DEVELOPMENT OF NOVEL ELECTROCHEMICAL MEASUREMENTS FOR WATER QUALITY

Manchester Metropolitan University

Athanasios V. Kolliopoulos

DEVELOPMENT OF NOVEL ELECTROCHEMICAL MEASUREMENTS FOR WATER QUALITY

Athanasios V. Kolliopoulos

Submitted in partial fulfilment of the requirements of Manchester Metropolitan University for the degree of Doctor of Philosophy

2014

School of Science and the Environment
Division of Chemistry and Environmental Science
Manchester Metropolitan University

ABSTRACT

This thesis reports the development of novel electrochemical methods applied for the quantification of important analytes in the field of water quality. Chapter 1 of this thesis focuses on the analytical methodologies used and the current requirements for low cost, environmental friendly and portable analytical tools into the field of water quality. In this chapter it is described how the analytical methodologies based on the use of screen-printed electrochemical sensors meets these requirements and why the development of such methodologies is the main purpose of this thesis.

Chapter 2 overviews the relevant fundamental electrochemical concepts with which this thesis is concerned. Chapter 3 gives a synopsis of the electrode materials as well as screen-printing upon which this thesis is based upon with a detailed overview not only of the screen-printing process, but also its current applications within the field of electrochemistry with particular attention paid towards the development of novel screen-printed electrode sensors applied into the field of water quality.

Chapter 4 describes the generic experimental methods used in this thesis. It gives details of the electrode materials, chemicals and real samples used in this thesis. Additionally it describes the screen-printing process on which the production of the in-door carbon based screen-printed sensors was based.

Chapter 5 reports the first examples of using electrochemical sensors for the target analytes selenium (IV), antimony (III) phenol and chlorophenols within drinking water; simplification of these analytical protocols is demonstrated through the production of screen-printed sensors.

Chapter 6 describes the development of screen-printed graphite sensors for the novel detection of dissolved phosphorus within environmental samples through the electrochemical

adaption of a colorimetric protocol. The electroanalytical protocol for the detection of dissolved phosphorus, a key parameter of eutrophication, was independently verified with ion chromatography and inductively coupled - plasma atomic emission spectroscopy.

Finally, Chapter 7 reports the first example of sensing cyclohexylamine and morpholine commonly used in industrial water as corrosion inhibitors for steam condensate treatment via indirect electrochemical protocol using screen-printed sensors. This is the first time that screen-printed sensors are applied into the detection of water treatment chemicals.

AIMS AND OBJECTIVES

The primary focus of this thesis is to develop novel electrochemical-based protocols to be applied into the field of water quality monitoring. The objectives of this study can be separated in three fields as described below.

Objectives:

1) Electrochemical detection of target analytes in drinking water.

2) Electrochemical detection of target analytes in environmental samples utilising screen-printed electrochemical sensors.

3) Electrochemical detection of target analytes in industrial water utilising screen-printed electrochemical sensors

ACKNOWLEDGMENTS

First and foremost I would like express my deepest gratitude to Professor Craig E. Banks for gifting me this opportunity but also for his continued support and everyday guidance over the past few years. I wouldn't have accomplished this research project if it wasn't for his enthusiastic encouragement and his effective management skills. I further would like to extend my sincere thankfulness to my friend Dr Dimitrios K. Kampouris who helped me from the very beginning not only with his extensive knowledge over the course of the project but also with his advices in everyday issues. I couldn't forget to mention Dr Jonathan Metters and his catalytic contribution in this project.

Importantly, I would like to offer a special thank you to all members of the Banks Research Group. The team spirit within the group has played a huge role in the research outcomes I have reached. Each one provided me with invaluable experience, for which I am grateful.

Finally I want to express my gratitude to the members of my family who have all played their own important roles in helping me achieve what I have to date.

TABLE OF CONTENTS

LIST OF TABLES

LIST OF SCHEMES

LIST OF FIGURES

ABBREVIATIONS

ASV	Anodic stripping voltammetry
AuSPE	Gold screen-printed macro electrode
BDDE	Boron-doped diamond electrode
CA	Chronoamperometry
CE	Counter electrode
CSV	Cathodic stripping voltammetry
CV	Cyclic voltammetry

DPASV	Differential pulse anodic stripping voltammetry
DPCSV	Differential pulse cathodic stripping voltammetry
DPV	Differential pulse voltammetry
ECL	Electrochemiluminescence
EIS	Electrochemical impedance spectroscopy
E_P	Peak potential
EPA	Environmental Protection Agency
EPPG	Edge-plane pyrolytic graphite
FIA	Flow injection analysis
GCE	Glassy-carbon electrode
HOPG	Highly ordered pyrolytic graphite
ICP-OES	Inductively coupled plasma optical emission spectroscopy
IR	Infra-red
I_P	Peak current
k^0	Electron chemical rate constant
LOD	Limit of detection
NPV	Normal pulse voltammetry
RE	Reference electrode
RSD	Relative standard deviation
PtSPE	Platinum screen-printed macro electrode
SCP	Stripping chronopotentiometry
SCE	Saturated calomel electrode

SEM	Scanning electron microscope
SIASV	Sequential injection anodic stripping voltammetry
SPE	Screen-printed electrode
SPGE	Screen-printed graphite electrode
SWASV	Square wave anodic stripping voltammetry
SWV	Square wave voltammetry
WE	Working electrode
WHO	World Health Organisation

CHAPTER 1

INTRODUCTION

Water is essential to all known forms of life and covers about 70 percent of the Earth's surface.[1] Water quality is termed as the chemical, physical and biological characteristics of water. Water quality defines the sustainability of ecological processes that support native fish populations, greenery and wetlands. A body of water according to its quality can be used by the communities for activities such as drinking, swimming, industrial processes and other commercial uses. Therefore water quality control is essential.[2] A major component of water quality control is water chemical analysis which produces quality data.

Modern water management requires quicker and more reliable characterization of important analytes, to allow for a more timely response. Traditionally, monitoring of water quality involves transportation of water samples to testing laboratories in order chemical, physical and biological characteristics to be determined.[3] Laboratory analytical techniques are expensive and time consuming. Additionally possible changing of water characteristics during the transportation can compromise the reflection of the analytical results obtained in the laboratories to the current water quality. Real-time monitoring can enable a short time response to water-quality concerns.[3] Recent advances in sensor technology have contributed to the progress in real-time monitoring capabilities for water quality.[4]

The most common instrumental techniques used into the field of water quality are presented in table 1.1. The electrochemical techniques are described extensively in chapter 2 of this thesis. Among the instrumental techniques most frequently used, optical and electrochemical have found applications in real-time monitoring of water quality.[5, 6] In contrast to optical detection, electrochemical sensors are not sensitive to light and they can be used for analysis of turbid samples.[7]

Table 1.1 A list of the most common instrumental techniques used into the field of water quality

Instrumental Techniques	Acronym
Mass Spectometry	
Electron Ionization Mass Spectrometry	EI-MS
Chemical Ionization Mass Spectrometry	CI-MS
Fast Atom Bombardment Mass Spectrometry	FAB-MS
Ion Cyclotron Resonance Mass Spectrometry	ICR-MS
Electrospray Ionization Mass Spectrometry	ESI-MS
Fourier Transform Mass Spectrometry	FT-MS
Secondary Ion Mass Spectrometry	SIMS
Gas Chromatography – Mass Spectrometry	GC-MS
Liquid Chromatography – Mass Spectrometry	LC-MS
Inductively Coupled Plasma – Mass Spectrometry	ICP-MS
Mass Spectrommetry-Mass Spectrometry	MS-MS
Optical Spectrometry	
Ultraviolet-Visible Spectrophotometry	UV-VIS
Atomic Absorption Spectrophotometry	AAS
Inductively Coupled Plasma Optical Emission Spectroscopy	ICP-OES
Atomic Fluoresence Spectroscopy	AFS
Infrared Spectrophotometry	IR
Nuclear Magnetic Resinance Spectroscopy	NMR
Fourier Transform Infrared Spectrophotometry	FTIR
Gas Chromatography-Infrared Spectroscopy	GC-IR
Electrochemical Techniques	
Potentiometry	
Voltammetry	
Amperomery	
Conductiometry	

New analytical tools and methodologies are required for real time monitoring of environmental pollutants and industrial process.[8] A major thrust of green analytical research activity is the development of low-cost analytical methodologies with reduced environmental impact and able to bring the analytical data close to the production operation.[8-10] The screen-printed derived sensors maintain the low cost production (when mass produced) through scales of economy.[11, 12] Additionally carbon based screen-printed sensors and especially the unmodified ones are disposable in nature and require a small volume of sample (even microliters[13]) making them environmentally friendly.[14, 15] Finally screen-printed analytical

sensors, containing the whole electrode system of counter, reference and working electrodes printed on the same substrate surface,[16] are considered to be the backbone of electrochemical sensors towards portable and decentralized (field) testing by even non-scientists because of their ease of use.[11, 17] For all of these reasons, screen-printed sensors meet the prerequisites and the current trends in green analytical chemistry for environmental and industrial process monitoring.

CHAPTER 2

INTRODUCTION TO ANALYTICAL ELECTROCHEMISTRY

Electrochemistry is concerned with the interaction between electrical and chemical effects. Different phenomena (*e.g.* electrophoresis and corrosion) and numerous devices (electrochromic displays, electroanalytical sensors, batteries, and fuel cells) and technologies (the electroplating of metals and the large-scale production of aluminium and chlorine) are included under the general field of electrochemistry. [18] Analytical electrochemistry is one of the largest parts of the field of electrochemistry which deals with the measurement of electrical quantities such as potential, current, or charge and their relationship to chemical reactions[18, 19]. Such electrical measurements have found a plethora of applications, including environmental monitoring, industrial quality control, and biomedical analysis.

2.1 ELECTROANALYTICAL TECHNIQUES

Electroanalytical techniques are based on an electrochemical process, which occurs at the electrode-solution interface which is in contrast to many chemical measurements that involve homogeneous solutions. The electrochemical process requires a system of at least two electrodes (conductors) and a contacting sample (electrolyte) solution, which constitute the electrochemical cell. Electroanalytical techniques focus on the processes and factors that affect the transport of charge across the interface between an electrode and an electrolyte, which are the electronic and the ionic conductors respectively. [18] The two necessary electrodes of the electrochemical cell are termed the working electrode and the reference electrode. The working electrode responds to the target analyte, while the reference electrode is of constant potential, which is independent of the composition of the contacting sample solution.

Electrochemical cells can be either galvanic or electrolytic cells. In galvanic cells, chemical energy converts into electrical energy by a spontaneous chemical reaction at the electrodes of the cell. In electrolytic cells, electrical energy from an external source, converts into chemical energy at the electrodes where a non-spontaneous chemical reaction occurs. Table 2.1 shows the classification of electroanalytical techniques according to the measured and controlled electrochemical parameter.

Table 2.1 Classification of the electroanalytical techniques according to the measured and controlled parameters. E = electrode potential, f = frequency, F = function of the parameter, G = conductivity, i = electric current, R = resistance, w = mass of deposition, Z = impedance, DMC = Dropping Mercury Electrode and t = time.

Measured Parameter	Controlled Parameter	Electrochemical Technique
$\boldsymbol{E}$	$i = 0$	Direct Potentiometry
$\boldsymbol{E}$	$i =$ stable	Potentiotitrimetry
$\boldsymbol{E = F(t)}$	$i =$ stable	Chronopotentiometry
$\boldsymbol{R}$ or $\boldsymbol{1/R}$ $(\boldsymbol{G})$	$E, f =$ stable	Conductometry
$\boldsymbol{Z = F(f)}$	$E =$ stable	Impedance Voltammetry
$\boldsymbol{w}$	$i =$ stable or $E =$ stable	Electrogravimetry
$\boldsymbol{i = F(E)}$	$E = F(t)$	Voltammetry (general)
$\boldsymbol{i = F(E)}$	$E = F(t)$(DMC)	Polarography
$\boldsymbol{i}$	$E =$ stable	Amperometry
$\boldsymbol{i = F(t)}$	$E =$ stable	Chronoamperometry
$\boldsymbol{Q}$ or $\boldsymbol{\int_0^t idt}$	$E =$ stable	Potentiostatic Coulometry
$\boldsymbol{Q}$ or $\boldsymbol{it}$	$E =$ stable	Amperostatic Coulometry
$\boldsymbol{Q = F(t)}$	$E =$ stable	Chronocoulometry

Equilibrium and dynamic techniques are the two types of electroanalytical techniques depending on the analytical signal for quantification.[19] In the case of equilibrium techniques, the measured parameter is the potential applied across an electrode's membrane. An external source keeps the chemical system at equilibrium (static at zero current 'situation'). The potential, which arises across the electrode's membrane, depends on the concentration of the analyte. Potentiometric and conductometric techniques are equilibrium techniques. In the

case of dynamic techniques, the measured parameter is the current based on the charge-transfer processes at the interface of the electrode and the solution. The static (controlled) parameter in this case is the potential (potentiostatic techniques) and not the current (no-zero current 'situations'). Voltammetric coulometric and electrogravimetric techniques are potentiostatic techniques. This thesis is concerned with potentiostatic or controlled-potential techniques.

2.2 FARADAIC PROCESSES

Faradaic and non-faradaic processes are the two types of processes that occur at electrodes. In the case of faradaic processes, charges (*e.g.* electrons) are transferred across the electrode-solution interface, resulting in oxidation or reduction. Such reactions are governed by Faraday's law, *i.e.* the amount of chemical reaction caused by the flow of current is proportional to the amount of electricity passed.[18] The total amount of the chemical equivalents of the reactants that are oxidised or reduced is given by the Faraday equation:

$$eq = \frac{Q}{F} \qquad (2.1)$$

where eq are the chemical equivalents of the reactants that are oxidised or reduced Q is the charge that is transferred across the electrode-solution interface and is given by: $Q = it$ (for stable current) or $Q = \int_0^t idt$ (for non-stable current), F is the Faraday constant (96485.38 coulomb eq^{-1}) which is the total charge of N electrons (N: Avogadro's number = 6.022×10^{23}) $F = NQ_e$ (Q_e is the charge of an electron = 1.602×10^{-19} Coulomb). The current as a result of Faradaic processes is termed a *Faradaic current*.

In the case of non-faradaic processes, there is not an actual charge transfer across the electrode-solution interface causing oxidation or reduction. Thus, the electrode can be modelled as capacitor. When the potential of the electrode or the solution composition is altered, non-faradaic processes such as adsorption and desorption can occur at the interface of the electrode, therefore an external current (capacitive current) can flow. Note that both faradaic and non-faradaic processes occur when electrode reactions take place.

Controlled-potential techniques intend to obtain the faradaic current response which is related to the concentration of the target analyte.[19] This objective is achieved by monitoring the transfer of electron(s) during the redox process of the analyte:

$$O + ne^- \leftrightarrow R \tag{2.2}$$

where O and R are the oxidised and reduced forms, respectively, of the redox couple. The potential region where this reaction will occur must make the electron transfer thermodynamically or kinetically favourable. For systems controlled by the laws of thermodynamics, the potential of the electrode is related to the activity of the species at the surface [where a_o and a_R simply represent the activities of the oxidised and reduced forms, respectively at the surface of the electrode] according to the *Nernst equation*:[18-21]

$$E = E^O - \frac{RT}{nF} \ln \frac{a_R}{a_O} \tag{2.3}$$

where E^o is the standard potential for the redox reaction, R is the universal gas constant (8.314 J K^{-1} mol^{-1}), T is the temperature (in Kelvin), n is the number of electrons transferred in the reaction, and F is the Faraday constant (96,485.33 C mol^{-1}). In highly dilute (ideal) aqueous solutions, where the ions do not actually interact with each other, it can assumed that activity is equal to concentration. The *Nernst equation* can then be expressed in the following form:

$$E = E^O - \frac{RT}{nF} \ln \frac{C_R}{C_O} \tag{2.4}$$

where C_R and C_O are the concentration of the reduced and oxidised forms respectively at the surface of the electrode. At a temperature of 25^0C and considering that lnx = 2.303logx the *Nernst equation* becomes:

$$E = E^O - \frac{0.059}{n} \log \frac{C_R}{C_O} \tag{2.5}$$

Current-potential plots constitute a voltammogram (see later). The shape and magnitude of this voltammetric response are governed by the faradaic and non-faradaic processes involved in the electrode reaction. The total current consists in the sum of the non-faradaic charging background current and the faradaic current.[20, 22]

2.3 FACTORS THAT DEFINE THE MEASURED CURRENT

As mentioned at equation (2.2), electrochemically redox reactions involve the electroactive (charged) species of the oxidised and reduced forms of a redox couple. For simplicity, the term electroactive species A for both the oxidised O and the reduced R forms of the redox couple is used interchangeably. Additionally, either the reduction or the oxidation half electrochemical reactions of the equation (2.2) are called half reactions. In a controlled-potential technique when the potential of the working electrode allows the half reaction of the electroactive species A to take part, the measured current is governed by the factors below:

- The rate of the mass transport with which the electroactive species A are transferred to the electrode's surface in order to replenish the species that already reacted and maintain the faradaic current.
- The rate of the electron transfer across the interface.
- The rate of other different chemical phenomena that come before the half reaction like homogeneous or heterogeneous chemical equilibriums in which the species A participate such as kinetics and catalysis and absorption of the species A into the surface of the electrode.

The slowest factor defines the measured current. In these cases, the current is characterized as a mass-transport limited current, electron-transfer limited current and reaction-rate limited current respectively. The mass transport rate is the factor that most voltammetric techniques seek to control the measured current. Such systems are called *nernstian* or *reversible*, because they obey thermodynamic relationships.

2.3.1 MASS-TRANSPORT LIMITED CURRENT

The mass transport can be accomplished with one or more of the modes below:

Migration – movement of charge particles (ions) under the influence of an electric field. The force F that is applied at these particles is given as $F = Eq$ where E is the electric field strength and q is the charge of the particles. The electric field is the result of the potential gradient between the electrodes across the solution.

Diffusion – movement of particles (charged and uncharged) under the influence of a concentration gradient within the solution (between the surface of the electrode and the bulk solution).

Natural convection – movement of particles with hydrodynamic transport due to density gradients caused by thermal inhomogeneity.
These three modes of mass transport are illustrated in figure 2.1.

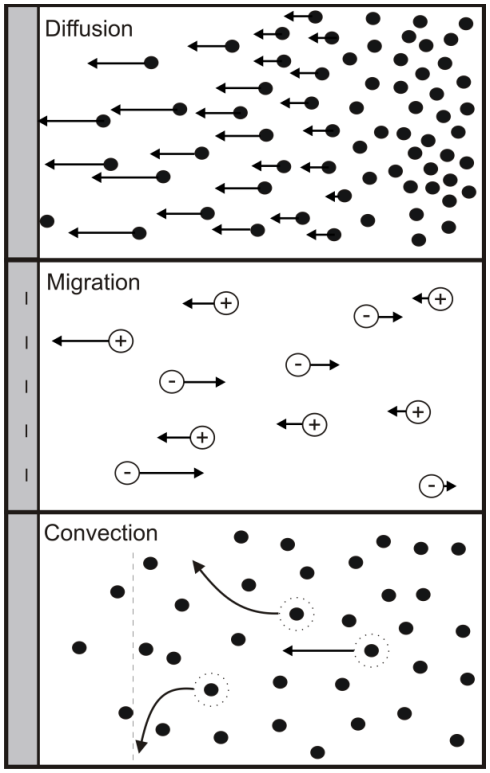

Figure 2.1 The modes of mass transport at an electrode surface. Reproduced from Ref[19].

In most voltammetric techniques, experimental conditions are chosen so that the mass transport is affected exclusively by a single mechanism, typically diffusion[23] as it is considered to be a mechanism that ensures a reproducible rate of electroactive species

transfer which is analogous to the their concentration in the bulk solution without using any mechanical means. Migration can be eliminated by adding supporting electrolyte. Supporting electrolyte is electrolyte, which is not electroactive at the potential range where the electroactivity of the determined species (analyte) is not expected. The relatively high concentration of the ions (at least 100 times higher than the concentration of the analyte) of the supporting electrolyte neutralize the gradient of the potential by eliminating the electric field between the two electrodes. Additionally the supporting electrolyte reduces the ohmic resistance of the solution and optimize the conditions for a particular analytical method (*i.e.* by regulating the pH of the solution or by complexing other ions).

Flux (J) is an important parameter relating to electrochemical process. Flux is defined as the number of molecules penetrating a unit area of an imaginary plane in a unit of time. The units of flux are: mol s^{-1} cm^{-2}. Under mass transport conditions occurring exclusively by diffusion, the flux of the electroactive species *A* from the bulk solution to the electrode is called diffusional flux and can be illustrated by Fick's first law:[21]

$$J_A(x,t) = -D_A[\frac{\partial C_A(x,t)}{\partial x}] \qquad (2.6)$$

where $J_A(x,t)$ is the flux of the species *A* (at distance x and time t), in mol s^{-1} cm^{-2}. $\frac{\partial C_A(x,t)}{\partial x}$ is the concentration gradient (at distance x from the electrode and time t) in mol cm^{-3} cm^{-1}. D_A is the diffusion coefficient of the species *A* in cm^2 s^{-1}. The diffusion coefficient is the measure of the velocity of the species *A* when they move under the influence of the concentration gradient. The negative sign in the equation (2.6) signifies that the flux of the mass performed to the opposite direction to that the concentration increases from the region of higher concentration to the region of lower concentration. The relation of the concentration to time and distance can be calculated by Fick's second law:

$$\frac{\partial C_A}{\partial t} = D_A \frac{\partial^2 C_A}{\partial x^2} \qquad (2.7)$$

Fick's first law illustrates the proportional relation of flux to the slope of the concentration gradient when the movement of the electroactive species is limited solely by diffusion. This requires the suppressing of the migration and natural convection. A more general equation known as the *Nernst-Planck equation*, describes mathematically the flux of

the electroactive species to the electrode surface taking into account the migration and natural convection as modes of mass transport:[19]

$$J_A(x,t) = -D_A \frac{\partial C_A(x,t)}{\partial x} - \frac{zFD_A C_A(x,t)}{RT} \frac{\partial \varphi(x,t)}{\partial x} + C_A(x,t) V_A(x,t) \qquad (2.8)$$

where D_A is the diffusion coefficient of the electroactive species *A*, $\frac{\partial C_A(x,t)}{\partial x}$ is the concentration gradient at distance x and time t, $\frac{\partial \varphi(x,t)}{\partial x}$ is the potential gradient, *z* is the charge of the electroactive species *A* and $V_A(x,t)$ is the hydrodynamic velocity at distance x. The above equations for flux are given in one dimension.

The magnitude of the current is related to the flux of the species A by the following:

$$i = nAFJ_A \qquad (2.9)$$

where *F* is the Faraday constant, *A* is the electrode area and *n* is the number of electrons per molecule involved. Combining equations (2.6) and (2.9) yields the relation of the current caused by diffusion of the electroactive species *A* and their concentration gradient.

$$i = -nFAD_A \frac{\partial C_A(x,t)}{\partial x} \qquad (2.10)$$

The concentration profile diagram (Fig. 1.2) explains the current-time relationship. The solid lines represent the real distribution diagram of the concentration whereas the extended dashed lines represent the simplified linearized model according to Nernst equation, which reflects the reality with sufficient accuracy. $\boldsymbol{C_{(b)}}$ is the concentration of the electroactive species *A* at the bulk solution and at the surface of the electrode when the electrode is in equilibrium with the bulk solution (i = 0). After the reach of a potential where there is exchange of electrons between the electrode and the electroactive species *A*, a concentration gradient is created close to the surface of the electrode. The distance δ in the linearized model is called the diffusion layer and is the region where there is depletion of the

electroactive species *A*. The diffusion layer, δ, in two dimensions is given by the following equation:

$$\delta = \sqrt{2Dt} \tag{2.11}$$

the diffusion layer if the solution is not renewed (no stirring conditions) expands (δ_1, δ_2, δ_3 at t_1, t_2, t_3 respectively) as time passes to the bulk solution. In this case the gradient of the concentration ($\frac{\partial C_A}{\partial x}$) reduces gradually and thereby the flux of the electroactive species *A* to the electrode (according to Fick's first law); consequently the faradaic current depletes.

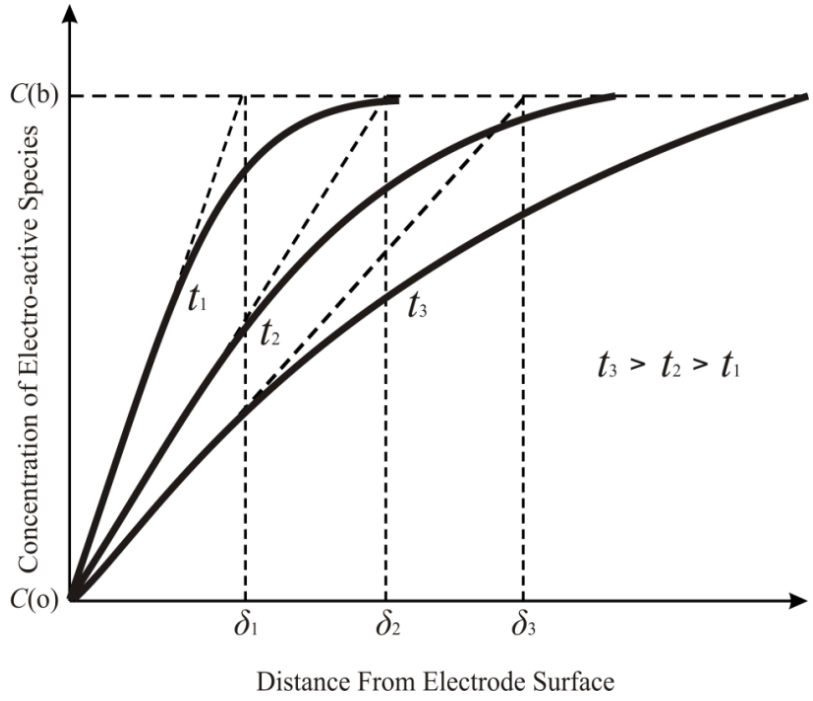

Figure 2.2 Distribution diagram of the concentration for different times *t*. Reproduced from Ref [19]

2.3.2 ELECTRON-TRANSFER LIMITED CURRENT

The current-potential relationship is different when the mass transport is sufficiently fast and the factor that controls the reaction is the rate of the electron transfer. The electron transfer step occurs between the conduction band of the electrode and an orbital of the molecules O or R $(O + ne^- \underset{k_{ox}}{\overset{k_{red}}{\longleftrightarrow}} R)$. The rate of the reduction, V_{red} is given by:

$$V_{red} = k_{red} C_O(0,t) \tag{2.12}$$

while the reversed (oxidation) reaction, V_{ox} is given by:

$$V_{ox} = k_{ox} C_R(0,t) \tag{2.13}$$

where k_{red} and k_{ox} are the rate constants of the reduction and the oxidation half reactions respectively. These constants depend on the operating potentials according to the following relationships:[19]

$$k_{red} = k^0 \exp[-\alpha n F(E - E^O)/RT] \tag{2.14}$$

$$k_{ox} = k^0 \exp[(1-\alpha) n F(E - E^O)/RT] \tag{2.15}$$

where k^0 is the standard rate constant (in cm s^{-1}) and α is the transfer coefficient. The standard rate constant k^0 reveals the the reaction between the electrode material used and the particular reactant, while the transfer coefficient α reflects the symmetry of the free energy curve with respect to the reactants and products and its values are between zero and unity. For symmetric curves, the value of α will be close to 0.5.

The two half-reactions currents are proportional to rate of the half-reactions respectively:

$$i_{red} = nFAV_{red} \tag{2.16}$$

$$i_{ox} = nFAV_{ox} \tag{2.17}$$

and since the net reaction rate is:

$$V_{net} = V_{red} - V_{ox} \tag{2.18}$$

the overall current is given by the combination of (2.12), (2.13), (2.16), (2.17)

$$i_{net} = i_{red} - i_{ox} = nFA[k_{red} C_o(0,t) - k_{ox} C_R(0,t)] \tag{2.19}$$

by substituting (1.14) and (1.15) in (1.19):

$$i_{net} = nFAk^0\{C_o(0,t)\exp[-\frac{anF(E-E^0)}{RT}] - C_R(0,t)\}\exp[\frac{(1-a)nF(E-E^0)}{RT}] \qquad (2.20)$$

which depicts the current-potential relationship for reactions controlled by the rate of electron transfer.

2.4 VOLTAMMETRIC TECHNIQUES-EQUIPMENT

In voltammetric techniques, the potential of the working electrode changes in a controlled manner. It alters linearly, by steps or pulses in a strictly controlled manner. This is the reason why the use of potentiostat and a third electrode known as the counter or the auxiliary electrode is necessary. The potentiostat receives the waveform of the potential $E(t)$ from a waveform generator and applies a potential $E_{applied}$ between the working electrode and the counter electrode in order for the potential of the working electrode (in relation to the reference electrode) to follow the waveform $E(t)$. The current is monitored as a voltage across a resistor (in series with the electrolytic cell), which is amplified and recorded with the assistance of current-to-voltage –i/V converters. Diagrammatic presentation of instrumentation in voltammetric experiments is given in Figure 2.3:

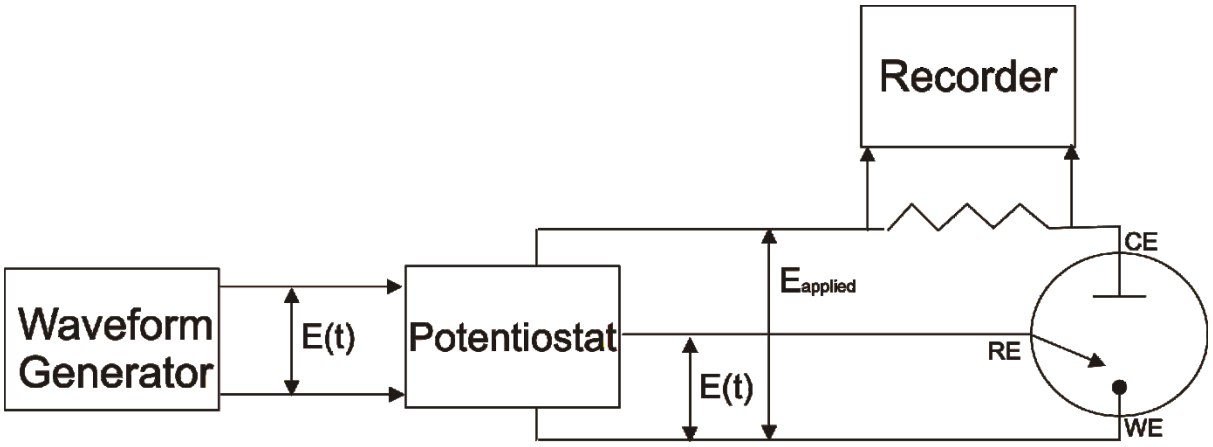

Figure 2.3 Electronic schematic of instrumentation in voltammetric experiments (WE: working electrode, CE: counter electrode, RE: reference electrode).

The three-electrode cell configuration consists of the working (small surface electrode), counter and reference electrode and is used to perform electroanalytical measurements into the sample solution. The potential of the reference electrode according to which the potentiostat controls the potential of the working electrode, must be independent of the solution. The counter electrode, which is usually constructed of inert metals, ensures the electrical neutrality of the solution providing the appropriate charges depending on the process accomplished on the working electrode. The potentiostat forces whatever current is required through the working electrode in order for the working electrode to achieve the desired potential at any time. This "electron pressure" forces the chemical species to gain or lose an electron (reduction or oxidation respectively). The current over the circuit of the working electrode, counter electrode and sample solution is measured as mentioned above. [18, 19] A typical three-electrode electrochemical cell for controlled-potential experiments is shown in Figure 2.4.

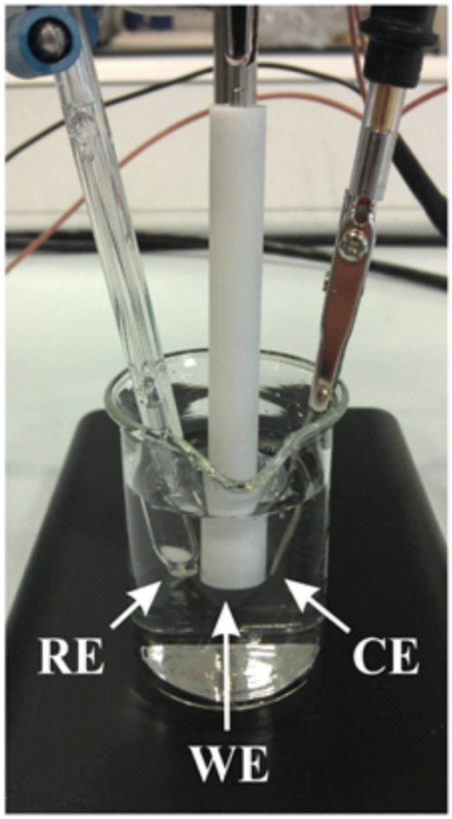

Figure 2.4 A typical voltammetric cell. The reference electrode (RE) is a saturated calomel electrode. The working electrode (WE) is an edge-plane pyrolytic graphite electrode and the counter electrode (CE) is a platinum wire. All the three electrodes immersed into an electrolyte solution.

In many cases, the solution in the voltammetric cell must not contain dissolved oxygen. The molecule O_2 is electroactive and interferes with the detection of the analyte by providing intense voltammetric signal. Additionally it is an oxidative agent, which can act in a synergistic or antagonistic way on the controlled electrochemical processes with a negative influence upon the repeatability and reliability of the measurements being performed. In these cases it is imposed the solution to be degased by the transmission of an electrochemically inert gas (like nitrogen) through the appropriate supply piping.

The controlled-potential techniques exhibit high sensitivity, selectivity towards electroactive species, portable and low cost instrumentation. Extremely low (nanomolar) limits of detection can be achieved with very small sample volumes (5-20 μL).[19]Additionally the extensive array of electrode materials permits the assay of unusual sample environments.[22]

2.5 CYCLIC VOLTAMMETRY

Cyclic Voltammetry (CV) is the most widely used voltammetric technique. It consists of linearly scanning the potential of the working electrode between two values, E_1 and E_2 using a triangular waveform (Figure 2.5). The potential of the working electrode swept from the initial value E_1 to the value E_2 with the same rate and then returns to the value E_1 with the same rate but in the opposite direction. Scanning from the value E_1 to E_2 only constitutes *Linear Sweep Voltammetry* while the whole cycle of the potential scanning ($E_1 \rightarrow E_2 \rightarrow E_1$) constitutes the *Cyclic Voltammetry* and it is accomplished in a range of time between *milliseconds* to *hours* depending on the chosen scan rate which can be from mVs^{-1} to hundreds of Vs^{-1} and on the difference between the two values E_1 and E_2. One cycle usually provides enough qualitative and quantitative information about the redox process, otherwise the cycle described above is repeated.

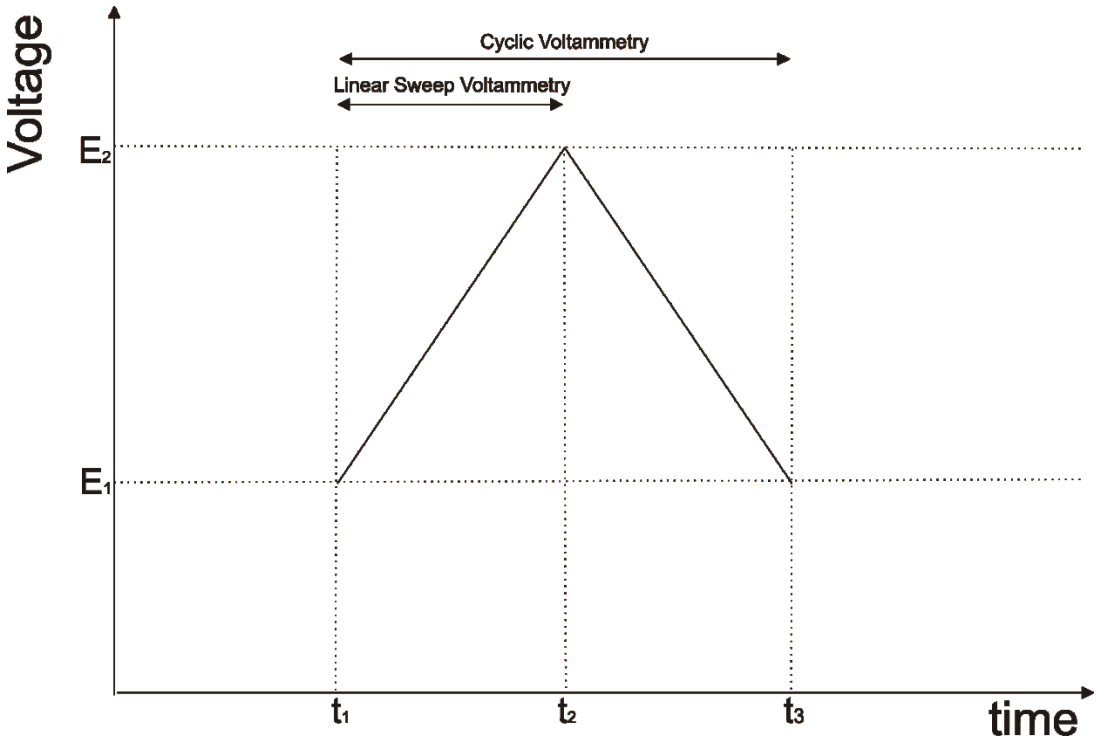

Figure 2.5 Typical triangular potential waveform used in the generation of a cyclic voltammogram.

During the potential sweep, the current which flows through the voltammetric cell is recorded as a function of the potential of the working electrode. The graph of current versus potential is termed a *cyclic voltammogram.* Figure 2.6 presents a typical cyclic voltammogram obtained in a solution containing 1mM Potassium Ferrocyanide in supporting electrolyte 1M KCl using a boron-doped diamond electrode (BDDE) as a working electrode, Saturated Calomel Electrode (SCE as reference electrode) and platinum wire (Pt as counter electrode). The voltammogram corresponds to conditions, which allow the mass transport to occur predominately via diffusion (no stirring).

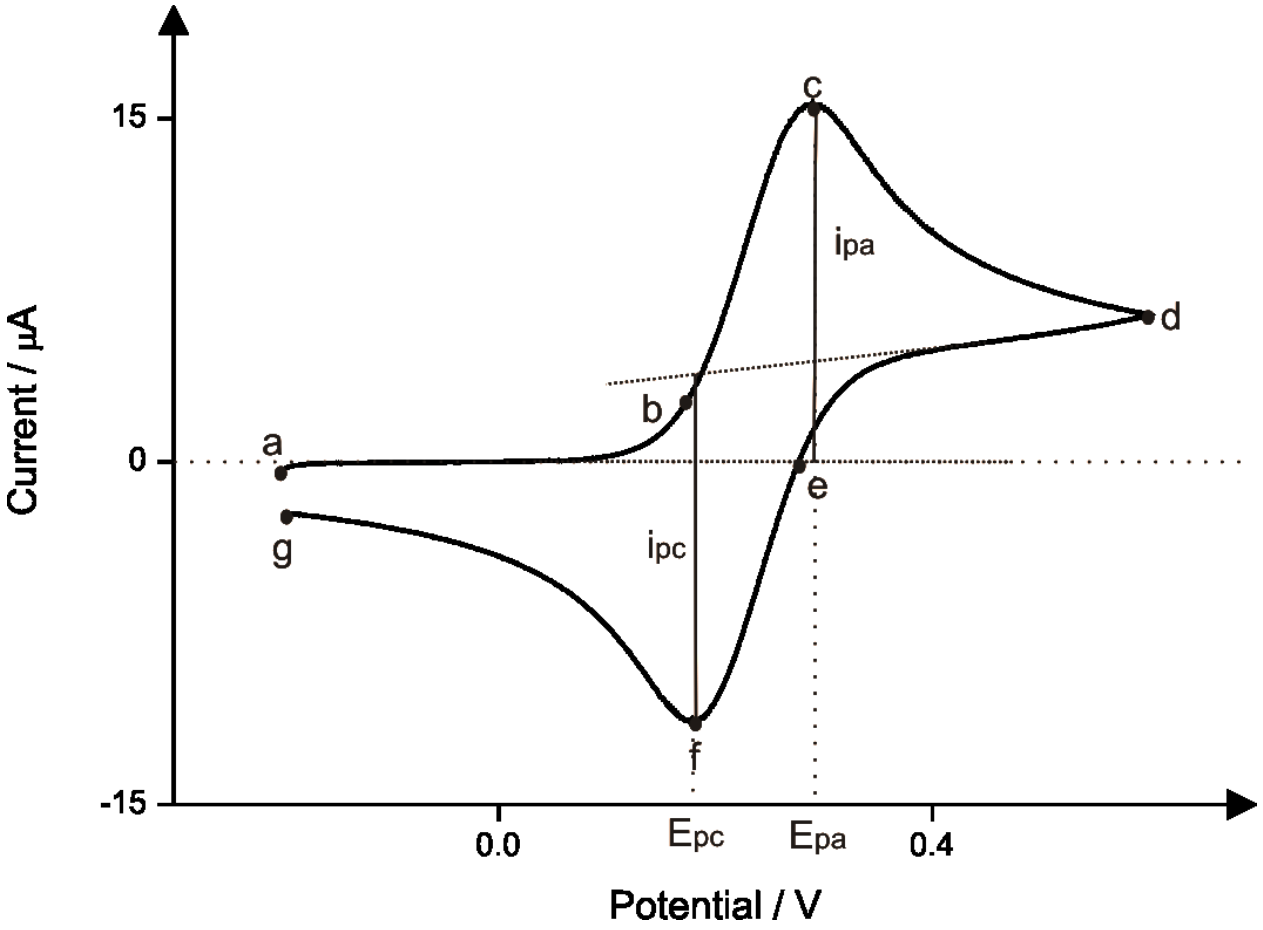

Figure 2.6 Cyclic voltammogram in consequence of the electrochemical response of a BDDE (using a SCE reference and /Pt counter) in a solution comprising 1mM Potassium Ferrocyanide and supporting electrolyte 1M KCl. Scan rate: 50 mV/s.

The potential scan of the working electrode starts at the point *a* (see fig 1.6) which corresponds to the initial potential E_1 (-0.20V vs SCE), where the ferro ions (Fe^{2+}) are not oxidised yet to ferri ions (Fe^{3+}). The oxidation of the Ferro ions has been started at point *b* and reaches a maximum (anodic) value i_{pa} at point *c* which corresponds to potential value E_{pa}. After that, the anodic current reduces as a result of the depletion of ferro ions on the surface of the working electrode since the limited time for the replenishment of the ferro ions by diffusion from the bulk solution (diffusion limited current). Point *d* corresponds to the potential E_2 (-0.6V vs SCE) where the direction of the potential scanning changes. Until the point *e* the current is still anodic as the result of the continuing oxidation of ferro ions. At

point *e* starts the reduction of the ferri ions which are formed during the previous half cycle of the potential scanning. The current reaches a maximum (cathodic) value i_{pc} at point *f* which corresponds to potential *Epc.* Consequently, the anodic current reduces because of the depletion of ferri ions on the surface of the working electrode. Point *g* corresponds to the initial potential E_1 and the cycle of the potential scanning is integrated. The small current observed at this point is capacitive current.

A cyclic voltammogram can be used for both qualitative and quantitative analytical purposes. The potentials of the peak currents are characteristic of each electroactive species (under specified conditions and scan rate). The maximum current (peak current) is measured by the extension of the base line before the peak and under stable scan rate is proportional to the concentration of the electroactive species. Cyclic voltammetry reveals information for the reversibility and the nature of the redox process. A redox process can be reversible, irreversible or quasi-reversible. It depends on if it is controlled exclusively by mass transport or not. Examples of cyclic voltammograms for all the three mentioned redox processes are shown in Figure 2.7.

For a reversible redox couple where the rates of all associated chemical reactions and the charge transfer are very rapid compared to the rates of the mass-transfer processes, the difference of the two potentials (peak separation) which correspond to the peak currents (at 298 K) is given by[22]:

$$\Delta E_{\mathrm{p}} = E_{\mathrm{pa}} - E_{\mathrm{pc}} = 0.057 / n \tag{2.21}$$

where *n* is the number of electrons which takes part in the half-reaction. Additionally the standard reduction potential for a redox couple is given by:

$$E^{0} = \frac{E_{\mathrm{pa}} + E_{\mathrm{pc}}}{2} \tag{2.22}$$

Finally the peak current is given by the Randles-Ševčík equation[24]:

$$I_{\mathrm{p}} = 0.4463 \frac{(Fn)^{3/2}}{(RT)^{1/2}} AD^{1/2} Cv^{1/2} \tag{2.23}$$

Leading to (at 25^0C): $I_p = (2.69 \times 10^5) n^{3/2} A C D^{1/2} v^{1/2}$ (2.24)

where F is the Faraday constant, n is the number of electrons transferred in the redox process, A is the electrode area (in cm^2), D is the diffusion coefficient of the electroactive species (in $cm^2\ s^{-1}$), C is their concentration (in mol cm^{-3}) and v is the applied scan rate (in V s^{-1}). The peak current is proportional to the analyte concentration. Additionally the anodic and cathodic peak currents are equal for a reversible redox system. As the reversibility of electrode half reaction reduces, the peak separation increases. Furthermore, the peak of the opposite scanning can be completely absent. In addition, the magnitude of the individual peaks is reduced (see figure 2.7).

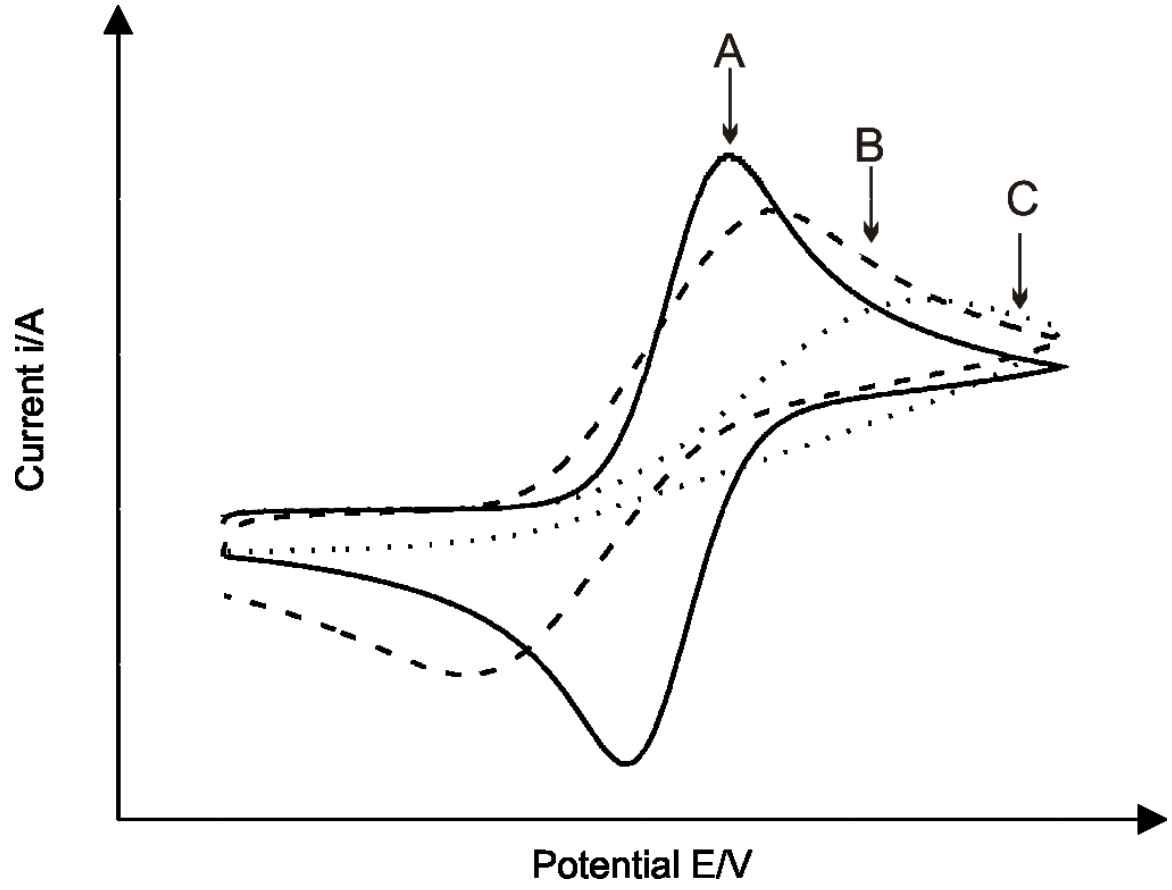

Figure 2.7 Typical cyclic voltammograms corresponding to: reversible (solid line), quasi-reversible (dashed line) and irreversible (dotted line) electrode half-reactions.

For an irreversible or quasi-reversible system, where the rate of the charge transfer is sluggish compared to the rate of the mass-transfer process, the peak potential is given by the equation[19]:

$$E_p = E^0 - \frac{RT}{an_aF}[0.78 - \ln\frac{k^0}{D^{1/2}} + \ln(\frac{an_aFv}{RT})^{1/2}] \quad (2.25)$$

where a is the transfer coefficient k^0 is the standard heterogeneous rate constant mentioned before at electron transfer limited reactions 1.3.2, n_a is the number of electrons participate in the charge-transfer step. The peak current at 25^0C is given by the equation:

$$i_p = (2.99\times10^5)n(an_a)^{1/2}ACD^{1/2}v^{1/2} \quad (2.26)$$

A system can be considered quasi-reversible when $10^{-1} > k^0 > 10^{-5}$ (cm s^{-1}).[19] From equation 2.25, it is obvious that the peak potential is displaced when the scan rate changes. Equation 2.26 shows that the peak current is still proportional to the bulk concentration of the analyte but it will be lower in height as it depends on the charge-transfer coefficient a whose values are between 0 and 0.5.

2.5.1 ELECTROCHEMICAL REACTION MECHANISMS

So far, it has been exclusively considered an electrochemical *E* reaction where the process involves the transfer of electrons. This chapter considers the intervention of a subsequent chemical reaction to this process as described below:

$$O + ne^- \longleftrightarrow R \text{ followed by } R \longrightarrow Z \quad (2.27)$$

which according to the notation of Tesla and Reinmouth[25] is described as an *EC* reaction. The product of the electrochemical step *R* is removed from the surface of the electrode during the following chemical step resulting in a smaller reverse peak to the corresponding cyclic voltammogram. In case that the chemical reaction progresses very rapidly that all of *R* has

been removed from the surface of the working electrode by being converted into Z, no reverse peak is being observed. Further information about the rates of the coupled reaction can be obtained by the peak ratio of the forward and reverse peaks (which is not equal to 1) and by varying the scan rate. Table 2.2 summarizes the electrochemical mechanisms involving coupled chemical reactions.

Table 2.2 Electrochemical mechanisms involving coupled chemical reactions. Reproduced from reference[26]

Reversible electron transfer process, no follow-up chemistry; an E_r step: $O + ne^- \longleftrightarrow R$
Reversible electron transfer process followed by a reversible chemical reaction; E_rC_r: $O + ne^- \longleftrightarrow R$ $R \longleftrightarrow Z$
Reversible electron transfer process followed by an irreversible chemical reaction; E_rC_i: $O + ne^- \longleftrightarrow R$ $R \longrightarrow Z$
Reversible chemical reaction followed by a reversible electron transfer process; C_rE_r: $Z \longleftrightarrow O$ $O + ne^- \longleftrightarrow R$
Reversible electron transfer process followed by an irreversible regeneration of starting materials; E_rC_i': $O + ne^- \longleftrightarrow R$ $R \longrightarrow Z + O$
Multiple electron transfer processes with an intervening reversible chemical reaction; $E_rC_rE_r$: $O + ne^- \longleftrightarrow R$ $R \longleftrightarrow Z$ $Z + ne^- \longleftrightarrow Y$
Multiple electron transfer processes with an intervening irreversible chemical reaction; $E_rC_rE_r$: $O + ne^- \longleftrightarrow R$ $R \longrightarrow Z$

$$Z + ne^- \longleftrightarrow Y$$

2.6 STRIPPING VOLTAMMETRY

Special categories of electroanalytical techniques are the stripping techniques such as stripping voltammetry and stripping potentiometry. Stripping voltammetry allows the detection of different chemical species (mainly metal ions) at the same time and at very low concentrations.

Stripping techniques are two-step techniques and this increases their sensitivity. The first step of all the stripping techniques is called the pre-concentration step where deposition of a small amount of the analyte at the surface of the working electrode takes part. The deposition of the analyte is carried out under conditions such as intense stirring of the solution or by using rotating electrodes in order to manage as quick and reproducible mass transport as possible. The pre-concentration step mainly proceeds by mass transport. Although in some stripping techniques, the pre-concentration step proceeds by absorption or chemical bonding of the analyte on the surface of the working electrode and it is called non-faradaic pre-concentration. In the second step, which is, called stripping step an electrochemical stripping, in case of stripping voltammetry, or chemical stripping, in case of stripping potentiometry, occurs.

Before the pre-concentration step, the solution is degasificated usually by bubbling with an inert gas such as nitrogen, argon or helium in order to substitute the dissolved oxygen. The scope of this substitution is to avoid the chemical oxidation of the pre-concentrated metal ions. Between the two steps, there is an equilibration phase where the stirring of the solution is stopped. At this phase, the amalgam of the metals deposited onto the surface of the working electrode is homogenized. Figure 2.8 shows the steps in stripping voltammetry (specifically in anodic stripping voltammetry). The pre-concentration step is usually 0.5-30 minutes whereas the equilibration phase 15-30 seconds.[27]

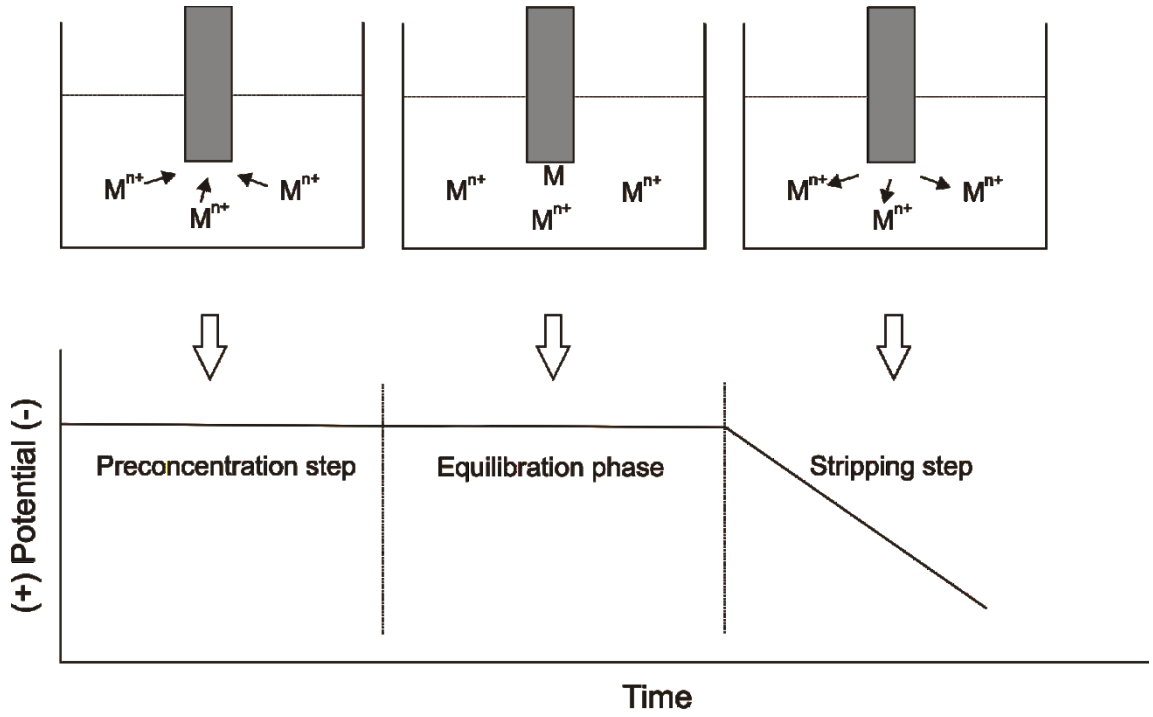

Figure 2.8 Typical potential-time profile showing the steps in Anodic Stripping Voltammetry.

There are two types of stripping voltammetry, Anodic Stripping Voltammetry (ASV) and Cathodic Stripping Voltammetry (CSV). In anodic stripping voltammetry the peak currents are anodic currents. An anodic stripping voltammogram of Cd^{2+}, Pb^{2+} and Sb^{3+} is shown at figure 2.9. The pre-concentration step was performed on a glassy-carbon electrode at potential of -1V (vs saturated calomel electrode) for 60 seconds in order to reduce a small amount of the ions in the solution to their metals on the working electrode. The stripping of the metals was realised by scanning to potential of + 0.5V where all the three metals have been re-oxidized. The peak height of each stripping/analytical signal is proportional to the concentration of the metal ions into the solution.

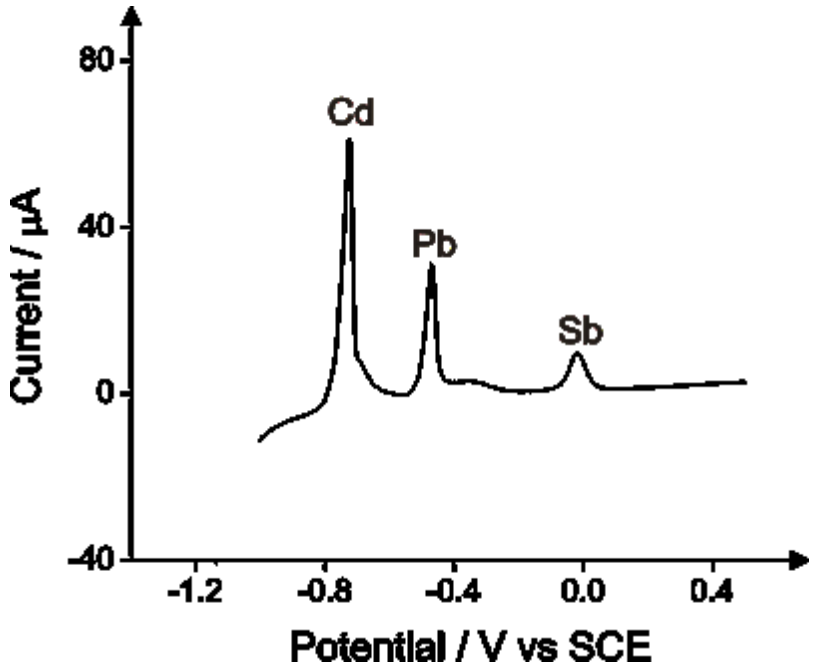

Figure 2.9 Anodic Stripping Voltammetry (in the same aqueous solution) of cadmium (Cd) lead (Pb) and Antimony (Sb). Working electrode: glassy-carbon electrode. Reference electrode: saturated calomel electrode. Counter electrode: Platinum wire.

In cathodic stripping voltammetry, the potential scan is performed in the opposite (cathodic) direction and the peaks are due to cathodic current. The cathodic stripping voltammetry has limited applications and has been used mainly for the detection of substances which oxidise the metal of the working electrodes[27] forming insoluble compounds with them during the pre-concentration step. Such substances are the halide ions (Cl^-, Br^-, I^-), SCN^-, S^{2-} and organic compounds with thiol groups. Typical electrode half-reactions are shown below:

Detection of halide ions (X^-):

Pre-conc. step: $$yM(\text{electrode}) + nX^- \rightarrow M_yX_n(s) + ne^- \quad (2.28)$$

Stripping step: $$M_yX_n + ne^- \rightarrow yM(\text{electrode}) + nX^- \quad (2.29)$$

Detection of compounds with thiol group:

Pre-conc. Step : $M(\text{electrode}) + nRSH \rightarrow (RS)_{\text{n}}M(s) + nH^{+} + ne^{-}$ (2.30)

Stripping step: $(RS)_{\text{n}}M(s) + nH^{+} + ne^{-} \rightarrow M(\text{electrode}) + nRSH$ (2.31)

2.7 CHRONOAMPEROMETRY

Chronoamperometry is a technique involving scanning the potential of the working electrode in steps and not linearly as in previously mentioned voltammetric techniques. The potential of the working electrode steps from a value (E_1) where faradaic process does not occur to a potential (E_2) within a potential region where the redox reaction becomes so rapid that the concentration of electroactive species at the surface of the electrode is nearly zero. (Figure 2.10). The solution in the electrochemical cell remains unstirred. This stepping of the potential creates a concentration gradient at the surface of the electrode producing flux of electroactive species to the electrode surface where they react rapidly. The flux of the electroactive species and hence the current is proportional to concentration gradient around the electrode surface as the mass transport under these conditions (unstirred solution) is solely by diffusion. The current is monitored in relation to time. Initially the current is very large as the potential step occurs instantly. As the time progresses the slope of the concentration of the electroactive species at the surface of the electrode decreases and accordingly the diffusion-limited current. The relation of the current (at a planar electrode) with time is given by the Cottrell equation:[19]

$$i(t) = \frac{nFACD^{1/2}}{\pi^{1/2}t^{1/2}} \qquad (2.32)$$

Chronoamperometry is usually used for measuring diffusion coefficients or the surface area of working electrodes.[28] Chronoamperometry is often used for the study of mechanisms of electrode processes.

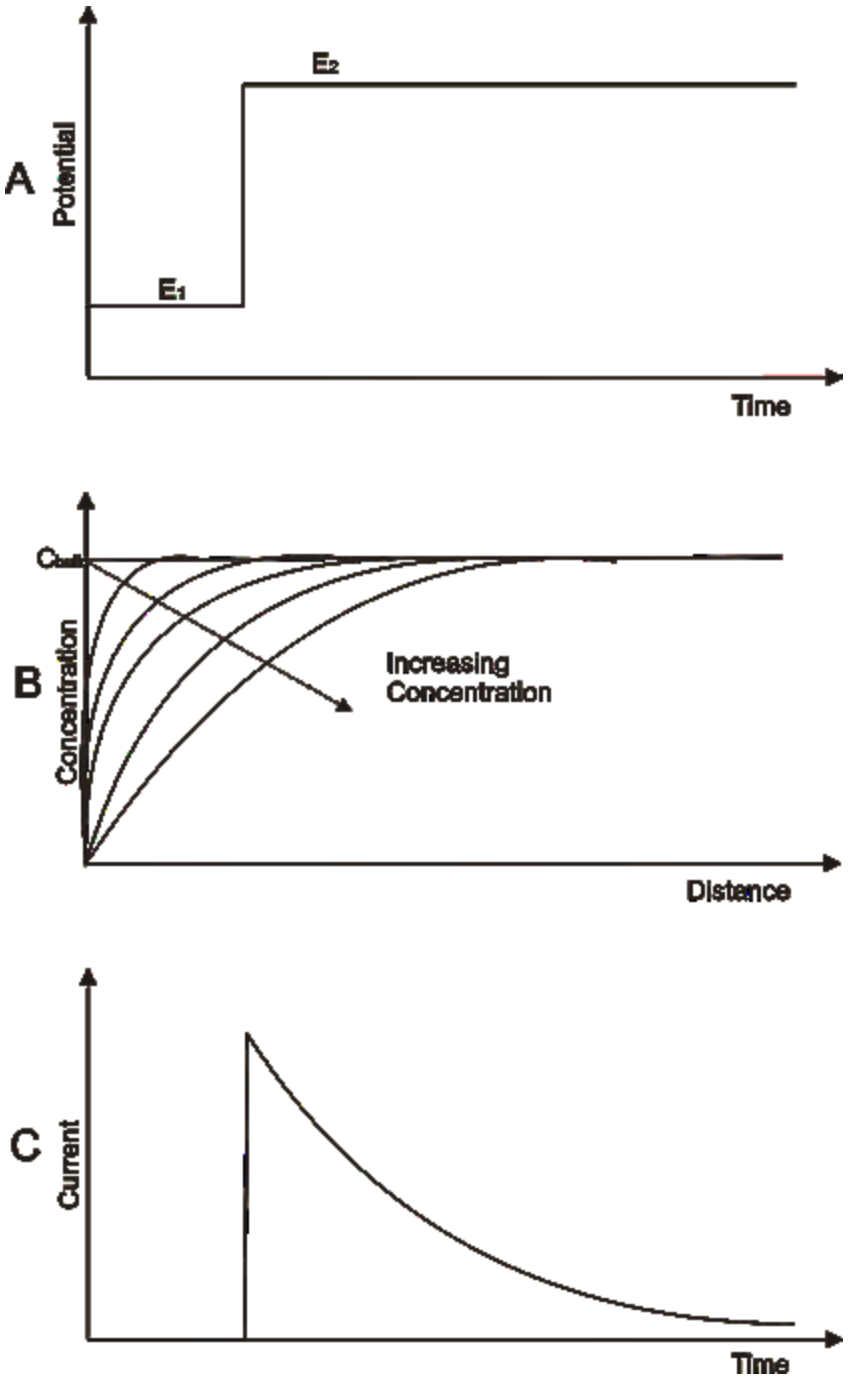

Figure 2.10 Chronoamperometric experiment: (A) Potential-Time waveform, (B) change of concentration profiles with time, (C) resulting current time response. Reproduced from Ref [19]

Pulse Voltammetric techniques use complex potential waveforms consisting of combinations of sweeps and steps. The most important pulse voltammetric techniques are introduced in Figure 2.11

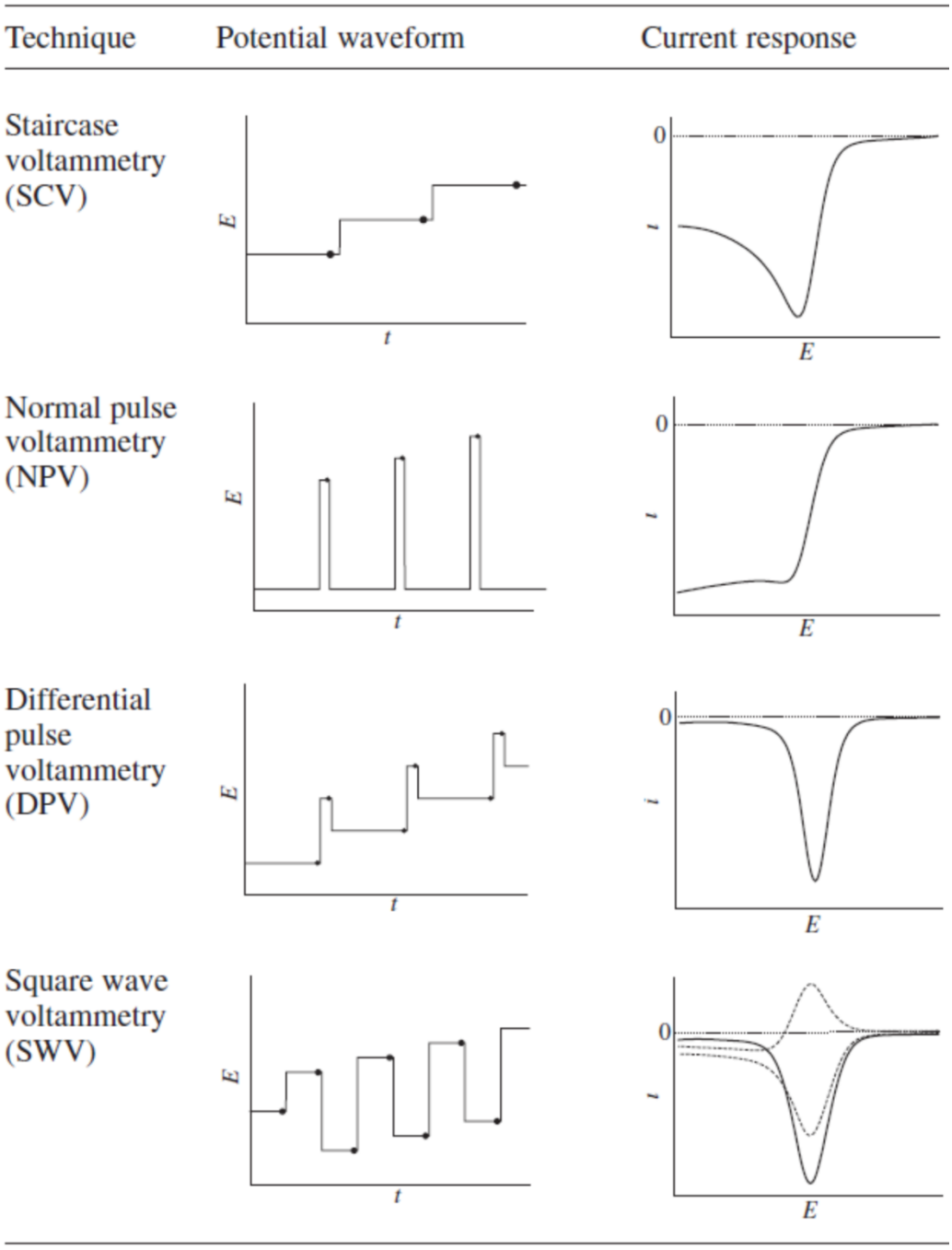

Figure 2.11 Most important pulse voltammetric techniques. The dot in potential waveforms indicate the time when the current is sampled. The current response (voltammogram) refers to the reduction of a reversible redox couple. Reproduced from Ref [24].

The current, in pulse voltammetric techniques is recorded at the end of the forward pulse just before each flank. In DPV and SWV, the currents are recorded at both forward and reverse pulses as a function of the applied staircase potential. The difference between the two currents is called the net current and it is larger than the two component parts. SWV can employ scan rates of 1 Vs^{-1} instead of sweep rates of 1-10 mVs^{-1} of DPV.[18] Thus an experiment by SWV requires much less time than by DPV.

In SWV, a square-wave cycle is superimposed on each staircase signal as is shown in the potential-time waveform at figure 2.12. The frequency of the signal f is the reverse of staircaise period: $f = 1/\tau$ whereas the duration of each pulse is the half of the staircase period: $t_p = \tau/2$. The magnitude of each pulse, E_{sw} which is square–wave amplitude. The height of the staircase waveform is called the potential increment ΔE. The difference between the currents measured on two pulses (forward and backward) of the same step is registered as net current: $I = I_f - I_b$

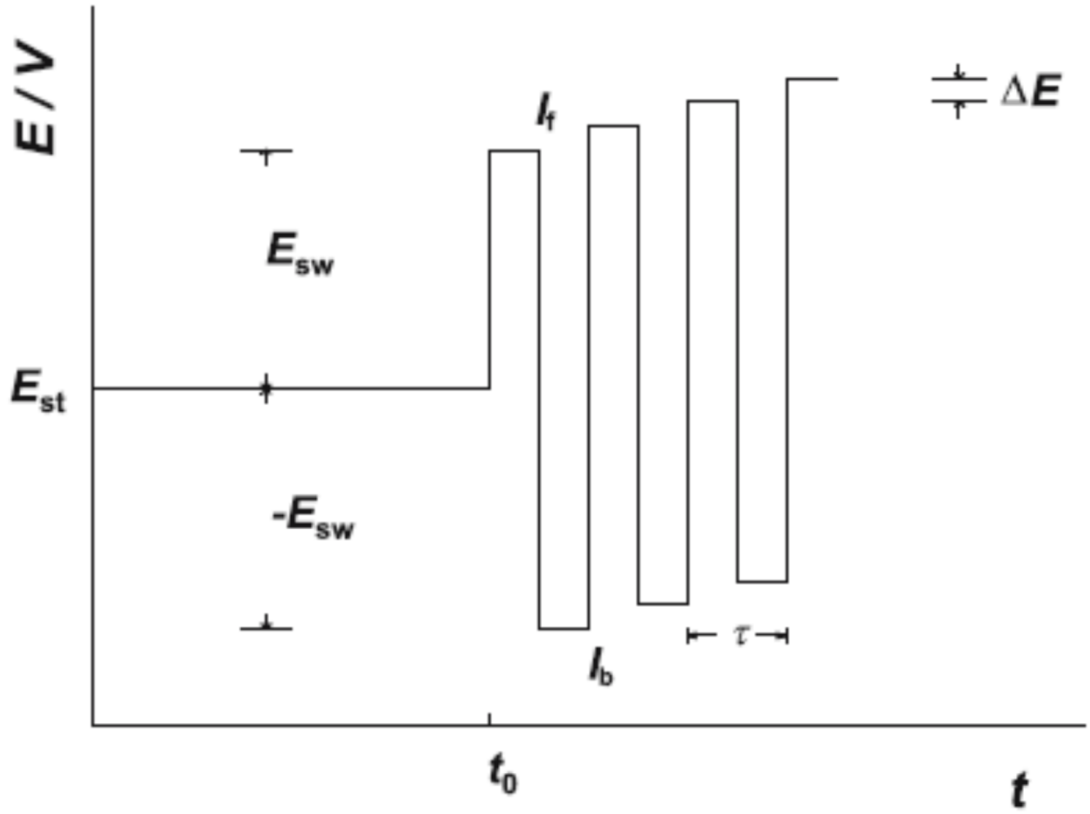

Figure 2.12 Potential-time waveform scheme in SWV. $\boldsymbol{E_{st}}$is the starting potential, $\boldsymbol{E_{sw}}$ is the square-wave amplitude, $\boldsymbol{\tau}$ is the staircase period, $\boldsymbol{\Delta E}$ is the potential increment, $\boldsymbol{I_f}$and $\boldsymbol{I_b}$ are the forward and backward currents respectively which are sampled at the end of each pulse. Reproduced from Ref [29].

The advantages of SWV are the very fast experiment time because of the fast scan rates that can be achieved (very fast reactions can be studied) and the high sensitivities because of the discrimination of the capacitive contributions.

2.9 QUANTIFICATION TECHNIQUES

The main purpose of this thesis is to develop novel electrochemical sensors and analytical protocols by using screen-printing technology to produce electrochemical configurations for the determination and online monitoring of target analytes in water samples with significant importance for the environmental or industrial water chemistry. The analytical signal of the voltammetric techniques that have been used is the peak current produced by the oxidation or reduction of either the target analyte (direct detection) or the product of the reaction of the target analyte with a specific mediator (indirect detection). The relation of the peak current and the concentration of the target analyte is investigated by using analytical quantification techniques such as calibration curve technique (or working curve technique) and multiple standard-addition technique.

A calibration curve is a plot that presents how the analytical signal (in this case the peak current) changes accordingly to the concentration of the target analyte. The plot is on a cartesian plane where the values on x-axis represent the concentration (X) and on y-axis the analytical signal (Y). A series of standard solution (containing known concentrations of the target analyte near to the unknown's expected concentration) is measured. The N measurements of each standard solution are depicted by N points (P_1,X_1), (P_2,X_2),…,(P_N, X_N). In order to use the calibration curve method the analytical signal and the concentration of the target analyte must have linear relationship. Theoretically, this is a fact in case of the peak current and the concentration of the electroactive species according to the Nernst equation we saw previously. The least number of measured points must be three ($N \geq 3$) for the general linear relationship:

$$P = aX + b \tag{2.33}$$

where the value a represent the sensitivity of the analytical method and b is a constant. The values a and b are determined using linear regression analysis and especially the method of

least squares after the rejection of the points plotted which obviously refrain from linear (usually because of experimental errors). As it is shown in figure 2.13 the value a is given by the slope of the calibration curve and the value b by the intersection of the calibration curve with the y-axis. Linearity is defined by the coefficient of determination denoted R^2. The R^2 value in statistics exhibits how close the measured points fit the calibration curve. It can range from 0 to 1 where the value 1 describes ideal linearity over the data range. The value of the coefficient determination in the range 0.960 to 0.999 would be sufficient in order to conclude that the analytical signal of the sensor is linear over the range of concentrations studied for the target analyte.

Another key parameter is the statistical limit of detection (LOD). (LOD) is the statistical determined minimum concentration of the target analyte, which corresponds to an analytical signal significantly different from the analytical signal of the blank. As shown in figure 2.13, $(LOD) = 3s_b/a$ where s_b is the standard deviation of the blank and a is the slope of the constructed calibration curve.[26] This approach to determine the (LOD) is common in the literature in order to benchmark an electrochemical system. Although a different estimation of the (LOD) is possible using this approach and many readers are directed towards.[30, 31] It is important to note that the (LOD) is a theoretical value and IUPAC make considerable efforts in order to completely clarify the definition of (LOD) which needs to be relatively simple as it is widely used.[26]

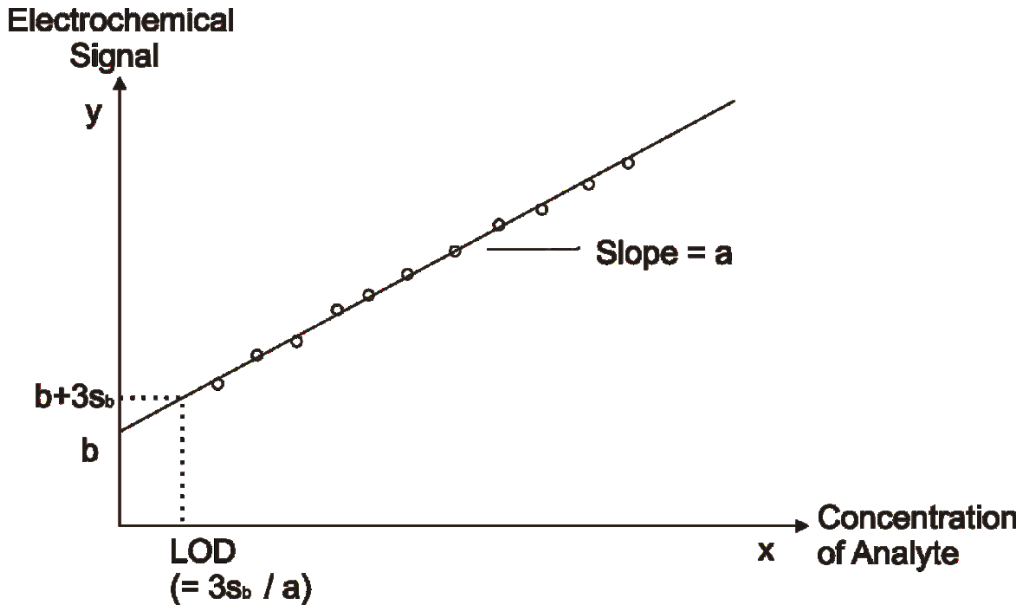

Figure 2.13 Typical calibration plot constructed for the determination of the theoretical limit of detection. Each point depicts a measurement of a standard solution.

Typically, LODs are reported in model systems/buffer solutions only. The analytical signal in 'real' samples depends on factors such as the presence of other substances (not the target analyte) which cannot be under experimental control. The presence of such substances can cause positive or negative errors upon the determination of the slope a as well as the constant b. This phenomenon is called the *matrix effect*. In order to overcome the matrix effect the standard solutions must have as much as possible the same composition with the measured samples regarding the substances that can affect the value of the analytical signal.

In the standard addition technique, unknown concentrations of the target analyte can be determined in a 'real' sample. The sample is placed in the electrochemical cell. If the sample is diluted, then the dilution coefficient must be taken into account when the unknown concentration is being determined. Known amounts of the target analyte are then added consecutively into the sample by adding small volumes of a dense standard solution of the target analyte in order that the volume of the final solution remains practically constant. In this case, *N + 1* measurement need to be performed. One measurement at the initial sample before the additions and *N* measurements after each consecutive addition; Figure 2.14 overviews this. The measurements refer to the equations: $P_0 = aX_{\text{unknown}}$, $P_1 = a(x_{\text{unknown}} + \Delta x_1)$, $P_2 = a(x_{\text{unknown}} + \Delta x_2)$, …, $P_N = a(x_{\text{unknown}} + \Delta x_{\text{N}})$. The values $\Delta x_1, \Delta x_2,.., \Delta x_N$ correspond to the standard additions where the amount of the analyte added each time is: Δx_1 , $(\Delta x_2 - \Delta x_1)$, $(\Delta x_3 - \Delta x_2 - \Delta x_1)$,…, $(\Delta x_N - \Delta x_{N-1} - \Delta x_{N-2} - \cdots - \Delta x_1)$. The system of the *N + 1* equation has only two unknown factors (a and x_{unknown}) and therefore is over defined. As a result, the unknown concentration of the target analyte at the initial sample can be well defined. A typical diagram for the graphical determination of the unknown concentration is shown in figure 2.14

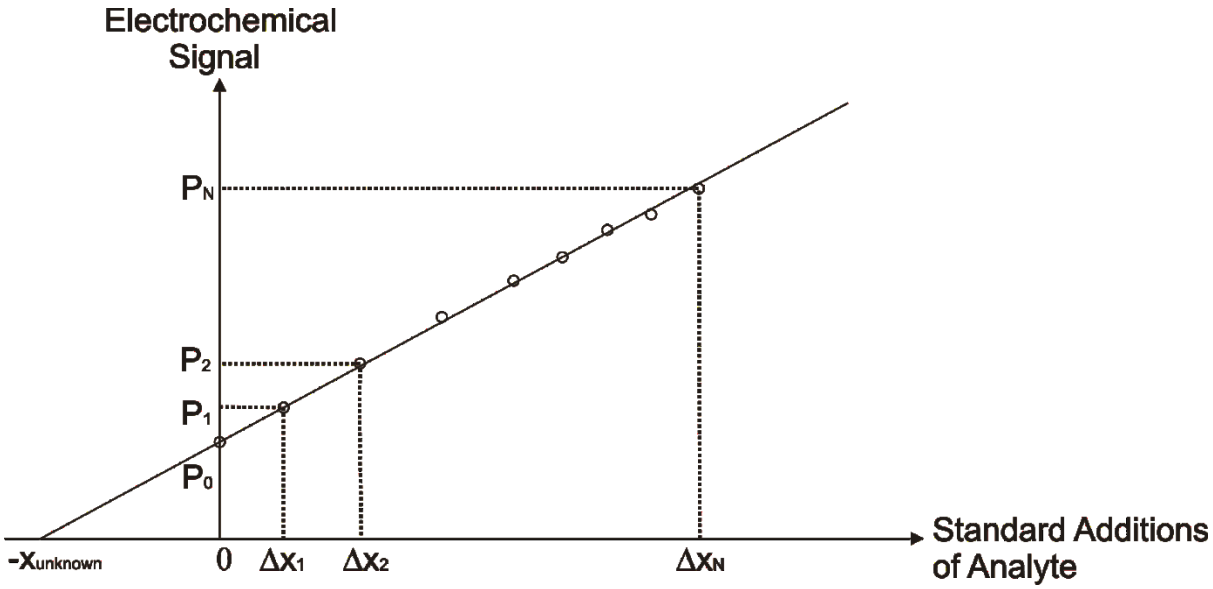

Figure 2.14 Typical diagram for the electrochemical detection of a target analyte by using the multiple standard method technique. Multiple standard consecutive additions are taking place. The initial unknown concentration of the target analyte is found on the intersection between the constructed line and the x-axis.

The point of each measurement are plotted and the straight line of best fit (least square method) used. The extension of the best fit line intersects the x-axis (at the part of negative values) to the point which corresponds (in absolute value) the unknown initial concentration of the target analyte x_{unknown}. In multiple standard addition technique, the matrix effect is overcome since the matrix of the solution practically remains the same.

CHAPTER 3

ELECTRODE MATERIALS AND THE SCREEN-PRINTING TECHNIQUE

The electrochemical processes within an electrochemical cell take place at the surface of the working electrode. Consequently, the material selected for use as a working electrode influences the performance of the voltammetric procedure. The working electrodes should provide high electrical conductivity, chemically inertness, low and stable background current, reproducible physical and chemical properties for the potential range of the studied redox systems. Finally, they must be low-cost fabricated and non-toxic.[19, 24] The materials of the working electrodes used as electronic conductors in electroanalysis are metals, various forms of carbon and in some cases, metal oxides and polymers.

The most popular metal electrodes involve noble metals (particularly gold and platinum) and the liquid metal, mercury. The high rate of electron transfer observed at metal electrodes surfaces when compared to traditionally carbon-based electrodes is their biggest advantage. Although the toxicity of mercury and the formation of surface oxides limit the conductivity of the electrode and can be mistaken for signals, are some of the reasons why metal electrodes are being considered second choice after that of carbon electrodes.[22]

Carbon-based electrodes are highly utilised in electroanalysis as they combine many properties of an ideal working electrode. They are characterised by large potential windows, chemically inertness, readily availability and low cost. Carbon materials that have been used for the fabrication of working electrodes include: graphite of spectral purity, boron-doped diamond (BDD), glassy-carbon (GC), pyrolitic graphite (PG), highly oriented pyrolytic graphite (HOPG), amorphous carbon, carbon black and carbon fibres each with different physicochemical properties.

Graphite-based screen-printed electrodes are widely used in this thesis. Screen-printed electrodes are the achievement of the implementation of the screen-printing technique for the fabrication of electrodes. The screen-printed derived electrodes are very low cost sensors and easily modified. They are disposable in nature and require small volume of sample (~microliters). Furthermore they have ease of use and portability for into the 'field' applications. These reasons establish screen-printed electrodes as a natural selection in electroanalytical applications over conventional (solid) carbon based electrodes.

3.1 METAL ELECTRODES

Various metal electrodes have been used as working electrodes in electroanalysis. Almost any metal electrode can be applied including platinum, gold, nickel, palladium and mercury with mercury gold and platinum the most commonly used. The metal electrodes can be in either bulk or thin-film form. The hydrogen evolution restricts the cathodic window for most of them such as platinum. Consequently, one must be cautious not to operate very close to the limits of the electrochemical window of the used combination of electrolyte solution and metal working electrode. Another undesired side effect is the formation and reduction of surface oxides which can alter the electrode reaction kinetics for certain redox systems resulting in problems with reproducibility of the electroanalytical measurement.[24] Nevertheless, metal electrodes can be utilised over a large anodic window exhibiting fast electrode-transfer kinetics for many redox systems. Mercury gold and platinum working electrodes applied into the field of water analysis are explored in this subchapter.

Mercury has been used extensively as electrode material because of its high hydrogen overvoltage which extends the cathodic window (compared to other metal electrodes).[19] The readily renewable high reproducible surface of the mercury working electrodes is another advantage which makes mercury a very attractive choice since 1920s with the discovery of dropping mercury electrode (DME)[32]. In the late 1950s the innovated construction of hanging mercury drop electrode (HDME) established mercury as the most promising electrode material. [33] The mercury film electrode is the third type of mercury electrodes, which are most frequently used. Nevertheless, the high toxicity of mercury has contributed to its unfavourable use as electrode material last decade.[34] Applications of mercury working electrodes in water quality are detailed in the following table (table 3.1).

Table 3.1 A list of various applications of the use of mercury electrodes utilised in water analysis through the use of voltammetric techniques.

Analyte	Matrix	Working Electrode	Technique	Limit of detection	Ref.
Mo(VI)	Mineral water	HMDE	CSV	0.2 pg mL^{-1}	35
As(III), As(V)	Natural water	HMDE	DPCSV	0.5 μgL^{-1}	36
Pb(II)	Natural water	HDME	CSV	$1.2x10^{-8}M$	37
Co(II) and Ni(II)	Seawater	HDME	CSV	6 pM and 0.45 nM	38
Co(II)	Seawater, Tap water, Mineral water	HDME	CSV	0.02 μgL^{-1}	39
Mo(VI)	Natural water	HDME	CSV	$1x10^{-8}M$	40
Fe(II) and Fe(III)	seawater	HDME	CSV	$6x10^{-10}M$	41
Al(III)	Seawater and freshwater	HDME	CSV	30 ngL^{-1}	42
Cu(II), Cd(II), Pb(II)	Seawater	HDME	DPCSV	0.24 nM, 0.12 nM and 0.3 nM	43
Ti(IV)	Sea, river and rain waters	HDME	CSV	$7x10^{-10}$ M	44, 45
V(V)	Seawater	HDME	CSV	0.3nM	46
Total dissolved iodine	Seawater, freshwater and brackish water	HDME	SWV	0.1 nM	47

While a wide choice of solid metal electrode are available for use in electroanalysis, gold and platinum are the most commonly used. The gold and platinum electrodes usually come as short wires or disc electrodes (stationary or rotating).[48] As mentioned before for metal solid electrodes, both gold and platinum electrodes exhibit very favourable electron transfer kinetics and a large anodic potential range. On the other hand, their limited cathodic

potential range compared to mercury because of the low hydrogen overvoltage in aqueous solution (depending on the pH, between -0.2 and -0.5V) limits their applications in water analysis.[19] Both gold and platinum electrodes undergo oxide film formation at anodic potentials, which can slow down the electron transfer of the analytical reaction or react with the analyte minimizing reproducibility. [49] The contribution of these difficulties is less in non-aqueous media, where metal solid electrodes are often an ideal choice.[48] Unlike mercury electrodes, metal solid electrodes present a heterogeneous surface. For that reason, the use of such electrodes requires precise electrode polishing and pre-treatment in order to increase reproducibility and achieve as rapid electron transfer kinetics as possible. The mechanical polishing should be under ultraclean conditions using deagglomerated alumina powders (ranging from 0.05 to 1 μm) as a fine sludge in ultra-pure water.[22] Except for mechanical polishing, which is the most commonly used mode of solid electrode preparation, alternatives such as heat treatment, electrochemical polarisation and solvent cleaning are used on occasion.[18] Metallic electrodes can be modified either electrochemically or chemically and many analytical applications can benefit from this. Recent applications of gold and platinum working electrodes used in water analysis with voltammetric techniques are presented in the next Table (Table 3.2).

Table 3.2 A list of various applications of gold and platinum electrodes utilised towards the analysis of analytes in water samples through the use of voltammetric techniques.

Analyte	Matrix	Working Electrode	Technique	Limit of detection	Ref
As(III) and Sb(III)	Seawater	GE	ASV	Below 0.1 nM	50
Total iron	Tap and marine water	ω-Thio nitrilotriacetic chemically modified GE	DPCSV	30 ngL^{-1}	51
Sulfide	Seawater and Hydrothermal samples	GE	SCP	58 nM	52
As(V)	Seawater	Manganese coated GE	ASV	0.2 nM	53
Mercury (II)	Tap, River and waste water	Thiophenol functionalized single-walled carbon nanotubes modified GE	SWASV	3 nM	54
Pb(II)	Natural waters	ω-mercapto alkyl/aryl sulfonates modified GE	ASV	0.4 μgL^{-1}	55
Cu(II)	River water	meso-2,3-dimercaptosuccinic acid modified GE	CV	1.29 $\mu g\ L^{-1}$	56
Nitrate	Seawater	electrodeposited silver nanoparticles modified GE	CV	10 μM	57
Diquat (herbicide)	River water	Platinum Electrode modified with natural phosphate	SWV	5.32nM	58
Pb(II)	River water	Platinum electrode modified with hydroxyapatite	SWV	20nM	59

3.2 CARBON-BASED ELECTRODES

Carbon is the most widely utilised electrode material in electroanalytical chemistry and it is available in a large variety of structures: graphite, glassy carbon (GC), amorphous carbon, diamond, carbon nanotube and carbon fiber, each with different electrochemical properties.

Carbon atom can form many allotropes due to its electron configuration: $(1s)^2(2s)^2(2p)^2$. The small energy difference between the s-orbital and the three p-orbitals of the outer shell enables the excitation of an electron from the 2s-state into the 2p-state. This results in the formation of hybrid orbitals sp, sp^2 and sp^3 with regard to the combination of the 2s-orbital with one, two or all the three 2p-orbitals. Among the allotropic forms of carbon its crystalline structures of diamond and graphite are widely used electrode materials. At the diamond crystal, the carbon atoms arranged in a tetrahedral configuration with sp^3-hybridised covalent bonding between them. Graphite has an hexagonal structure where the carbon atoms in a trigonal configuration of sp^2-hybrised bonding.[24] Graphite is comprised of a series of parallel graphene layers, termed basal-planes. Unlike the covalent bonding of the atoms in the same layer, parallel layers are hold together by weak van der Waals forces. These weak interactions between the graphene layers make graphite a good lubricant.

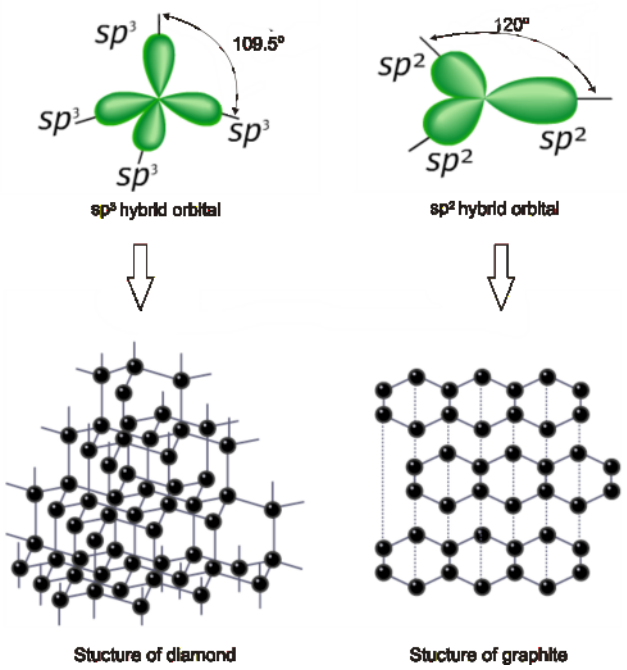

Figure 3.1 Diamond and graphite structures derived from the sp^3 and sp^2 hybridisation orbitals of the carbon atoms respectively.

Graphite crystals can exist in different microstructures. This is according to the stacking of the basal planes which can be in an hexagonal or rhombohedral structures as shown in figure 3.2.

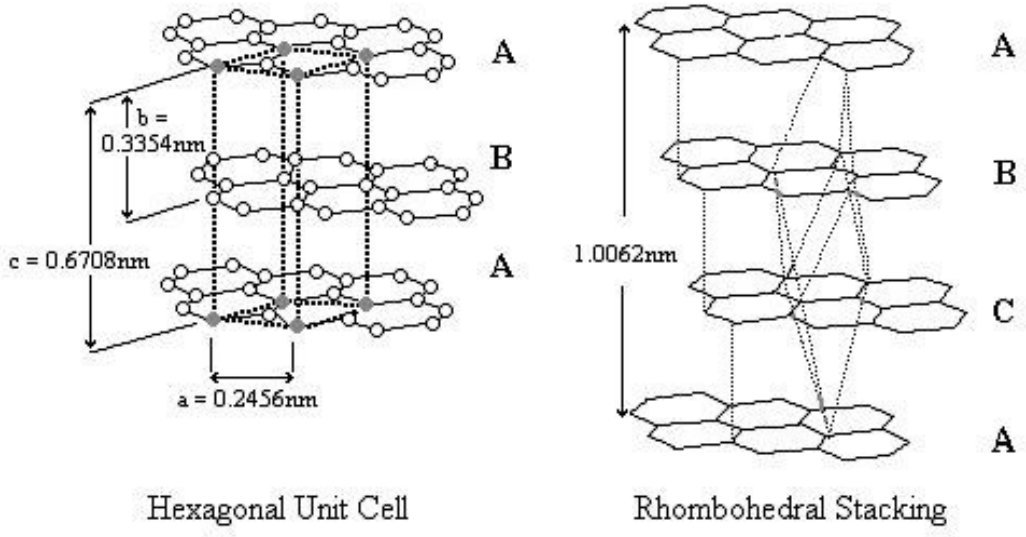

Figure 3.2 Hexagonal and rhombohedral graphite stacking arrangements. Reproduced from ref [60]

The most commonly found arrangement is hexagonal (or alpha or Bernal stacking) where the first sheet is exactly on top of the third sheet (-ABA- sequence). The rhombohedral structure which is thermodynamically less stable and can convert to the hexagonal structure after heat treatment (1300^{o}C) displays a –ABCA- sequence. In this case the first basal layer is superimposed by the forth one. There is difference between the two structures in the distance of the two 'A' basal layers, ca. 0.6708 and 1.0062 nm for hexagonal and rhombohedral stacking, respectively.

According to the orientation of the basal layer, it has two faces (zig-zag and arm-chair) as shown in figure 3.3. These two formations display different electron conductivities.

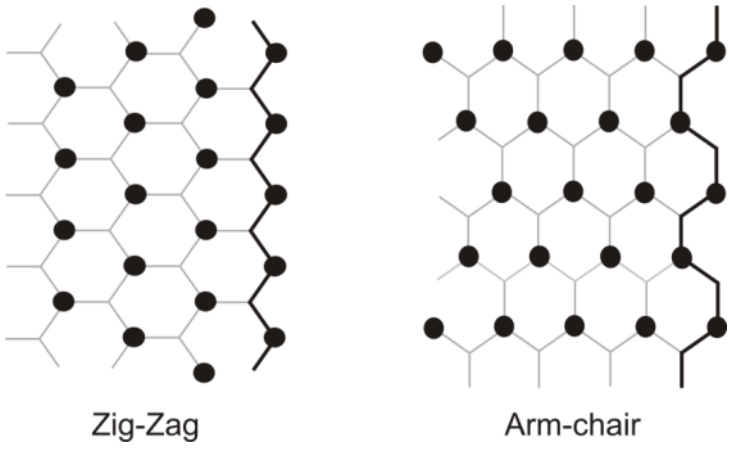

Figure 3.3 Schematic of a zig-zag and arm-chairs basal layer configurations.

Additionally to the basal-plane is what researchers call 'edge-plane' and is formed through the outer sites on the perimeter of the basal-plane layers of the graphite. The surface energies of the basal and edge-plane sites are reported to be 0.11 J/m^2 and 5 J/m^2 respectively. This significant difference contributes to the faster reaction rate of the edge-plane and should be taken into account during the construction of a graphite electrode. Thus edge-plane and basal-plane pyrolytic graphite electrodes (EPPG and BPPG respectively) are fashioned from high ordered pyrolytic graphite (HOPG).

3.2.1 BORON-DOPED DIAMOND ELECTRODE

Due to its structure which has been described previously, diamond presents unusual material properties such as the high hardness (1 x 10^4 kg mm^{-2}), high thermal conductivity (2600 W m^{-1} K^{-1}) and high charge carrier mobilities (electron mobility: 2200 cm^2 V^{-1} s^{-1}, hole mobility: 1600 cm^2 V^{-1} s^{-1}).[61]

The energy required to excite an electron from its bound state to a free state where it can take part in conduction is very high for diamond (5.5 eV)[62]. In terms of band theory, diamond presents large band-gap which is the difference of the energy between the 'valence band' (occupied by electrons sp^3-sp^3 bonding orbitals for diamond) and the 'conduction band' (empty sp^3-sp^3 anti-bonding orbitals for diamond). The large band-gap implies no electrical conductivity for un-doped diamond which normally cannot be used as an electrode material.[61] In order to increase the electrical conductivity, diamond has been doped by certain elements like boron, phosphorus and nitrogen.[63] Boron is the most widely used dopant to produce doped-diamond electrodes because of its low charge carrier activation energy 0.37 eV.[64] The addition of boron atoms in the regular diamond's crystal lattice (doping) can be achieved by chemical vapour deposition technologies (CVD) or by ion implantation through high pressure, high temperature (HPHT) doped-diamond particle production.[61, 63]

Boron-doped diamond electrode exhibits very high overpotential for both hydrogen and oxygen evolution.[65, 66] This contributes to a wide potential window in aqueous solutions (up to 3V)[67] which is one of the largest potential window in aqueous solutions so far measured.[61] This combining with the low background currents and great stability in different media establish Boron-Doped Diamond Electrode (BDDE) a useful working electrode in applications such as water treatment[64-66] and water analysis. Recent applications of BDDE as working electrode in water analysis using voltammetric techniques are presented in Table 3.3.

Table 3.3 Recent applications of BDDE utilised in the analysis of water samples through the use of voltammetric techniques.

Analyte	Matrix	Working Electrode	Technique	Limit of detection	Ref.
Atrazine (pesticide)	River water	BDDE	SWV	10 nM	[68]
Picloram (herbicide)	Tap and natural water	BDDE	CV and DPV	70 nM	[69]
Mn(II)	Seawater	BDDE	CSV	9 nM	[70]
Pb(II)	Drinking water	BDDE	ASV	2 nM	[71]
Benzo[a]pyrene (PAH's)	Tap water	BDDE	CV	0.72 μgL^{-1}	[72]
Chemical Oxugen Demand (COD)	Wastewater	BDDE with Ultrasound	CA	192 μgL^{-1}	[73]
Pentachlorophenol	River water	BDDE	SWV	15.5 μgL^{-1}	[74]
Cd(II) and Pb(II)	River water	BDDE	SWV	1-50 μgL^{-1}	[75]
Carbaryl (insecticide)	River water	BDDE	SWV	10 μgL^{-1}	[76]
Methylparaben	River water	BDDE	SWV	103 μgL^{-1}	[77]
Total inorganic arsenic	Wastewater	Au-coated BDDE	DPASV	0.01 μgL^{-1}	[78]
2,4,6-trinitrotoluene	Seawater	BDDE	SWV	25 μgL^{-1}	[79]
Carbendazim and Fenamiphos (pesticides)	River water	BDDE	SWV	9 μgL^{-1}	[80]

3.2.2 GLASSY-CARBON ELECTRODE

Glassy carbon (GC) or vitreous carbon is the most widely used carbon-based electrode for electroanalysis.[24, 81] It is manufactured by slow carbonization of a pre-modeled polymeric resin (phenol-formaldehyde or polyacrylonitrile) at temperature range from 300 ^{0}C to 1200 ^{0}C in order to remove the oxygen, nitrogen and hydrogen.[19, 24, 29] The structure of glassy carbon consists of thin, tangled ribbons of cross-linked graphite-like sheets.[19] Unlike other carbon-based electrodes it is essentially pore-less and consequently impermeable to

liquids and gases.[24] It exhibits lower thermal and electrical conductivity.[82] Recent applications of glassy-carbon electrodes in water analysis using voltammetric techniques are shown in Table 3.4.

Table 3.4 Recent applications of GCE utilised in the analysis of water samples through the use of voltammetric techniques.

Analyte	Matrix	Working Electrode	Technique	Limit of detection	Ref
Cd(II)	Tap lake and sea water	Sulfisoxazole modified GC	CV	0.033 nM	83
Fenitrithion (pesticide)	Tap water	GC	SWV	78 μM	84
Propanil and Monalide (pesticides)	River lake and tap water	Nickel oxide modified GC	DPV	0.05 and 0.21 μM	85
Catechol, Resorcinol and Hydroquinone	River, lake and sanitary wastewater	Graphene–chitosan composite film modified GC	DPV	750 nM	86
Reactive Red 231 (dye)	River water	GC	DPV	10 μM	87
Paraquat (Herbicide)	River water	Dihexadecylhydrogenphosphate modified GC	SWV	10 nM	88
4-Chlorophenol	River, lake and tap water	multi-wall carbon nanotubes and nano nickel hydroxide modified GC	DPV	0.5 μM	89
Phenol	Tap water	3,3'-diaminobenzidine (DAB) modified GC	CV	10 nM	90
Bisphenol A	Commercial Mineral water	functionalized single-walled carbon nanotubes and poly(3,4-ethylenedioxythiophene) modified GC	CV	0.03 μM	91
Butylparaben preservative)	River water	multi-wall carbon nanotubes modified GC	ASV	20 nM	92

Cu(II)	Tap and lake water	amino-functionalized mesoporous silica modified GC	ASV	0.9 μgL^{-1}	93
Nitrite	Well water	Gold nanoparticles decorated on cobalt porphyrin-modified GC	DPV	60 nM	94
Total iron	Tap and mineral water	chitosan-modified GC	CSV	20 μgL^{-1}	95
Pb(II)	Tap water	Etodolac modified GC	SWASV	0.167 nM	96

3.3 SCREEN-PRINTED ELECTRODES

The main thrust of this thesis deals with the implementation of the screen-printing technique for the fabrication of screen-printed electrodes suitable for water analysis. Consequently, the rest of this chapter is concerned with the introduction of screen-printing technology and the overview of recent literature utilising screen-printed electrodes as sensors for the water quality.

The origin of screen-printing technology as an advanced form of stencilling dates as far back as 30,000 B.C when negative prints of the human hand have been found as stencilling examples in Paleolithic cave paintings.[97] Stencils are reported to be used by the Egyptians and Greeks at 2500 B.C. in order to decorate tombs and paint murals.[97, 98] In China at 500 A.D. stencilling reported to be used for the reproduction of Buddha's images while at the same time Japanese culture used stencilling to decorate bulk amounts of fabric.[97] The evolution from stencilling to the modern day techniques of screen-printing related to work of Englishman Samuel Simon who patented a fabric printing system based on a wooden frame and a brush which made the printing operation across the stencil drawn onto bolting cloth.[97, 98] In 1920 Albert Kosloff proposed screen-printing on paper by using a rubber-bladed squeeze in order to push the ink through the stencil which was supported by a wooden frame.[98] A major breakthrough was achieved in 1940 when the first photographic stencil was developed.[99] The screen-printing techniques used today are governed by the same principle of these early systems. The evolution of the equipment used in screen-printing contributes to the

increment of its application. The fabrication of screen-printed electrodes constitutes one such newly developed application.

Some remarkable advantages of the screen-printed electrodes over the conventional carbon based electrodes are due to the flexibility of the screen-printing process in terms of design and fabrication of the electrodes. The measurement of multiple analytes in one single sample can be realized by unique screen-printed designs. Electro-catalysts can be either deposited upon the screen-printed sensor or incorporated into its bulk. The advantages of using screen-printed sensors lead to the expectation that many more applications of either unmodified 'as-is' or modified (through novel modification) screen-printed sensors will arise.

3.3.1 SCREEN-PRINTED SENSOR FABRICATION

Screen-printing is a general method for the deposition of patterned coatings onto flat surfaces.[100] Screen-printing involves the spread of a thixotropic fluid by squeezing through a gauze or mesh screen onto a surface beneath. The thixotropic fluid can be ink or other viscous compound and in case of the screen-printed electrode it contains substances including graphite, carbon black, solvents and polymeric binder.[16] The design of the mesh screen defines the shape and size of the electrode, which is printed onto the desired surface of controlled pattern and thickness.

The utilisation of commercial machines for the fabrication of screen-printed sensors is a common practice. The screen-printing machines contribute to the improvement of repeatability of the printing process allowing the mass production of standardized sensors.

Figure 3.4 shows a schematic representation of screen-printing process for manufacturing of electrodes. The substrate (on which the electrode is to be printed) is located just below the screen in a way in order to ensure that the ink will be deposited in the desired position. Above the screen the ink is applied and squeegee sweeps across at a controlled velocity forcing the ink through the defined open areas in the screen onto the substrate.[101] Once the squeegee passes the screen (the mesh) peels away, leaving the ink on the substrate. The ink (thixotropic liquid) stays on the substrate because of its higher (to a certain extent) surface tension with the rough surface of the substrate rather than with the smooth wires of the screen (mesh).[101] This screen-printing process is an off-contact process in which the screen mesh is separated from the substrate by a small specified distance. In this case, substrate and screen mesh come in contact only under the pressure of the squeegee and they

snap back after this action. Contact screen-printing process is used when a solid metal stencil (which cannot be stretched) is utilized to print solder paste.[101] The off-contact process is exclusively used for the fabrication of screen-printed sensors.

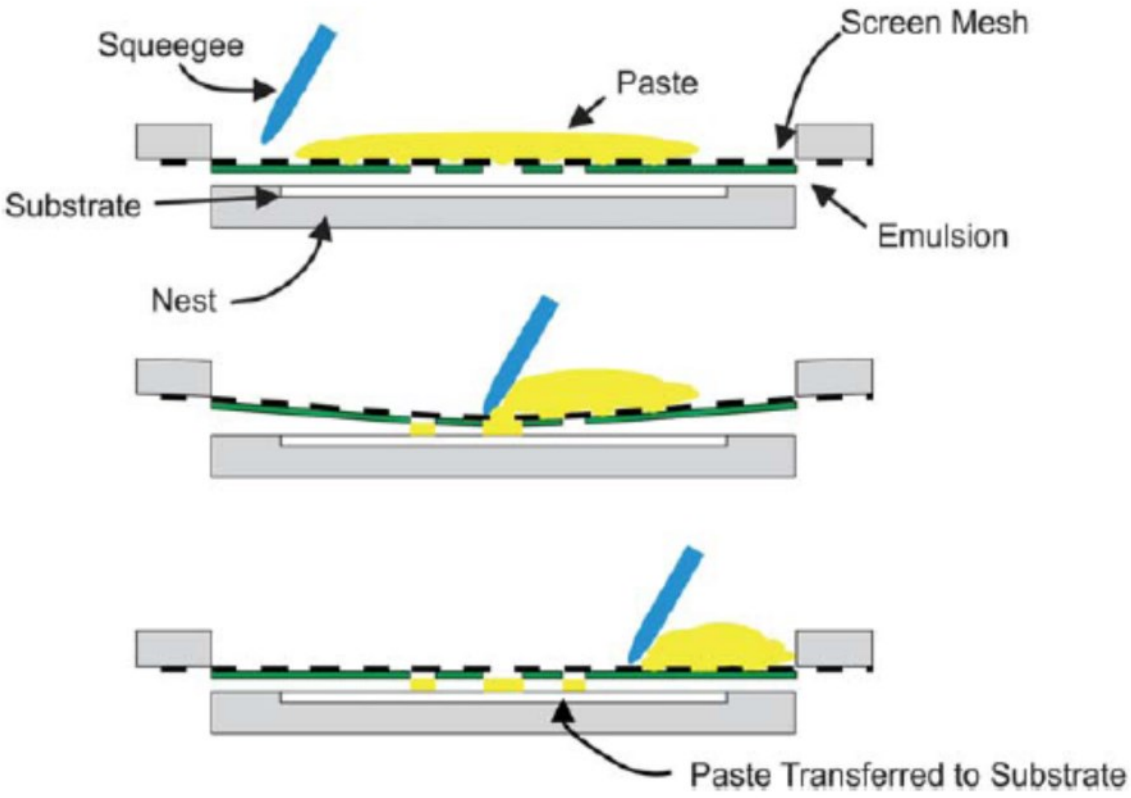

Figure 3.4 Cross-sectional representation of the basic screen-printing process for the manufacturing of electrochemical sensors. Figure reproduced from reference[16]

The current requirements for more reproducible screen-printed electrodes with intricate designs call for the optimisation of the screen-printing process. Paramount importance for this thrust is the careful consideration and selection of technical aspects such as the substrate, screen-mesh, inks and squeegee.

Many substrate materials in different thickness and size suitable for screen-printed electrodes have been reported such as Polyester[102-106], Polyvinyl Chloride [107-110], Polyimide[111, 112] Alumina[113-115], ceramic[116-118], paper (cellulose)[119], Polyethylene terephthalate (PET) foil[120] and textile[121] . Among the plethora of materials used for fabrication of electrochemical sensors, Polyester and Polyvinyl Chloride are the most popular for fabrication of electroanalytical sensors. In this thesis polyester is the substrate material used for the fabrication of SPEs.

The selection of the appropriate screen and particular the screen-mesh is a critical aspect for consideration. The screen usually consists of a frame upon which a woven mesh is stretched. The mesh material must be precisely woven, flexible, smooth, inert to various solvents and chemicals and economic.[122] The most common mesh materials are polyester, nylon and stainless steel. Polyester is flexible the most resilient with long lifetime and can be used onto uneven surfaces. Nylon is the most elastic of the three materials but it cannot be used with high viscosity inks due to its low resilience. Stainless steel exhibits good control of ink deposition producing high standards of line definition but it cannot be used on uneven surfaces because of its poor flexibility.[122] Apart from the material, the size and density and the orientation of the threads (comprising the screen-mesh) as long as the open area (%) of the mesh must be of consideration in order to ensure that the printed deposit will be uniform and reproducible.

As has been eluded to, the squeegee constitutes a technical aspect for consideration. A squeegee is basically a flexible blade whose function is to forces ink through the mesh onto the substrate.[122] A squeegee's material must be resistant to solvents and inks used. Neoprene and especially polyurethane are the most common used materials.[122] Shape and contact angle (with the mesh) are important parameters. In this thesis for the fabrication of the screen-printed sensors, a Polyurethane blade with contact angle at 60^0 has been utilised.

The most critical parameter of the screen-printing process is considered to be the printing medium. For screen-printed electrodes ink and paste are mainly used as printing mediums. Even if paste is characterised by higher viscosity, the words ink and paste are generally (including this thesis) used interchangeably. All inks consist of four ingredients: 1) an active element which determines the electrical properties of the printed film, 2) an adhesive element which provides the adhesion property on the substrate, 3) an organic binder which gives the ink the desired fluid characteristics for screen-printing and additionally keeps the active and adhesive elements in suspension and 4) a solvent or thinner which decrease the viscosity of the very thick organic binder in order to permit screen-printing (solvent together with the organic binder are referred to as vehicle).[123, 124] According to the active element used the ink can be classified as conductive or dielectric. Conductive ink made from conductive active elements such as carbon, silver, platinum, gold, palladium or metal alloys and it forms the conductive track of the screen-printed sensors. Dielectric ink is made from polymer or ceramic powders and forms the insulating layer of the screen-printed sensors.[124] The immobilization of the ink onto the substrate is very important and comes through a curing

process which involves thermal curing or ultraviolet radiation.[124] Adhesion elements used are glass frit, metal oxides or both depending on the desired adhesion mechanism.[123] Ethyl cellulose and various acrylics are the most commonly used organic binders. Typical materials used as solvents or thinners are terpineol, butyl carbitol and some complex alcohols.[123]

Schematic representation of the in-house fabricated screen-printed carbon electrode mainly used in this thesis is shown in figure 3.5. The sensor involves all the three necessary electrodes required for its use in voltammetric techniques. In this case the working and the counter electrode are carbon based whereas the reference electrode is a Ag/AgCl electrode. The four layers printed on the substrate require four different screen-meshes and three different inks.

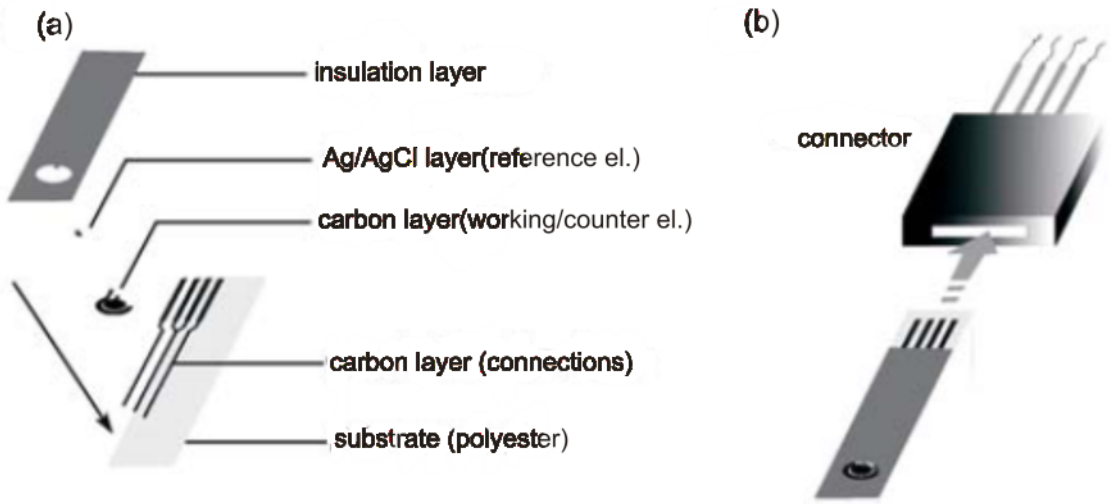

Figure 3.5 (a) Schematic representation of the screen-printed three electrode configuration (four screen-printed layers). (b) connector used for the electrical connection of the sensor with the potentiostat. Figure reproduced from reference[125]

Scanning Electrode Microscope (SEM) images of an unmodified screen-printed graphite electrode (the working electrode) are shown in figure 3.6.

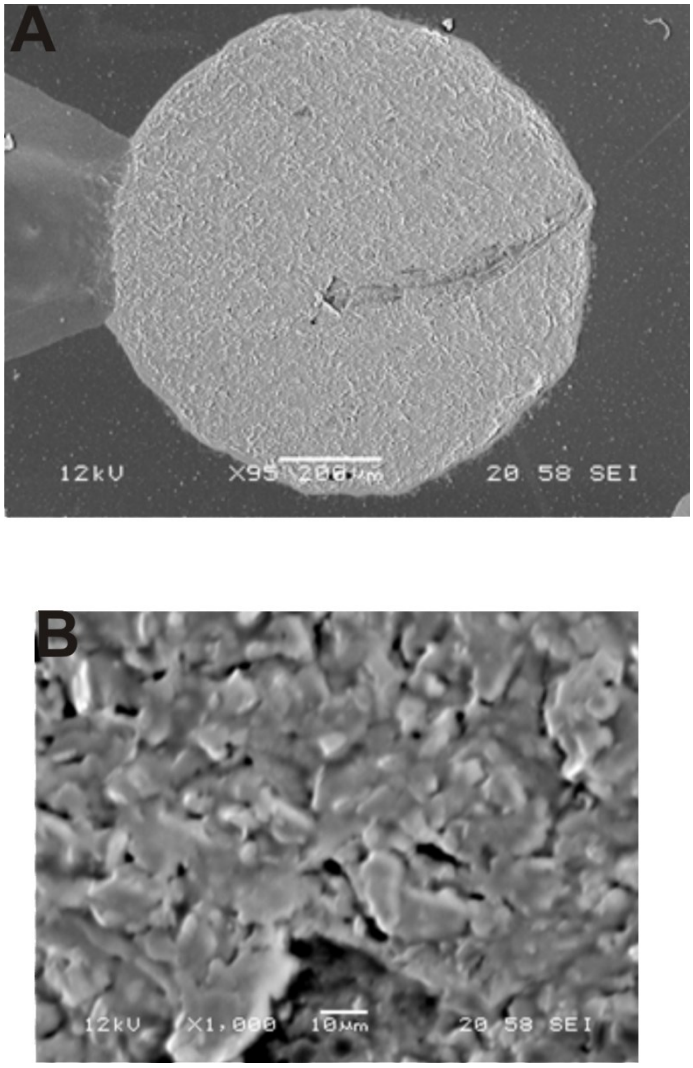

Figure 3.6 Scanning Electrode Microscope (SEM) images of a screen-printed graphite electrode (A) the graphite working electrode with diameter 1 mm and (B) the working electrode magnified 20 times.

3.3.2 FUNDAMENTALS OF SCREEN-PRINTED ELECTROANALYTICAL SENSORS

The urgent interest in economical, specific and real time techniques suited to water-monitoring applications push the boundaries of screen-printing technique for increasingly sensitive and 'all in one' sensors with intuitive designs. This has resulted the increased

interest for the fundamental understanding of the electrochemical reactivity at the screen-printed sensors which has been rarely studied.[9] Additionally various ways of modification of screen-printed electrochemical sensors with plethora of materials has been reported with a view to increasing either their sensitivity or their specification. Advantageous sensor designs have been investigated so as to improve the mass transport of the target analyte.

The electron-transfer reactivity and consequently the analytical performance of the screen-printed graphite sensors is reported to be strongly influenced by the exact ink formulation and the printing and curing conditions.[105, 126] Notable work by Choudhry *et al*. has shown how various concentrations of the polymeric binder within the ink can affect the electrode morphology. It is demonstrated that as the concentration of the polymer binder within the ink increases the heterogeneous electron-transfer rate constant decreases.[127] Work by Šljukić *et al.* has shown that performance of macro screen-printed electrode can be improved through the use of power ultrasound.[128] Ultrasound insonation was demonstrated to remove electrode's surface active species and increase the mass transport of analyte. The removal of the active species from the electrode surface eliminates the surface passivation during the electroanalytical measurement keeping the electrode 'active'. Novel work from Davies *et al.* contributed to the understanding of the individual roles of the edge-plane and basal-plane regions in the electrochemical response of a graphite surface. They displayed that at basal-plane highly ordered pyrolytic graphite electrodes the edge-plane sites are responsible for the voltammetric response, with the basal plane being effectively inert.[129]

In order to change the electrochemical properties or to improve selectivity and sensitivity in an analytical determination the working electrode can be modified.[130] Electroanalytical applications of modified metal, boron-doped diamond and glassy-carbon electrodes were presented previously. The screen-printed carbon electrodes as well as carbon paste electrodes can be modified not only at their surfaces but also in the whole bulk (interior).[131] The modification can be classified as *intrinsic* and *extrinsic modification* depending on whether the functional groups of the conductive components of the ink are modified or the modifier added to the material as a plus component.[131]

An example of intrinsic modification is pre-anodization of screen-printed carbon electrodes which involves the application of highly positive potential to the working electrode in order to oxidize the surface of the carbon particles containing in the ink.[9, 131] Pre-anodization contributes to the improvement of the electron transfer with the analyte. Applications of pre-anodized screen-printed electrodes has been reported for the detection of

dopamine in the presence of high concentration of ascorbic acid[132] and for the electrocatalytic oxidation of phenols.[133]

Extrinsic modification can be classified further by the way the reagents (modifiers) are placed in the screen-printed carbon electrode at surface and bulk modification. At the surface modification the modifier is placed on the surface of the electrode in thin layers, films or membranes whereas at the bulk modification the modifier is placed directly in the ink and thus the whole electrode material is modified.[131] Modifiers used in order to improve the electroanalytical performance of the screen-printed electrodes are metal oxides such as copper oxide, nickel oxide, ruthenium oxide, manganese oxide and most commonly bismuth oxide for many analytical applications. Many target analytes which are not electroactive cannot be detected directly unless an electro-catalyst mediator is used for their indirect determination. Plethora of mediators such as Prussian Blue, crown ethers, nickel hexacyanoferrate, cobalt phthalocyaninde have been successfully incorporated into the ink[9] and much more (even enzymes) have been used as surface modifiers at screen-printed carbon electrodes. (Applications of modified screen-printed electrodes in water analysis are presented in section 2.3.3)

Most of the applications with screen-printed electroanalytical sensors based on the use of macro-sized working electrodes where planar diffusion dominates mass transport. However micro-sized electrodes where the diffusion layer thickness is of the same dimension as the diameter of the working electrode exhibit a non-planar diffusion layer (edge or radial diffusion). When radial diffusion becomes dominant the mass transport and consequently the current density increases.[22]

Since a platinum microdisk working electrode was introduced by Davies and Brink[134] for the detection of oxygen in animal tissues several uses of microelectrodes have been reported.[135] Despite the high current density microelectrodes exhibits the current response of a single microdisc electrode is small resulting in a narrowing range of electroanalytical applications. This disadvantage has been overcome by the fabrication of microbands or arrays of non-interacting microelectrodes.[136] Microelectrode arrays are usually fabricated by photolithography or laser ablation with high fabrication costs resulting the prohibition of their mass production.[105] The notable work of Kadara *et al.* [104] for fabrication of flexible and disposable microelectrodes using solely screen-printing contributed to the decrease of the manufacturing cost of the screen-printed microelectrodes. Applications of these low cost screen-printed carbon electrodes for the detection of Manganese (II) has been reported.[105]

Nevertheless this approach is limited by the dielectric which produces shallow recessed microelectrodes.[105] The development of versatile and screen-printed microelectrodes, which combine the advantages of screen-printing technique and the improvement mass transport microelectrodes exhibits, is very promising for further applications in water analysis.

3.3.3 SCREEN-PRINTED SENSORS FOR WATER ANALYSIS

Electrochemical sensors have employed disposable and portable screen-printed electrodes for water monitoring such as heavy metals and organic compounds detection as well as for water quality tests in drinking water, environmental and industrial samples. Selected and recently developed sensors for heavy metal detection for metalloids, non-metals detection including common water quality tests and for organic compounds determination are listed in the Tables 2.5-2.7 respectively. The heavy metals analysis is a great challenge for scientists due to their major impact toward human health and the environment. The development of fast, simple, portable and low cost analytical methods for the heavy metals has been object of investigation for decades and therefore plethora of applications of electrochemical sensors for the detection of heavy metals have been reported so far. Recent developments of electrochemical sensors based on screen-printed working electrodes for heavy metals detection within environmental aqueous samples using voltammetric techniques are listed in Table 3.5.

Table 3.5. Recent applications of screen-printed electrodes for heavy metal detection utilised in water analysis through the use of voltammetric techniques.

Analyte	Matrix	Working Electrode	Technique	Limit of detection	Ref
Hg(II)	Rain, river and industrial waste water	Gold nanoparticles-modified SPCE	SWASV	0.8 μgL^{-1}	137
Pb(II), Cd(II)	Seawater	plasticizer mixed with mercury acetate modified SPCE	SWASV	1.8 and 2.9 μgL^{-1}	138
Vanadium	Tap water	Gold-nanoparticles and alkaline phosphatase modified SPCE	CA	4 μM	139

Hg(II)	Ambient water	Screen-Printed Gold Electrode (SPGE)	SWASV	1.1 μgL^{-1}	140
Pd(II), Pt(II), Rh(II)	River water	Bismuth film modified SPCE	DPASV	0.008 μgL^{-1}, 0.006 μgL^{-1} and 0.005 μgL^{-1}.	141
Pb(II)	Drinking, river and ground water	Functionalized mesoporous silica nanoparticles modified SPCE	SWASV	0.1 μgL^{-1}	142
Tl(I)	Lake water	Bismuth precursor compounds modified SPCE	ASV	1 μgL^{-1}	143
Pb(II)	River water	Calixarene modified SPCE	DPASV	5 μgL^{-1}	144
Cr(VI)	Drinking water	Multi-walled carbon nanotubes/quercetin modified SPE	DPV	0.3 µM	145
Pb(II)	Surface water	SPCE	SWASV	5 μgL^{-1}	146
Cu(II)	Tap and Estuarine water	4-carboxyphenyl modified SPCE	ASV	5 nM	147
U(VI)	Tap and Estuarine water	4-carboxyphenyl modified SPCE	CSV	0.7 nM	148
Cd(II) and Pb(II)	Rainwater	SPCE	DPV	100 nM and 500 nM	149
Pb(II) and Cd(II)	Mineral water	Antimony and Tin SPE	ASV	0.9 μgL^{-1} and 1.8 μgL^{-1}	150

The replacement of commonly used methods for monitoring pH, dissolved oxygen and biochemical oxygen demand by disposable screen-printed electrodes has attracted major attention. Recent applications of screen-printed electroanalytical sensors for these physical elements of analyses along with the detection of metalloids such as arsenic ions and non-metals with great ecological impact such as forms of nitrogen and phosphorus occurred in nature are listed in Table 3.6.

Table 3.6. Recent applications of screen-printed electrodes for water quality tests along with metalloid and non-metal detection in water analysis through the use of electroanalytical techniques.

Analyte	Matrix	Working Electrode	Technique	Limit of detection	Ref
Hydroxide ions	Aqueous solutions	Nickel oxide bulk modified SPCE	CV and CA	23 μM	151
pH	Aqueous solutions	Phenanthraquinone modified SPCE	CV	1-13	152
pH	Rock CO_x pore water.	CeO_2-based oxides SPE	Potentiometry	5.5-13.2	153
pH	Aqueous solutions	Nitrosophenyl modified SPCE	CV and SWV	1-14	154
Dissolved oxygen	Ground water and Tap water	Copper-plated SPCE	Amperometry	1 mgL^{-1}	155
Biochemical Oxygen Demand (BOD)	Aqueous solutions	CdS modified SPCE	ECL	20 ppb in Dissolved Oxygen	156
Sulfide	Wastewater	Coprinus cinereus peroxidase modified SPCE	CV and CA	0.3 μM	157
NADH and Nitrite	Aqueous solutions	Screen-printed graphite microband electrodes	CV	0.48 μM and 0.05μM	158
Nitrite	Tap water	Poly(3,4-ethylenedioxythiophene) modified SPCE	CV	1.72 μM	159
Nitrite	Rainwater	Amine-functionalised polystyrene latex beads self-assembled on polyaniline modified SPCE	Amperometry	7.4 μM	160

Nitrite	Aqueous solutions	Manganese dioxide SPCE	CV	2.5 μM	161
Nitrate and Nitrite	Tap water and mineral water	Dispersion of carbon black modified SPCE	DPV	65 nM	162
Phosphates	Pond water samples	Cobalt phthalocyanine modified SPCE	CA	62 μgL^{-1}	163
As(III)	Tap water	Platinum nanoparticle modified SPCE	CV	5.68 μgL^{-1}	164
As(III)	Tap water	Acetylcholinesterase modified SPCE	CA	11 nM	165
As(III)	Canal water	Gold nanoparticle modified SPCE	ASV	3 μgL^{-1}	166
As(III)	Ground and surface water	Gold modified SPCE	SIASV	0.5 μgL^{-1}	167

Many organic compounds with broadly industrial and agricultural use exhibit negative impact toward the human health and the environment. For that reason, the detection of such organic compounds in environmental and industrial samples is highly desirable to meet the corresponding electroanalytical challenges. Recent applications of screen-printed electrodes for detections of phenolic compounds, pesticides, herbicides and polycyclic aromatic hydrocarbons (PAHs) are listed in Table 3.7.

Table 3.7. Recently developed screen-printed sensors for the detection of organic compounds of environmental interest.

Analyte	**Matrix**	**Working Electrode**	**Technique**	**Limit of detection**	**Ref**
Carbamate and Organophosphorous pesticides	Wastewater and River water	Co-phthalocyanine and Prussian Blue-modified SPCE	Amperometry	24 μgL^{-1} and 0.5 μgL^{-1}	168

Hydroquinone and Catechol	Tap water	Prussian Blue modified SPCE	DPV	0.12 μM and 0.43 μM	169
Phenol	River water	Surface-immobilized gold nanoparticles (and tyrosinase modified SPCE	SWV	47 μgL^{-1}	170
Aminophenol isomers	River water	SPCE	NPV	0.05-0.16 μM	171
Organophosphorous pesticides	Seawater	Acetylcholinesterase modified SPCE	CA	4-7 μgL^{-1}	172
Paraoxon Carbofuran (pesticides)	Tap water	Cholinesterase modified SPCE	CA	0.165 μgL^{-1} and 0.047 μgL^{-1}	173
Phenol	Synthetic seawater	Pseudomonas putida cells modified SPCE	CA	0.1 μM	174
Phenanthrene (Polycyclic Aromatic Hydrocarbons, PAHs)	River and Tap water	Phenanthrene-9-carboxaldehyde and alkaline phosphatase modified SPCE	CA	5 and 6.3 μgL^{-1}	175
Paraoxon (Organophosphorous insecticide)	Drinking water	Mono-enzymatic acetylcholinesterase modified SPAuE	CA	2 μgL^{-1}	176
Catechol and chlorpyrifos (pesticide)	Tap and River water	Iridium oxide nanoparticles and tyrosinase modified SPCE	CA	0.08 μM and 0.003 μM	177
Bisphenol A	Lake and Fresh water	Poly(3,4-ethylenedioxythiophene) and poly(styrene sulfonate) modified SPCE	CA	19 nM	178

CHAPTER 4

EXPERIMENTAL METHODS

This chapter covers generic experimental methods used throughout this thesis. It focuses on the description of the electrodes that have been used and especially the fabrication of the screen-printed carbon-based sensors with which this thesis is mainly concerned. Additionally this chapter reports common characteristics of reagents, solvents, equipment and methodologies that are utilised in this thesis. In the following chapters the particular methodological differences are highlighted.

Screen-printed carbon-based electrodes (denoted as SPGEs) are three electrode configurations which had a geometric working electrode area of 3 mm diameter, Ag/AgCl reference and carbon counter electrodes. They were fabricated in-house with appropriate stencil designs using a microDEK 1760RS screen-printing machine (DEK, Weymouth, UK). Note that this screen-printed electrode design has been previously reported[166, 179-182] "as is" without electrode pre-treatment or modification in various electroanalytical endeavours. For fabrication of the SPGEs, first a carbon ink formulation (Product Code: C2000802P2; Gwent Electronic Materials Ltd, UK) utilised for the efficient connection of all three electrodes and the electrode material for both the working and counter electrodes was screen-printed onto a polyester (Autostat, 250 micron thickness) flexible film. The carbon ink layer was cured in a fan oven at 60 degrees for 30 minutes. Next a silver/silver chloride reference electrode was included by screen-printing Ag/AgCl paste (Product Code: C2040308P2; Gwent Electronic Materials Ltd, UK) onto the polyester substrates which was subsequently cured once more in a fan oven at 60 degrees for 30 minutes. Finally, a dielectric paste (Product Code: D2070423P5; Gwent Electronic Materials Ltd, UK) was then printed onto the polyester substrate to cover the connections and define the active electrode areas including that of the working electrode (3 mm diameter). After curing at 60 degrees for 30 minutes the SPGEs are ready to be used. These electrodes have been characterised electrochemically in a prior paper and have heterogeneous rate constants of 1.08×10^{-3} cm s^{-1}.[183] No pre-treatment of the electrode surface; chemically or electrochemically was carried out prior to measurements. Figure 4.1 depicts typical scanning electron microscope images of the graphite working electrode surface demonstrating the electrodes uniform structure, with graphitic flakes evident upon the surface.

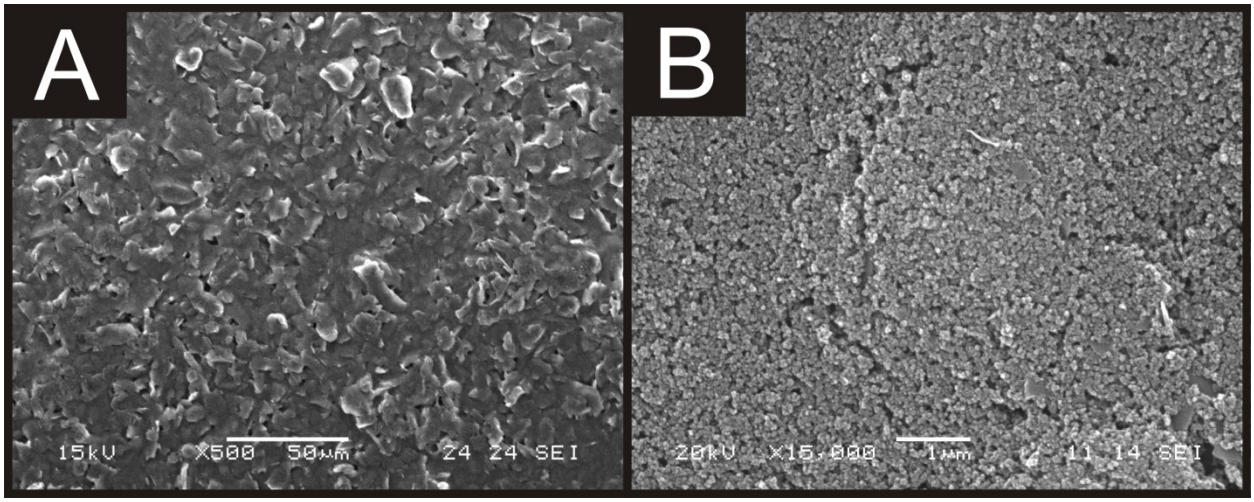

Figure 4.1 Typical SEM images depicting the graphite working electrode surface of the SPGE at magnifications of x 500 (A) and x 15000 (B).

A glassy-carbon electrode (GCE) (3 mm diameter, BAS, USA) a boron-doped diamond electrode (BDDE) (3 mm diameter, BAS, USA) and a gold electrode (AuE) (1 mm diameter, BAS, USA) were also utilised with a platinum wire counter and a Saturated Calomel Electrode (SCE) as the reference electrode completing the circuit. The BDDE, GCE and AuE were all thoroughly cleaned and polished with 1 micron and 0.25 micron-sized diamond sprays prior to use.

Voltammetric measurements were carried out using μ AUTOLAB Type III potentistat by Metrohm Autolab B.V. The pre-concentration step during the anodic stripping voltammetry at subchapters 5.1 and 5.2 by using screen-printed raphite electrodes was carried out without stirring the solution.

The limits of detection (LOD) are theoretical values as have been described in subchapter 2.9. In cases where dilution of the real water samples has been made, the level of dilution has been taken into account and consequently the limits of detection refer to the real water samples unless otherwise stated. The limits of quantification (LOQ) are the starting values of the linear ranges mentioned each time unless otherwise stated.

All chemicals used were obtained by Sigma Aldrich unless otherwise stated. Deionised water of resistivity 18.2 MΩ cm was used for the preparation of all solutions. All glassware was washed in 15.8 M nitric acid prior to use. All solutions were thoroughly degassed using nitrogen gas prior to analysis.

The next chapter considers some novel electroanalytical methods for the detection of antimony and selenium as well as organic compounds such as chlorophenols in drinking water.

CHAPTER 5

ELECTROANALYSIS IN DRINKING WATER

This chapter considers the development of novel sensors for electroanalysis in drinking water. The first examples of electroanalytical sensing of selenium (IV) and antimony (II) utilising screen printed graphite electrodes are exhibited in subchapters 5.1 and 5.2 respectively. In subchapter 5.3 the direct and the proposed indirect electroanalytical detection of Phenol and three chlorophenols is examined by using boron-doped diamond electrode.

EXPERIMENTAL

The drinking water utilised was obtained using the laboratory drinking water tap which was ran for a minute before a sample being obtained. The sample was stored at room temperature and used within a day of sampling. In subchapter 5.1 the drinking water was simply modified to pH 1.02 (that of the $HCLO_4$). In subchapter 5.2 the drinking water sample was modified to pH 3.5 using acetic acid (pH 2.8). Finally in case of subchapter 5.3 the drinking water sample was modified to pH 10 using sodium hydroxide. In all three cases the modified drinking water sample spiked to a concentration of 0.1 M potassium chloride, acting as an electrolyte before electroanalytical measurements were commenced.

5.1 ELECTROANALYTICAL SENSING OF SELENIUM (IV) UTILISING SCREEN-PRINTED GRAPHITE MACRO ELECTRODES

5.1.1 ABSTRACT

The electroanalytical determination of selenium (IV) via anodic stripping voltammetry is shown to be possible for the first time using screen-printed graphite electrodes. The deposition potential and time was optimised allowing a linear range from 10 to 1000 μg L^{-1} in 0.1 mol L^{-1} $HClO_4$ to be realised with a limit of detection (3σ) found to correspond to 4.9 μg L^{-1}. Utilising these screen-printed graphite electrodes, the detection of selenium (IV) in drinking (tap) water is shown to be feasible allowing a detection limit (3σ)

of 19.2 μg L^{-1} (taking into account the level of dilution by adding perchloric acid) to be realised which is below the levels set by the United States Environmental Protection Agency. Such an approach suggests the possibility of a disposable screening tool for selenium (IV) in drinking water samples.

5.1.2 INTRODUCTION

Selenium is a trace element present in environmental and biological systems and whilst being a highly essential micronutrient for all animals, including humans at trace levels, selenium can be extremely toxic if the intake dose exceeds 400 μg per day; the need for a simple methodology for its monitoring within relevant samples is clearly evident.[184-187]

Within the environment, selenium exists in several oxidation states (VI, IV, 0, −II) with selenium (IV) by far the most toxic.[188] Guidelines for the levels of selenium within drinking water sources have been outlined by the European Union and the United States Environmental Protection Agency (EPA) with maximum concentrations of 10 μg L^{-1} and 50 μg L^{-1} being suggested respectively.[189-192] Continuous flow hydride generation atomic fluorescence spectrometry,[193] Inductively Coupled Plasma Atomic Emission Spectroscopy (ICP-AES)[194] and ICP-Mass Spectroscopy[195, 196] are just some of the many analytical methods that have been proposed for the determination of selenium (IV) in trace levels. Additionally, electrochemical methods such as stripping voltammetric techniques for selenium (IV) detection in food samples,[197] atmospheric precipitates[198] and within natural water sources[199] have been reported.

Electrochemical methods of determination are particularly attractive due to their potentially low cost nature and key ability to allow for 'in-field' analysis through the ease of portability. One particular type of electrochemical sensors which epitomises the advantages offered via electrochemistry is the screen-printed sensor. Screen-printing can produce economical one-shot disposable sensors which can be used for the rapid, sensitive and portable analysis of many target analytes in a plethora of areas.[200] Further to this the art of screen-printing allows further miniaturisation of electrochemical sensors which, in addition to allowing facile development of 'in-field' sensors as described, allows sample sizes to be dramatically reduced with low-microlitre range volumes being viable. In such instances electrode materials including mercury[198], gold[201], platinum, bismuth film[199], silver[202] ceramic composite[203] have been utilised. Table 5.1 gives a thorough overview of reported

electrochemical methodologies for the detection of selenium; from inspection of Table 5.1 it is evident that screen-printed graphite sensors are yet to be realised for this analytical target, with only one such application reported by Wang *et al.,* using gold film modified carbon-based screen-printed sensors.[204]

Consequently, the anodic stripping voltammetry of selenium (IV) using graphite screen-printed sensors in $HClO_4$ is reported for the first time to be feasible in drinking water samples at levels relevant to the United States Environmental Protection Agency.

Table 5.1 A summary of electrochemical reports towards the detection of selenium (IV).

Electrode Configuration	**Linear Range**	**Limit of Detection**	**Additional Comments**	**Reference**
Gold disc	5 – 15 µM	1.2 µM	The effect of common interferents; lead, copper nickel and zinc is observed.	[205]
Gold microband array	0.1 – 10 µM	25 nM		
Hanging copper amalgam drop	Up to 50 µM	0.25 nM	Interefence from different metals and surfactants is observed.	[188]
Mercury film coated glassy-carbon	Up to 50 μgL^{-1}	0.1 μgL^{-1}	Detection within biological and environmental samples (water, horse kidney and mussel).	[206]
Hanging mercury drop electrode	1.2 – 75 μgL^{-1}	α	Detection within different milk samples.	[207]
Hanging mercury drop electrode	0.02 – 6 µM	α	Detection within garlic samples.	[208]
Gold	0.5 – 291 ngL^{-1}	α	Electrodes made from recordable compact discs.	[209]

Mercury film coated glassy carbon	5 – 50 ng/mL	0.37 ng/mL	The effect of bovine albumin is studies. Sea water samples are also analysed.	[210]
Mercury film coated glassy carbon	10 – 60 μgL^{-1}	0.4 μgL^{-1}	The effect of common interferents; lead, copper and iron is observed.	[211]
Hanging mercury drop electrode	0.04 – 0.4 µg/mL	α	Detection within tea leaf samples.	[212]
Gold	5 – 100 ng/mL	α	N/A	[213]
Bismuth coated glassy-carbon	2 – 30 μgL^{-1}	0.1 μgL^{-1}	Detection within multivitamins and human hair.	[214]
Rotating gold disc	α	0.04 μgL^{-1}	The effect of common interferents; lead, copper and mercury is observed.	[215]

α = Information not disclosed

The detection of selenium (IV) is known to be possible via anodic stripping voltammetry[213, 216-218] and consequently the effect of the deposition potential on the voltammetric peak height of the anodic stripping peak was first studied using the screen-printed graphite electrodes (denoted throughout as SPGEs), through applying different deposition potentials and quantitatively monitoring the resulting linear sweep voltammograms each time. The solution consisted of 10 mg L^{-1} selenium (IV) in 0.1 mol L^{-1} $HClO_4$ (pH 1.02) with the deposition time fixed at 100 seconds with the initial potential at 0.0 V; perchloric acid was chosen due to recent reports.[205] Figure 5.1 shows a plot of the stripping peak height as a function of the applied deposition potential where the peak height at potentials from 0.0 V to - 0.4 V is negligible. At potentials more cathodic than -0.4 V the peak height increases steeply until -0.8 V, after this point, the peak diminishes; consequently, a deposition potential of -0.6 V was selected for use within the consequential analysis. The electrochemical reduction of selenium (IV) in acidic solution is known to depend upon the applied voltammetric potential and is complex.[205, 219]

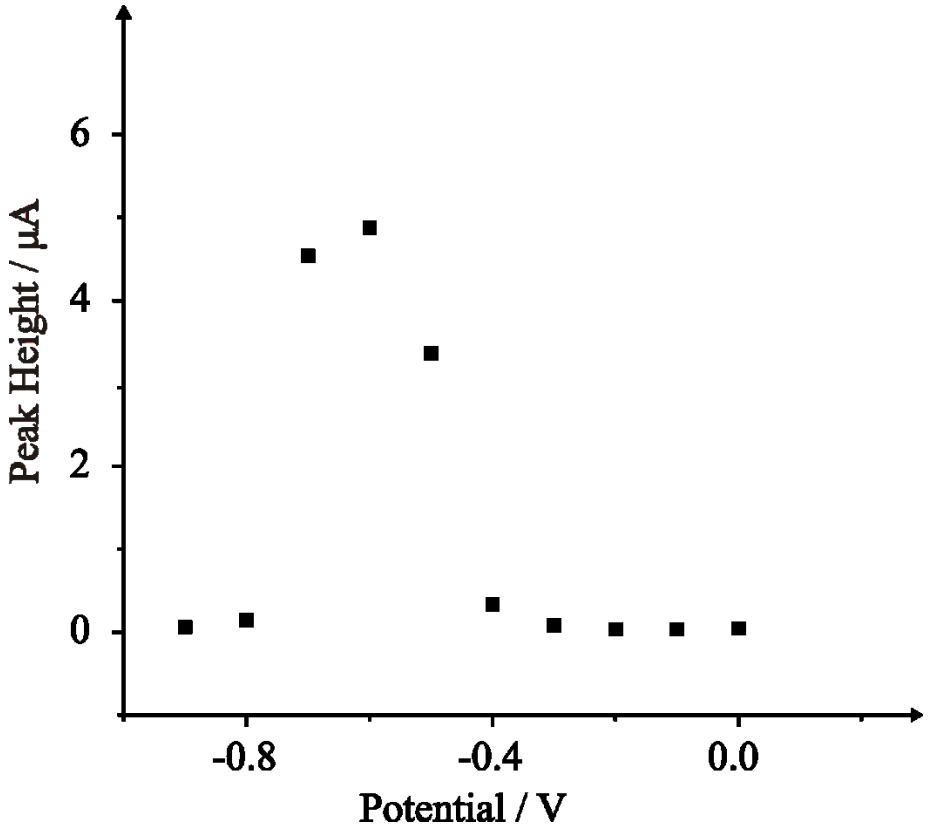

Figure 5.1 The effect of deposition potential upon the observed voltammetric peak height for the sensing of 10 mg L^{-1} selenium (IV) in 0.1 mol L^{-1} $HClO_4$ with a deposition time of 100 seconds using a SPGE. Scan rate: 50 mVs^{-1}.

Selenium (IV) is of greatest interest to electrochemists as it is the only form of selenium which is electroactive. In acidic media, the reduction of selenium (IV) is proposed to follow two different pathways determined by the potential applied during electrochemical analysis as described by equations 3.1 and 3.2:[205, 219-222]

$$H_2SeO_3 + 4H^+ + 4e^- \rightarrow Se + 3H_2O \quad (3.1)$$

$$H_2SeO_3 + 6H^+ + 6e^- \rightarrow H_2Se + 3H_2O \quad (3.2)$$

It has been suggested that the reaction proposed within equation 3.2 arises as a direct result of equation 3.1, which is then followed by a further reduction of selenium (0) to selenium (II) through equation 3.3:[219]

$$Se + 2H^+ + 2e^- \rightarrow H_2Se \quad (3.3)$$

When high potentials (typically between 0.0 V and +0.4 V, depending on the reference electrode utilised) are selected for the reduction reaction, equation 3.1 is adhered to.[220, 222] Alternatively, at more electronegative potentials the formation of H_2Se is common as the reactions described within equations 3.2 and 3.3 occur more readily. Further to this, selenium hydride is known to undergo a co-proportionation reaction in acidic media whilst in the presence of selenous acid, leading to the production of so-called red selenium as explained in equation 3.4:[209, 222]

$$H_2SeO_3 + 2H_2Se \rightarrow 3Se + 3H_2O \quad (3.4)$$

Arguably the most critical parameter when attaining electrochemical measurement using the method of anodic stripping voltammetry (ASV) is the deposition time as it can not only dictate the sensitivity of the measurement, but length of the analytical protocol. In light of this, Figure 5.2 demonstrates the effect of deposition time upon the voltammetric peak height resulting from measurement of selenium (IV) at a fixed concentration of 10 mg L^{-1} in 0.1 mol L^{-1} $HClO_4$ and a fixed deposition potential of -0.6 V utilising the SPGE. Evidently, a greater voltammetric peak height is observed with increasing deposition time with no plateau arising as is typical in anodic stripping voltammetry. In order to avoid a reduction in the practicality of the electrochemical methodology through having a lengthy analytical protocol, a deposition time of 300 seconds was chosen.

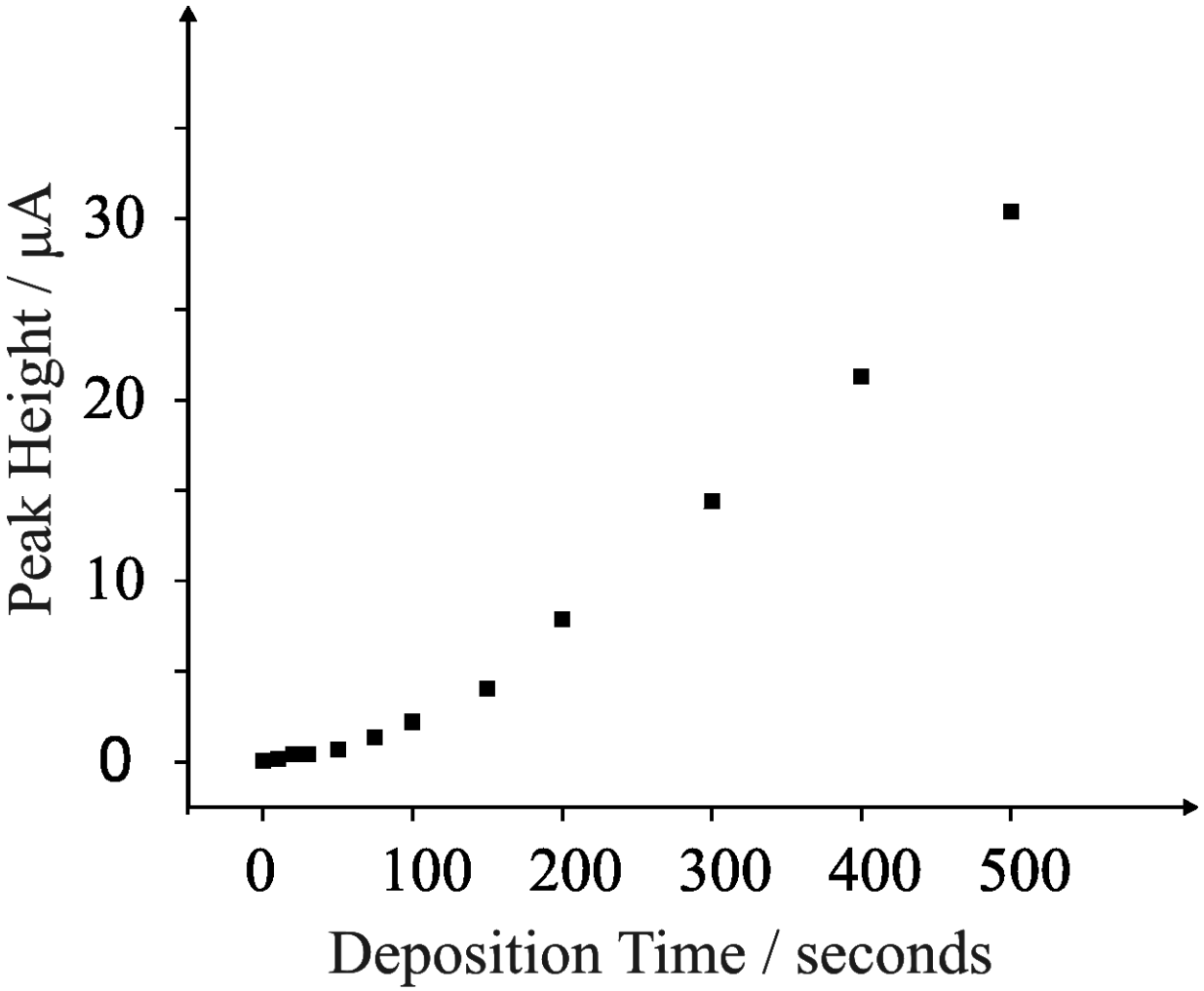

Figure 5.2 The effect of deposition time upon the voltammetric peak height response for 10 mg L^{-1} selenium (IV) in 0.1 mol L^{-1} $HClO_4$ using an SPGE. Deposition potential: -0.6 V. Scan rate: 50 mVs^{-1}.

Next, attention was turned to exploring the electroanalytical response of the SPGEs. Figure 5.3 shows the linear sweep voltammetric response over a range of selenium (IV) additions over the range of 10 to 300 µg L^{-1} in 0.1 mol L^{-1} $HClO_4$ utilising a single SPGE.

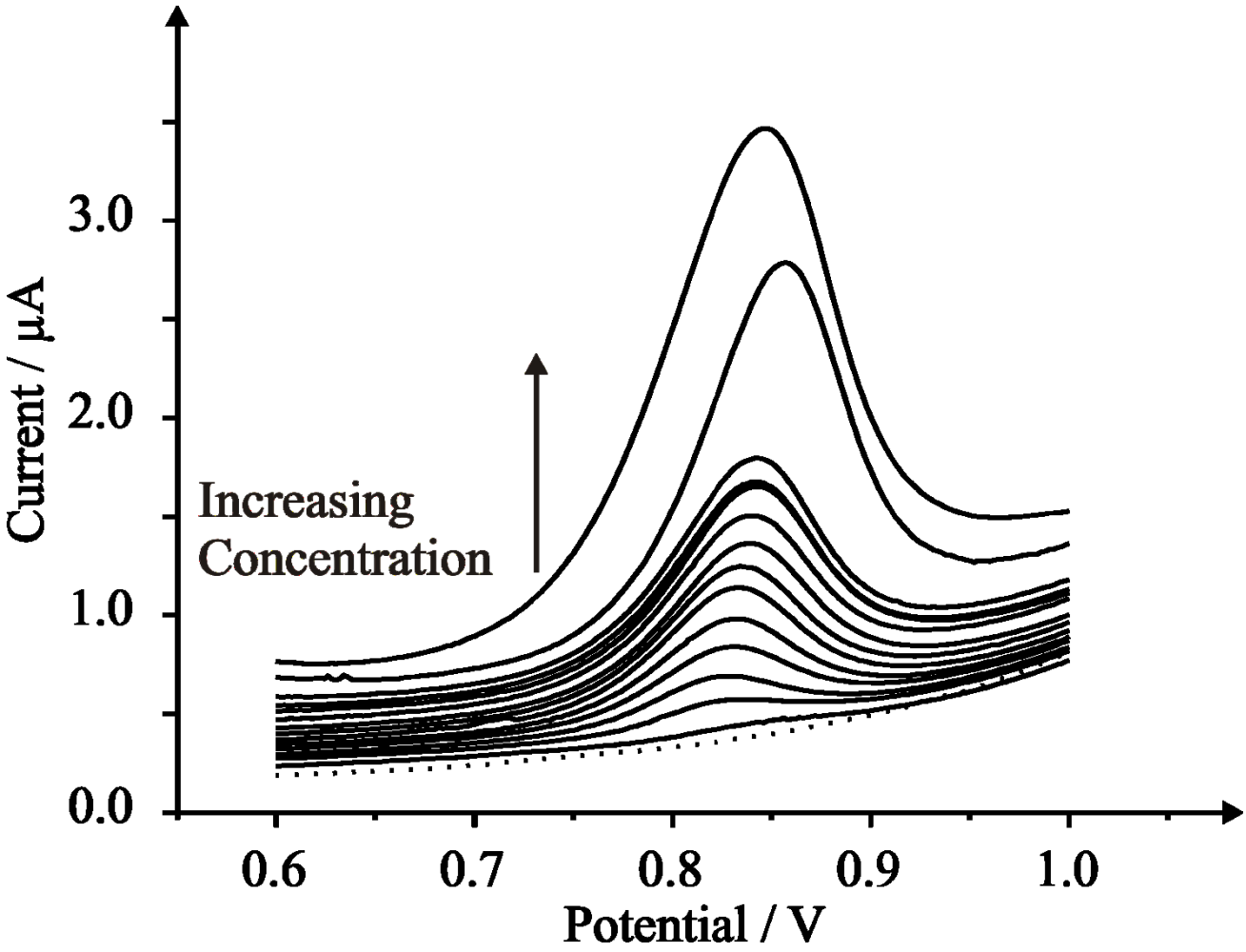

Figure 5.3 Linear sweep voltammetric response of a single SPGE upon additions of selenium (IV) (10 – 300 µg L^{-1}) in to 0.1 mol L^{-1} $HClO_4$. Deposition potential: -0.6 V; Deposition time 300 seconds. Dotted line: without selenium (blank). Scan rate: 50 mVs^{-1}.

It is apparent that using the same electrode over the entire concentration range allows for a good linear relationship ($I_P/\mu A = 8.2$ x 10^{-3} $\mu A/\mu g L^{-1} - 5.6$ x 10^{-3} μA; $R^2 = 0.99$) as depicted in Figure 5.4 between the concentration of selenium (IV) and the resultant peak height (µA). Furthermore, the theoretical limit of detection (3σ) for selenium (IV) when utilising a single SPGE for each concentration was determined to be 5.3 µg L^{-1}.

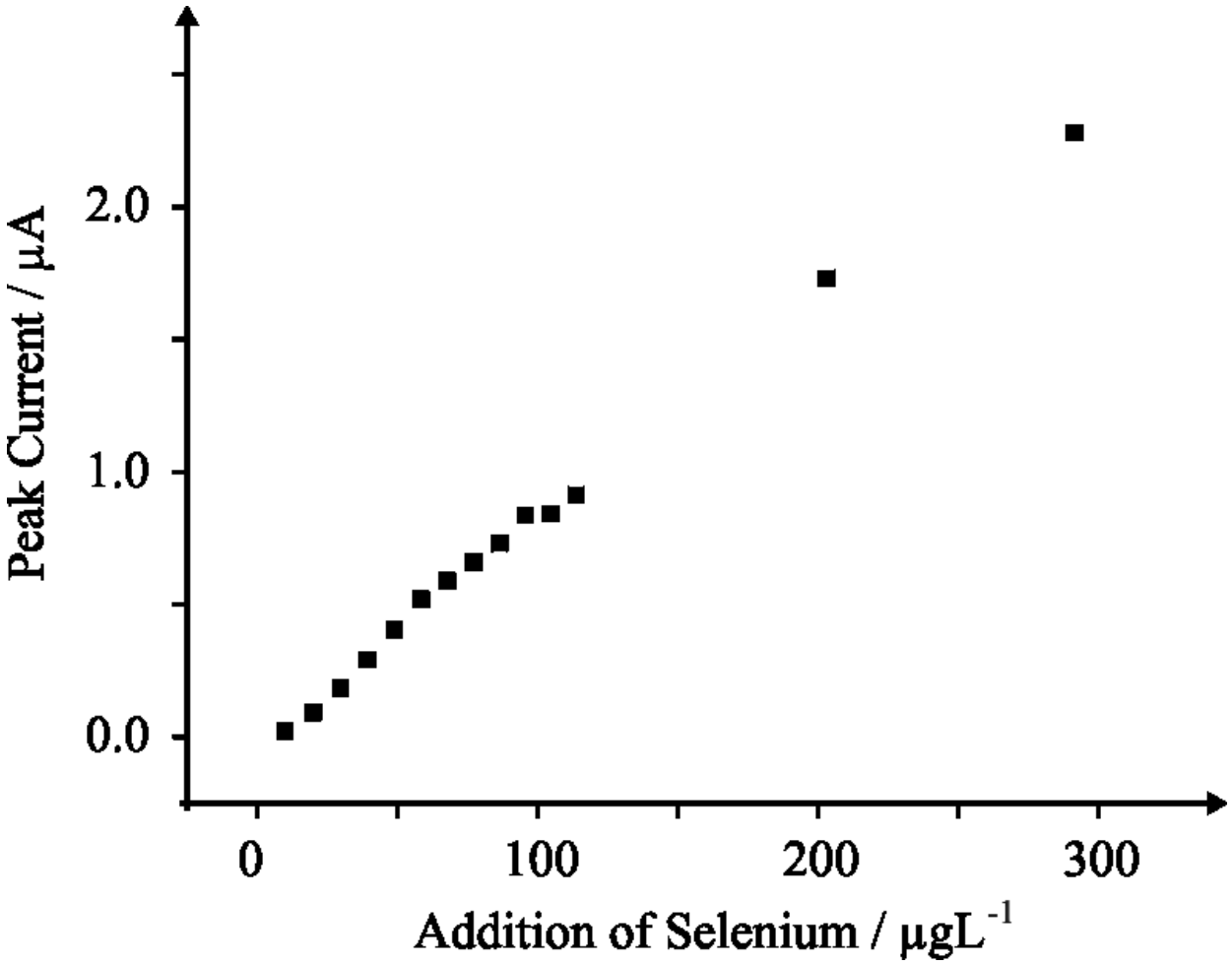

Figure 5.4 A typical calibration plot corresponding to additions of selenium (IV) (10 – 300 µg L^{-1}) into 0.1 mol L^{-1} $HClO_4$ using an SPGE. Deposition potential: -0.6 V; Deposition time 300 seconds. Scan rate: 50mVs^{-1}.

Next, the electroanalytical response was explored using a single SPGE for *each* concentration. Using a deposition potential of -0.6 V for 300 seconds the resulting voltammograms using different SPGE for each concentration of selenium (IV) in 0.1 mol L^{-1} $HClO_4$ are displayed in Figure 5.5 which demonstrates the presence of a clear peak at ~ + 0.8 V.

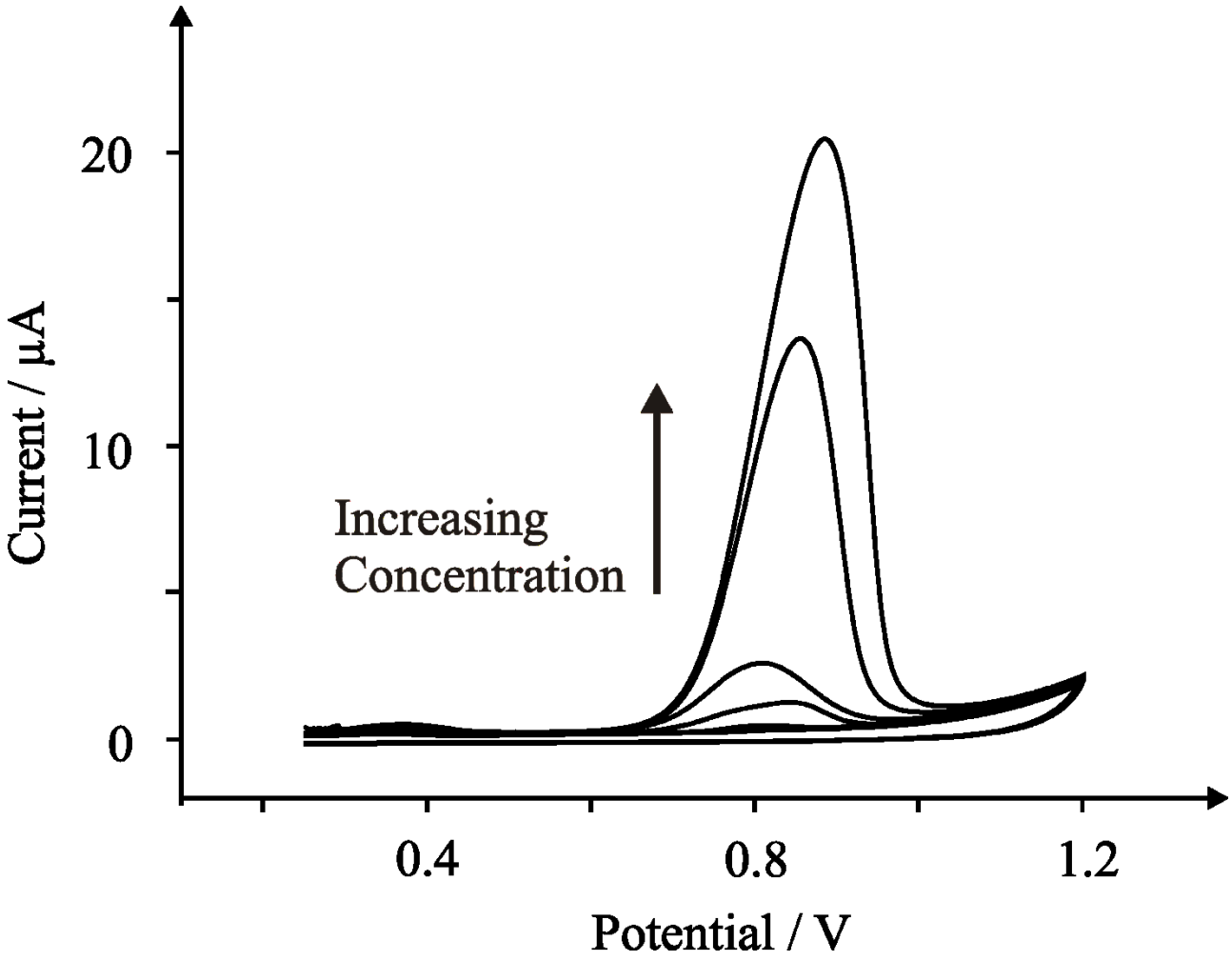

Figure 5.5 Typical cyclic voltammetric responses of increasing selenium (IV) concentrations (0 – 10000 µg L^{-1}) in 0.1 mol L^{-1} $HClO_4$ using a different SPGE for each addition. Scan rate: 50 mVs^{-1}.

Calibration plots corresponding to the increasing concentration of selenium (IV) versus the voltammetric peak height (µA) are presented in Figure 5.6. As is clear in Figure 5.6, two linear ranges are evident when utilising separate SPGEs for each concentration. A linear response ($I_P/\mu A = 1.3 \times 10^{-3}\ \mu A/\mu g L^{-1} - 3.0 \times 10^{-2}\ \mu A;\ R^2 = 0.99$) is observed between 10 to 250 µg L^{-1} of selenium (IV) with a second, steeper linear range ($I_P/\mu A = 2.5 \times 10^{-3}\ \mu A/\mu g L^{-1} - 4.2 \times 10^{-1}\ \mu A;\ R^2 = 0.99$) observed upon additions of selenium (IV) up to 1000 µg L^{-1} for the anodic stripping voltammetry measurement of selenium over a concentration range of 10 to 1000 µg L^{-1}. The detection limit (3σ) of selenium (IV) was calculated to correspond to 4.9 µg L^{-1}. An excellent linear and reproducible response is observed when utilising a single SPGE for each measurement which is possible due to the ease of mass production of reproducible SPGEs. Clearly such a response indicates the potential utilisation of a SPGE

over an entire range of analysis, with the option for utilisation of 'fresh' SPGE's upon each measurement with no deviation in sensitivity or reproducibility

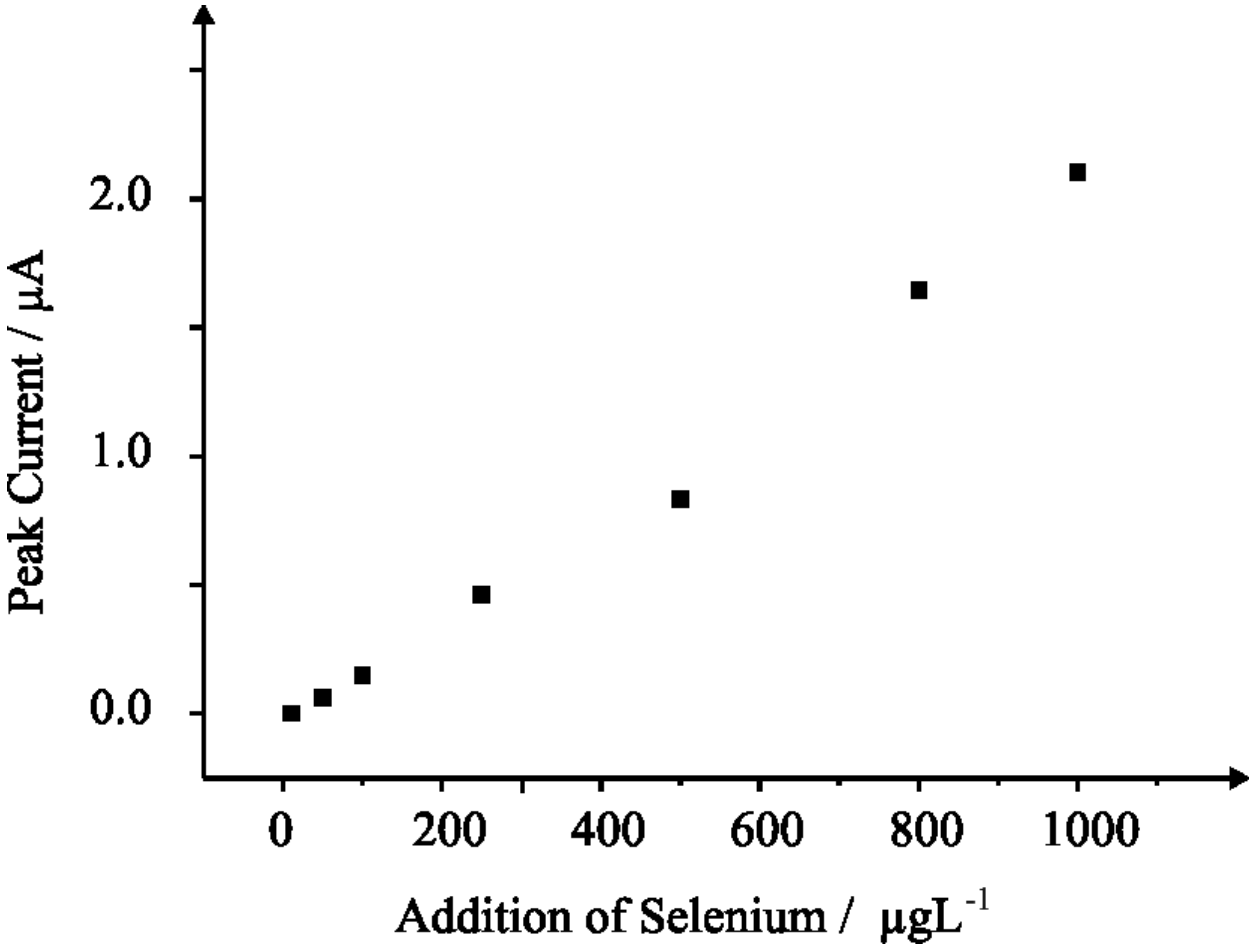

Figure 5.6 A typical calibration plot corresponding to the addition of selenium (IV) (10 – 1000 μg L^{-1}) into a solution of 0.1 mol L^{-1} $HClO_4$ using a different SPGE for each addition. Deposition potential: - 0.6 V; Deposition time 300 seconds. Scan rate: 50 mVs^{-1}.

Finally, further insight into the robust nature of the analytical protocol was sought through the detection of selenium (IV) in drinking (tap) water. Additions of selenium (IV) were made into a sample of tap water (adjusted to pH1 with $HClO_4$ prepared as described in the Experimental section) over the concentration range of 30 to 1000 μg L^{-1}. A deposition time of 300 seconds, held at a potential of -0.6 V was utilised for all measurements. The corresponding calibration plot is shown in Figure 5.7, where a *new* SPGE was utilised upon each addition of selenium (IV). A linear response for the sensing of selenium (IV) within drinking water was achieved ($I_P/\mu A = 5.0 \times 10^{-4}\ \mu A/\mu gL^{-1} - 4.0 \times 10^{-3}\ \mu A;\ R^2 = 0.99$), a reduction in the sensitivity of the protocol is evident when compared with analysis under

ideal conditions in 0.1M $HClO_4$ solution as is expected in real samples. The detection limit (3σ) of selenium (IV) within drinking water adjusted to pH1 with $HClO_4$ was calculated to be 19.2 μg L^{-1}. While this is higher than the EU limit, the limit of detection still falls below that stipulated by the United States Environmental Protection Agency and could potentially be used as a disposable and economical screening tool.

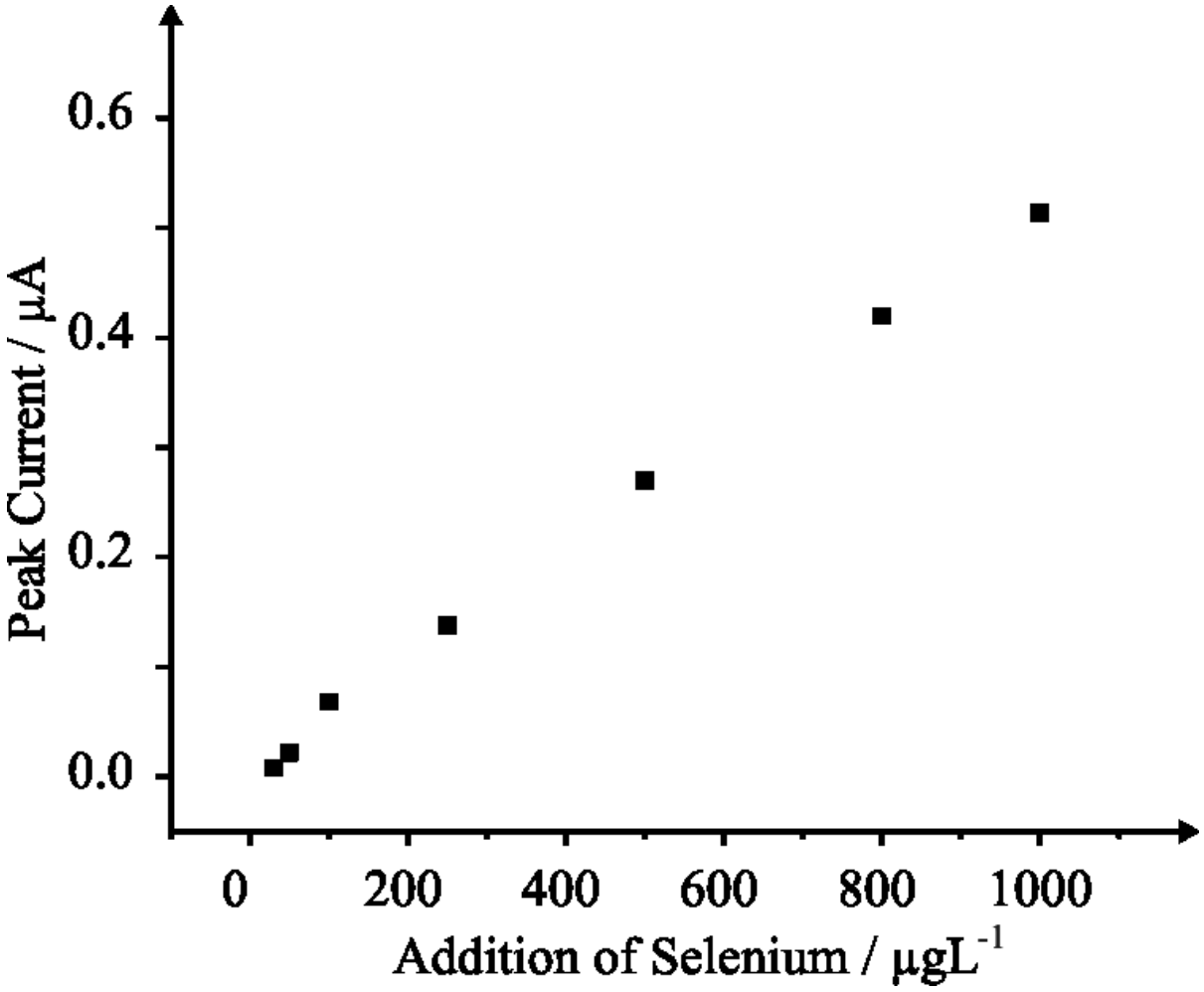

Figure 5.7 A typical calibration plot derived from additions of selenium (IV) into a tap water sample adjusted to pH1 with $HClO_4$ over the concentration range of 30 – 1000 μg L^{-1} using a different SPGE upon each addition. Deposition potential: -0.6 V; Deposition time 300 seconds. Scan rate: 50 mVs^{-1}.

5.1.4 CONCLUSIONS

The first example sensing of selenium (IV) in 0.1 mol L^{-1} $HClO_4$ using screen-printed graphite electrodes has been reported. These simplistic and cost effective screen-printed sensors provide an appealing alternative to expensive gold based electrodes which are traditionally used for the sensing of selenium (IV). The flexible screen-printed graphite electrodes were demonstrated to allow for the low level sensing of selenium (IV) in tap water samples, in addition to analysis under ideal conditions. Such sensors provide a potential solution to the common problem of the transition of laboratory-based analytical procedures to real world applications in the 'field' combining the low-cost benefits of carbon based materials with ease of mass production and facile use of screen-printed sensors. The next section considers the electroanalytical sensing of antimony (III) in drinking water.

5.2 SCREEN-PRINTED GRAPHITE ELECTROCHEMICAL SENSORS FOR THE VOLTAMMETRIC DETERMINATION OF ANTIMONY (III)

5.2.1 ABSTRACT

In this section, the electroanalytical determination of antimony (III) is explored using disposable and economical unmodified screen-printed graphite macro electrodes. These sensors are found to allow the sensing of antimony (III) *via* anodic stripping voltammetry over the range of 1 to 910 μg L^{-1} in pH 3.5 acetate buffer solutions with a limit of detection found to correspond to 0.58 μg L^{-1}. The analytical protocol is applied to the sensing of antimony (III) in drinking water samples where a limit of detection was found to correspond to 1.2 μg L^{-1}. The observed detection limits are well below that of those have been imposed as maximum antimony (III) concentrations in drinking water by the European Union (4.5 μg L^{-1}) and World Health Organisation (20 μg L^{-1}).

The effect of interferences upon the electroanalytical protocol are also explored, where only copper (II) ions are found to be problematic due to the close proximity of the antimony and copper stripping peaks. Proof-of-concept that copper interference can be eliminated is demonstrated through the application of a complexing agent.

5.2.2 INTRODUCTION

Antimony is a toxic element which the vast majority of the world's population are exposed to regularly and is found within both environmental and biological samples.[223] The increasing use of antimony in industry and its relative toxicity mean it is established as a pollutant. Industrially, antimony is used in the fabrication of fire retardants,[224] glass and ceramics,[224] batteries[225] and in the production of polyethylene terephthalate (PET) bottles where antimony is used as a catalyst.[226]

Four oxidation states of antimony subsist; -III, 0, III and V however, antimony is generally reported to exist within the environment in two forms, that is, antimony (III) and antimony (V).[227] The trivalent compounds of antimony are generally considered to be more toxic than the pentavalent ones.[228] Exposure to antimony at high levels is reported to cause respiratory irritation, 'antimony dermatitis',[229] pneumoconiosis and gastrointestinal symptoms.[227, 230] Additionally antimony trioxide may be carcinogenic to humans although studies are inconclusive, while animal studies have reported lung tumours in rats exposed to

antimony trioxide *via* inhalation; as such the U. S. Environmental Protection Agency does not currently classify antimony as a carcinogen.[223, 231, 232] In contrast with their potential toxicity, the therapeutic properties of antimony compounds have also been explored with organic pentavalent antimonials (antimony (V)) having been used for the treatment of Leishmaniasis,[233, 234] whilst sodium antimony tertate (antimony (V)) is used in urinary schistosomiasis treatment.[235]

In environmental aqueous samples which are not polluted, the concentration of total antimony are typically below 1 μg L^{-1}.[236] This concentration increases in areas where activities such as mine drainage occurs and also close to industries where antimony compounds are routinely used or produced.[237] In accordance with the reported toxicity and potential risk to human health posed by antimony, the European Union have imposed a maximum antimony concentration 4.5 μg L^{-1} within drinking water.[238] Similarly, the World Health Organization recommend that antimony levels do not to exceed 20 μg L^{-1}.[237]

At present, various different analytical techniques exist for the measurement and monitoring of antimony in environmental and biological samples, these include; Fluorometry, Spectrophotometry, Atomic Absorption Spectrometry,[239-242] High Pressure Liquid Chromatography with Mass Spectrometric detection[243] and Flow Injection Analysis with Hydride Generation Atomic Fluorescence detection.[244] Detection limits of 0.1 μg L^{-1} or lower can typically be achieved with analytical spectroscopic methods using hydride generation however, such techniques are expensive and pose real limitations when considering portability and operation skill level required (as is the case with each of the techniques listed earlier).[239]

One potential alternative to the described techniques, which has the ability to offer cost effective, rapid and reliable monitoring of antimony, is electrochemical measurement.[232, 245] Electrochemically, various techniques have been used with many different electrodes such as hanging mercury drop electrodes, graphite-mercury film electrodes, gold film electrodes, edge-plane pyrolytic graphite, glassy-carbon and carbon-paste electrodes.[232] Further improvement and potential 'real-world' application of electrochemistry for the determination of antimony is offered through the incorporation of screen-printed sensors, which allow for the production of electrochemical sensors capable of utilization within the 'field' through exploitation of a fabrication methodology which enables mass production of highly reproducible, single-shot electrodes.[245-248] As such, modified carbon screen-printed electrodes have been used for the determination of antimony (III) and total antimony.[246, 247, 249, 250] In

these reports, the existing screen-printed carbon-based working electrode have been modified with mercury film,[246] with gold[249] and silver[247] nanoparticles. More recently, Compton *et al.* reported upon a study for the monitoring of antimony (III) utilising a range of unmodified carbon electrodes including edge plane pyrolytic graphite electrode, glassy-carbon electrode, boron-doped diamond electrode and for the first time screen-printed electrodes purchased from DropSens.[251, 252] Critically however, the group determined that the screen-printed electrodes utilised were unsuitable for the monitoring of antimony due to the absence of linearity in the response obtained over the analytical range selected, suggesting that such observations were owing to the complications of avoiding oxygen in the system.[251] A further complication noted was interference from the ink; such ink contamination precluded useful measurements for the sensing of antimony (III). The authors concluded that at present no satisfactory unmodified carbon based screen-printed electrodes have been reported for the sensing of antimony (III).[251]

In this section, the sensing of antimony (III) using bare/unmodified screen-printed graphite electrodes has been proposed, without the requirement for any further modification or potential cycling. These screen-printed sensors are also shown to be feasible for the detection of antimony (III) in drinking water samples at levels relevant to the United States Environmental Protection Agency and World Health Organisation.

5.2.3 RESULTS AND DISCUSSION

First attention was turned to the electrochemical detection of antimony (III) in a pH 3 acetate buffer solution *via* cyclic voltammetry using a screen-printed graphite electrode (denoted throughout as SPGE). It is evident upon inspection of figure 5.8 the reduction of antimony (III) to antimony (0) occurs at a cathodic potential of – 1.1 V (vs. Ag/AgCl) with the corresponding oxidative stripping peak being observed at an anodic potential of – 0.3 V (vs. Ag/AgCl). A current "cross-over" is evident from inspection of figure 5.8 which is due to a nucleation and growth mechanism where the initial deposition of antimony nuclei on the SPGE surface serves to increase the rate of further deposition such that on the reverse sweep the cathodic current flows at less negative potentials than those required for the initial deposition.

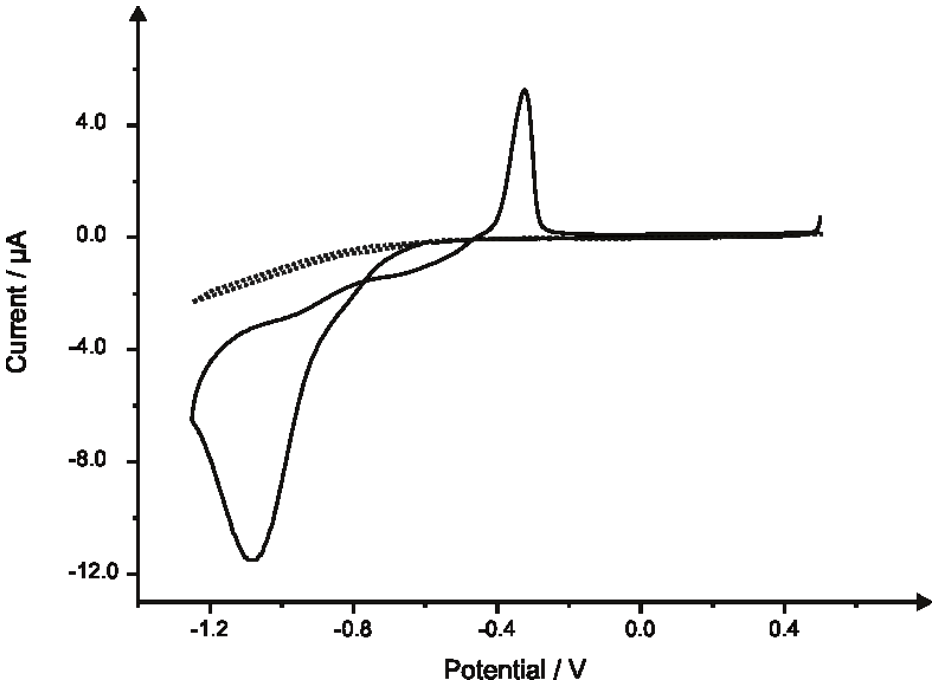

Figure 5.8 Cyclic voltammograms obtained in the absence (dotted line) and presence (solid line) of 10 mg L^{-1} antimony (III) in a pH 3 acetate buffer. Scan rate: 50 mVs^{-1}.

In order to simplify the analytical protocol, linear sweep anodic stripping voltammetry (ASV) was utilised for the sensing of antimony (III) and consequently the effect of the deposition potential on the voltammetric peak height of the stripping peak was first studied, using the SPGEs, through the application of different deposition potentials. The solution comprised of 7 mg L^{-1} antimony (III) in a pH 3.5 acetate buffer solution with the deposition time fixed at 100 seconds and the initial starting potential the same as that of the chosen deposition potential. Figure 5.9 depicts an analysis of the plot of the observed stripping peak height due to the electrochemical stripping of antimony (0) to antimony (III) as a function of the applied deposition potential, where the peak height at deposition potentials from -0.5 V to -1.0 V (*vs*. Ag/AgCl) appear to be negligible. At deposition potentials more cathodic than -1.0 V (*vs*. Ag/AgCl) the peak height increases steeply until -1.25 V (*vs*. Ag/AgCl), after this point the peak diminishes; consequently, a deposition potential of -1.25 V (*vs*. Ag/ AgCl) was selected for use within the consequential analysis.

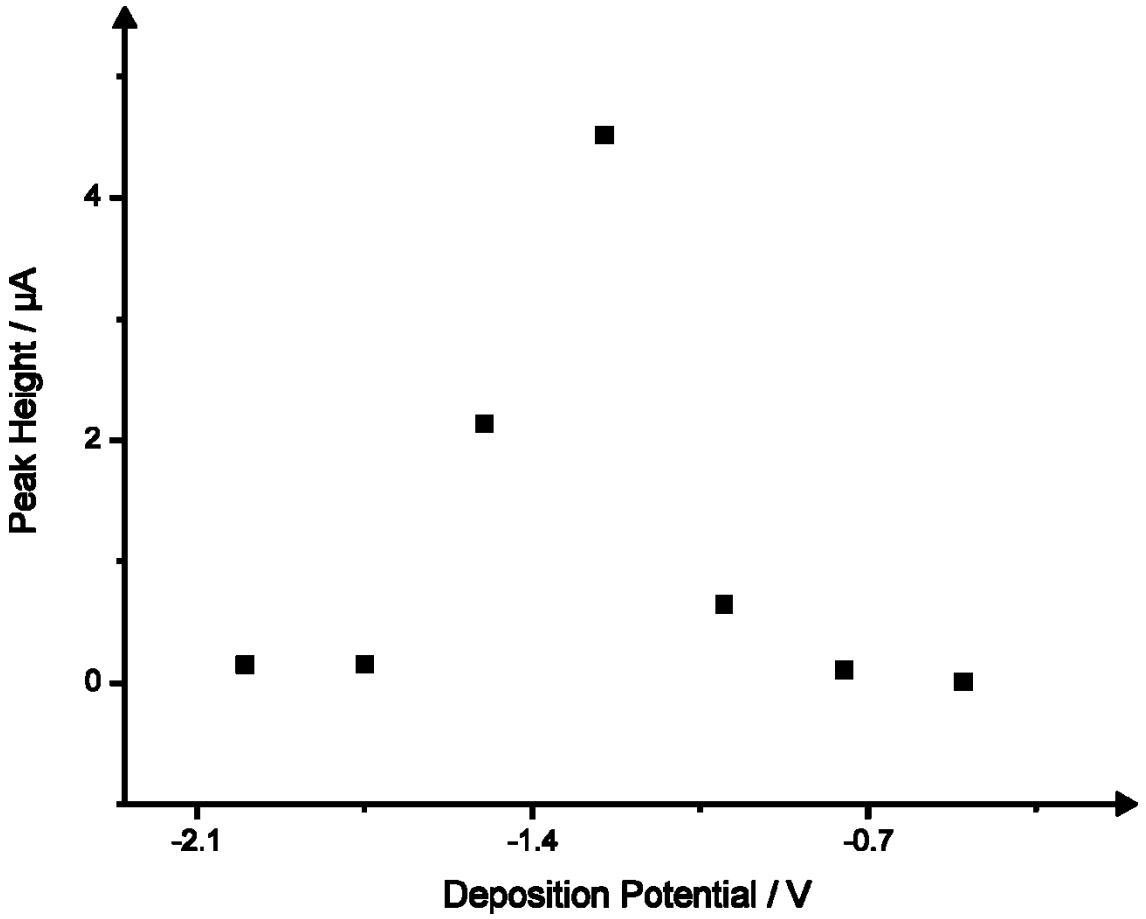

Figure 5.9 The effect of deposition potential upon the observed voltammetric peak height for the sensing of 7 mg L^{-1} antimony (III) in a pH 3.5 acetate buffer solution, using a deposition time of 100 seconds using a SPGE. Scan rate: 50 mVs^{-1}.

Arguably the most critical parameter when attaining electrochemical measurement using the method of anodic stripping voltammetry is the deposition time as it can not only dictate the sensitivity of the measurement, but also the length of the analytical protocol. In light of this, figure 5.10 demonstrates the effect of deposition time upon the voltammetric peak height resulting from measurement of antimony (III) at a fixed concentration of 7 µg L^{-1} in acetate buffer solution pH 3.5 and a fixed deposition potential of -1.25 V (*vs*. Ag/AgCl), utilising the SPGEs. Evidently, a greater voltammetric peak height is observed with increasing deposition time with no plateau arising as is typical in anodic stripping voltammetry. In order to avoid a reduction in the practicality of the electrochemical methodology through having a lengthy analytical protocol, a deposition time of 125 seconds was chosen.

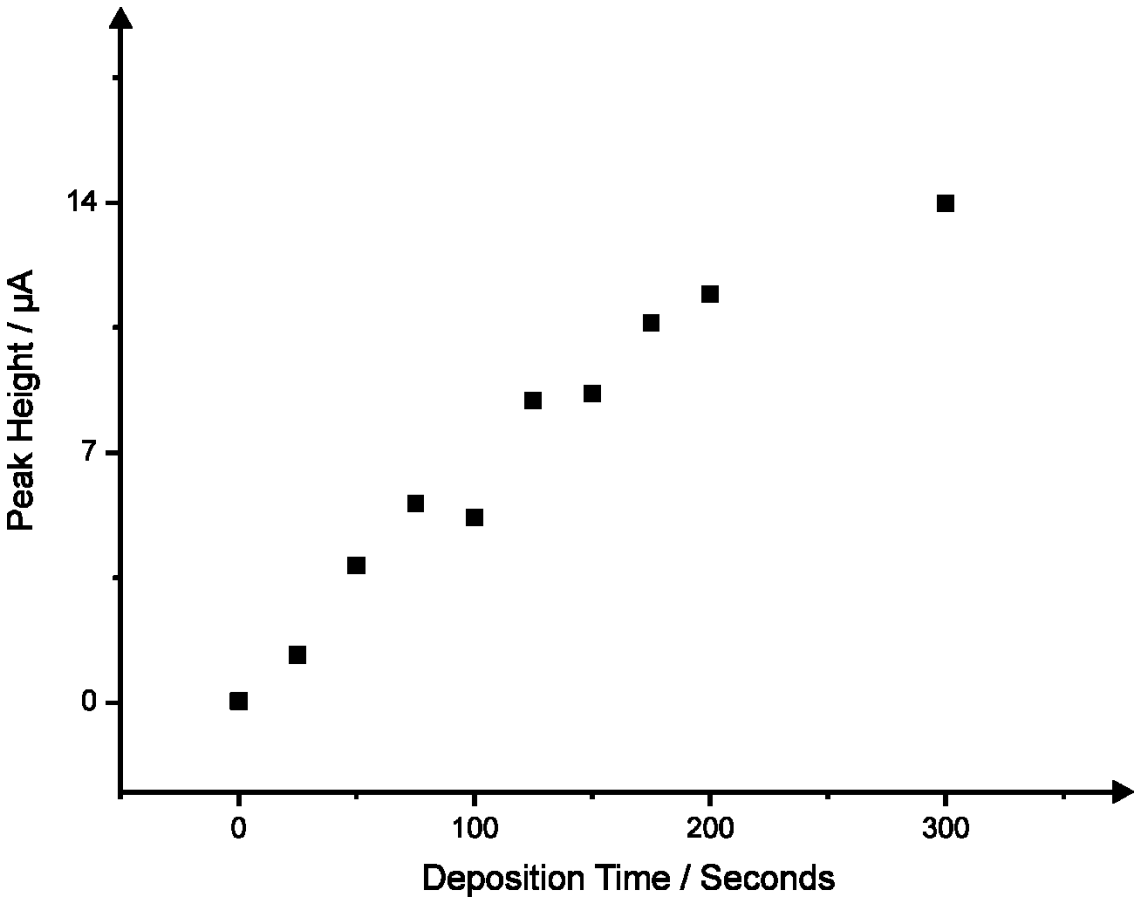

Figure 5.10 The effect of deposition time upon the voltammetric peak height response for 7 mg L^{-1} antimony (III) in a pH 3.5 acetate buffer solution. Deposition potential: - 1.25 V (*vs*. Ag/AgCl). Scan rate: 50 mVs^{-1}.

Next, attention was turned to exploring the electroanalytical response of the SPGEs. Figure 5.11 A shows the linear sweep voltammetric responses as a result of antimony (III) concentrations made over the range of 1 to 910 µg L^{-1} into a pH 3.5 acetate buffer solution, utilising a single SPGE for all the concentrations explored. A stripping peak corresponding to the electrochemical stripping of antimony (0) to (III) is evident at a voltammetric potential of – 0.35 V (*vs*. Ag/AgCl) where analysis of the observed stripping peak as a function of antimony (III) concentration results in two linear ranges, the first being over the concentration range 1 to 40 μgL^{-1} ($I_P/\mu A = 3.5 \times 10^{-2}\,\mu A/\mu gL^{-1} - 1.1 \times 10^{-2}\,\mu A$; $R^2 = 0.984$; $N = 4$) and the second 40 to 910 μgL^{-1} ($I_P/\mu A = 2.8 \times 10^{-3}\,\mu A/\mu gL^{-1} - 5.2 \times 10^{-1}\,\mu A$; $R^2 = 0.993$; $N = 6$) as depicted in figure 5.11 B. Furthermore, utilising the linear range determined over

the lower concentration range, the limit of detection (3σ) for antimony (III) was determined to correspond to 0.58 μg L^{-1}.

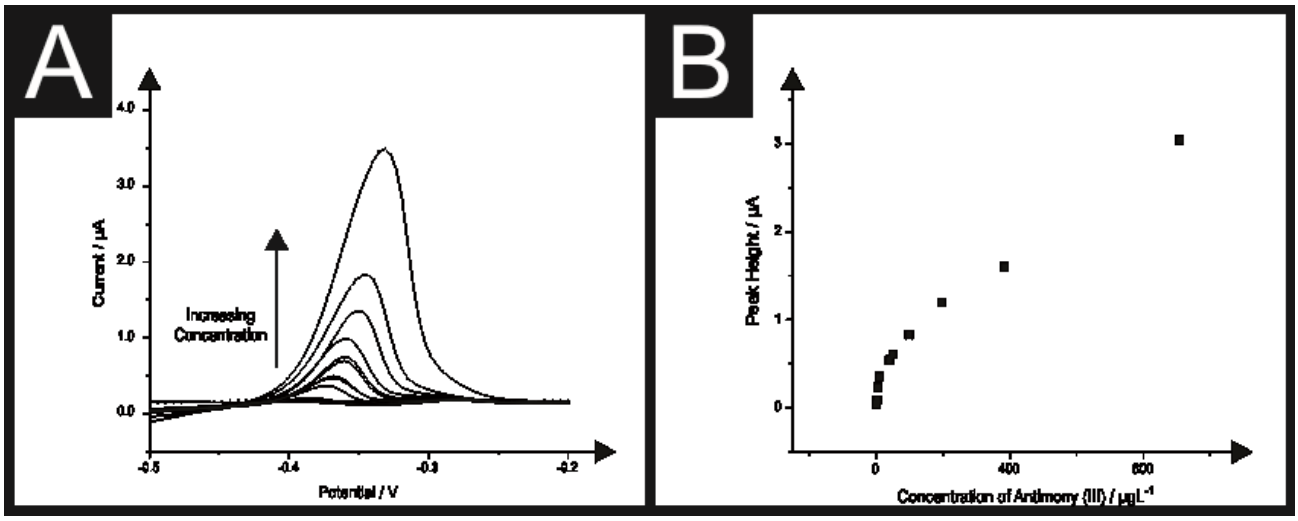

Figure 5.11 A) Linear sweep voltammetric response of a SPGE upon additions of antimony (III) (1 – 910 μg L^{-1}) in a pH 3.5 acetate buffer solution. Deposition potential and time: - 1.25 V (*vs*. Ag/AgCl); 125 seconds. Scan rate: 50 mVs^{-1}. B) A typical corresponding calibration plot from analysis of data presented in A).

A review of the current literature relating to electrochemical detection of antimony (III) reveals that screen-printed sensors modified with silver[249] and gold[247] nanoparticles have been utilised allowing for antimony (III) detection levels of 0.083 μg L^{-1} and 0.12 μg L^{-1}. Additionally in many instances carbon based electrode materials have been modified or combined with a complexing agent prior to utilisation, for example Brainina and co-workers[253] have utilised a N,N,N′,N′-tetramethyl-p-phenylenediamine modified graphite macro electrode enabling antimony (III) limits of detection of 3.65 μg L^{-1}, whilst others have reported the use of iridium oxide for sensing with a boron-doped diamond electrode allowing detection limits of 85.2 μg L^{-1} [254]. Evidently, although not offering the lowest limit of detection, the screen-printed graphite electrode reported herein offers not only a competitive detection limit, but also simplification of the analytical procedure through the alleviation for the requirement of electrode modification or use of complexing agents. For further insights into the different electrochemical techniques and electrode configurations utilised for the sensing of antimony (III) the reader is directed to an elegant and authoritative review by Toghill *et al*.[232] It is imperative to note that in addition to offering a competitive limit of

detection in comparison with existing reports, critically the SPGE also allows for the detection of antimony (III) at concentrations well *below* that of the maximum concentrations of 5 and 20 μg L^{-1} prescribed by the European Union[238] and World Health Organisation[237] respectively.

Finally, further insight into the robust nature of the analytical protocol was sought through the detection of antimony (III) in drinking (tap) water. Additions of antimony (III) were made into a sample of drinking water (prepared as described in the Experimental section) over the low concentration range of 2 to 80.3 μg L^{-1} selected since these best represent concentrations likely to be realised in true analytical samples. A deposition time of 125 seconds, held at a potential of -1.25 V (*vs*. Ag/AgCl) was utilised for all measurements. The corresponding calibration plot is shown in figure 5.12, where a *new* SPGE was utilised upon each addition of antimony (III). As was observed for additions of antimony (III) into 'ideal' solutions, *viz* figure 5.11 B, two linear ranges were observed, the first being over the concentration range 2 to 9 μg L^{-1} ($I_P/\mu A = 3.0 \times 10^{-2}\ \mu A/\mu g L^{-1} - 1.3 \times 10^{-1}\ \mu A$; $R^2 = 0.945$; $N = 3$) and the second 9 to 80.3 μg L^{-1} ($I_P/\mu A = 7.8 \times 10^{-3}\ \mu A/\mu g L^{-1} - 2.4 \times 10^{-1}\ \mu A$; $R^2 = 0.991$; $N = 4$). A reduction in the sensitivity of the protocol is evident when compared with analysis under ideal conditions in acetate buffer solution pH 3.5 as is expected in real samples. The detection limit (3σ) of antimony (III) within drinking water was calculated to be 1.2 μg L^{-1} which once more allows for the sensing of antimony (III) well below the limits recommended by the European Union[238] and World Health Organisation.[237] Additionally, the inclusion of error bars (figure 5.12) demonstrates the excellent inter-reproducibility of the screen-printed sensors, suggesting the use of the analytical protocol for the routine sensing of antimony (III) in real samples.

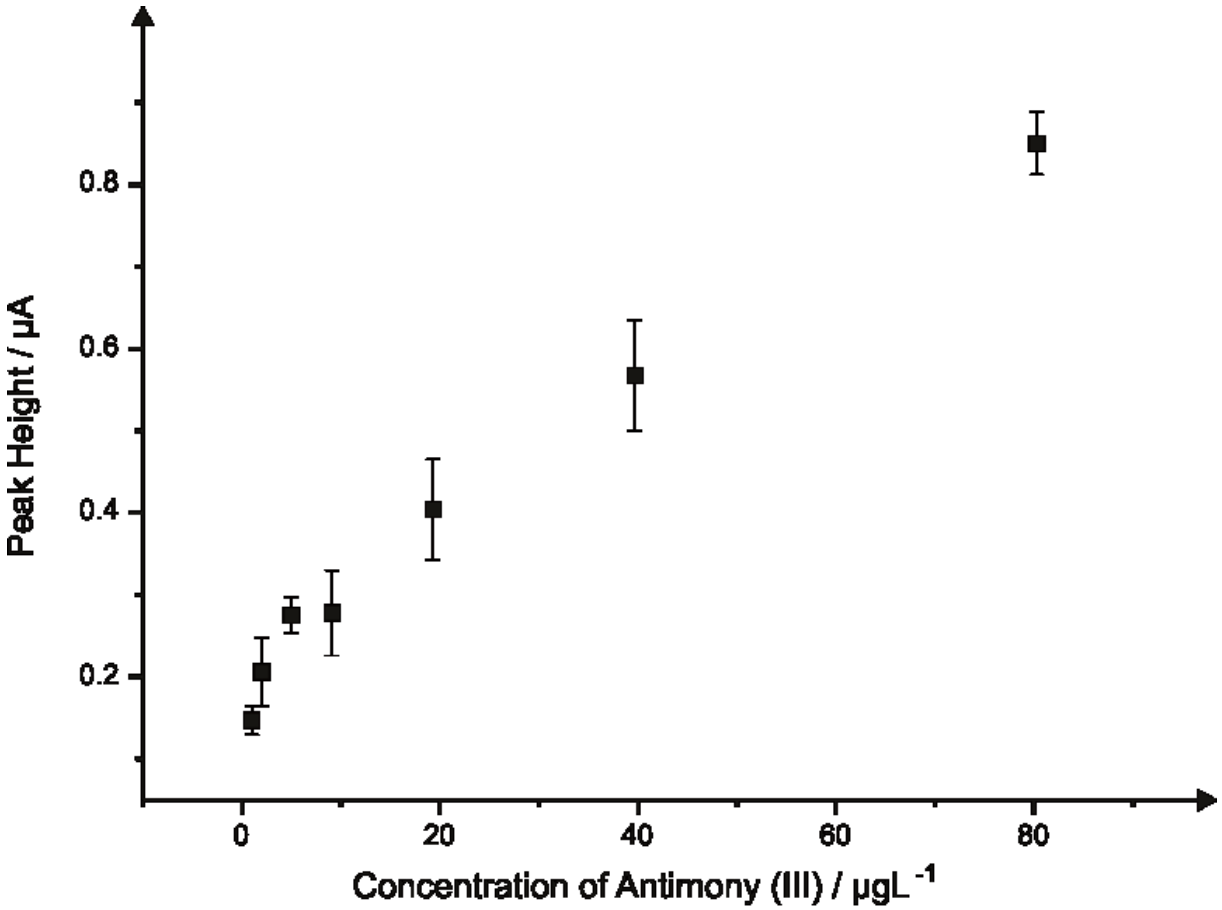

Figure 5.12 Typical calibration plot derived from additions of antimony (III) into a drinking water (tap) sample over the concentration range of 2-80.3 µg L^{-1} using a *different* SPGE for each concentration. Deposition potential and time: -1.25 V; 125 seconds. Scan rate: 50 mVs^{-1}. Error bars (N=3).

Although, no substantial decrease in the analytical protocol is evident when applied into antimony (III) determination in real drinking samples, the presence of interferences, likely to be encountered in other samples must be considered. The interference of other common metals upon the detection of antimony (III) is shown in figure 5.13. Linear sweep voltammetric measurements were undertaken using the SPGEs in separate solutions containing 3 mg L^{-1} cadmium (II), 3 mg L^{-1} lead (II), 3 mg L^{-1} zinc (II) and 3 mg L^{-1} copper (II) in a pH 3.5 acetate buffer. Inspection of figure 5.13 reveals that of the potential metallic interferents studied, only copper is observed to result in a voltammetric peak at a potential (-0.07 V (*vs*. Ag./AgCl)) close to that of antimony (- 0.22 V (*vs*. Ag/AgCl)).

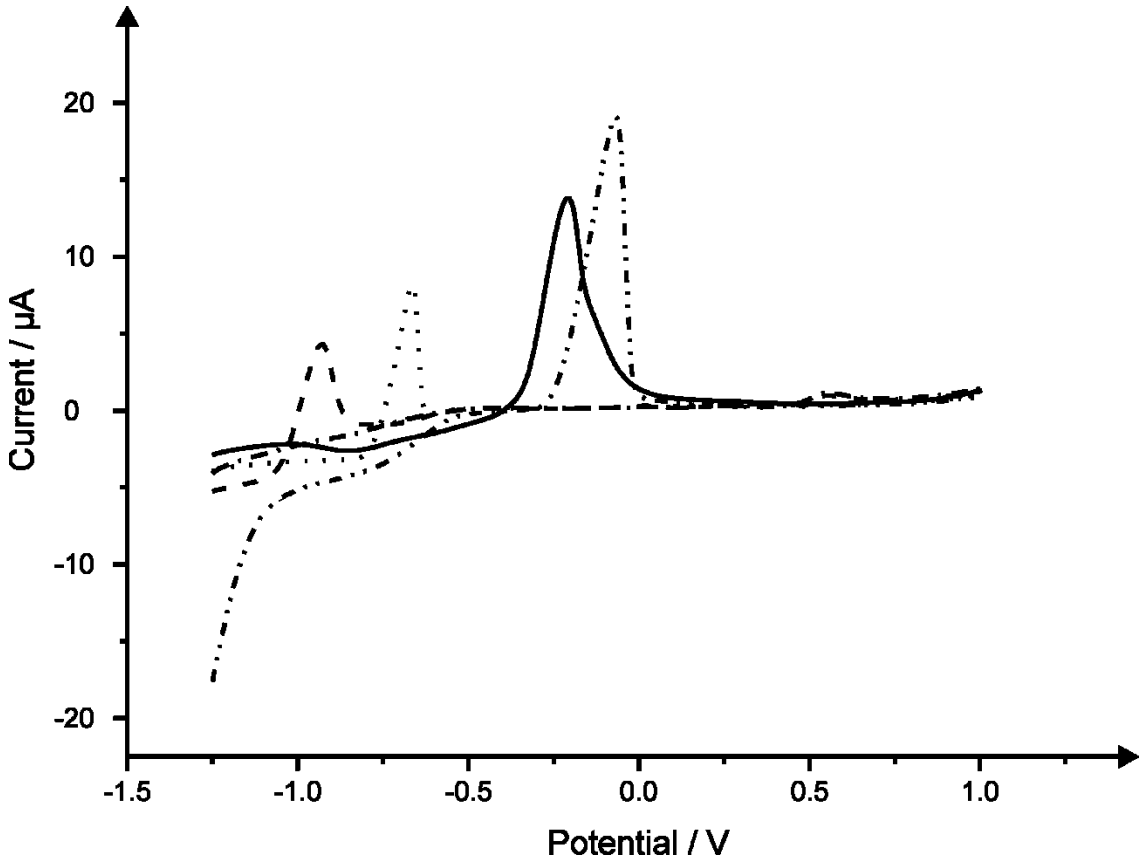

Figure 5.13 Determination of the effect of the presence of common metal ion interferents; 3 mg L^{-1} cadmium (II) (dashed line), 3 mg L^{-1} lead (II) (dotted line), 3 mg L^{-1} zinc (II) (dash dot line) and 3 mg L^{-1} copper (II) (dash dot dot line) on the detection of 10 mg L^{-1} antimony (III) (solid line) using the SPGEs via anodic stripping voltammetry in a pH 3.5 acetate buffer solution. Deposition potential and time: -1.25 V (*vs*. Ag/AgCl); 125 seconds. Scan rate: 50 mVs^{-1}.

The copper interference has been proposed to be eliminated by applying less cathodic deposition potential, especially when mercury electrode have been utilised.[255, 256] In the case of the SPGEs, changing the deposition potential to the less cathodic potentials will reduce the observed sensitivity and approach the limits of our protocol. Importantly the effect of the potential interferents noted when each exist within the same antimony solution was also studied. To allow for this, the voltammetric response obtained in bank pH 3.5 acetate buffer which was then consequently spiked to a concentration of 10 mg L^{-1} antimony (III) and further to this an addition of 3 mg L^{-1} cadmium (II), 3 mg L^{-1} lead (II), 3 mg L^{-1} zinc (II) and 3 mg L^{-1} copper (II) was made. The resultant voltammograms are depicted in figure 5.14 where it is clear that the presence of copper (II), as suspected earlier, poses a significant

problem in relation to the monitoring of antimony (III) resulting in a greatly diminished antimony (III) with the potentials of the two analytes overlapping under the given electrochemical parameters.

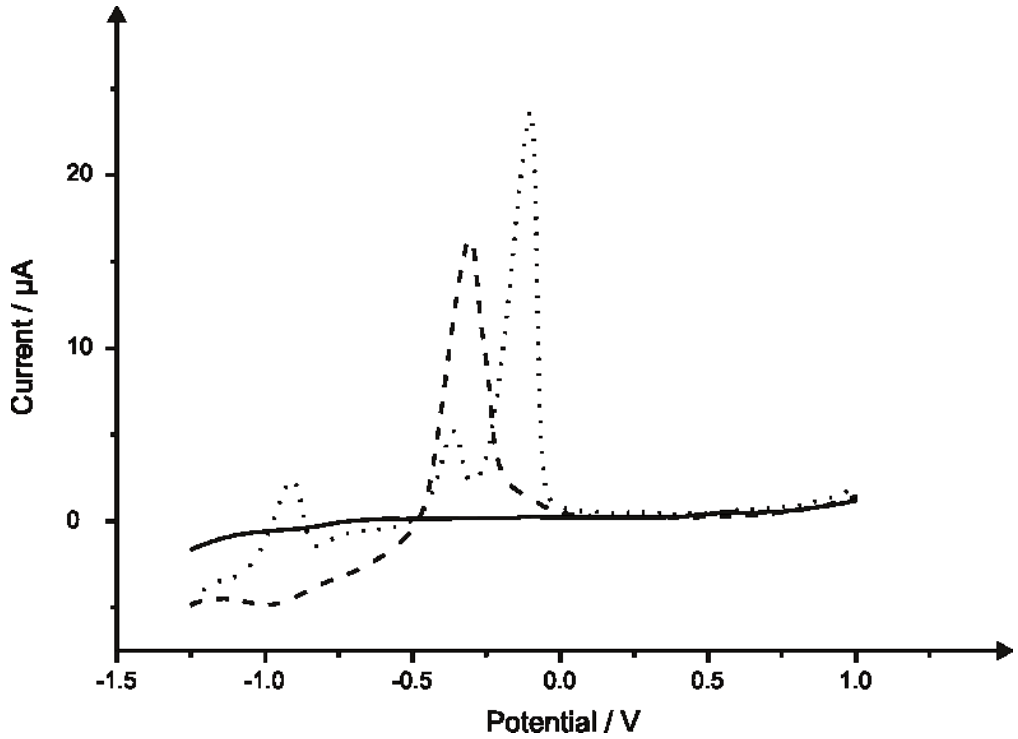

Figure 5.14 Linear sweep voltammograms resulting from analysis in pH 3.5 acetate buffer (solid line), 10 mg L^{-1} antimony (III) (dashed line) and 10 mg L^{-1} antimony (III) in the presence of common metal ion interferents (3 mg L^{-1} cadmium (II), 3 mg L^{-1} lead (II), 3 mg L^{-1} zinc (II), and 3 mg L^{-1} copper (II)) (dotted line), using the SPGEs *via* anodic stripping voltammetry. Deposition potential and time: -1.25 V (*vs*. Ag/AgCl); 125 seconds. Scan rate: 50 mVs^{-1}.

Out of the various reports detailing the detection of antimony, many note the interference posed by the presence of copper, though do not proceed to offer any potential solutions to the apparent problem.[247, 249, 257] Interestingly it is noted that this potential inference from the presence of copper may be overcome through the introduction of a complexing agent; potassium ferrocyanide (II) which can be added into the antimony solution. As is demonstrated in figure 5.15, the peak observed at a potential of -0.07 V (*vs*. Ag./AgCl) attributed to the stripping of copper which poses a clear risk of interference when studying antimony (II), can be alleviated through complexation of the copper in solution with the ferrocyanide (II) as is explained by the following equation:[258]

$$2Cu^{2+}(aq) + [Fe(CN)_6]^{4-}(aq) \leftrightarrow Cu_2[Fe(CN)_6](s) \qquad (3.5)$$

Clearly this therefore prevents the copper stripping peak arising and as such enables the monitoring of antimony in copper contaminated solutions without interference of the analytical protocol.

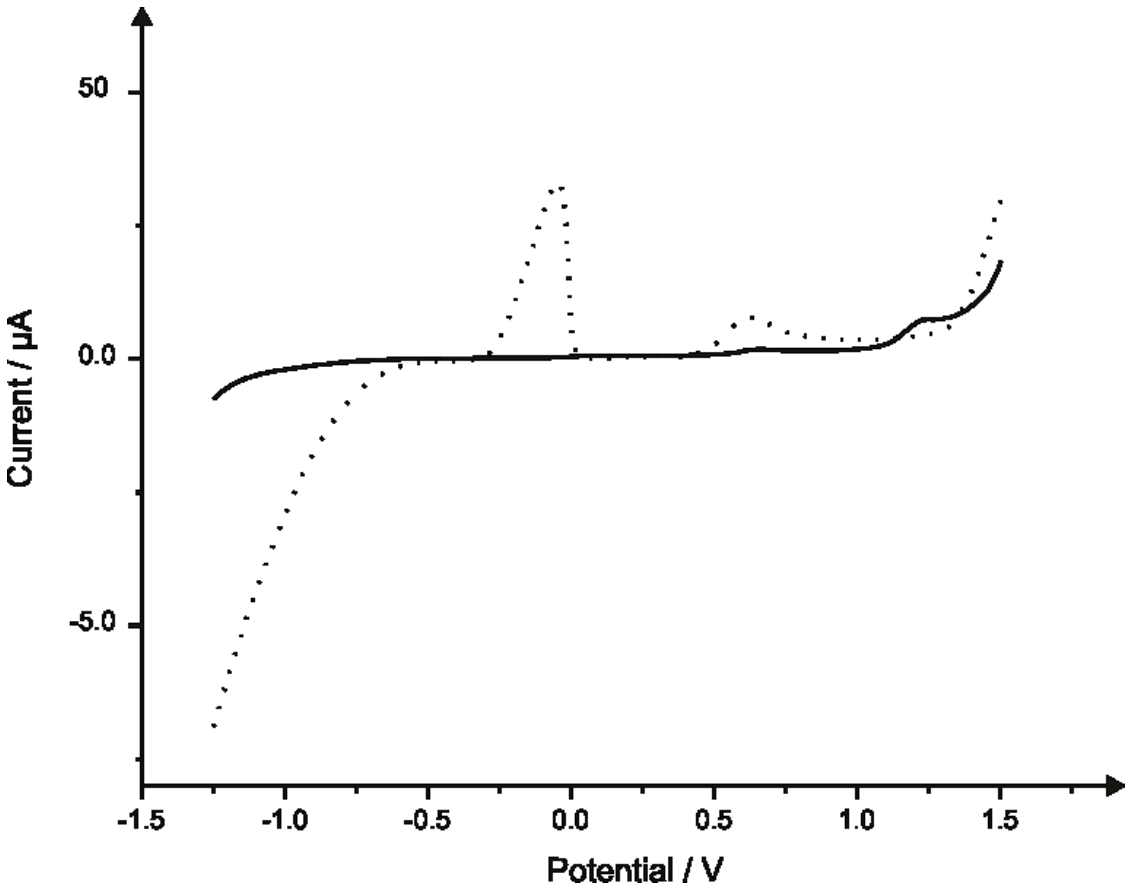

Figure 5.15 Linear sweep voltammograms obtained in the absence (solid line) and presence (dotted line) of 0.1 M potassium ferrocyanide (II) within a solution of 10 ppm copper (II) in a pH 3.5 acetate buffer solution using a SPGE. Deposition potential and time: -1.25 V (*vs*. Ag/AgCl); 125 seconds. Scan rate: 50 mVs^{-1}.

Finally, although the use of ferrocyanide (II) is confirmed to successfully alleviate interference caused by copper (*viz* figure 5.15) it is also important to determine the effect, if any, of ferrocyanide (II) upon the sensitivity of the electrochemical technique towards the monitoring of antimony (III). Additions of antimony (III), over the range 250 – 1400 µg L^{-1}, were once more made into an acetate buffer of pH 3.5 in the presence of 0.1 mM potassium

ferrocyanide (II), shown in figure 5.16. Although the sensing of antimony (III) was successful in the presence of ferrocyanide (II), deviations in behaviour from that observed under ideal conditions were observed. It was determined experimentally that when utilising the optimised electrochemical conditions the gradient obtained under 'ideal' conditions (*3.7* x 10^{-3} $\mu A/\mu gL^{-1}$) was reduced in the presence of ferrocyanide (II) (*1.4* x 10^{-3} $\mu A/\mu gL^{-1}$) with a reduction in the observed voltammetric signal of ~62.2 % when the complexing agent is utilised. Additionally, it is important to note the observation that in the presence of ferrocyanide (II) the monitoring of antimony (III) at concentrations below 250 µg L^{-1} is not possible due to the afore mentioned reduction in analytical sensitivity of the protocol but allows for the alleviate of the copper ion interference.

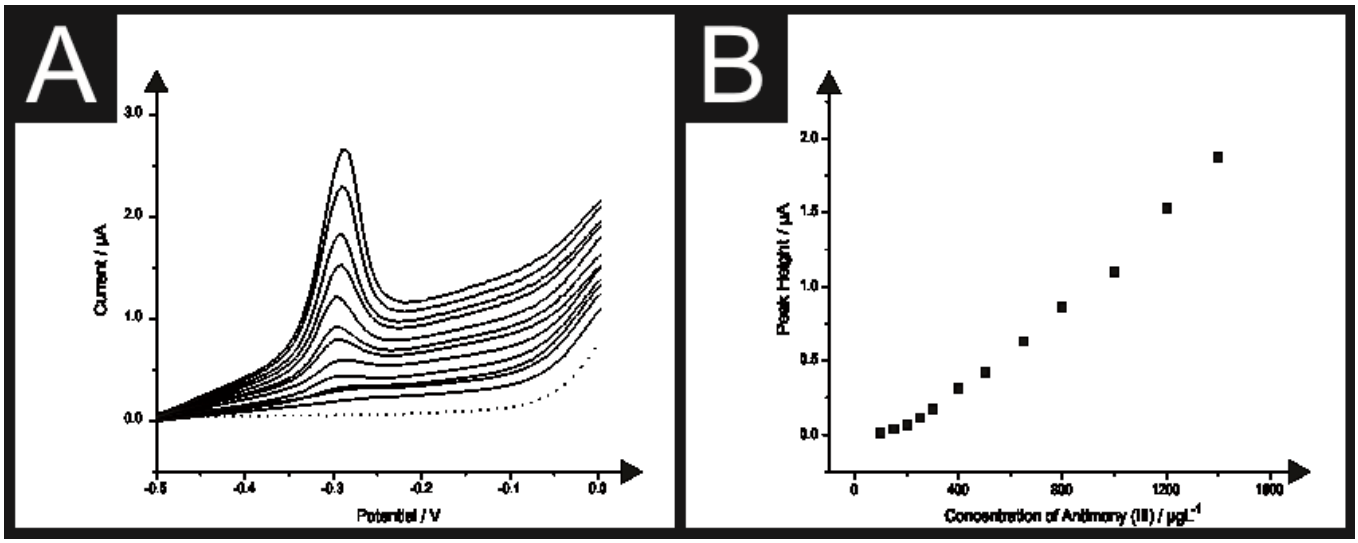

Figure 5.16 A) Linear sweep voltammetric response of a SPGE following additions of antimony (III) (250 – 1400 µg L^{-1}) into a pH 3.5 acetate buffer solution containing 0.1 mM potassium ferrocyanide (II). Deposition potential and time: -1.25 V (*vs*. Ag/AgCl); 125 seconds. Scan rate: 50 mVs^{-1}. B) A typical corresponding calibration plot from the analysis of the data presented in A).

5.2.4 CONCLUSIONS

The first example sensing of antimony (III) in acetate buffer solution pH 3.5 using bare unmodified screen-printed graphite electrodes has been reported in this thesis/section. These simplistic and cost effective screen-printed sensors provide an appealing alternative to expensive and toxic mercury based electrodes which are traditionally used for the sensing of

antimony (III). The flexible screen-printed graphite electrodes were demonstrated to allow for the low level sensing of antimony (III) in drinking water samples, in addition to analysis under ideal conditions. In both cases the levels are well below the limits recommended by the European Union[238] and World Health Organisation.[237] Additionally, the potential problematic occurrence of interference has been explored, highlighting a potential solution to such problems likely to be encountered in-the-field through the utilisation of potassium ferrocyanide (II). Note however the introduction of potassium ferrocyanide (II) was determined to result in a reduction in the observed peak intensity of ~ 60 % with unsuccessful determination of antimony (III) concentrations below 250 μg L^{-1}. These screen-printed sensors provide a potential solution to the common problem of the transition of laboratory-based analytical procedures to real world applications in the 'field' combining the low-cost benefits of carbon based materials with the ease of mass production and facile use of screen-printed sensors for the detection of a key analyte.

5.3 COMPARISON OF THE DIRECT AND INDIRECT ELECTROANALYTICAL DETECTION OF PHENOLS

5.3.1 ABSTRACT

The indirect determination of phenol, 2-Chlorophenol, 4-Chlorophenol and 2,4-Dichlorophenol through an electrochemically adapted optical method is reported for the first time. This electrochemical adaptation allows the determination of the above mentioned phenols without the use of an oxidant agent. Additionally other pyrazoline substitution products are evaluated for the detection of phenol. Finally the comparison of the direct (without mediator) and the proposed indirect determination (with 4-Aminoantipyrine) of the phenol and the three chlorophenols is presented. The limitation of the proposed electroanalytical protocol is quantified for all the four analytes.

5.3.2 INTRODUCTION

Chlorinated phenols represent a group of commercially produced, substituted phenols and cresols referred to as chlorophenols and chlorocresols. Chlorinated phenols are used as intermediates in the synthesis of dyes, pigments, phenolic resins and pesticides [259]. Certain chlorophenols also are used directly as flea repellents, fungicides, wood preservatives [260] mould inhibitors, antiseptics, disinfectants and anti-gumming agents for gasoline [261]. The chlorination of tap water may also produce CPs [262]

The reaction of phenolic materials with 4-aminoantipyrine, a pyrazoline substitution product, in the presence of potassium ferricyanide at a pH of 10 forms a stable reddish-brown coloured antipyrine dye. The amount of colour produced is a function of the concentration of phenolic material. [263] [264] These dyes are measured spectrophotometrically at 510nm and is the official analytical method for the determination of phenolic compounds in many countries. [265] The proposed reaction is shown in scheme 5.1 [266]

Scheme 5.1 Possible reaction of 4-Aminoantipyrne with phenol to produce the Quinoneimine dye. [267]

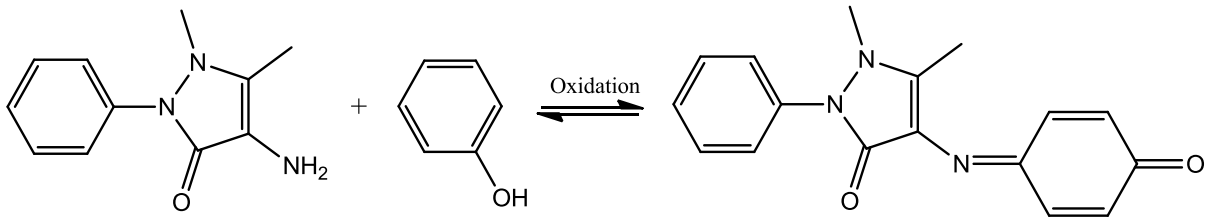

Elsenstaed, who first proposed this method, has studied the reactive limits of 69 phenols and 17 naphthols. His conclusions were as follows [266]:

- There must be at least one free phenolic hydroxyl group in the molecule for a positive test; Substituent in the para position to the hydroxyl group prevent the reaction except as follows: halogen, carboxyl, sulfonic acid, hydroxyl and methoxyl. These groups are probably expelled;
- A nitro group in the ortho position prevents reaction and a nitro group in meta position inhibits the test but not completely;
- Coupling of aminoantipyrine with the phenol takes place in the para position rather than in the ortho position

- When the para position is blocked by an alkyl, aryl, ester, nitro, benzoyl, nitroso, or aldehyde groups, no colour reaction takes place even if the ortho positions are unsubstituted.
- Phenols in sewage determined by 4-AAP optical method are phenolic compounds in which there is no substituent in the para position (of the previous conclusion) to the hydroxyl group except for halogen, COOH, SO_3H, OH, OCH_3 groups.

This section of the thesis deals with the electrochemical adaptation of the 4-Aminoantipyrine optical method [268, 269] introduced above which avoids the use of an oxidant agent, which is commonly included in the optical protocol. The electrochemical method is applied on the detection of phenol, 2-Chlorophenol, 4-Chlorophenol and 2,4-dichlorophenol. The evaluation of other pyrazoline substitution products on the detection of phenol is also explored. Finally the comparison of the direct and the proposed indirect determination of the phenol and the three chlorophenols is presented to evaluate the proposed electrochemically adapted protocol.

5.3.3 RESULTS AND DISCUSSION

First, the cyclic voltammetry responses of seven different pyrazoline substitution products was explored in a pH 10 carbonate buffer solution towards the detection of 10 mg L^{-1} phenol. Pyrazolines are the five –membered heterocyclic chemical compounds which have two adjacent nitrogen atoms within the ring and one endocyclic double bond. [270] Figures 5.17-5.23 depict the responses of 4-dimethylaminoantipyrine, Antipyrine, 3-methyl-1-(2-phenylethyl)-2-pyrazolin-5-one, 4. 3-amino-1-(1-naphthylmethyl)-2-Pyrazolin-5-one, 4-amino-1,2-dimethyl-3-pentadecyl-3-pyrazolin-5-one hydrochloride, 3-amino-1-(2-amino-4-methylsulfonylphenyl)-2-pyrazolin-5-one hydrochloride and 4-Aminoantipyrine in the presence and absenceof 10 mg L^{-1} Phenol. The chemical reaction of 4-Aminoantipyrine with the target phenol produces a product which is electrochemically active and produces a new reduction peak at -0.5V, as is shown in figure 5.23. The new peak which arises in figure 5.18 at +0.1V is because of the direct reduction of phenol (see later in figure 5.31) and is not due to its reaction with the antipyrine. Antipyrine is the only pyrazoline of the seven which does not have an amine group bonded with the pyrazoline ring. For this reason, it was not expected to react with the oxidised form of phenol producing the Schiff base according to Scheme 5.1.

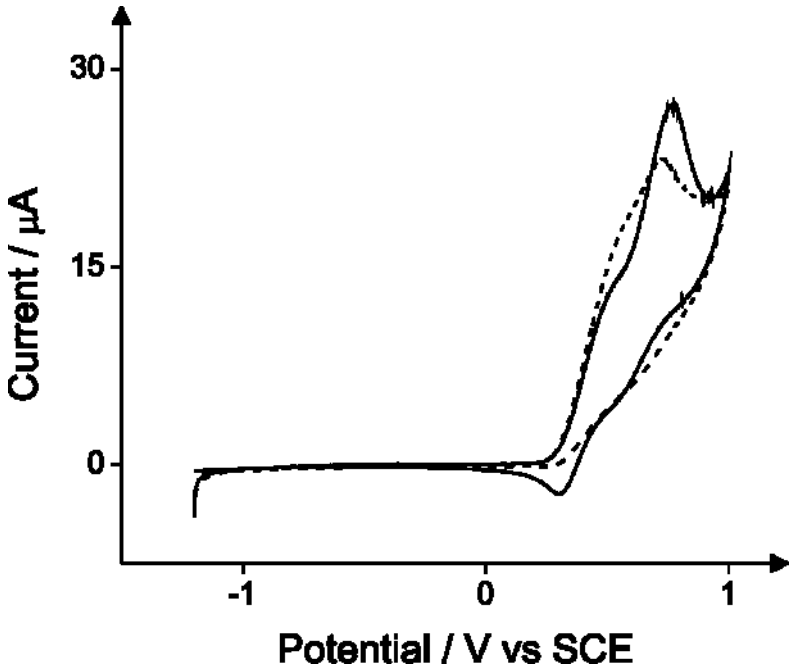

Figure 5.17 Cyclic Voltammetric response of the BDDE/SCE/Pt in the absence (solid line) and presence (dashed line) of 10 mg L^{-1} phenol obtained in pH 10 carbonate buffer solution containing 400 mg L^{-1} 4-dimethylaminoantipyrine (CAS Number: 58-15-1). Start Potential: -1.2V, first vertex potential: 1V, end potential: -1.2V. Scan rate: 50 mV/s

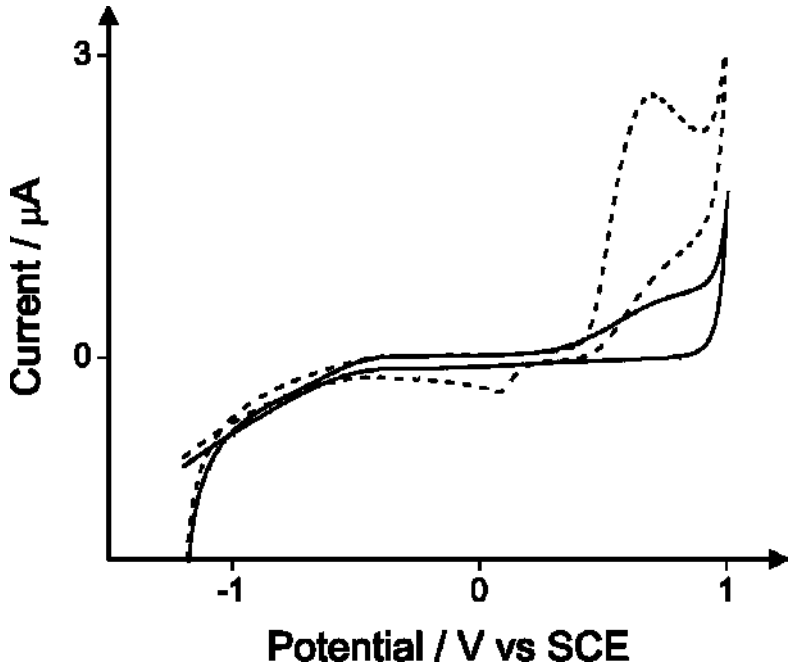

Figure 5.18 Cyclic Voltammetric response of the BDDE/SCE/Pt in the absence (solid line) and presence (dashed line) of 10 mg L^{-1} phenol in pH 10 carbonate buffer solution containing 400 mg L^{-1} Antipyrine (CAS Number: 60-80-0). Start Potential: -1.2V, first vertex potential: 1V, end potential: -1.2V. Scan rate: 50 mV/s

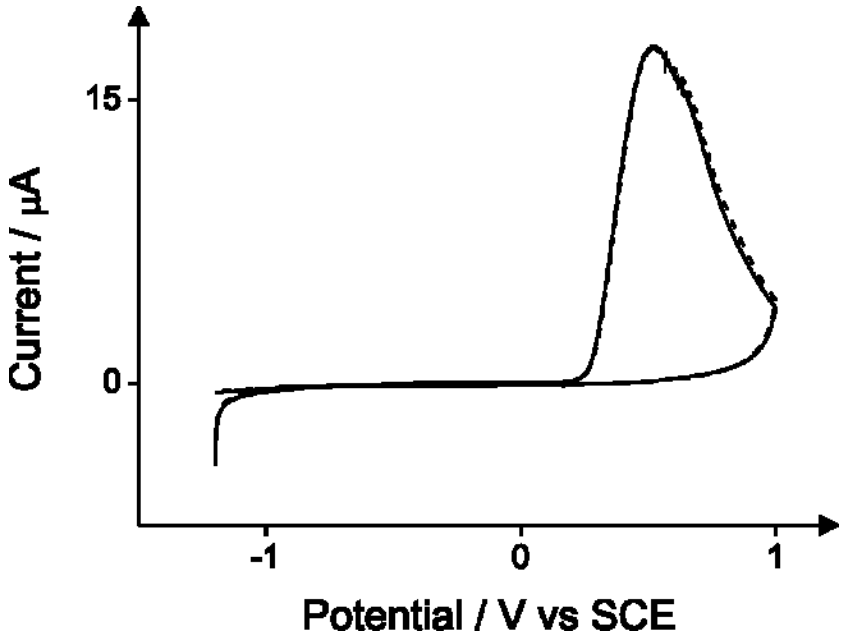

Figure 5.19 Cyclic Voltammetric response of the BDDE/SCE/Pt in the absence (solid line) and presence (dashed line) of 10 mg L^{-1} phenol in pH 10 carbonate buffer solution containing 400 mg L^{-1} 3-methyl-1-(2-phenylethyl)-2-pyrazolin-5-one. Start Potential: -1.2V, first vertex potential: 1V, end potential: -1.2V. Scan rate: 50 mV/s

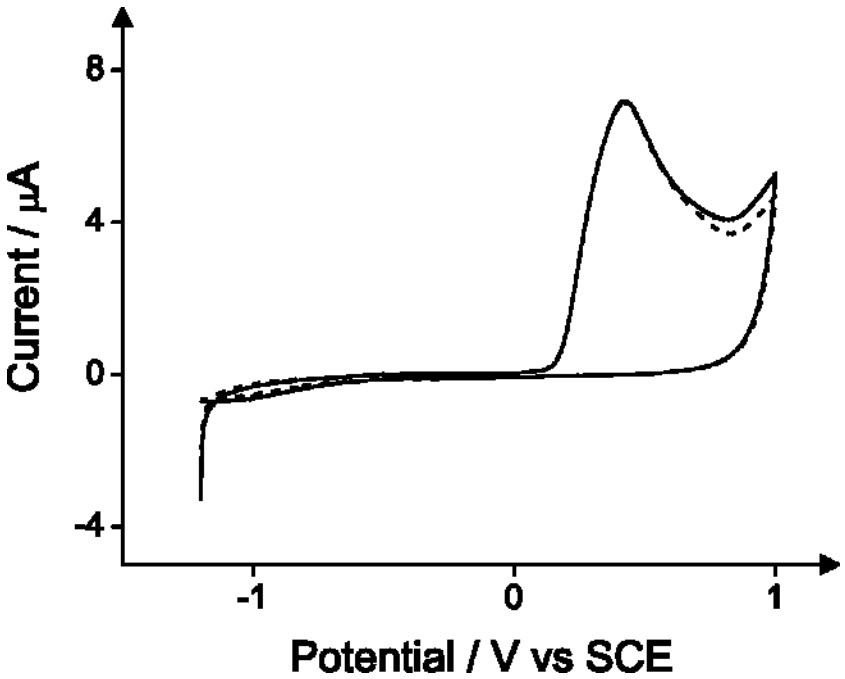

Figure 5.20 Cyclic Voltammetric response of the BDDE/SCE/Pt in the absence (solid line) and presence (dashed line) of 10 mg L^{-1} phenol in pH 10 carbonate buffer solution containing 400 mg L^{-1} 3-amino-1-(1-naphthylmethyl)-2-Pyrazolin-5-one. Start Potential: -1.2V, first vertex potential: 1V, end potential: -1.2V. Scan rate: 50 mV/s.

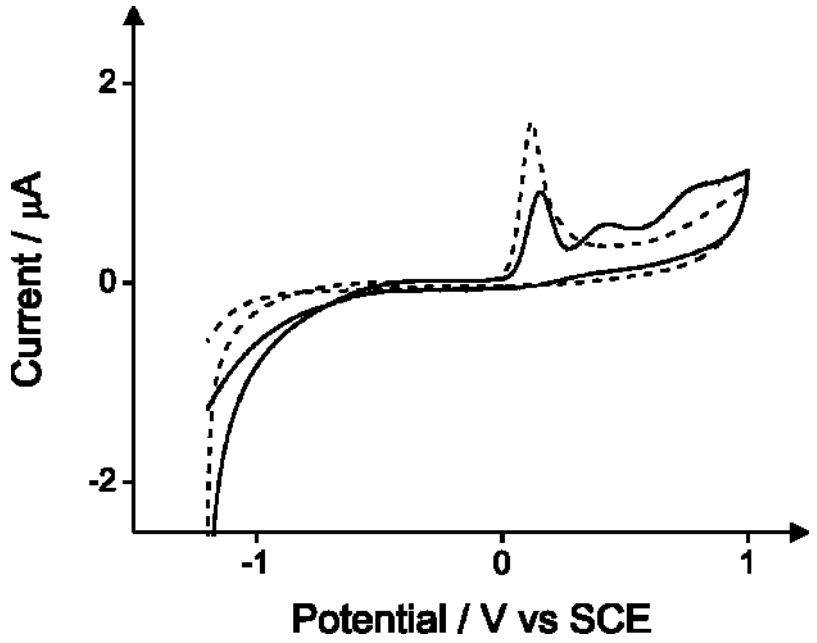

Figure 5.21 Cyclic Voltammetric response of the BDDE/SCE/Pt in the absence (solid line) and presence (dash line) of 10 mg L^{-1} phenol in Carbonate Buffer Solution pH 10 containing 400 mg L^{-1} 4-amino-1,2-dimethyl-3-pentadecyl-3-pyrazolin-5-one hydrochloride. Start Potential: -1.2V, first vertex potential: 1V, end potential: -1.2V. Scan rate: 50 mV/s

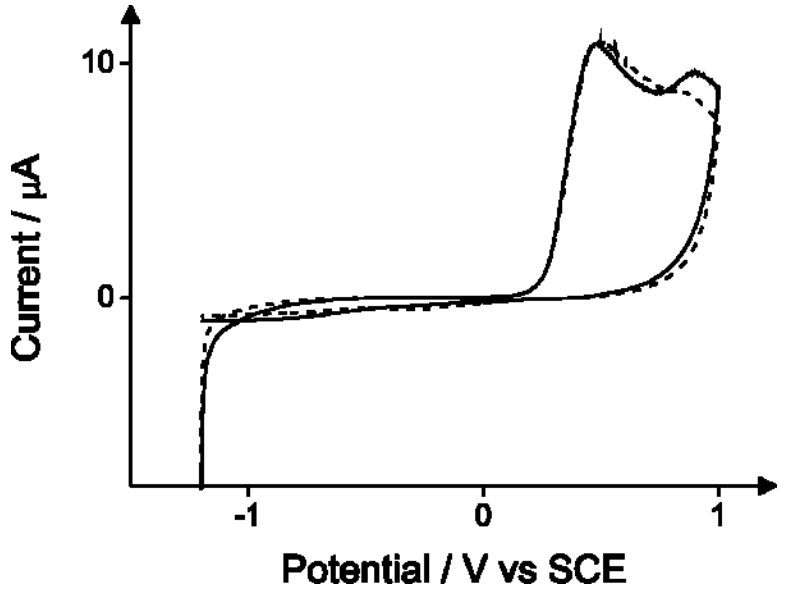

Figure 5.22 Cyclic Voltammetric response of the BDDE/SCE/Pt in the absence (solid line) and presence (dash line) of 10 mg L^{-1} phenol in pH 10 carbonate buffer solution containing containing 400 mg L^{-1} 3-amino-1-(2-amino-4-methylsulfonylphenyl)-2-pyrazolin-5-one hydrochloride. Start Potential: -1.2V, first vertex potential: 1V, end potential: -1.2V. Scan rate: 50 mV/s

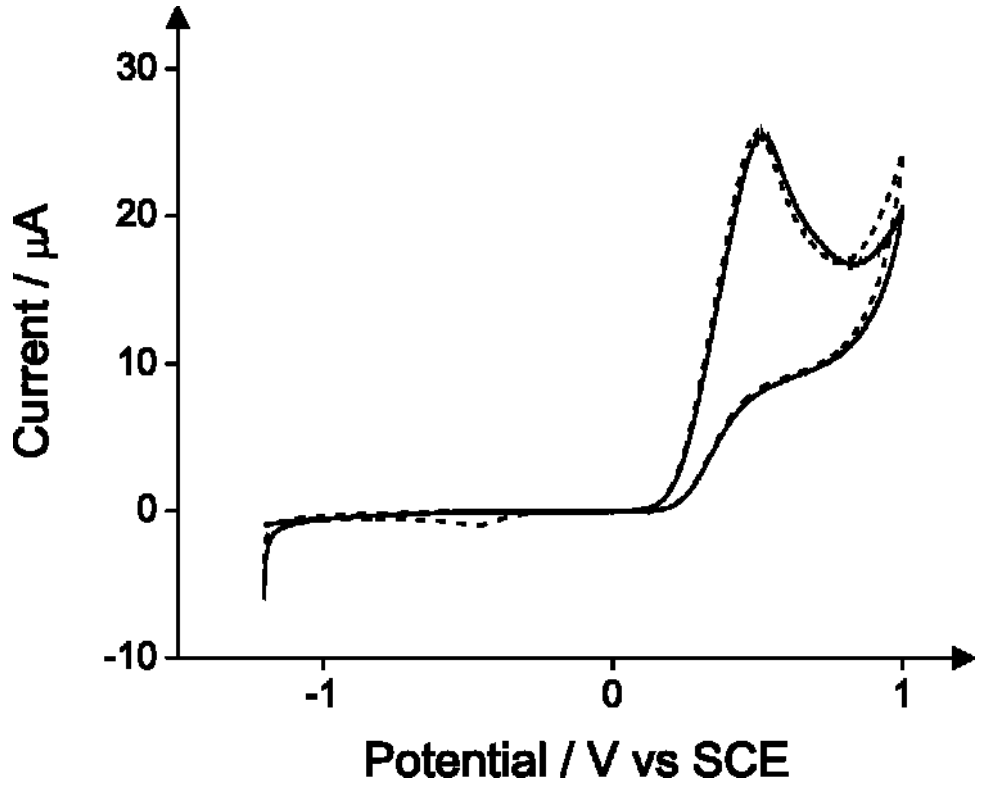

Figure 5.23 Cyclic voltammetric response of the BDDE/SCE/Pt in the absence (solid line) and presence (dashed line) of 10 mg L^{-1} phenol in pH 10 carbonate buffer solution containing 400 mg L^{-1} 4-Aminoantipyrine. Start Potential: -1.2V, first vertex potential: 1V, end potential: -1.2V. Scan rate: 50 mV/s

The reaction of the 4-Aminoantipyrine with the target phenol needs first the electrochemical oxidation of phenol to occur. For this purpose potassium ferricyanide is used in the standard optical method. The electrochemical oxidation of phenol alleviates the need of any oxidising agent. Figure 5.24 demonstrates that the use of ferricyanide ions at concentration 0.16 mg/mL does not optimise the analytical method. Additionally the potassium ferricyanide is of electrochemically active and as it can be seen in figure 5.25, its reduction to ferrocyanide at high concentration (1.6 mg/mL) induces a peak that overlaps with the analytical signal.

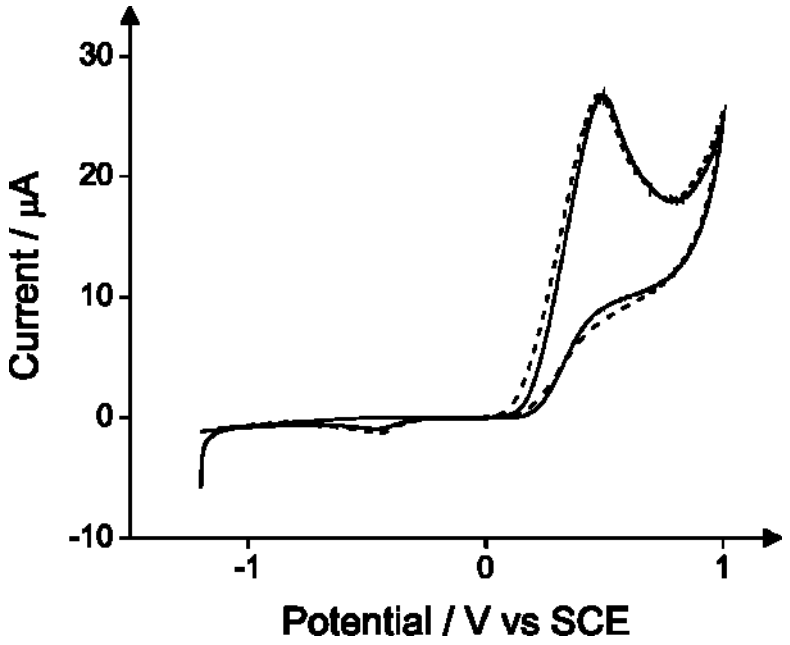

Figure 5.24 Cyclic voltammetric response of the BDDE/SCE/Pt upon 10 mg L^{-1} phenol in pH 10 carbonate buffer solution containing 400 mg L^{-1} 4-Aminoantipyrine in the absence (solid line) and presence (dash line) of 160 mg L^{-1} Potassium Ferricyanide. Start Potential: -1.2V, first vertex potential: 1V, end potential: -1.2V. Scan rate: 50 mV/s

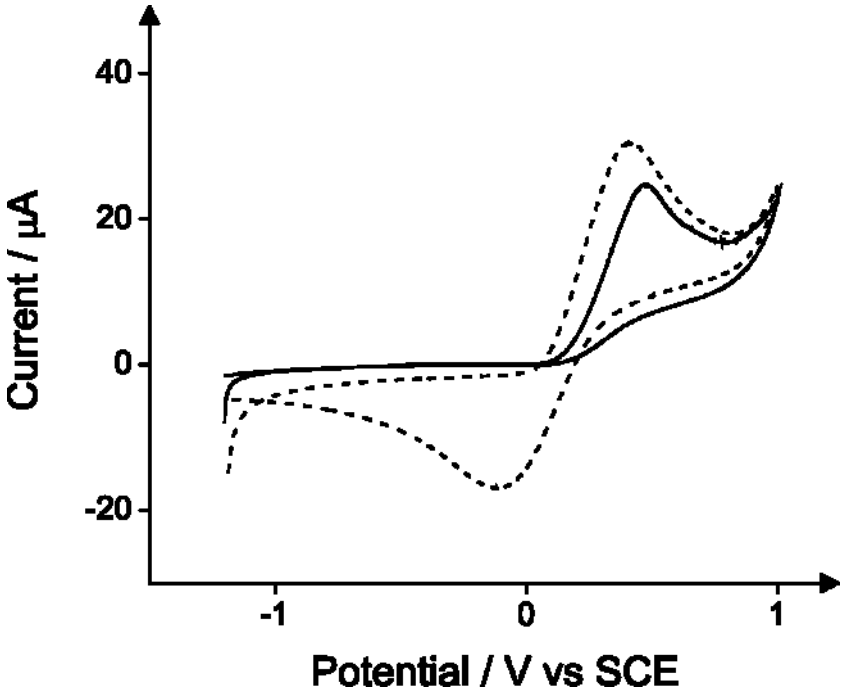

Figure 5.25 Cyclic voltammetric response of the BDDE/SCE/Pt recorded in pH 10 carbonate buffer solution containing 400 mg L^{-1} 4-Aminoantipyrine with the addition of 160 (solid line) and 1600 (dash line) mg L^{-1} Potassium Ferricyanide. Start Potential: -1.2V, first vertex potential: 1V, end potential: -1.2V. Scan rate: 50 mV/s

The pH is a crucial parameter which needs to be explored. As depicted in figure 5.26, it is evident that pH 10 is the optimum for the electrochemically detection of phenols with 4-Aminoantipyrine as at pH 10 the highest peak height has been observed.

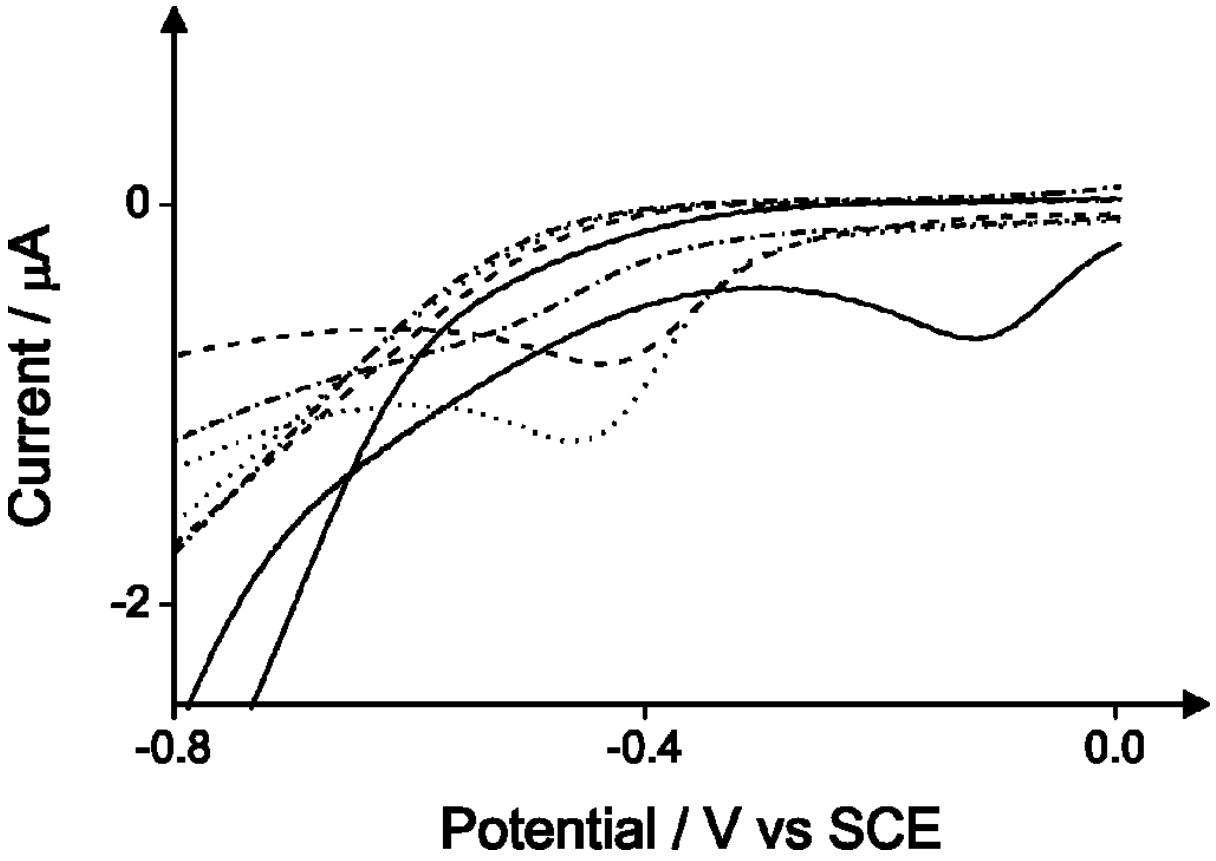

Figure 5.26 Voltammetric response (reductive curves) of the BDDE/SCE/Pt recorded within pH 3.5 acetate buffer solution (solid line), Phosphate Buffer solution (PBS) pH 7.5 (dashed line), Carbonate Buffer Solution (CBS) pH 10 (dotted line) and NaOH Buffer Solution pH 13 (dashed dotted line) containing 400 mg L^{-1} 4-Aminoantipyrine with the addition of 10 mg L^{-1} Phenol. Start Potential: -1.2V, first vertex potential: 1V, end potential: -1.2V. Scan rate: 50 mV/s

The detection of phenol and three chlorophenols, namely 2-Chlorophenol, 4-Chlorophenol and 2,4-Dichlorophenol in drinking water was the main subject of this investigation. The limits of detection (LOD) for these four compounds with the proposed method using cyclic voltammetry on boron-doped diamond electrode are 500 µg L^{-1}, 300 µg L^{-1}, 750 µg $L^{-1}$and 1000 µg L^{-1} respectively in drinking water adjusted to pH 10. Corresponding calibration plots are shown in figures 5.27-5.30.

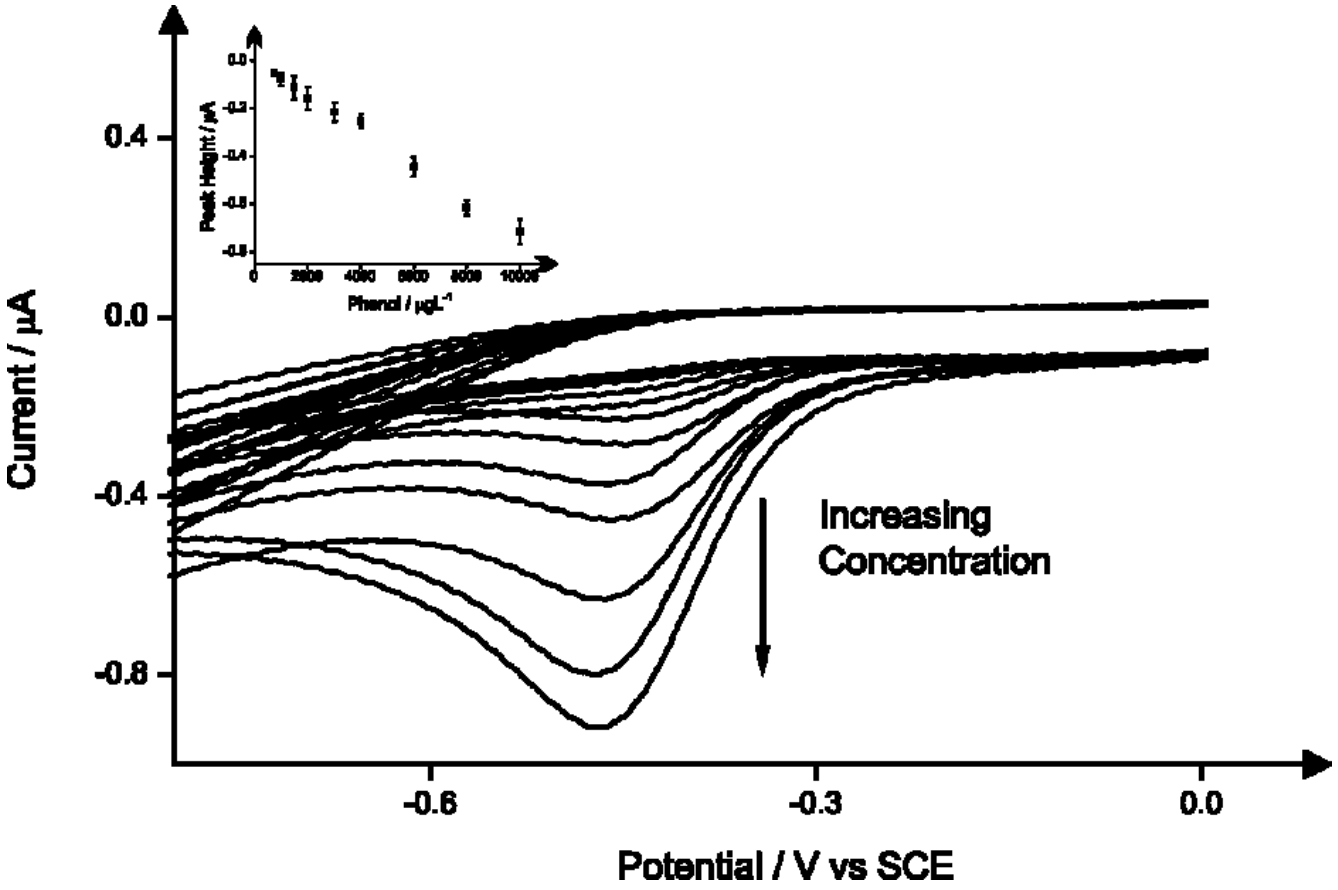

Figure 5.27 Cyclic voltammetric response (reductive peak) arising from additions of phenol into drinking water (tap) sample adjusted to pH 10 using a BDDE/SCE/Pt . The solution contains 400 mg L^{-1} 4-Aminoantipyrine with the additions of phenol in µg L^{-1}. Start Potential: -1.2V, first vertex potential: 1V, end potential: -1.2V. Scan rate: 50 mV/s. Error bars arise from three measurements.

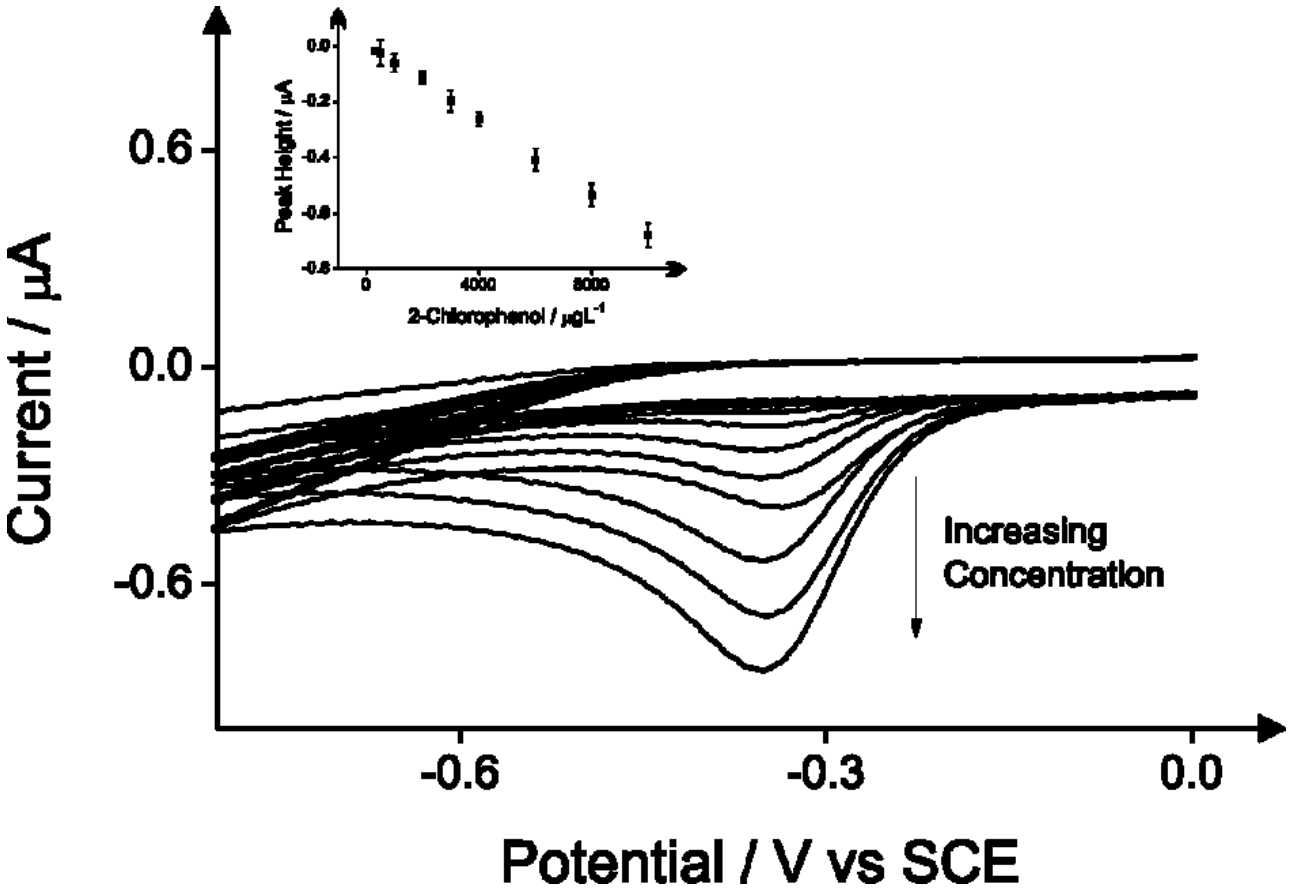

Figure 5.28 Cyclic voltammetric response (reductive peak) arising from additions of 2-Chlorophenol into drinking water (tap) sample adjusted to pH 10 using a BDDE/SCE/Pt . The solution contains 400 mg L^{-1} 4-Aminoantipyrine with the additions of 2-Chlorophenol in µg L^{-1}. Start Potential: -1.2V, first vertex potential: 1V, end potential: -1.2V. Scan rate: 50 mV/s. Error bars arise from three measurements.

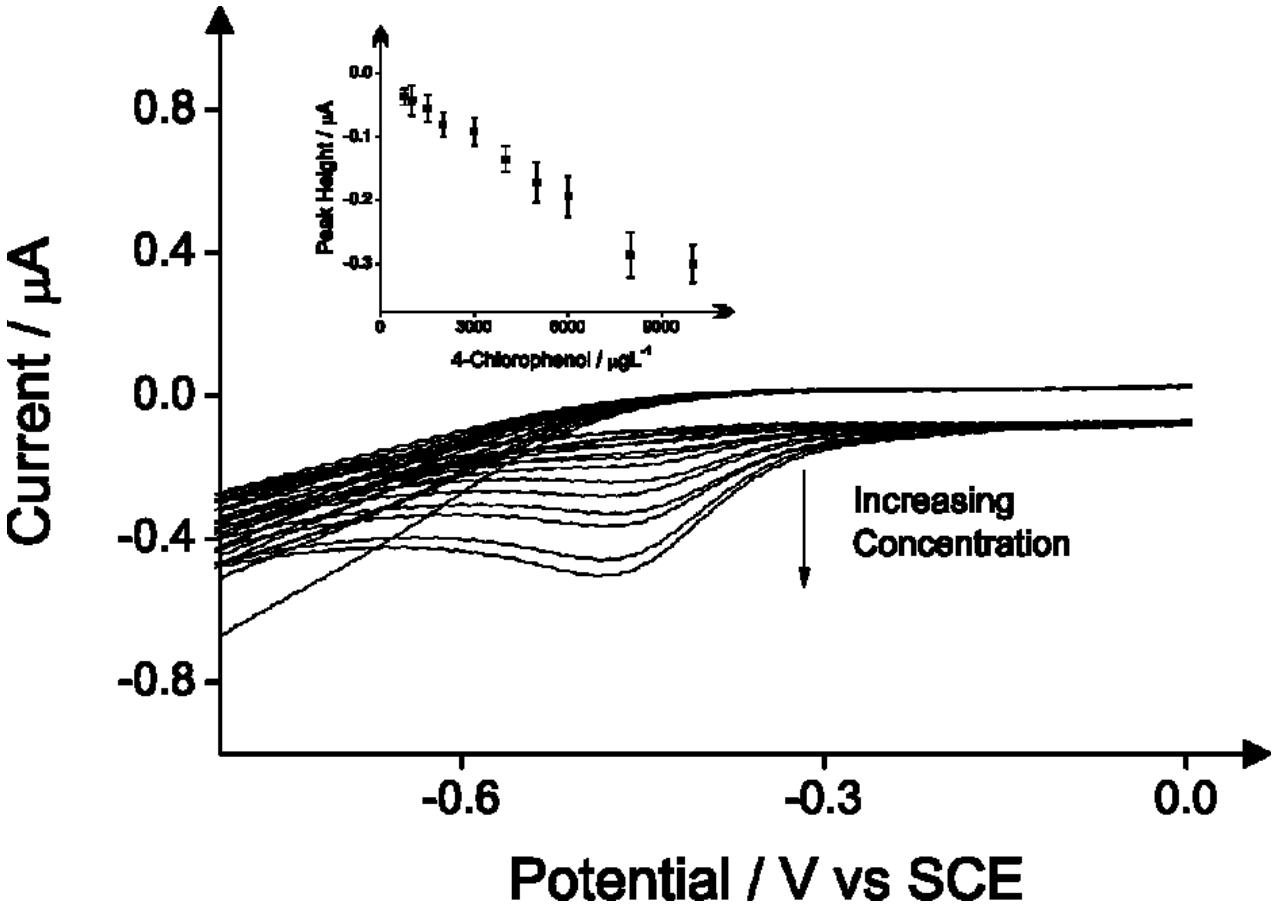

Figure 5.29 Cyclic voltammetric response (reductive peak) arising from additions of 4-Chlorophenol into drinking water (tap) sample adjusted to pH 10 using a BDDE/SCE/Pt . The solution contains 400 mg L^{-1} 4-Aminoantipyrine with the additions of 4-Chlorophenol in µg L^{-1}. Start Potential: -1.2V, first vertex potential: 1V, end potential: -1.2V. Scan rate: 50 mV/s. Error bars arise from three measurements.

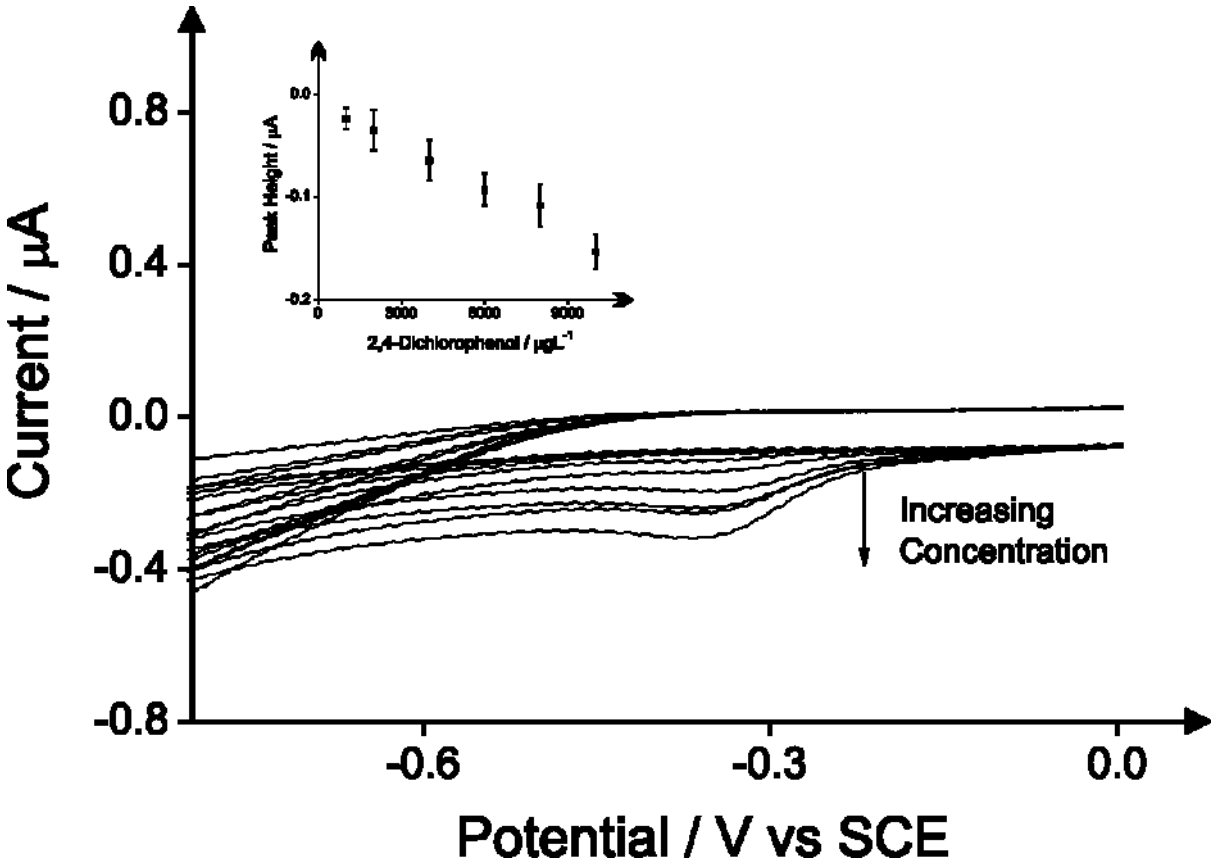

Figure 5.30 Cyclic voltammetric response (reductive peak) arising from additions of 2.4-Dichlorophenol into drinking water (tap) sample adjusted to pH 10 using a BDDE/SCE/Pt . The solution contains 400 mg L^{-1} 4-Aminoantipyrine with the additions of 2,4-Dichlorophenol in µg L^{-1}. Start Potential: -1.2V, first vertex potential: 1V, end potential: -1.2V. Scan rate: 50 mV/s. Error bars arise from three measurements.

The relative high detection limits of the proposed electrochemical method with the 4-AAP leads this work to consider the direct oxidation of phenol and chlorophenols, which is known to be attainable from inspection of the literature. [271-275] Consequently voltammetric responses of the boron-doped diamond electrode using the same experimental parameters without the addition of 4-AAP took place for Phenol, 2-Chlorophenol, 4-Chlorophenol and 2,4-Dichlorophenol. Calibration Plots for both the oxidation and reduction peaks of these four phenols are shown in figures 5.31, 5.32, 5.33, 5.34 respectively.

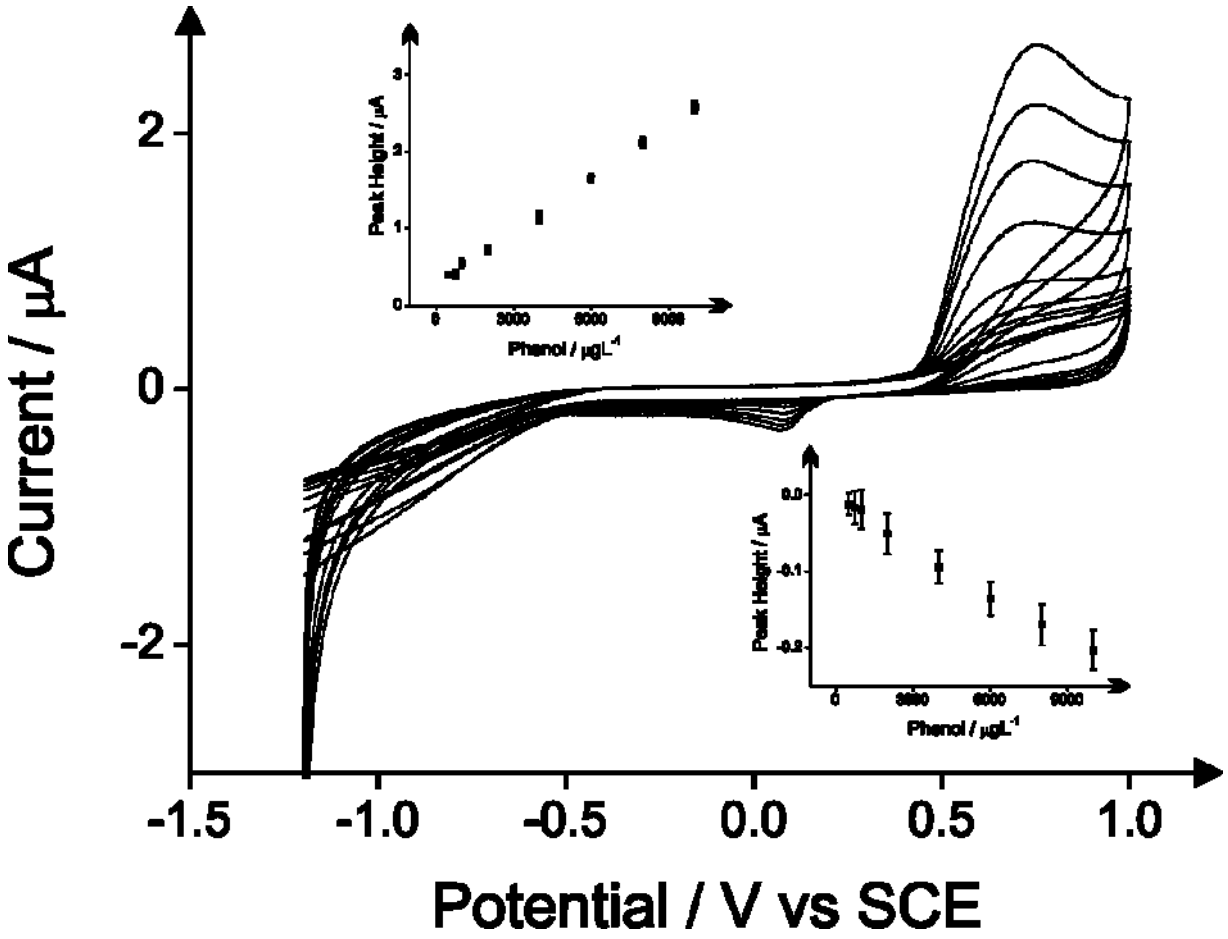

Figure 5.31 Cyclic voltammetric response of the BDDE/SCE/Pt upon additions of phenol into a drinking water (tap) sample adjusted to pH 10. Start Potential: -1.2V, first vertex potential: 1V, end potential: -1.2V. Scan rate: 50 mV/s. Error bars arise from three measurements.

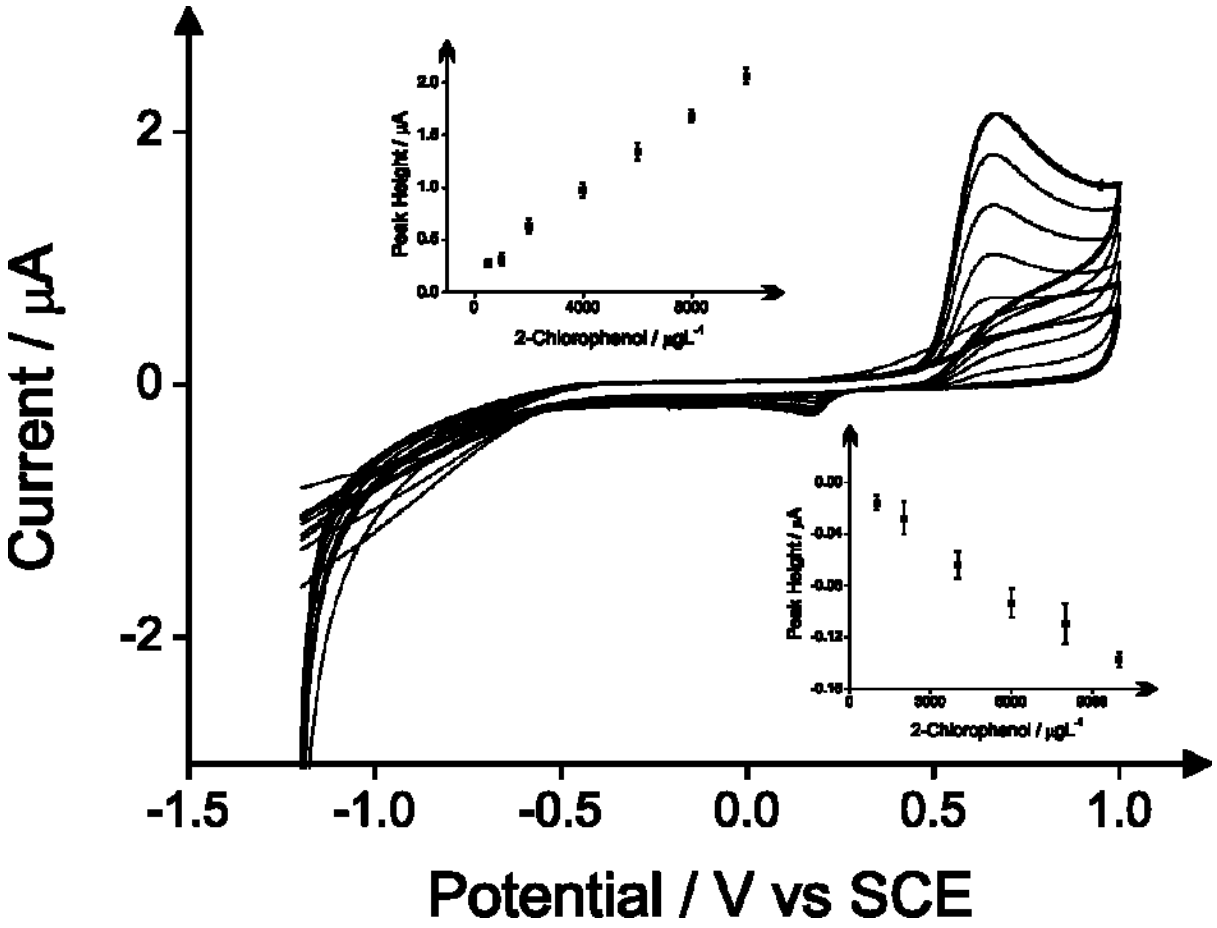

Figure 5.32 Cyclic voltammetric response of the BDDE/SCE/Pt upon additions of 2-Chlorophenol into a drinking water (tap) sample adjusted to pH 10. Start Potential: -1.2V, first vertex potential: 1V, end potential: -1.2V. Scan rate: 50 mV/s. Error bars arise from three measurements.

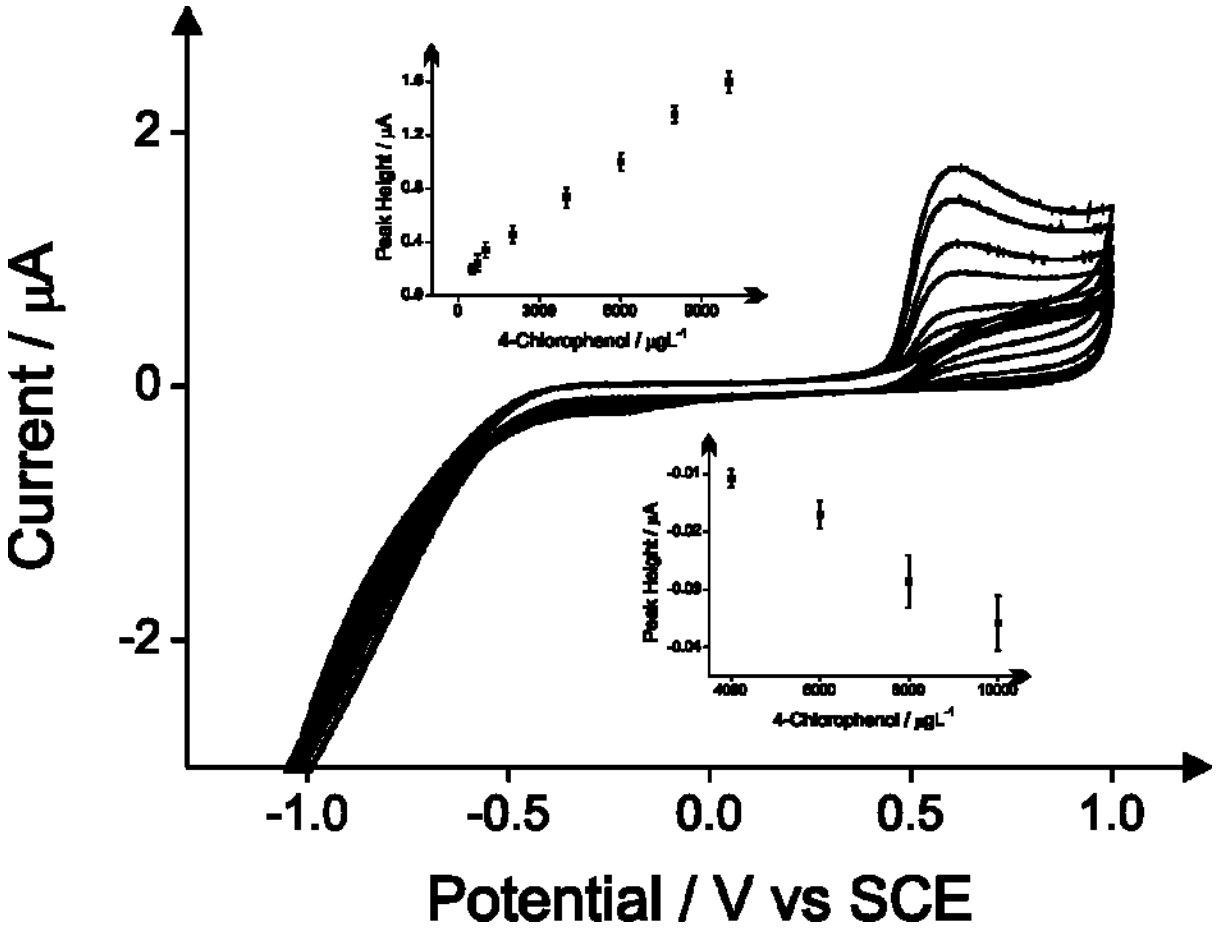

Figure 5.33 Cyclic voltammetric response of the BDDE/SCE/Pt upon additions of 4-Chlorophenol into a drinking water (tap) sample adjusted to pH 10. Start Potential: -1.2V, first vertex potential: 1V, end potential: -1.2V. Scan rate: 50 mV/s. Error bars arise from three measurements.

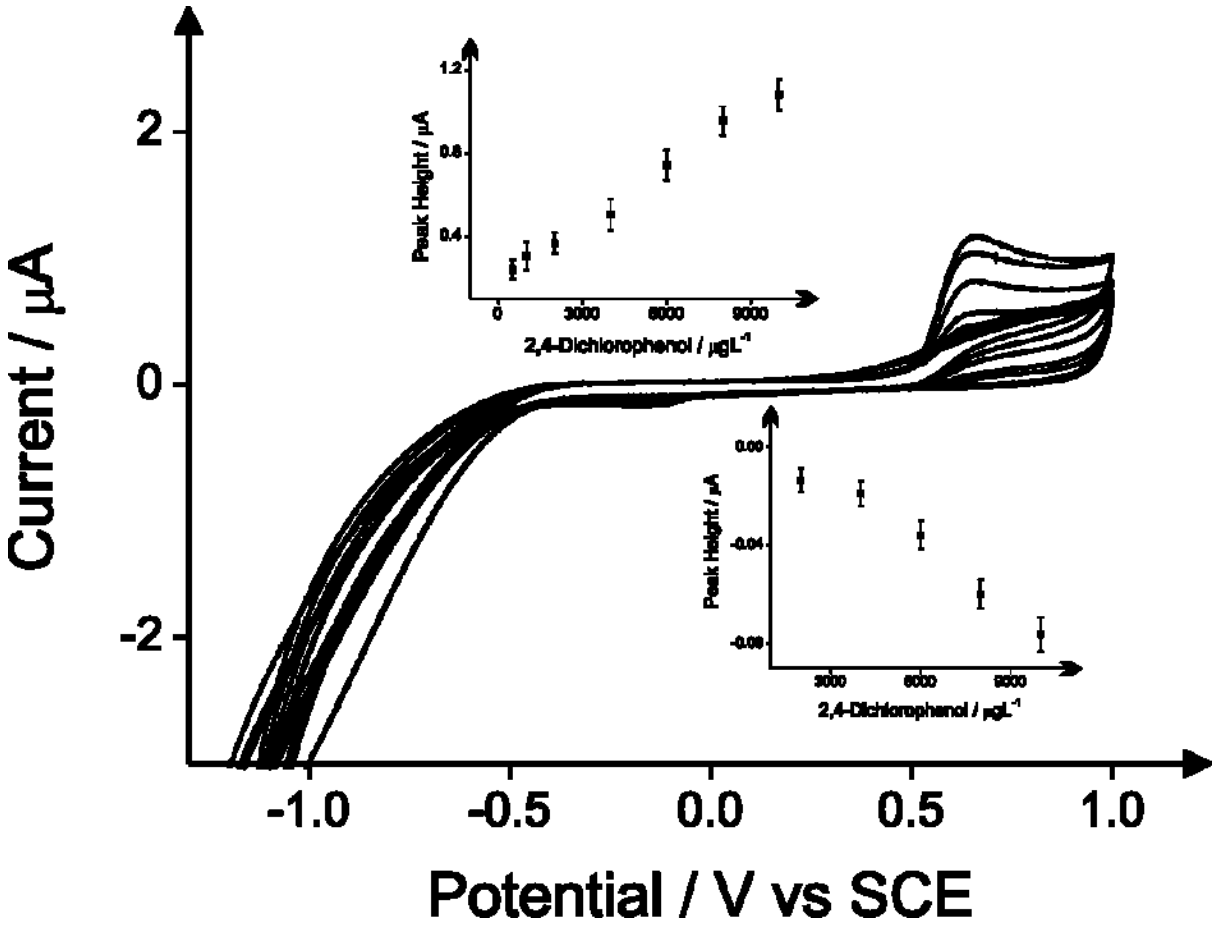

Figure 5.34 Cyclic voltammetric response of the BDDE/SCE/Pt upon additions of 2,4-Dichlorophenol into a drinking water (tap) sample adjusted to pH 10. Start Potential: -1.2V, first vertex potential: 1V, end potential: -1.2V. Scan rate: 50 mV/s. Error bars arise from three measurements.

Figure 5.35 is a comparison of the two reduction peaks in the case of 2-Chlorophenol by using or not 4-AAP. In the presence of 4-AAP the reduction peak prevails over the reduction peak oming from the direct reduction of 2-Chlorophenol in the absence of 4-AAP.

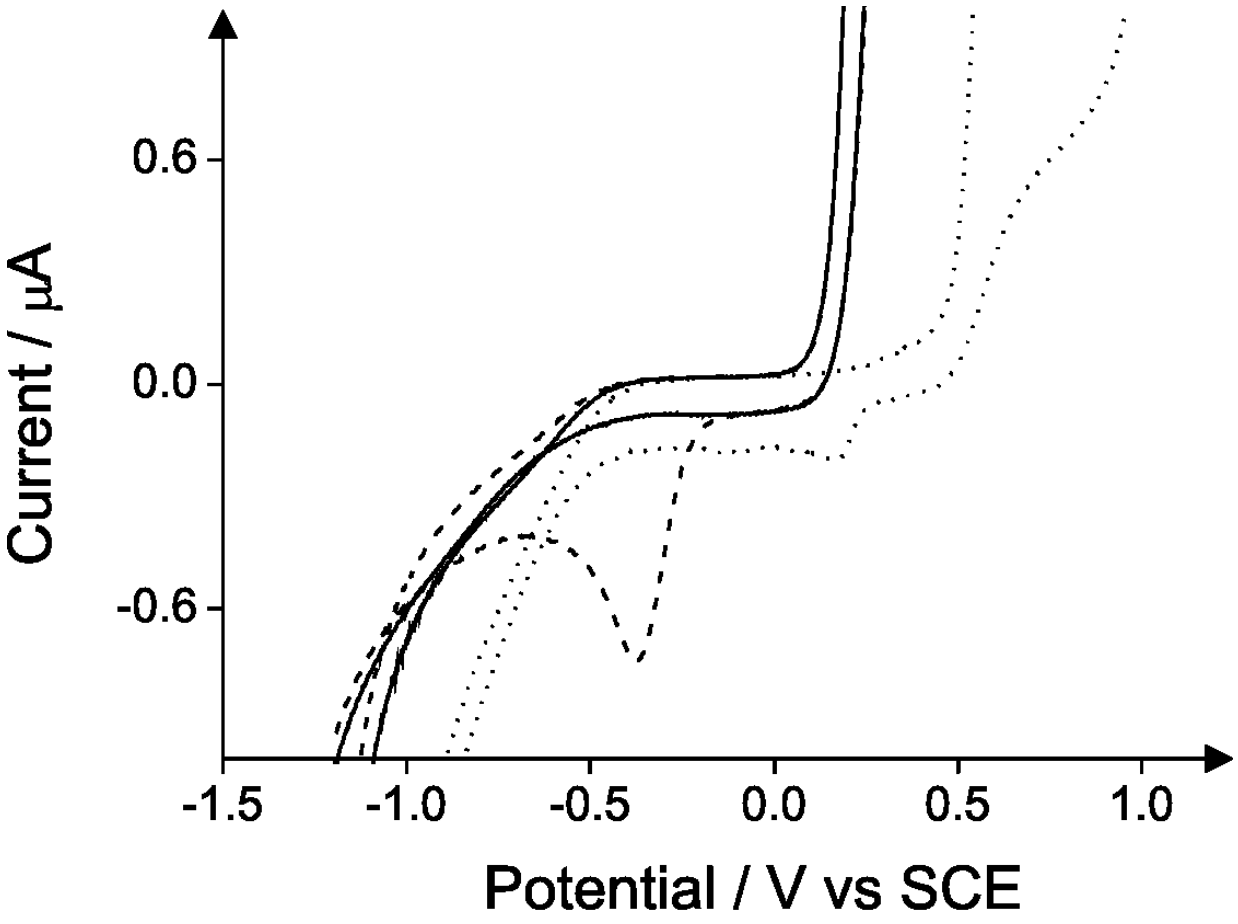

Figure 5.35 Cyclic voltammetric responses of the BDDE/SCE/Pt using 400 mg L^{-1} 4-AAP (solid line), 400 mg L^{-1} 4-AAP and 10 mg L^{-1} 2-Chlorophenol (dashed line) and 10 mg L^{-1} 2-Chlorophenol (dotted line) into a drinking water (tap) sample adjusted to pH 10. Start Potential: -1.2V, first vertex potential: 1V, end potential: -1.2V. Scan rate: 50 mV/s.

The comparison of the three analytical peaks for the electrochemical detection of phenols is presented in the four tables below (Tables 5.2 to 5.5) for each of the four phenols studied. The three analytical peaks refer to the oxidation peak of phenols without the addition of 4-AAP, the reduction peak of the oxidised phenols without the addition of 4-AAP and the reduction of the oxidised product of the reaction between the phenols and the 4-AAP. All the peaks are responses obtained using a boron-doped diamond electrode in drinking water adjusted pH 10, which was proved as the optimum electrode for this method based on literature reports due to its wide potential window, low background current and avoidance of passivation. These comparisons are based upon the lowest detection limits and the coefficient of determination that are possible. The potential where the voltammetric peaks appear is displayed as well.

In case of phenol limit of detection 500 μg L^{-1} is reached using all the three analytical peaks. The coefficient of the direct oxidation of Phenol is relatively higher (see Table 5.2). In case of 2-Chlorophenol the reduction peak of its product after its reaction with the 4-AAP displays the lowest limit of detection which is 300 μg L^{-1}(see Table 5.3). In case of 4-chlorophenol the lowest detection limit of 500 μg L^{-1} can be reached when the direct oxidation peak is used as analytical peak (see Table 5.4). Finally the detection of 2,4-Dichlorophenol by utilizing again the direct oxidation peak as analytical peak exhibits the lowest detection limit of 500 μg L^{-1} (see Table 5.5).

Table 5.2 Comparison of the analytical peaks for the direct (in the absence of 4-AAP) and indirect (in the presence of 4-AAP) electrochemical detection of phenol.

	Limit of detection ($\mu g\ L^{-1}$)	**Peak position (V) of 10 mg L^{-1} Phenol**	**R-Squared value**
Oxidation of Phenol	500	0.757	0.9973 (8 points)
Reduction of phenol	500	0.082	0.9934 (8 points)
Reduction of its product with 4-AAP	500	-0.465	0.9936 (9 points)

Table 5.3 Comparison of the analytical peaks for the direct (in the absence of 4-AAP) and indirect (in the presence of 4-AAP) electrochemical detection of 2-Chlorophenol.

	Limit of detection ($\mu g\ L^{-1}$)	**Peak position (V) of 10 mg L^{-1} 2-Chlorophenol**	**R-Squared value**
Oxidation of 2-Chlorophenol	500	0.669	0.9988 (8 points)
Reduction of 2-Chlorophenol	1000	0.172	0.9893 (6 points)
Reduction of its product with 4-AAP	300	-0.352	0.9940 (9 points)

Table 5.4 Comparison of the analytical peaks for the direct (in the absence of 4-AAP) and indirect (in the presence of 4-AAP) electrochemical de tection of 4-Chlorophenol.

	Limit of detection (µg L^{-1})	**Peak position (V) of 10 mg L^{-1} 4-Chlorophenol**	**R-Squared value**
Oxidation of 4-Chlorophenol	500	0.589	0.9973 (8 points)
Reduction of 4-Chlorophenol	4000	-0.179	0.9869 (4 points)
Reduction of its product with 4-AAP	750	-0.474	0.9831 (10 points)

Table 5.5 Comparison of the analytical peaks for the direct (in the absence of 4-AAP) and indirect (in the presence of 4-AAP) electrochemical detection of 2,4-Dichlorophenol.

	Limit of detection (µg L^{-1})	**Peak position (V) of 10 mg L^{-1} 2,4-Dichlorophenol**	**R-Squared value**
Oxidation of 2,4-Dichlorophenol	500	0.654	0.9924 (7 points)
Reduction of 2,4-Dichlorophenol	2000	-0.152	0.9650 (5 points)
Reduction of its product with 4-AAP	1000	-0.358	0.9860 (6 points)

5.3.4 CONCLUSIONS

The indirect determination of phenol, 2-Chlorophenol, 4-Chlorophenol and 2,4-dichlorophenol by electrochemically adapting the 4-Aminoantipyrine optical method is examined for the first time in drinking water. This electrochemical adaptation allows the determination of the phenol, 2-Chlorophenol, 4-Chlorophenol and 2,4-Dichlorophenol with limits of detection 500 μg L^{-1}, 300 μg L^{-1}, 750 μg L^{-1} and 1000 μg L^{-1} respectively without the use of an oxidant agent. Furthermore, other pyrazoline substitution products (apart from the 4-Aminoantipyrine) are evaluated for the detection of phenol. Finally the comparison of the direct (without mediator) and the proposed indirect determination (with 4-Aminoantipyrine) of the phenol and the three chlorophenols is presented. The detection limits achieved in drinking water by the proposed electrochemical indirect method are lower than that by the direct method in case of 2-Chlorophenol but higher in case of Phenol, 4-Chlorophenol and 2,4-Dichlorophenol comparing to the data received when their direct oxidation peak is analysed. Such work, thus then questions the need for the indirect electrochemical sensing protocol even with its advantage of alleviating the need for the oxidising agent.

CHAPTER 6

ELECTROANALYSIS IN ENVIRONMENTAL SAMPLES-EUTROPHICATION

ELECTROANALYTICAL SENSING OF DISSOLVED PHOSPHORUS UTILISING SCREEN-PRINTED GRAPHITE MACROELECTRODES

6.1 ABSTRACT

Phosphorus is one of the key indicators of eutrophication levels in natural waters where it exists mainly as dissolved phosphorus**.** Various analytical protocols exist to provide an offsite analysis and a point of site analysis is required. The current standard method recommended by Environmental Protection Agency (EPA) for the detection of total phosphorus is colorimetric and is based on the colour of the phosphomolybdate complex formed as a result of the reaction between phosphates and molybdates ions where ascorbic acid and antimony potassium tartrate are added and serve as reducing agents which convert all forms of phosphorus into orthophosphates. The work reported in this chapter details the electrochemical adaptation of the colorimetric determination of dissolved phosphorus using screen-printed graphite macroelectrodes; such work has not been reported before.

This novel indirect electrochemical sensing protocol allows the determination of dissolved phosphorus over the range 0.5 to 20 μg L^{-1} in pH 1 buffer solutions utilising cyclic voltammetry with a theoritical limit of detection (3σ) found to correspond to 0.3 μg L^{-1} of phosphorus. The reaction time and influence of foreign ions (potential interferents) upon this electroanalytical protocol is also investigated where it was found that unlike the standard colourimetric method, where a reaction time of 5 minutes is required before the colourimetric measurement is not necessary in the electrochemical adapted protocol. The electrochemical method was validated through the quantification of phosphates and total dissolved phosphorus determination in polluted water samples (canal water samples) with ion chromatography and ICP-OES respectively.

This novel electrochemical protocol exhibits advantages over the established and EPA recommended colorimetric determination for total phosphorus with lower detection limits and

shorter experimental times. Additionally this electrochemical adaptation allows the determination of phosphorus without the use of ascorbic acid and antimony potassium tartrate as reducing agents (as used in the colourmetric method) eliminating any possible interferences from the instability of ascorbic acid.

6.2 INTRODUCTION

The nutrients phosphorus and nitrogen play critical roles for living cells but their excess leads to nutrient pollution or over-enrichment [276] which is one of the most extended, expensive and challenging environmental problems.[277] High levels of nutrients is the main cause of eutrophication where growth of algal and plankton increase to a substantial extent (known as algal bloom).[278] Eutrophication results in reduction or elimination of dissolved oxygen which is crucial for fish and other aquatic life. Some algal blooms produce toxins [279-282] which are harmful for humans if they come in contact with this polluted water, consume tainted shellfish [280], or drink contaminated water.[283, 284] The biogeochemical cycle of phosphorus is vast but very slow [285] and human activities have caused significantly acceleration of the natural phosphorus cycle. The mining of phosphorus-rich rock to produce plant fertilizers is the major intervention of human activity in the phosphorus cycle.[286] The use of phosphorus in agriculture can contaminate natural water such as lakes and sea via rivers; the use of phosphorus within domestic detergents is another source of phosphorus in natural water through sewage disposal. [286]

Phosphorus can exist in natural water in three broad classes: orthophosphates, condensed phosphates (pyro-, meta-, and poly-) and organic phosphorus.[278] However, soluble phosphorus in natural water mainly consists of orthophosphates. Other forms of soluble phosphates like organic phosphates and polyphosphates are eventually hydrolysed into orthophosphates. Orthophosphates, according to pH, can exist as phosphoric acid (H_3PO_4), dihydrogen phosphate ($H_2PO_4^-$), hydrogenophosphate (HPO_4^-) and phosphate ion (PO_4^{3-}). The percentage distribution of orthophosphates is dependent upon the pH; such dependency is shown in figure 6.1. The low limits of the phosphorus concentrations in natural waters can be several micrograms per litre [287] and additionally it is the key indicator of eutrophication level in natural waters. [288]

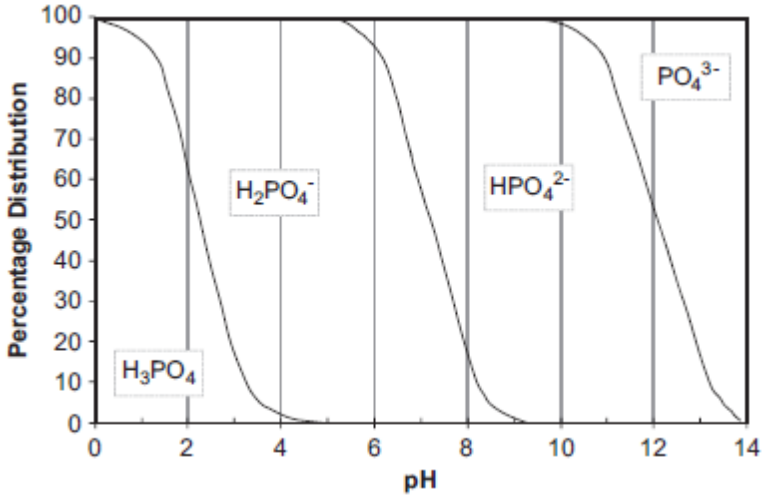

Figure 6.1 Percentage of orthophosphate species as a function of pH at 25^0C and 1 atmosphere pressure. Image taken from reference [289]

As small differences of phosphorus concentrations can have a pronounced impact on streams, less sensitive methods should be utilised only to identify serious eutrophication problems.[277] The measurement of low concentrations (less than 10 μg L^{-1}) of phosphorus in natural water makes the monitoring of phosphorus challenging. The majority of methods to quantify phosphorus are based on the detection of orthophosphates following a digestion process which involves acidifying and gently boiling in order to convert all the various forms of phosphorus (orthophosphate, condensed phosphate and organic phosphate) into orthophospates.[290] Through filtering of this sample, dissolved phosphorous can be determination or alternatively, not filtering allows total phosphorus to be determined. There are chromatographic [291] fluorescence [292] and spectrophotometric methods for the determination of total phosphorus.[293-295] The EPA recommended current standard method for the detection of phosphorus is colorimetric.[296] In this approach, ammonium molybdate, ascorbic acid and antimony potassium tartrate are all added in unison to acidified samples in order to form the blue coloured a-keggin anion, ammonium phosphomolybdate. The reaction is as follows:[297, 298]

$$7PO_4^{3-} + 12Mo_7O_{24}^{6-} + 72H^+ \Rightarrow 7PMo_{12}O_{40}^{3-} + 36H_2O \qquad (1)$$

The concentration of phosphate is proportional to the blue colour of the sample and is determined spectrophotometrically. This method suffers from refractive index errors and

turbidity interference.[287, 299] For this reason electrochemical methods have been explored and reported for phosphate detection. A variety of electrode substrates and analytical methods have been reported for the determination of phosphates as it is shown in Table 6.1. Such approaches have utilised metal electrodes, ion selective membranes enzyme based electrodes, [300-302] gold and glassy-carbon modified electrodes, [303] modified carbon paste electrodes, [302, 304] cobalt wire ion selective electrodes, [305, 306] lead ion selective electrodes, [307] and cobalt phthalocyanide modified screen-printed electrodes as amperometric sensors. [163, 308]

Table 6.1 Summary of amperometric and voltammetric methods for the detection of phosphates applied to its analysis in water samples.

Method	Linear Range (µg L^{-1} of P)	Limit of Detection (µg L^{-1} of P)	Application	Ref
Amperometric biosensor based on pyruvate oxidase for the determination of pyruvate and phosphate	30.97-309.7	30	Phosphates in buffer solution	300
Amperometric sensor based on platinum electrode based on bienzyme membrane with co-immobilized nucleoside phosphorylase and xanthine oxidase was used for the detection of enzymatically generated hydrogen peroxide	3-300	3	Phosphates in real samples	301
Electrochemiluminescence technique based on the combination of liquid–liquid extraction with benzene-modified carbon paste electrode	0.2-10	0.2	Phosphates in real samples	302
Anodic oxidation of molybdenum at gold and glassy-carbon working electrode	3.7-161.4	3.7	Phosphates in Seawater	303
Associated decrease in free lead ion concentration is measured by a lead ion-selective electrode		31	Phosphates in river water	307
Cobalt phthalocyanine	77-4026	62	Phosphates in	163

screen-printed carbon electrode (CoPC-SPCE)			pond water samples	
Reduction of phosphomolybdate complex at a carbon paste electrode	31-620	9	Phosphates in Seawater	[309]
Reduction of phosphomolybdate complex at a glassy carbon electrode by flow-injection amperometry incorpotrating an ion exchange preconcentration column	0.1-10	0.2	Dissolve phosphorus in fresh and marine samples	[299]

Consequently, in this chapter, the established colorimetric protocol by using molybdate ions as complexing agent is electrochemically adapted and thus there is no need of use of ascorbic acid and antimony potassium tartrate as reducing agents eliminating any possible interferences from the instability of ascorbic acid.[310, 311] The reduction of the phosphomolybdate ion is accomplished electrochemically. The present electro-analytical protocol maintains the high sensitivity and selectivity of the standard colorimetric method and additionally reaches lower detection limits, minimizes the experimental time and simplifies the procedure using fewer reagents. This indirect electroanalytical protocol is found to exhibit a limit of detection (3σ) of 0.3 μg L^{-1} of phosphorus over the range 0.5 to 20 μg L^{-1} applied successfully in canal water; through inspection of this

6.3 EXPERIMENTAL

The phosphate standard solutions were prepared with pre-dried (105°C for one hour) potassium dihydrogen phosphate. [290] The molybdate stock solution was a 0.8% w/v ammonium molybdate tetrahydrate solution. Interfering solutions were made with sodium nitrite, sodium nitrate and sodium bicarbonate. All the solutions including the sample from canal water were adjusted to pH 1 with 11N sulphuric acid[290] in accordance with the optical method in order to avoid possible interference of silicate.[287, 303]

The canal water utilised was obtained in a plastic container from Manchester's city centre. The sample was filtered with a 0.45μm filter from Millipore and then stored at room temperature and used within a day of sampling.

The persulfate digestion for the detection of total dissolved phosphorus (orthophosphates, organic and hydrolysable phosphorus) took place according the EPA's standard colorimetric method where 50 mL of 100 times diluted canal water were transferred into a 125 mL Erlenmeyer flask and 1 mL of 11 N sulfuric acid was added. After the addition of 0.4 g ammonium persulfate, the sample was mixed and boiled gently for 30-40 minutes until a final volume of about 10 mL is reached. It was left in order to reach the room temperature, diluted to 40 mL and filtered. 5.2gr of sodium bisulphite was added and the solution was mixed and placed in a 95°C water bath for 30 minutes.[290] The final solution was cooled and diluted to 50 mL. The total phosphorus was determined after this procedure according to the method used for the orthophosphates.

The ion chromatography for the detection of soluble orthophosphates in real sample performed by Dionex, ICS-2000 Ion Chromatography System accompanied by Dionex IonPac AG18 as guard column and Dionex IonPac AS18 as separation column.

The inductively coupled plasma optical emission spectrometry (ICP-OES) for the detection of the total dissolved phosphorus in real sample performed by Thermo Scientific DUO iCAP 6300 ICP Spectrometer.

In accordance to the EPA's standard colorimetric method, the concentrations of orthophosphates and total phosphorus in this paper are reported as phosphorus P which is approximately three times lower than the concentration in phosphates.

6.4 RESULTS AND DISCUSSION

The colorimetric method for the determination of orthophosphates requires antimony potassium tartrate and ascorbic acid as reducing agents. The proposed electrochemical adaptation of this method avoids the use of these reducing agents since the product ammonium phosphomolybdate of the complexing reaction can be electrochemically interrogated.

The voltammetric response of the SPGEs towards 640 mg L^{-1} ammonium molybdate tetrahydrate at pH 1 with and without the addition of 20 μg L^{-1} phosphorus is shown in figure 6.2. Two reduction peaks at +0.27V and at +0.13V are observed which are likely due to electrochemical reduction of Mo(VI)→Mo(IV) and Mo(IV)→Mo(II) respectively [287]. The two corresponding oxidation peaks observed at +0.16V and at +0.30V are likely due to the

electrochemical oxidation of Mo(II)→Mo(IV) and Mo(IV)→Mo(VI) respectively. Note that all 4 peaks increase with increasing concentration of phosphate providing an indirect electrochemical methodology.

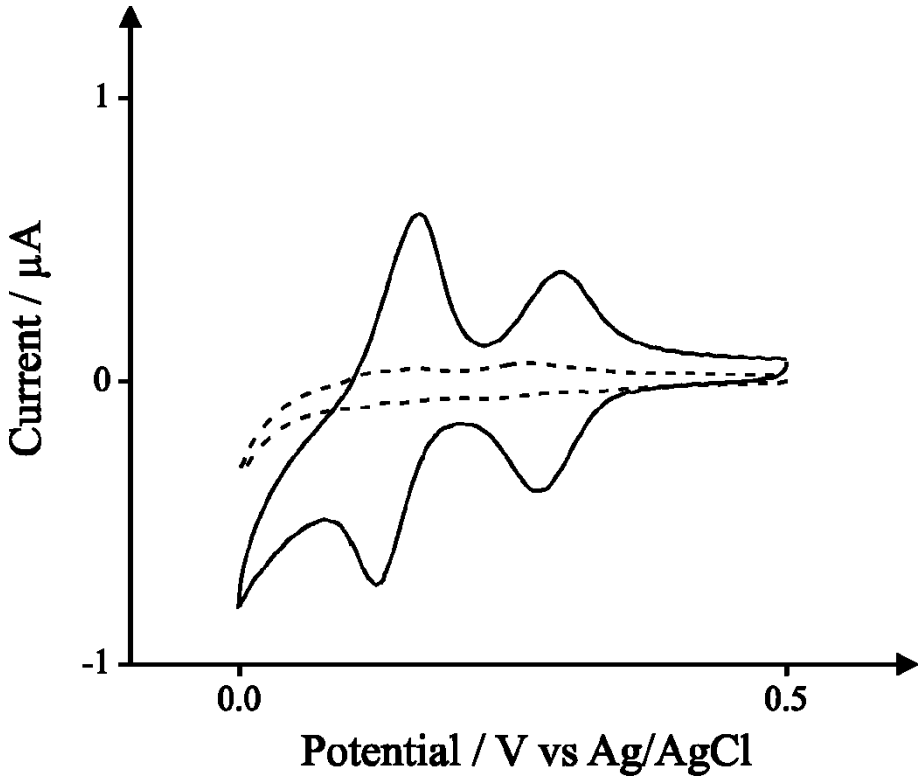

Figure 6.2 Cyclic voltammetry of SPGE upon solution containing 640 mg L^{-1} ammonium molybdate tetrahydrate at pH 1 with and without the addition of 20 µg L^{-1} phosphorus. Dashed line: without phosphorus. Solid line: with 20 µg L^{-1} phosphorus. Scan rate: 50mVs^{-1}.

The voltammetric responses observed from additions of phosphate into an ideal solution (pH 1) are depicted in figure 6.3 utilising SPGEs.

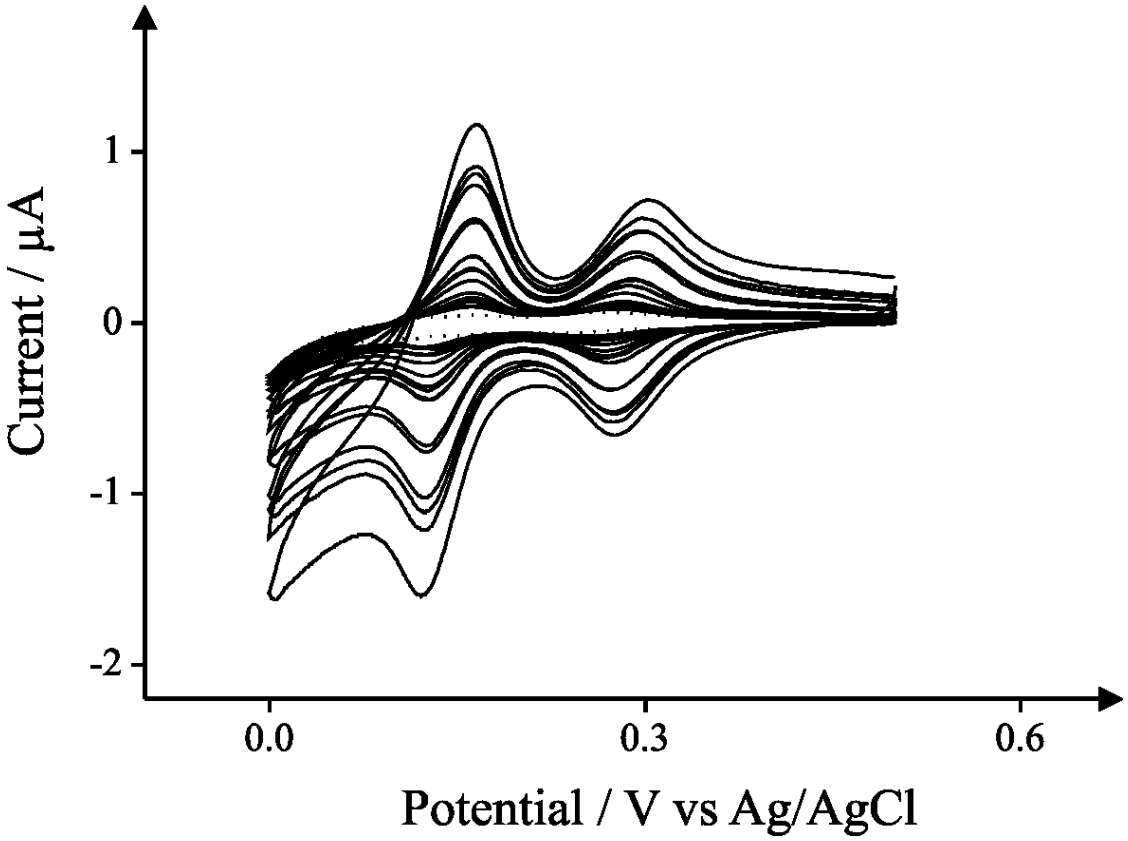

Figure 6.3 Typical cyclic voltammetric responses using a SPGE following additions of Phosphorus (0.5 – 100 µg L^{-1}) into an ideal solution (pH 1) containing 640 mg L^{-1} ammonium molybdate tetrahydrate. Note that a new SPGE is used for each addition. Dotted line: without phosphorus (blank). Scan rate: 50 mVs^{-1} *vs*. Ag/AgCl.

Figures 6.4-6.7 depict the calibration plots for all the four oxidation and reduction analytical peaks. The linear responses for the sensing of Phosphorus are as follows: for using the oxidation peak at +0.16V (see figure 6.4) ($I_P/\mu A = 2.76$ x 10^{-2} $\mu A/\mu gL^{-1}$ + 5.21 x 10^{-2} μA; $R^2 = 0.9938$ $N = 3$), for using the oxidation peak at + 0.30V (see figure 6.5) ($I_P/\mu A = 4.2$ x 10^{-3} $\mu A/\mu gL^{-1}$ + 12.12 x 10^{-2} μA; $R^2 = 0.7544$ $N = 3$), for using the reduction peak at + 0.27V (see figure 6.6) ($I_P/\mu A = -4.8$ x 10^{-3} $\mu A/\mu gL^{-1}$ -13.16 x 10^{-2} μA; $R^2 = 0.6898$ $N = 3$) and for using the reduction peak at + 0.13V (see figure 6.7) ($I_P/\mu A = -3.4$ x 10^{-2} $\mu A/\mu gL^{-1}$ -3.84 x 10^{-2} μA; $R^2 = 0.9979$ $N = 3$). The reduction peak at +0.13V was chosen as the analytical peak since it is found to exhibit the best linear relationship with the concentration of phosphorus

upon additions over the range 0-20 μL^{-1}; using this line of best fit,the theoretical limit of detection (3σ) for Phosphorus when utilising new SPGE for each addition was determined to be 0.3 $\mu g\ L^{-1}$.

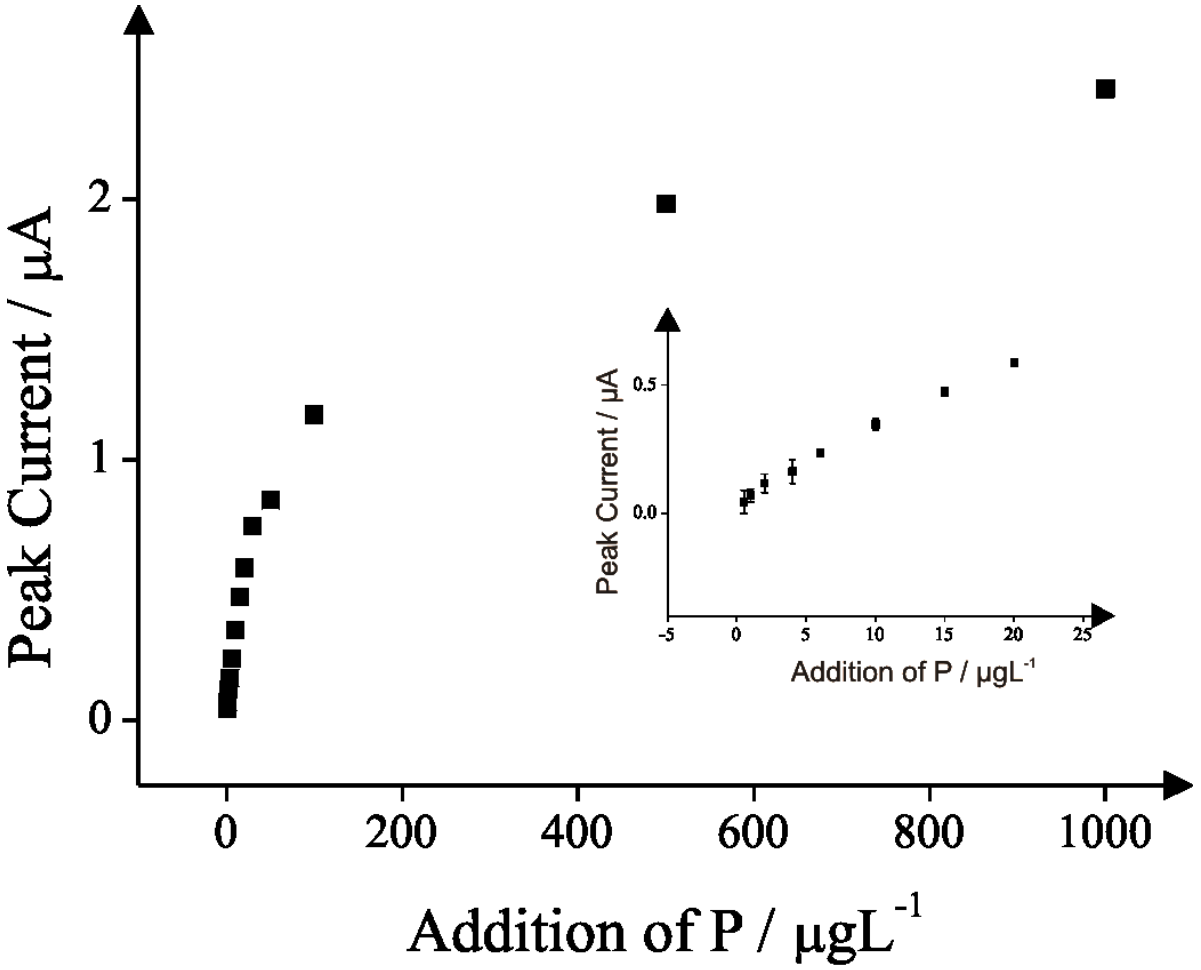

Figure 6.4 A typical calibration plot corresponding to additions of Phosphorus (0.5 – 100 $\mu g\ L^{-1}$) into an ideal solution (pH 1) containing 640 mg L^{-1} ammonium molybdate tetrahydrate. The data is from the analysis of the analytical oxidation peak observed at +0.16 V. Inset: zoom of the Calibration Plot for additions of Phosphorus (0.5 – 20 $\mu g\ L^{-1}$). A new SPGE is used for each addition. Error Bars in the inset arise from three measurements with new SPGE each time.

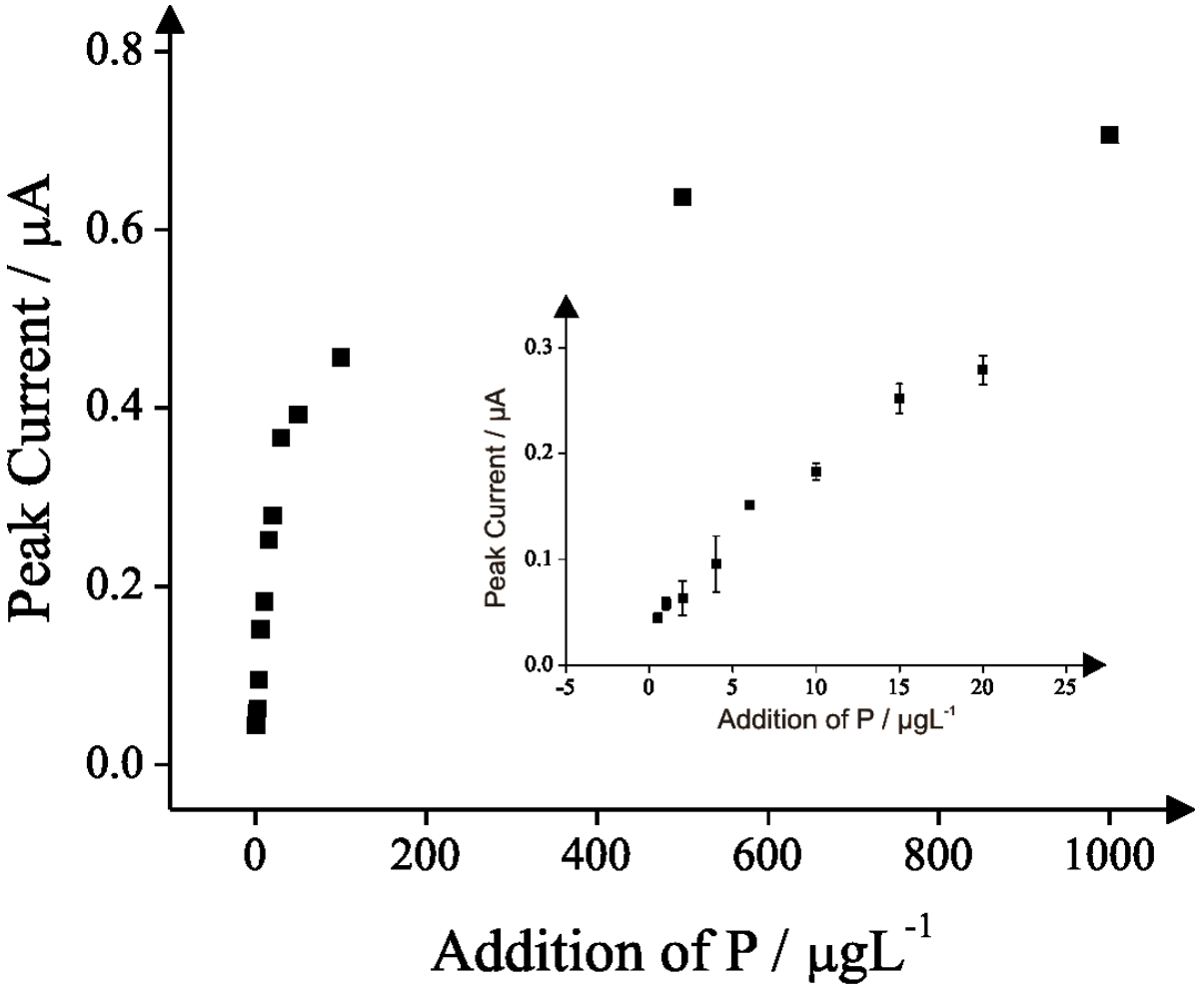

Figure 6.5 A typical calibration plot corresponding to additions of phosphorus (0.5 – 100 µg L^{-1}) into an ideal solution (pH 1) containing 640 mg L^{-1} ammonium molybdate tetrahydrate. The data is from the analysis of the analytical oxidation peak observed at +0.30 V. Inset: zoom of the Calibration Plot for additions of Phosphorus (0.5 – 20 µg L^{-1}). A new SPGE is used for each addition. Error Bars in the inset arise from three measurements with new SPGE each time.

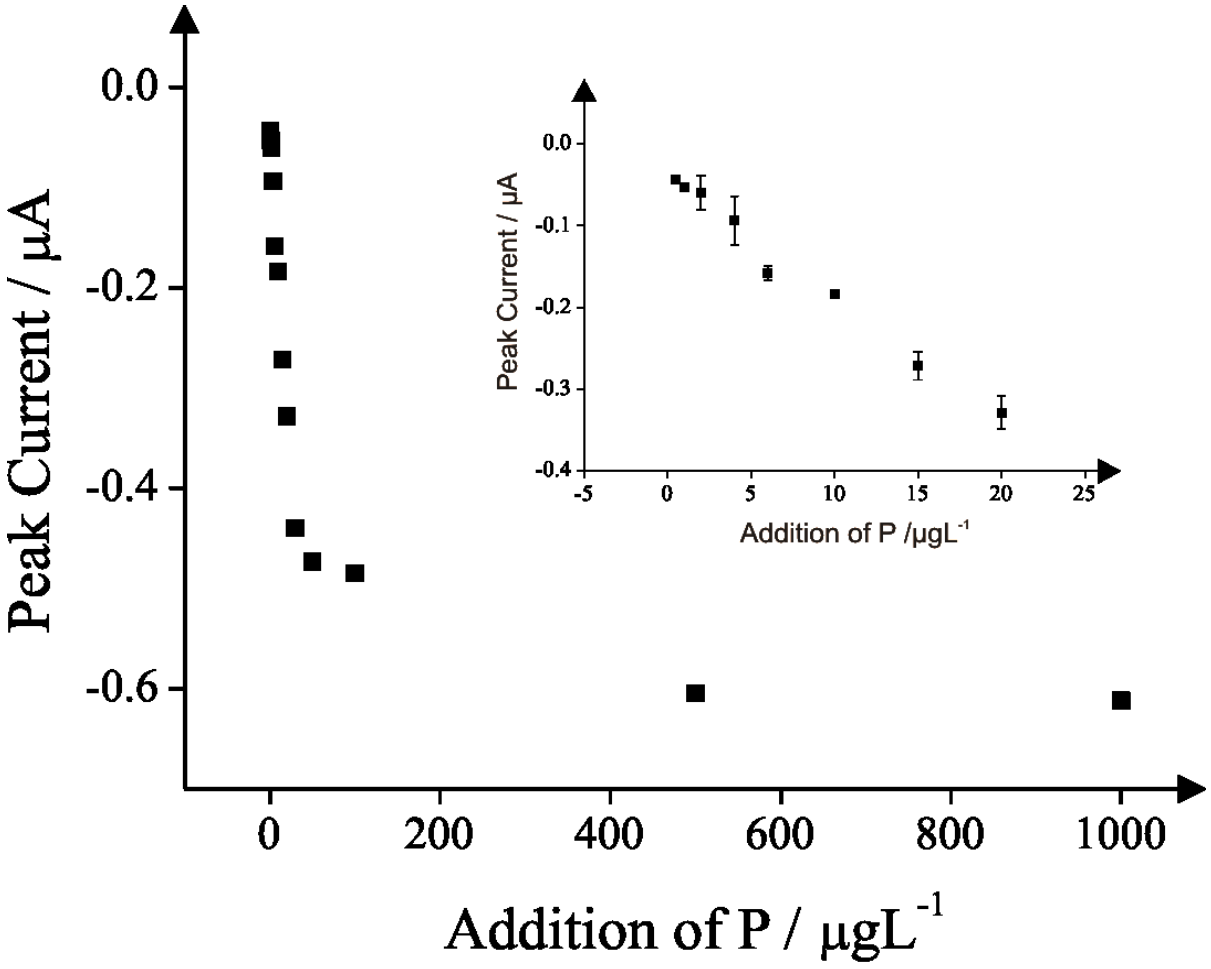

Figure 6.6 A typical calibration plot corresponding to additions of Phosphorus (0.5 – 100 µg L^{-1}) into an ideal solution (pH 1) containing 640 mg L^{-1} ammonium molybdate tetrahydrate. The data is from the analysis of the analytical reduction peak observed at +0.27 V. Inset: zoom of the Calibration Plot for additions of Phosphorus (0.5 – 20 µg L^{-1}). Error Bars in the inset arise from three measurements.

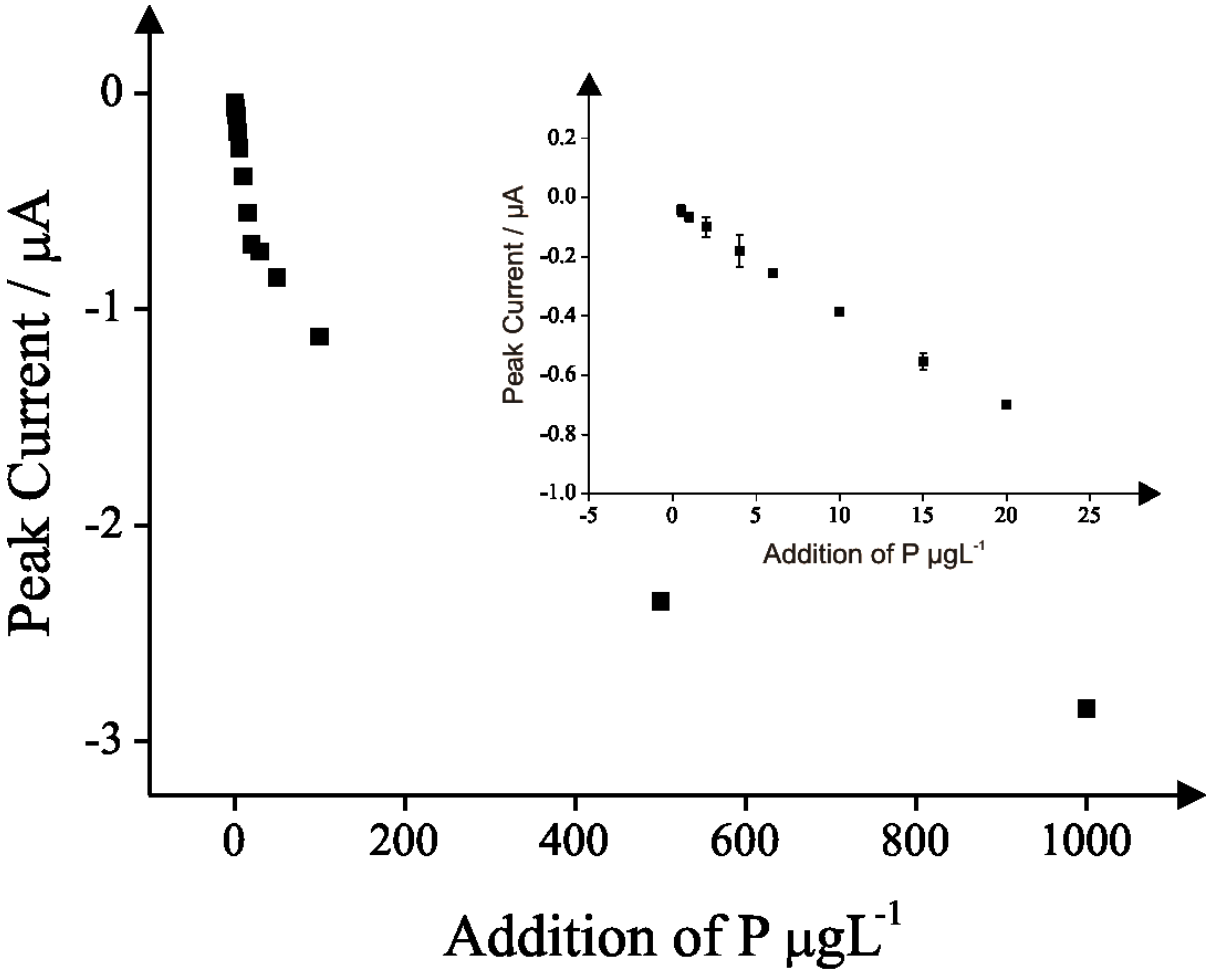

Figure 6.7 A typical calibration plot corresponding to additions of Phosphorus (0.5 – 100 µg L^{-1}) into an ideal solution (pH 1) containing 640 mg L^{-1} ammonium molybdate tetrahydrate. The data is from the analysis of the analytical reduction peak observed at +0.13 V. Inset: zoom of the Calibration Plot for additions of Phosphorus (0.5 – 20 µg L^{-1}). Error Bars in the inset arise from three measurements. Different electrode has been used each time.

In the EPA recommended optical method, the time of reaction is crucial and this is the reason why a minimum time of 5 minutes is suggested following the addition of all the chemicals in order to determine the concentration of phosphorus spectrophotometrically. The peak current of the reduction peak at + 0.13V in relation with the reaction time is shown in figure 6.8. It is clear from the figure that the reaction time doesn't affect voltammetric signature/analytical signal. This is because the electrochemical protocol does not require reducing agents as mentioned above.

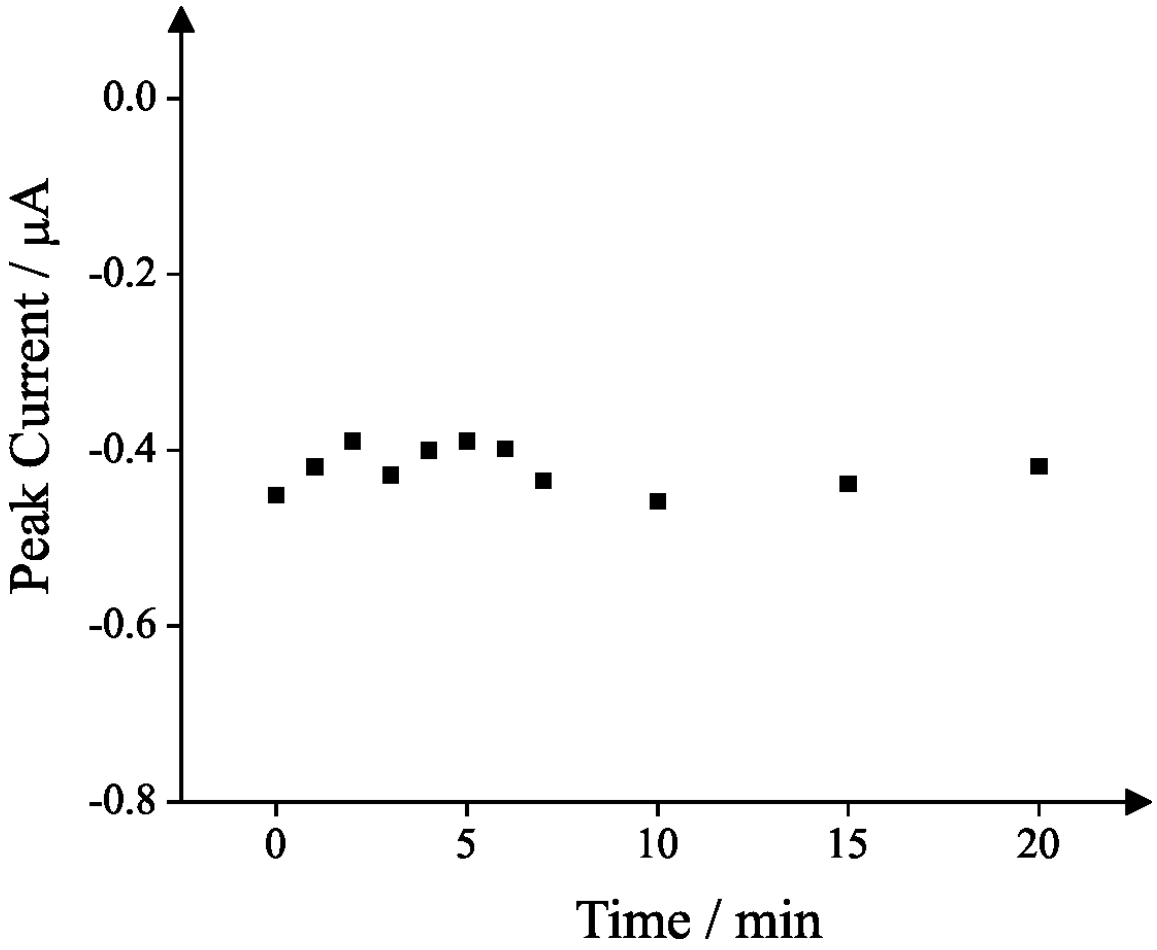

Figure 6.8 Analysis of the peak current of the reduction peak observed at +0.13V as a function of time. The solution contains 640 mg L^{-1} ammonium molybdate tetrahydrate and 20 µg L^{-1} Phosphorus in pH 1. New SPGEs were used for each measurement.

Next, potential interferences were explored. Interference from ions that might be found in water samples such as NO_2^-, NO_3^- and HCO_3^- have been studied and the results are depicted in figure 6.9. It can be concluded that the ions, which have been studied in concentrations five times higher than concentration of phosphorus, do not interfere with the proposed electrochemical method.

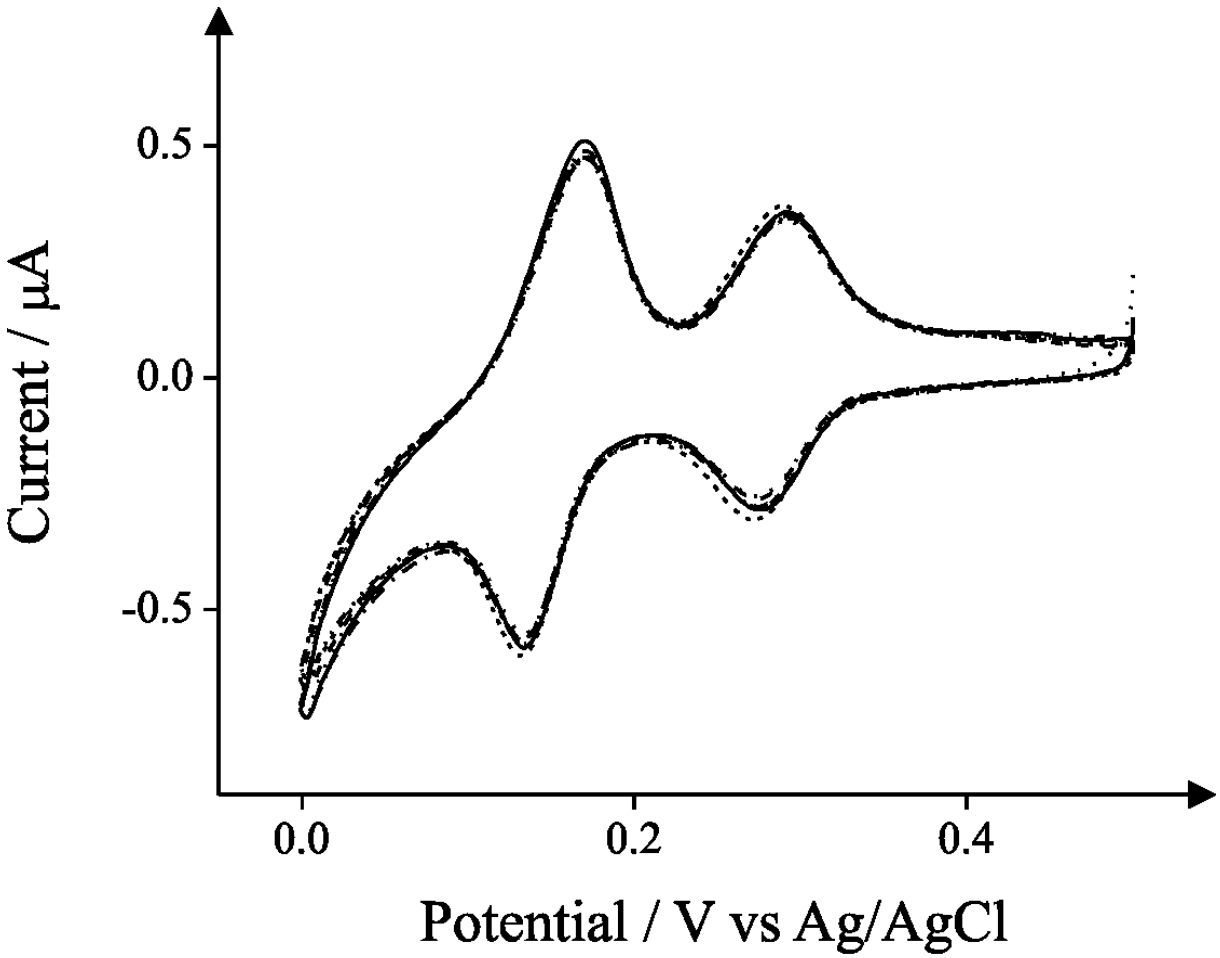

Figure 6.9 Typical cyclic voltammetric responses in the absence (solid line) and presence of 100 µg L^{-1} of the ions HCO_3^- (dotted line) NO_3^- (dashed) and NO_2^- (dashed-dotted line) in an ideal solution (pH 1) containing 640 mg L^{-1} ammonium molybdate tetrahydrate and 20 µg L^{-1} phosphorus. Scan Rate: 50 mVs^{-1} *vs* Ag/AgCl.

Attention was focused on determining the concentration of orthophosphates (as phosphorus) via standard addition techniques into canal water (diluted1:4) with deionised water (see experimental). Cyclic voltammetric responses using SPGE resulting from additions of phosphorus (1 – 20 µg L^{-1}) into the canal water sample (acidified to pH 1 with with H_2SO_4) containing 640 mg L^{-1} ammonium molybdate tetrahydrate are shown in figure 6.10. Analysis of the data presented in figure 6.10 reveals a linear response (see figure 6.11) for the sensing of orthophosphates using the reduction peak at +0.13 V ($I_P/\mu A$ = *-2.37* x 10^{-2} $\mu A/\mu gL^{-1}$ + *9.33* x 10^{-2} μA; R^2 = *0.9923* *N = 3*). The initial concentration of orthophosphates of the diluted (1:4) canal water can be determined at 3.94 µg L^{-1} of phosphorus. Consequently, the concentration of orthophosphates in the canal water was initially 4 x 3.94 = 15.7 µg L^{-1} as phosphorus. This value was confirmed by ion chromatography (Figure 6.12) where orthophosphates were independently determined to be 15 µg L^{-1} as phosphorus.

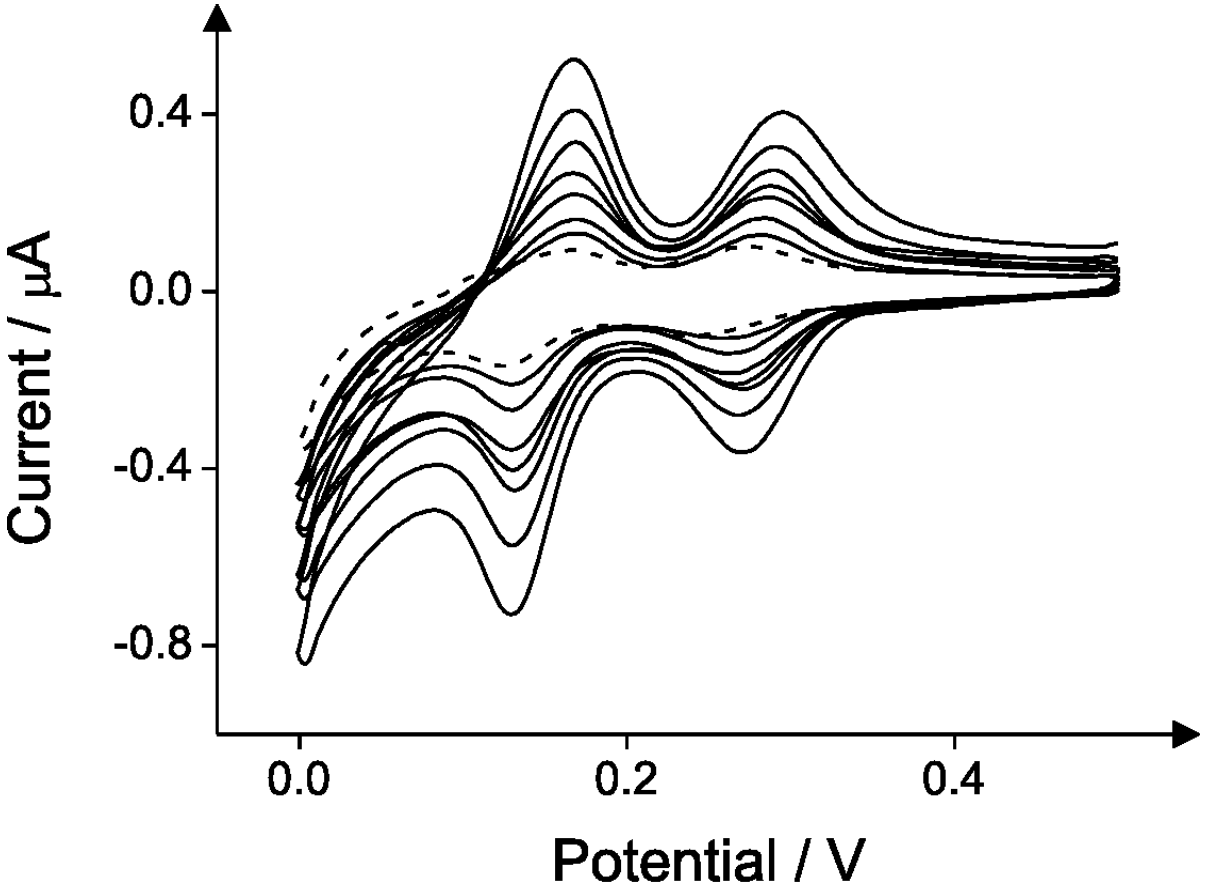

Figure 6.10 Cyclic voltammetric responses using SPGEs following additions of Phosphorus (1 – 20 µg L^{-1}) into a canal water (diluted 1:4) sample (adjusted to pH 1 with H_2SO_4) containing 640 mg L^{-1} ammonium molybdate tetrahydrate. A new SPGE is used for each addition. Dashed line: without phosphorus. Scan rate: 50 mVs^{-1} *vs*. Ag/AgCl.

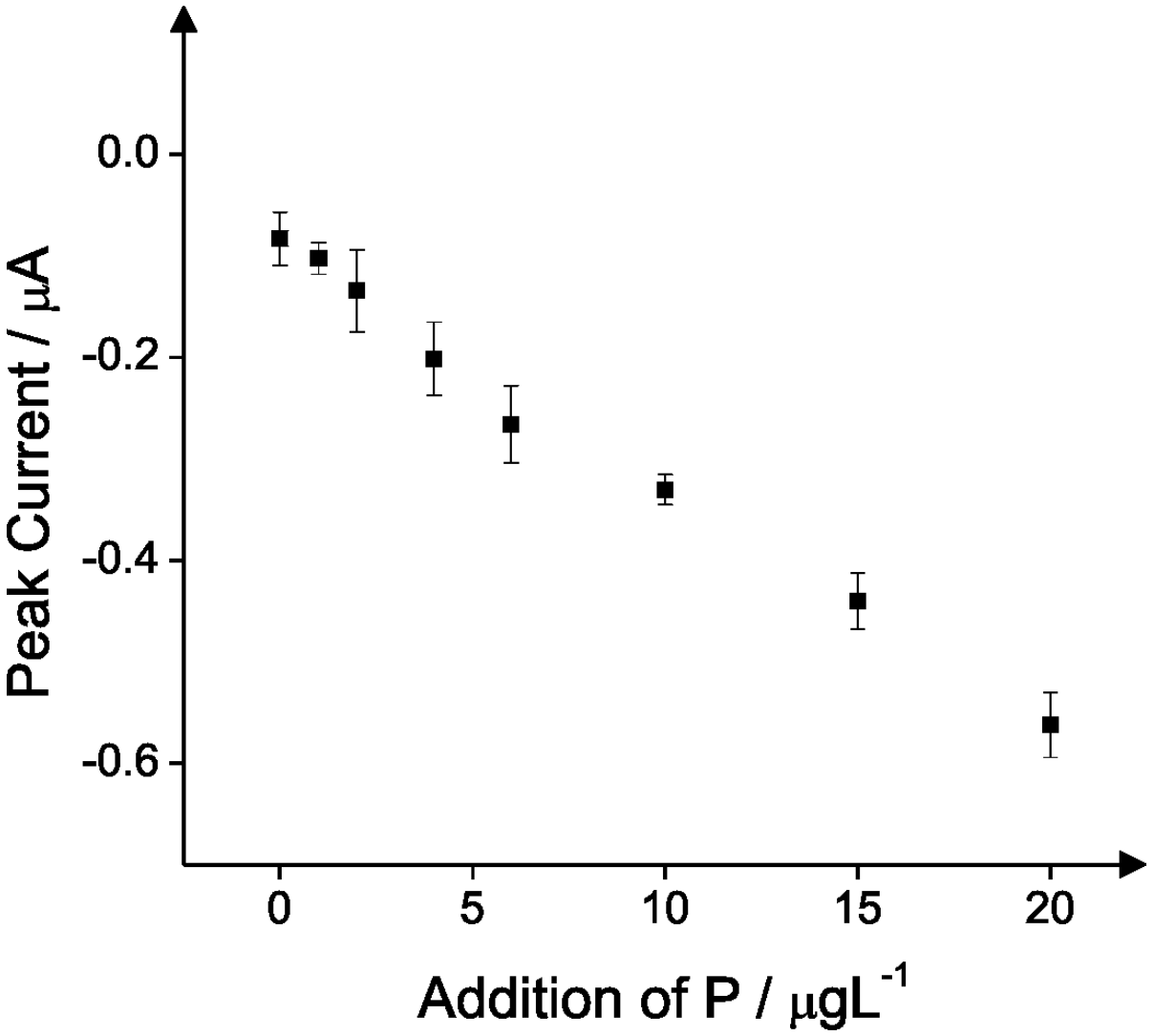

Figure 6.11 Analysis of the data presented in figure 6.10 producing a calibration resulting from additions of phosphorus (1 – 20 μg L^{-1}) into canal water (diluted 1:4 adjusted to pH 1 with H_2SO_4) using a standard addition protocol. Solution contains 640 mg L^{-1} ammonium molybdate tetrahydrate which was added prior to electrochemical measurements. Analytical reduction peak at + 0.13V is analysed to provide the data presented in this figure. A new SPGE is used for each addition. Error bars ($N = 3$)

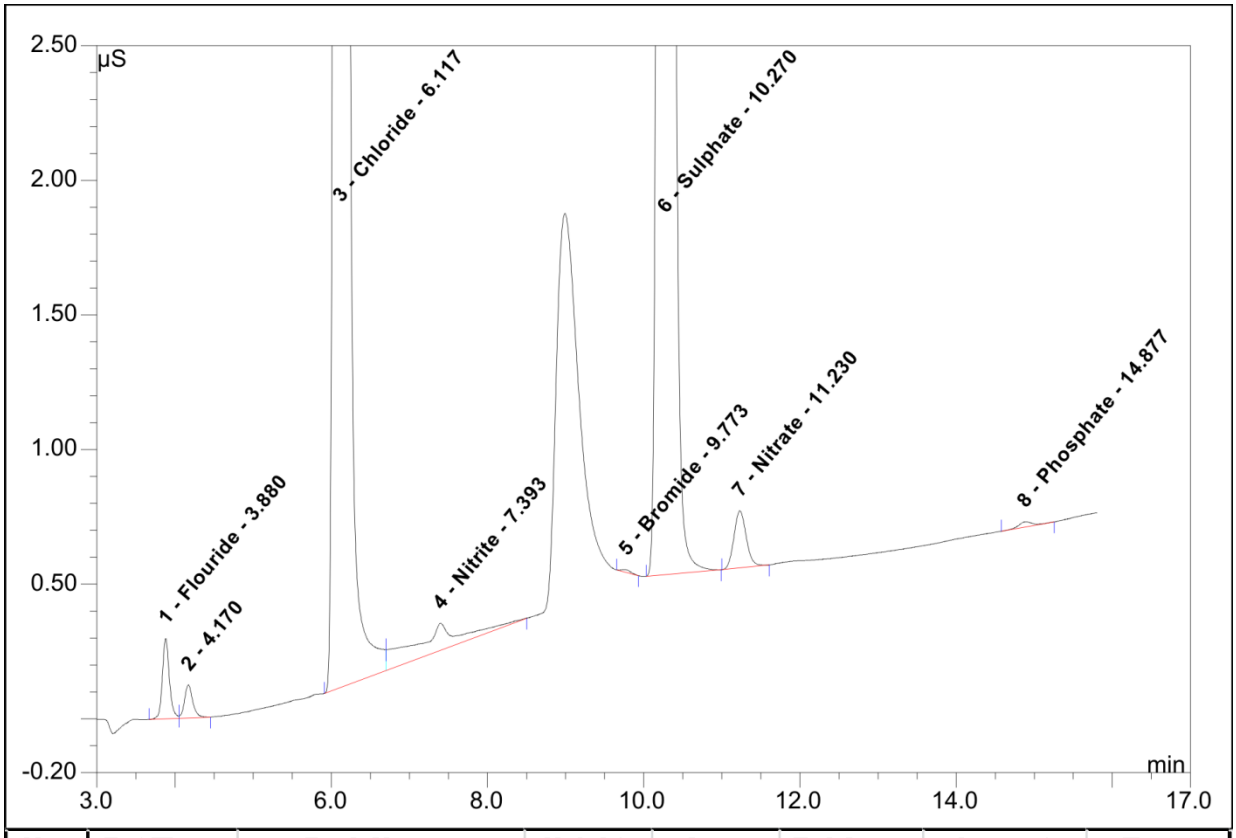

No.	Ret.Time min	Peak Name	Height µS	Area µS*min	Rel.Area %	Amount mg/l	Type
1	3.88	Flouride	0.299	0.031	0.37	0.072	BM
2	4.17	n.a.	0.123	0.015	0.18	n.a.	MB
3	6.12	Chloride	40.035	4.968	59.21	13.116	BM
4	7.39	Nitrite	0.100	0.068	0.81	0.392	MB
5	9.77	Bromide	0.010	0.001	0.02	0.013	BMB
6	10.27	Sulphate	20.704	3.264	38.90	16.974	BMB
7	11.23	Nitrate	0.212	0.039	0.46	0.278	BMB
8	14.88	Phosphate/Phosphorus	0.019	0.004	0.04	0.046/0.015	BMB
Total:			61.503	8.390	100.00	30.844	

Figure 6.12 Typical Ion chromatogram obtained in the analysis of the canal water sample. The concentration of orthophosphates is 46 µg L^{-1} as phosphates or 15 µg L^{-1} as phosphorus.

The total amount of dissolved phosphorus in the canal water sample was determined by using the standard addition technique in diluted canal water (1:100 with deionized water) after persulfate digestion (procedure detailed in the e*x*perimental section) in order to convert all the forms of phosphorus into orthophosphates. Cyclic voltammetric responses using SPGEs following additions of phosphorus (1 – 20 μg L^{-1}) in the digested sample (adjusted to pH 1 with H_2SO_4) containing 640 mg L^{-1} ammonium molybdate tetrahydrate are shown in figure 6.13. Analysis of the voltammetric responses shown in figure 6.13 reveals a linear response (see figure 6.14) for the sensing of orthophosphates using the reduction peak at +0.14 V was achieved ($I_P/\mu A$ = *-1.11* x 10^{-2} $\mu A/\mu g L^{-1}$ *-8.87* x 10^{-2} μA; R^2 = *0.9925* *N = 3*). The initial concentration of dissolved phosphorus of the diluted (1:100) canal water can be determined at 8.0 μg L^{-1}. Consequently the concentration of dissolved phosphorus in the canal water was initially 100 x 8.0 = 800 μg L^{-1} as phosphorus with relative standard deviation 8.1%. This value was confirmed by ICP-OES (Table 6.2) where dissolved phosphorus was determined to correspond to 885 μg L^{-1} with relative standard deviation 10.1%. Reasonable agreement between the proposed electrochemical method and the traditional ICP-OES suggests the electroanalytical protocol has merit.

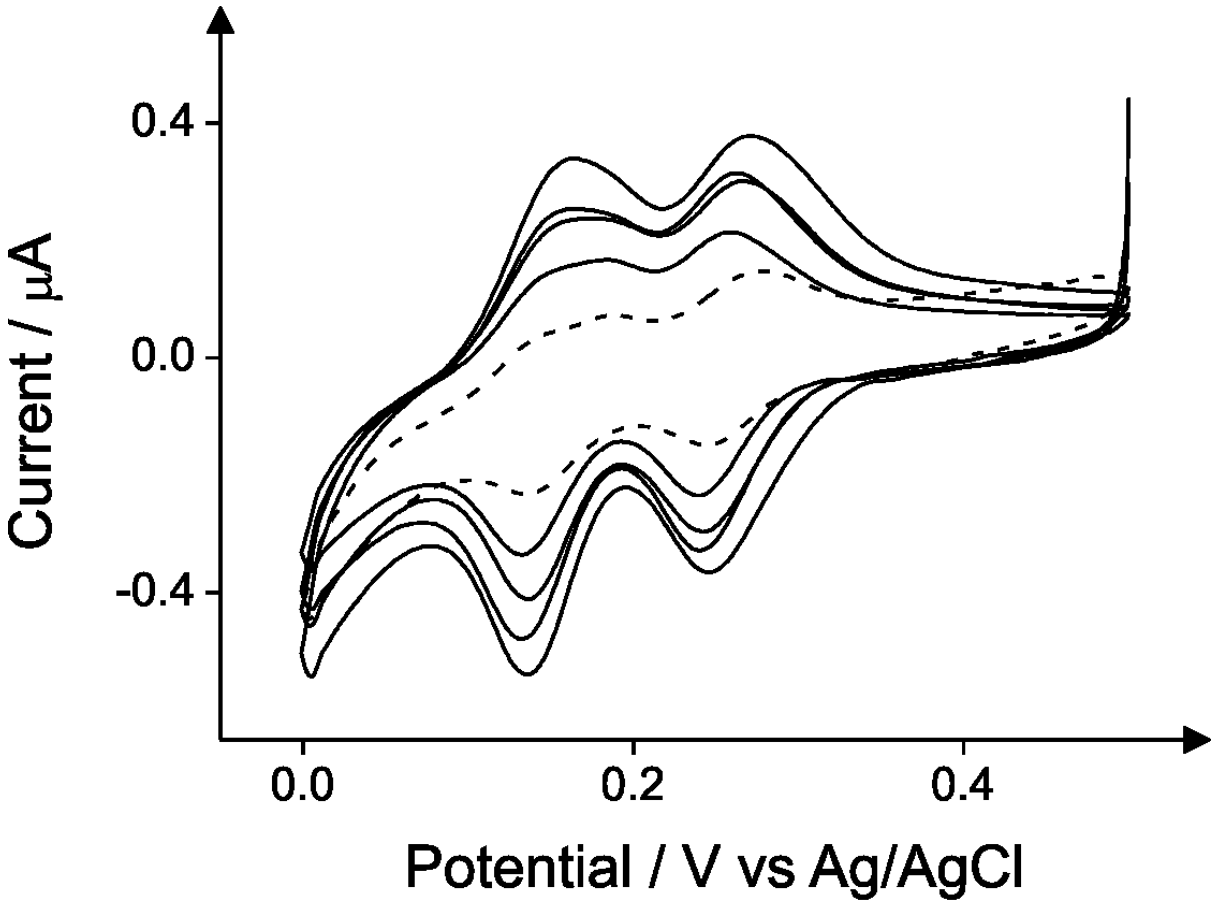

Figure 6.13 Cyclic voltammetric responses using SPGE as a result of additions of phosphorus (1 – 20 µg L^{-1}) into a digested canal water (diluted 1:100) sample (using persulfate see experimental). The pH of the canal water sample was adjusted to pH 1 with H_2SO_4. 640 mg L^{-1} ammonium molybdate tetrahydrate was added in the solution prior to electrochemical measurements. A new SPGE is used for each addition. Dashed line: without phosphorus. Scan rate: 50 mVs^{-1} *vs*. Ag/AgCl.

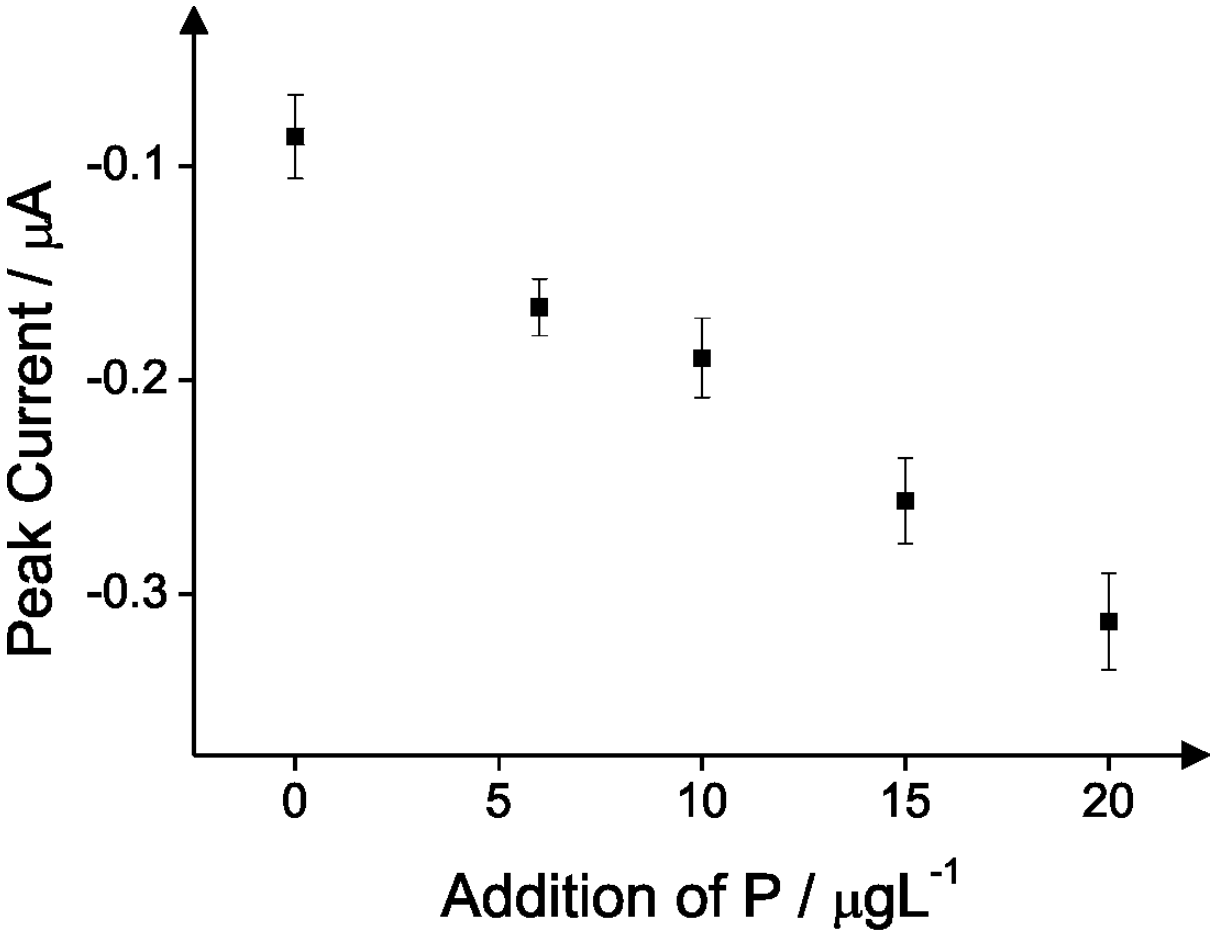

Figure 6.14 Analysis of the data presented in figure 6.13 producing a calibration plot resulting from additions of phosphorus (1 – 20 μg L^{-1}) into digested with persulfate canal water (diluted 1:100 and adjusted to pH 1 with H_2SO_4) using a standard addition protocol. Analytical reduction peak at + 0.13V is analysed to provide the data presented in this figure. A new SPGE is used for each addition. Error bars ($N = 3$)

Table 6.2 Results of the analysis of total phosphorus in canal water via ICP-OES. The concentration of total phosphorus is found to correspond to 885.2 μg L^{-1}.

	Standard Deviation	% RSD (Relative Standard Deviation)	Rep #1 (mgL^{-1})	Rep #2 (mgL^{-1})	Rep #3 (mgL^{-1})	Average (mgL^{-1})
Ca	1.4	0.9051	154.3	157.1	155.2	155.6
Cd	0.0142	159	0.0226	0.0099	-0.0057	0.0089
Cu	0.0075	12.27	0.0643	0.0663	0.0524	0.061
Fe	0.0225	23.72	0.0933	0.1183	0.0733	0.095
K	0.2	1.254	15.77	16.05	15.67	15.83
Mg	0.11	0.7826	13.93	14.14	13.97	14.01
Mn	0.0031	32.07	0.0094	0.013	0.0068	0.0097
Na	0.78	0.8764	88.29	89.71	88.44	88.81
Ni	0.0153	20.9	0.0884	0.0738	0.0577	0.0733
P	0.0895	10.11	0.9809	0.8712	0.8035	0.8852
Pb	0.2402	72.57	0.6017	0.2477	0.1435	0.331
S	1	0.4312	223.2	222	221.3	222.1
Zn	0.0281	37.71	0.1043	0.0709	0.0484	0.0745

6.4 CONCLUSIONS

The first example sensing dissolved phosphorus in ideal and a real sample (canal water) using screen-printed graphite electrodes has been reported using an indirect protocol. The proposed electroanalytical procedure is simple and utilises cost effective screen-printed sensors provide an appealing alternative to the existed standard colorimetric method which is traditionally used for the sensing of dissolved phosphorus. The screen-printed graphite electrodes were shown to allow for the low level sensing of dissolved phosphorus in canal water samples, in addition to analysis under ideal conditions. The proposed electroanalytical protocol is as sensitive and selective as the established standard colorimetric method but additionally it exhibits lower detection limits it requires less experimental time and it overcomes refractive index errors and turbidity interferences. The substitution of the reducing

agents such as ascorbic acid antimony potassium tartrate by electrochemical reduction of the phosphomolybdate ion contributes in the elimination of any possible interference from the instability of ascorbic acid. Such sensors provide a potential solution to the common problem of the transition of laboratory-based analytical procedures to real world applications in the 'field' combining the low-cost benefits of carbon based materials with ease of mass production and facile use of screen-printed sensors.

CHAPTER 7

ELECTROANALYSIS APPLIED IN THE SENSING OF TARGET ANALYTES IN INDUSTRIAL WATER

QUANTIFICATION OF CORROSION INHIBITORS USED IN THE WATER INDUSTRY FOR STEAM CONDENSATE TREATMENT: THE INDIRECT ELECTROANALYTICAL SENSING OF MORPHOLINE AND CYCLOHEXYLAMINE

7.1 ABSTRACT

Corrosion inhibitors are widely used in the water industry for steam condensate treatment. Due to their application into the food industry, the Food and Drug Administration (FDA) legislate that such inhibitors are not to exceed 10 mg L^{-1}. Various analytical protocols exist to provide but a point of site analysis is yet to be reported and is required by industry. Consequently, the first example of the indirect electroanalytical determination of cyclohexylamine and morpholine, two important corrosion inhibitors using disposable and economical screen-printed graphite macroelectrodes is reported for the first time in this chapter.

These two important analytes have been demonstrated to have no measureable direct electrochemical signatures in aqueous solutions using carbon and noble metal based macroelectrodes and, for the first time, an indirect electrochemical sensing protocol which utilises screen-printed graphite macroelectrodes is been proposed. This indirect approach utilises an EC type-mechanism using the compounds, N,N'-(1,4-phenylene)dibenzenesulfonamide and N-(4-Amino-2-Methyl-Phenyl)-Benzenesulfonamide as mediators. In this approach the mediators are electrochemically oxidised which then chemically react with the target analytes, cyclohexylamine and morpholine; the products of these reactions are then electrochemically interrogated and provide an indirect electroanalytical signal with which to quantify cyclohexylamine and morpholine. The two mediators are required for the two target analytes as one mediator cannot measure both.

It is demonstrated that this indirect sensing protocol allows the electroanalytical

detection of cyclohexylamine and morpholine over the range 1 to 10 mg L^{-1} in pH 10 carbonate buffer utilising cyclic voltammetry. This indirect electroanalytical protocol is found to exhibit a limit of detection (3σ) of 0.9 and 1 mg L^{-1} for cyclohexylamine and morpholine respectively which are *significantly below the FDA sanctioned levels*.

This indirect electroanalytical protocol utilising screen-printed sensors has the potential to be applied into-the-field enabling the measurement of these two neutralizing amines to ensure they do not exceed FDA guidelines.

7.2 INTRODUCTION

Water treatment for boilers is divided into external (physico-chemical) and internal (chemical) treatments. [312] External treatment involves the physico-chemical treatment of the raw water to produce a satisfactory quality boiler feed water such as ion exchange, water softening and filters for suspended solids. Internal treatment comprises the addition of chemicals for the treatment of the boiler feed water and steam condensate. The treatment of the boiler feed water controls mineral scaling, corrosion and general deposition in the boiler drums and tubes. The treatment of the steam condensate controls carbonic acid and dissolved oxygen corrosion of the steam condensate lines by the addition of chemicals either in the steam lines or directly into the boiler. [313, 314] The main components to be chemically treated in the steam condensate are carbon dioxide and oxygen. Bicarbonate and carbonate ions in feed water thermally decompose to carbon dioxide gas (CO_2) in the boiler water with the majority passing into the steam and forming carbonic acid in the condensate as described below:

$$CO_2 + H_2O \leftrightarrow H_2CO_3 \quad (1)$$

$$H_2CO_3 \leftrightarrow H^+ + HCO_3^- \quad (2)$$

$$HCO_3^- \leftrightarrow H^+ + CO_3^{2-} \quad (3)$$

Consequently, the pH of the condensate can decrease to very low levels, often below pH 3 which at this pH level is of course very corrosive resulting in corrosion and ultimately failure of metal pipelines. [315, 316]Additionally in the presence of oxygen, the corrosion rate increases and it is observed usually as localized pitting.[317] The cathodic reactions may occur either by the direct reduction of hydrogen ions, or *via* carbonates:[318]

$$2H^+ + 2e^- \rightarrow H_2 \quad (4)$$

$$H_2CO_3 + e^- \rightarrow HCO_3^- + 1/2H_2 \quad (5)$$

$$HCO_3^- \rightarrow CO_3^{2-} + 1/2H_2 \quad (6)$$

The anodic reaction occurs simply *via* the oxidation of iron:

$$Fe \rightarrow Fe^{2+} + 2e^- \quad (7)$$

There is experimental evidence for the presence of carbonate ($FeCO_3$) layer formation upon steel surfaces; [319] this corrosion layer is formed as described by Glezakou: [320]

$$Fe^{2+} + CO_3^{2-} \rightarrow FeCO_3 \quad (8)$$

$$Fe^{2+} + 2HCO_3^- \rightarrow Fe(HCO_3)_2 \quad (9)$$

$$Fe(HCO_3)_2 \rightarrow FeCO_3 + CO_2 + H_2O \quad (10)$$

Carbonate alkalinity can be minimized *via* de-alkalization and de-carbonation in the pre-treatment step, but in most medium and low pressure boilers this is not routinely undertaken.

In order to prevent acidic corrosion in the condensate lines (see above), carbon dioxide must be neutralized. This is performed by adding neutralizing amines (volatile amines) into the feed water; the addition of these amines adjusts the pH of the feed water into the range between 8 to 10, which is optimum for a mixed metallurgy system to avoid corrosion. [312] As these added amines pass into the boiler, they are also distributed into the steam, and condense with the steam and carbon dioxide. Apart from the neutralizing amines which inhibit the corrosion by controlling the condensate pH, filming amines are being used in steam condensate treatment. Filming amines form water repellent films upon metal surfaces inhibiting the corrosion process further by preventing the metals from contacting with the corrosive substances, such as oxygen and carbon dioxide.

The most common neutralizing amines utilised to reduce corrosion are cyclohexylamine, morpholine, and ammonia.[317, 321] Ammonia, with high concentration distribution ratios in steam to that in condensate (vapour/liquid distribution) transfers into steam easier than into the condensate and is not very effective for preventing the corrosion in the steam line close to the boiler.[312] Additionally, ammonia is not applicable for the boilers employing copper materials in the steam lines.[312] The detection of ammonia has been widely reported.[322, 323] Cyclohexylamine and morpholine are the amines of interest in

this work. The food industry uses steam extensively [295] and since the above chemicals are used to reduce/inhibit corrosion, contamination can occur with food products. As such, the Food and Drug Administration (FDA) limits the use of these amines. According to FDA Amine Standards-Title 21 CFR 173.310.d, both cyclohexylamine and morpholine are not to exceed 10 parts per million in steam. If the steam comes in contact with milk and milk products, the two amines are totally excluded.[324]

Cyclohexylamine and morpholine can be analysed by an array of analytical techniques such as High-Pressure Liquid Chromatography,[325, 326] Ion Chromatography,[327] or spectrophotometry [328] with detection limits in the required low part-per million (ppm) range. Electroanalytical techniques are sensitive portable and cost-effective especially through the use of screen-printed electrochemical sensors which have scales of economy.[16] Such an approach is promising for the measurement of chemicals in water treatment for on-site applications where rapid and accurate results are required.

In this chapter, an indirect electrochemical sensing protocol for cyclohexylamine and morpholine is described for the first time since they have no direct measurable electrochemical signatures. These two neutralizing amines are used extensively as anticorrosion agents of steam condensate lines and the proposed electrochemical protocol allows their sensing at limits below and close to the FDA legislation. The use of screen-printed sensors, which are disposable and easily portable, enables the sensing protocol to be potentially applied into-the-field.

First, the direct electrochemical detection of cyclohexylamine and morpholine was explored. In order to achieve this, cyclic voltammetric responses of 10 mg L^{-1} cyclohexylamine and morpholine using SPGE, BDDE, GCE and AuE were explored in a pH 10 buffer. The observed voltammetric profiles are presented in figures 7.1-7.8 where, for morpholine and cyclohexylamine, the similarity of the voltammograms with and without the analyte demonstrate that the direct electrochemical detection of morpholine and cyclohexylamine at pH 10 is *not possible* in the accessible aqueous potential window.

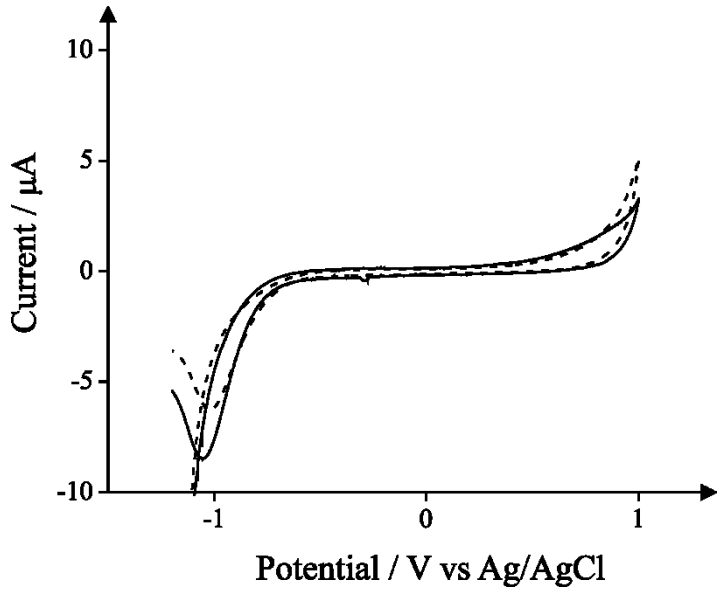

Figure 7.1 Typical cyclic voltammetric responses in the absence (solid line) and presence (dashed line) of 10 mg L^{-1} morpholine in pH 10 carbonate buffer solution recorded using SPGE. Scan rate: 50 mVs^{-1} *vs* Ag/AgCl

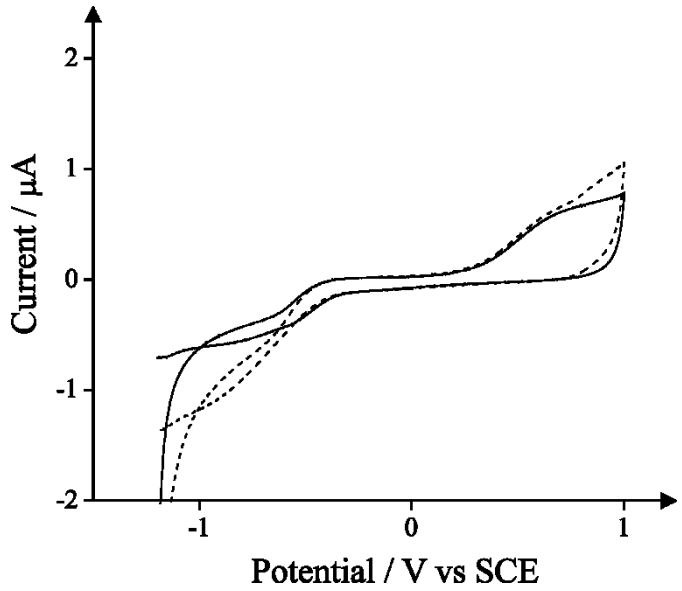

Figure 7.2 Typical cyclic voltammetric responses in the absence (solid line) and presence (dashed line) of 10 mg L^{-1} morpholine in pH 10 carbonate buffer solution recorded using BDDE. Scan rate: 50 mVs^{-1} *vs* SCE

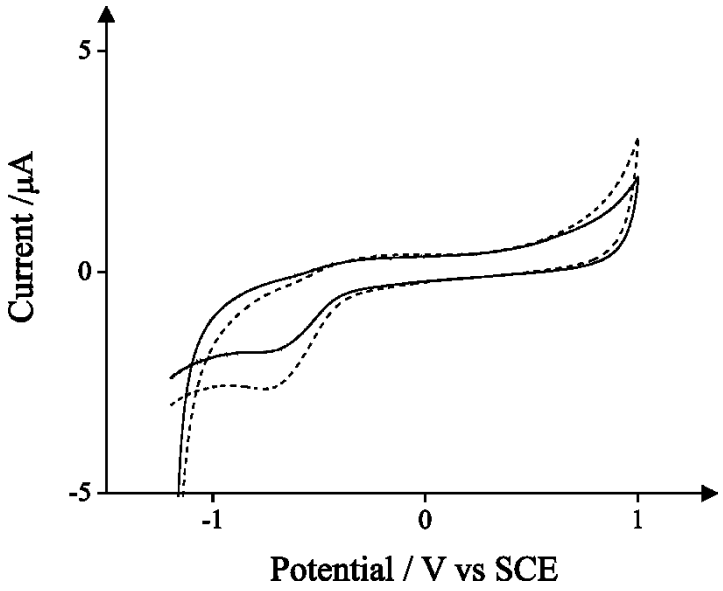

Figure 7.3 Typical cyclic voltammetric responses in the absence (solid line) and presence (dashed line) of 10 mg L^{-1} morpholine in pH 10 carbonate buffer solution recorded using GCE. Scan rate: 50 mVs^{-1} *vs* SCE

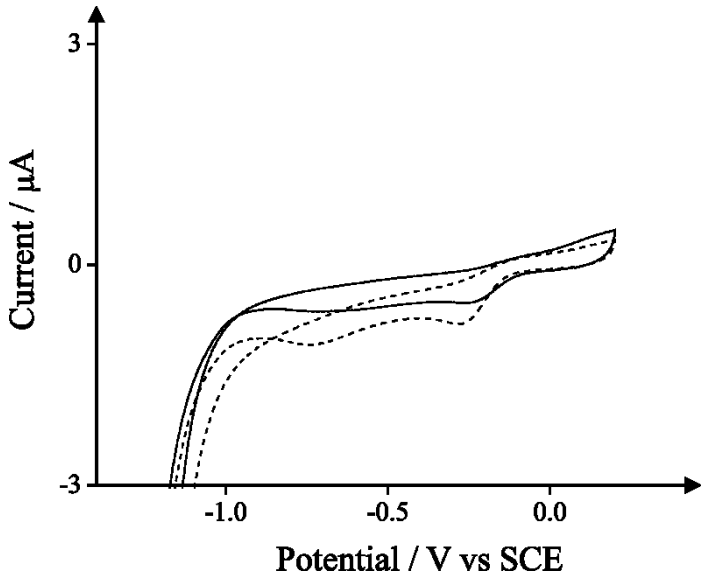

Figure 7.4 Typical cyclic voltammetric responses in the absence (solid line) and presence (dashed line) of 10 mg L^{-1} morpholine in pH 10 carbonate buffer solution recorded using AuE. Scan rate: 50 mVs^{-1} *vs* SCE

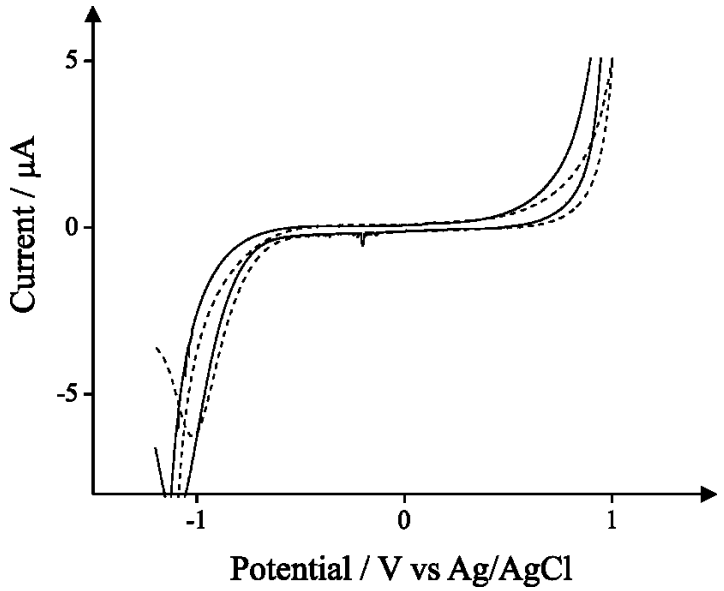

Figure 7.5 Typical cyclic voltammetric responses in the absence (solid line) and presence (dashed line) of 10 mg L^{-1} cyclohexylamine in pH 10 carbonate buffer solution recorded using SPGE. Scan rate: 50 mVs^{-1} *vs* Ag/AgCl

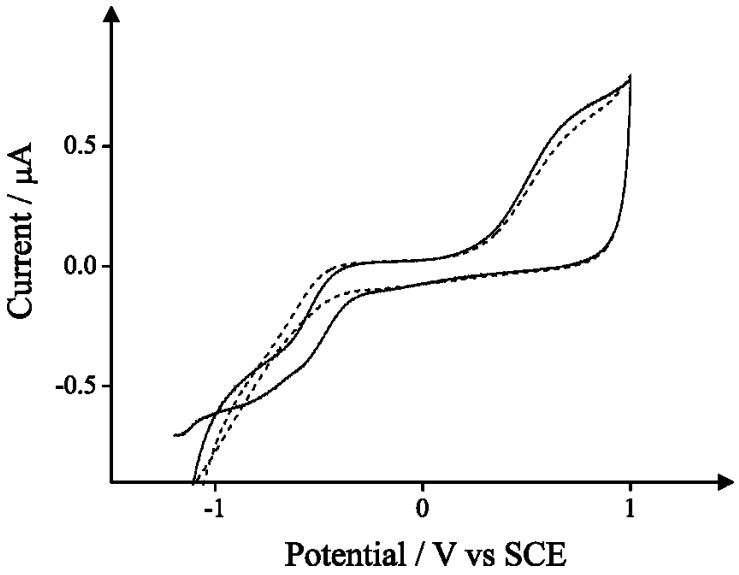

Figure 7.6 Typical cyclic voltammetric responses in the absence (solid line) and presence (dashed line) of 10 mg L^{-1} cyclohexylamine in pH 10 carbonate buffer solution recorded using BDDE. Scan rate: 50 mVs^{-1} *vs* SCE.

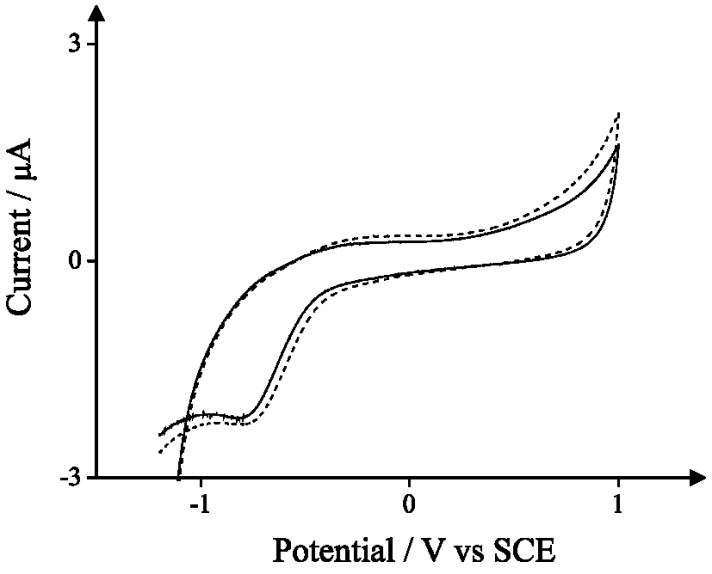

Figure 7.7 Typical cyclic voltammetric responses in the absence (solid line) and presence (dashed line) of 10 mg L^{-1} cyclohexylamine in pH 10 carbonate buffer solution recorded using GCE. Scan rate: 50 mVs^{-1} *vs* SCE

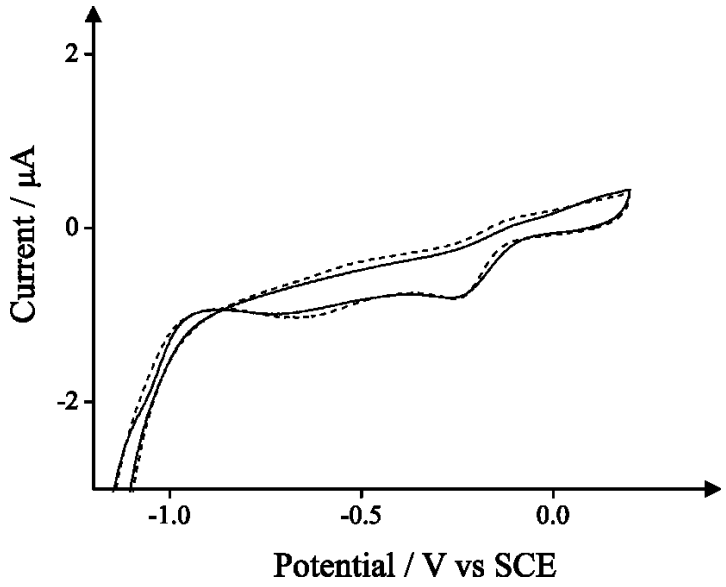

Figure 7.8 Typical cyclic voltammetric responses in the absence (solid line) and presence (dashed line) of 10 mg L^{-1} cyclohexylamine in pH 10 carbonate buffer solution recorded using AuE. Scan rate: 50 mVs^{-1} *vs* SCE

Inspired by prior work by Adams and Schowalter[329] who reported that morpholine and other amines such as dimethylamine, aniline, methylamiline and aliphatic primary amines chemically react with N,N'-(1,4-phenylene)dibenzenesulfonimide in organic solvents giving a variety of products which are dependent on the experimental conditions, in this work this novel system is electrochemically adapted. In this approach within aqueous solutions, we use the compound N,N'-(1,4-phenylene)dibenzenesulfonamide which is electrochemically oxidised (see Scheme 7.1, step 1) to the corresponding N,N'-(1,4-phenylene)dibenzenesulfonimide (producing a large oxidation wave) which then chemically reacts (Scheme 7.1, step 2) with the target amine at an appreciate rate. The product of this reaction is then electrochemically interrogated (Scheme 7.1, step 4) providing the analytical signal (see Scheme 7.1).

Scheme 7.1 Proposed EC mechanism for the indirect sensing of cyclohexylamine and the various electrochemical and chemical steps involved.

1) **Electrochemical step**: Electrochemical oxidation of mediator appears at +0.07 V.

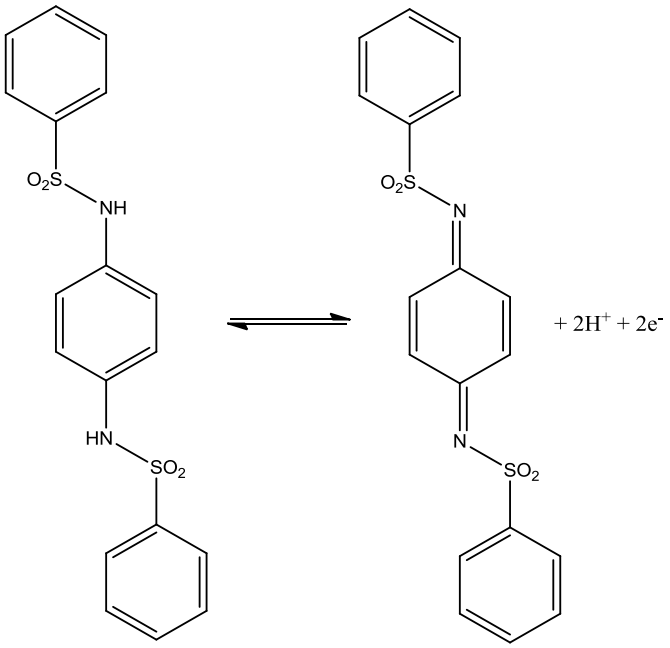

2) **Chemical step**: Reaction of Cyclohexylamine with the sulfonimide (oxidized form of the mediator).

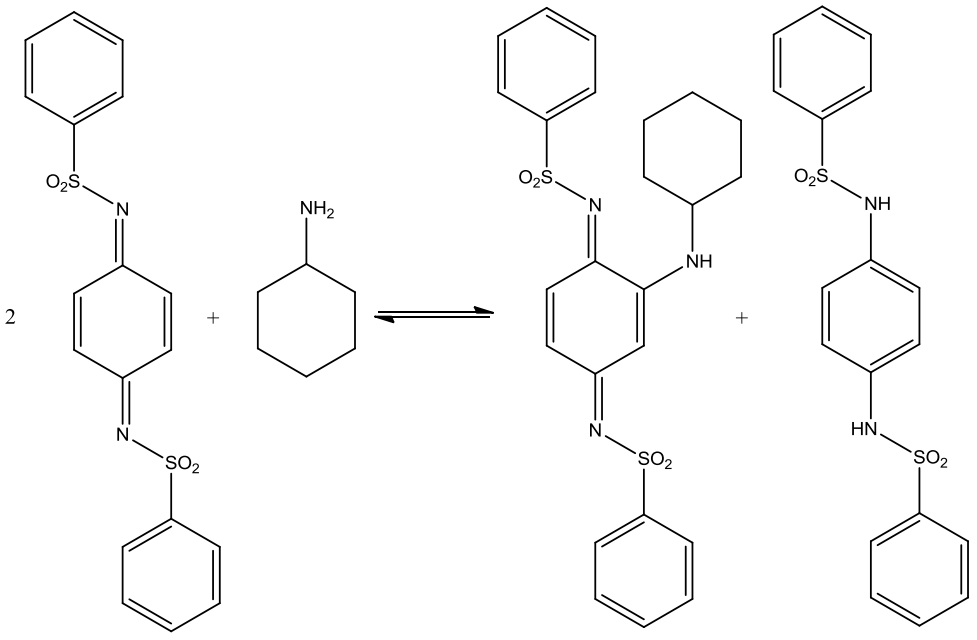

3) **Electrochemical step**: Reduction of Sulfonimide (oxidized form of the mediator) appears at +0.01 V.

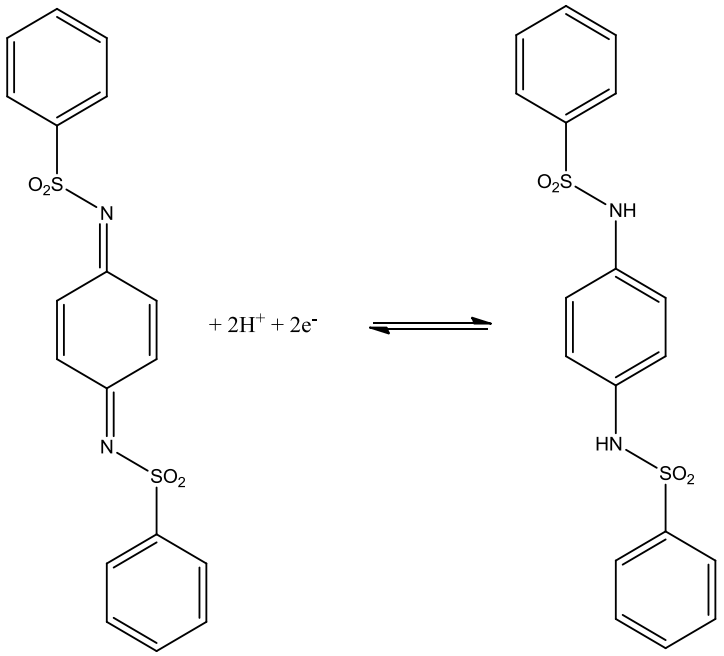

4) **Electrochemical step**: Reduction of the chemically formed product produces a new voltammetric signal at -0.2 V.

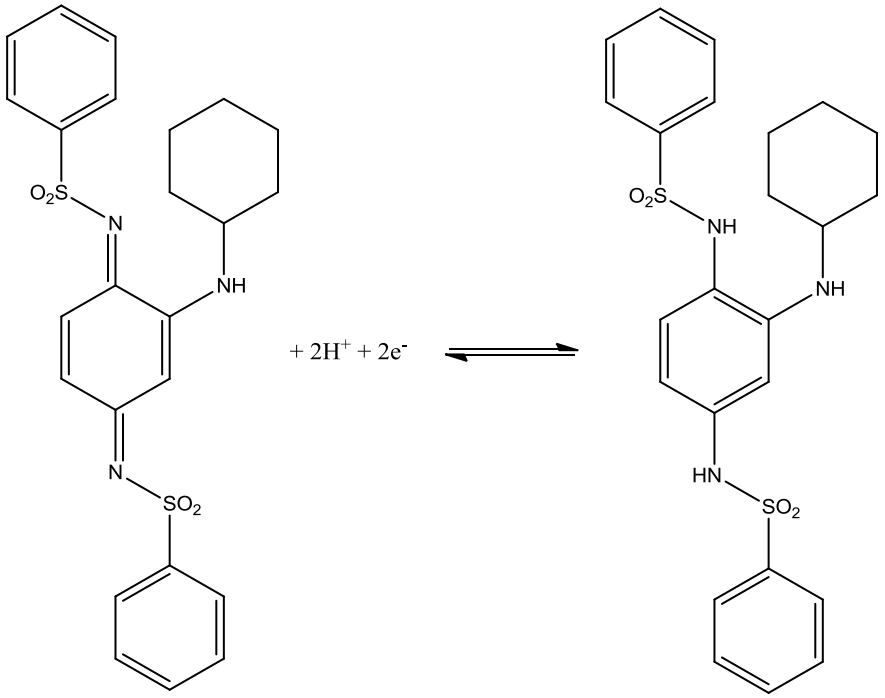

The plots of reduction peak potential *Ep vs*. pH for the mediators N-(4-Amino-2-Methyl-Phenyl)-Benzenesulfonamide and N,N'-(1,4-phenylene)dibenzenesulfonamide are shown in figure 7.9 and 7.10 respectively. In case of N-(4-Amino-2-Methyl-Phenyl)-Benzenesulfonamide (Figure 7.9) the plot shows a linear range with a gradient of 0.055 (*E/V= -0.055 +0.444 E/pH* R^2*=0.98)*. In case of N,N'-(1,4-phenylene)dibenzenesulfonamide (Figure 7.10) the plot shows a linear range with a gradient of 0.060 (*E/V= -0.060 +0.651 E/pH* R^2*=0.99)*. Such a value is close to that expected for 2 protons and 2 electrons process according to the electrochemical step (1) of the proposed mechanism (see Scheme 7.1) (59 mV per pH unit at 25 °C) as deduced from the following equation:

$$E = E^0 - 0.059\frac{m}{n}pH \qquad (11)$$

where E^0 is the standard reduction potential, m and n are the number of protons and electrons that participate in the reaction, respectively and the other symbols have their usual meaning.

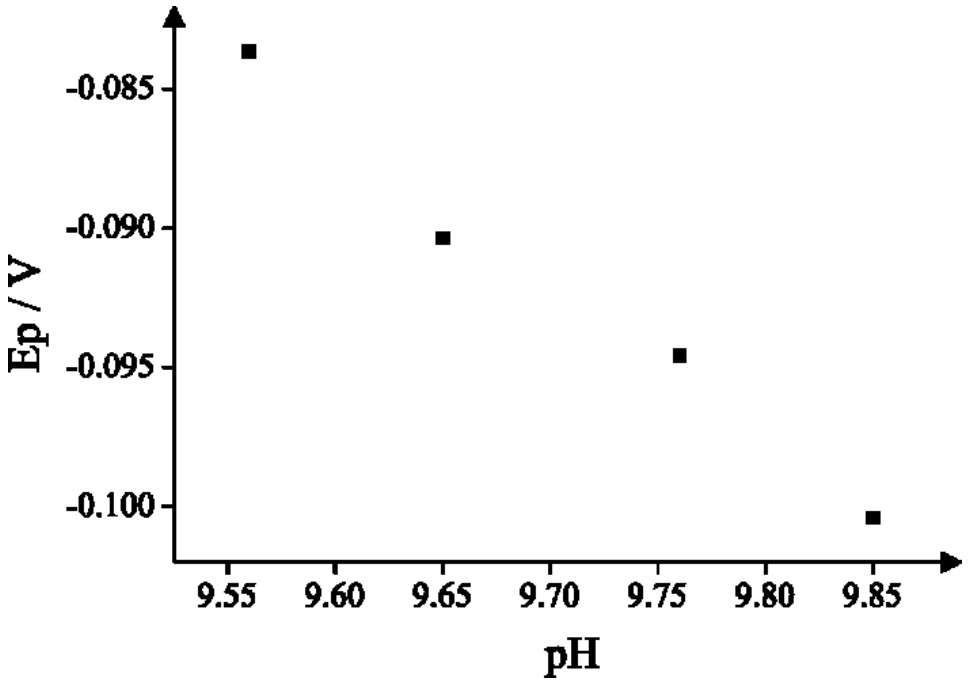

Figure 7.9 Plot of peak potential, E_P, as a function of pH for the electrochemical reduction of 100 μg mL^{-1} N-(4-Amino-2-Methyl-Phenyl)-Benzenesulfonamide in carbonated buffer solution at different pH values. In all cases, new SPGEs were utilised each time. Scan rate: 50 mV s^{-1} *vs.* Ag/AgCl.

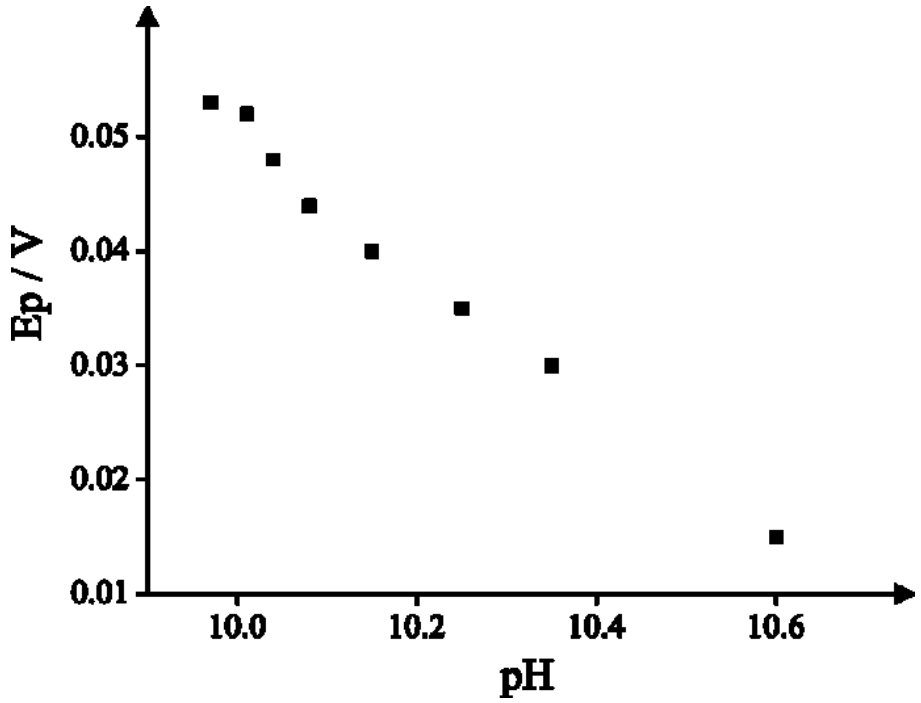

Figure 7.10 Plot of peak potential, E_P, as a function of pH for the electrochemical reduction of 100 μg mL^{-1} N,N'-(1,4-phenylene)dibenzenesulfonamide in carbonated buffer solution at different pH values. New SPGEs were utilised each time. Scan rate: 50 mV s^{-1} *vs.* Ag/AgCl

The above pH study of the mediators was untaken in order to reveal the likely electrochemical mechanism in operation for the mediators which involves an equal ratio of *m*-protons and *m*-electrons, where *m* and *n* equal 2; this process is summarised in Scheme 7.1, step 1.

Next, N,N'-(1,4-phenylene)dibenzenesulfonamide and N-(4-Amino-2-Methyl-Phenyl)-Benzenesulfonamide for the indirect sensing of cyclohexylamine and morpholine respectively were investigated as potential mediators for their electrochemical detection. In order to select the optimum pH for the detection of the two neutralizing amines with the mediators, three parameters were taken into account. The pKa values for cyclohexylamine and morpholine, the voltammetric responses of the SPGE upon the two mediators at different pH and the optimum pH range for a mixed metallurgy system, which is 8-10. [312] The pKa values for cyclohexylamine and morpholine are 10.6 [330]and 8.36 [331] respectively. The amine groups of both analytes are desirable to be as bases (pH above the pKa) and not as their conjugative acids, which do not react with the mediators.

The voltammetric responses of the mediators N-(4-Amino-2-Methyl-Phenyl)-Benzenesulfonamide and N,N'-(1,4-phenylene)dibenzenesulfonamide were investigated at

different pH values using the SPGE. Plots of their electrochemical oxidation peak currents versus the pH value are shown in figures 7.11 and 7.12 respectively. The highest peak current for N-(4-Amino-2-Methyl-Phenyl)-Benzenesulfonamide is observed in a pH range between 9 and 10. N,N'-(1,4-phenylene)dibenzenesulfonamide presents the highest peak current in the pH range between 9 and 12. For all the three above factors, pH 10 was selected as the optimum pH for the detection of the two neutralizing amines with the two mentioned mediators.

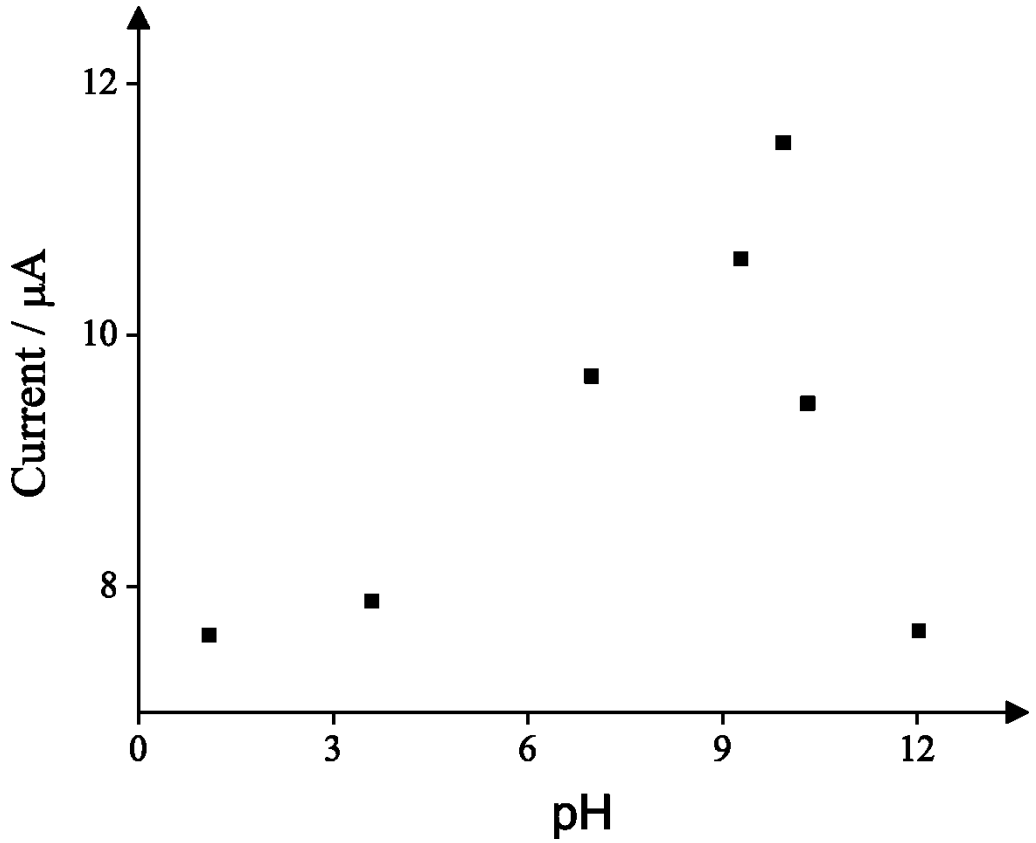

Figure 7.11 Analysis of the electrochemical oxidation peak current of 0.1 mg mL^{-1} N-(4-Amino-2-Methyl-Phenyl)-Benzenesulfonamide (Scheme 7.1, Step 1) at different pH values using SPGEs. Scan rate: 50 mVs^{-1}.

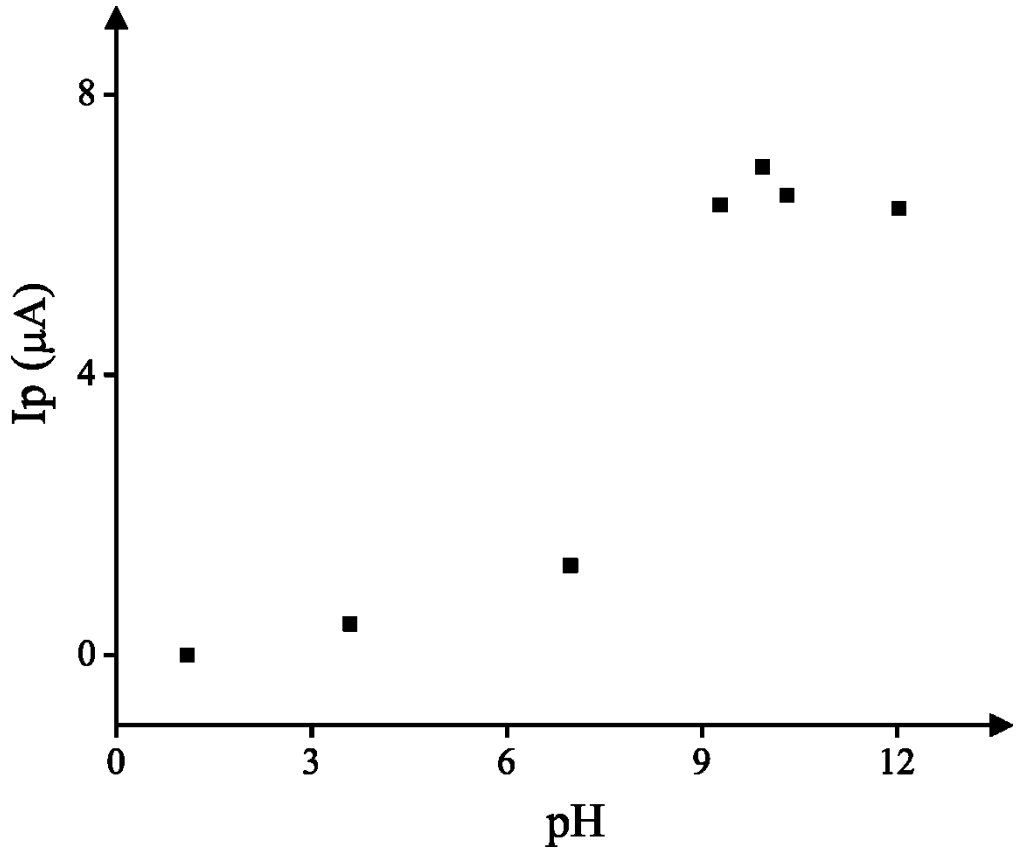

Figure 7.12 Analysis of the electrochemical oxidation peak current of 0.1 mg mL^{-1} N,N'-(1,4-phenylene)dibenzenesulfonamide at different pH values using SPGEs. Scan rate: 50 mVs^{-1}.

Figure 7.13 depicts typical cyclic voltammetric responses of SPGEs following additions of morpholine (1 – 10 mg L^{-1}) into a pH 10 carbonate buffer solution containing 0.1 mg mL^{-1} N-(4-Amino-2-Methyl-Phenyl)-Benzenesulfonamide. The electrochemical oxidation of the mediator is observed at +0.05V (*vs*. Ag/AgCl) while its corresponding electrochemical reduction peak is observed to occur at -0.04 V (*vs*. Ag/AgCl). This electrochemically oxidised mediator reacts chemically with the target amine, morpholine over appreciable and useful timescale (no waiting time is required). The reduction of this product appears as a new voltammetric signal, observed at -0.15 V (*vs*. Ag/AgCl) which increases in proportion to the concentration of morpholine. The calibration plot corresponding to increasing concentrations of morpholine versus the voltammetric peak height (μA) are depicted in Figure 7.14. The error bars for three different measurements are also shown. A linear response for the sensing of morpholine was achieved ($I_P/\mu A = -6.32$ x 10^{-2} $\mu A/mgL + 3.31$ x 10^{-2} μA; $R^2 = 0.9882$ N =

3). Furthermore, the limit of detection (3σ) for morpholine was determined to be 1.0 mg L^{-1}; the linear range and limit of detection are for FDA monitoring of these neutralizing amines.

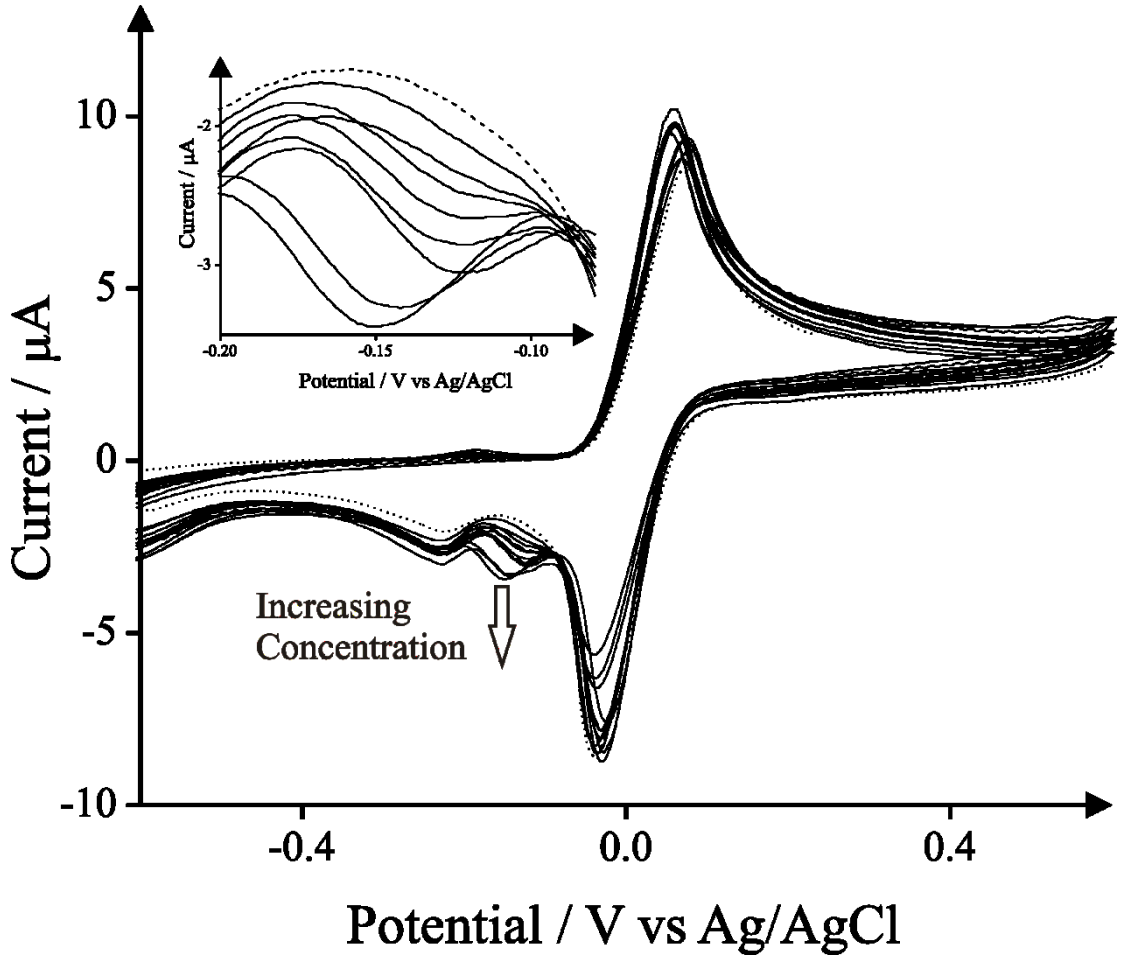

Figure 7.13 Typical cyclic voltammetric responses using SPGEs following additions of morpholine (1 – 10 mg L^{-1}) into a pH 10 carbonate buffer solution containing 0.1 mg mL^{-1} N-(4-Amino-2-Methyl-Phenyl)-Benzenesulfonamide. Note that a new SPGE is used for each addition. Inset: zoom of the peak at potential -0.15 V (*vs*. Ag/AgCl). Scan rate: 50 mVs^{-1}.

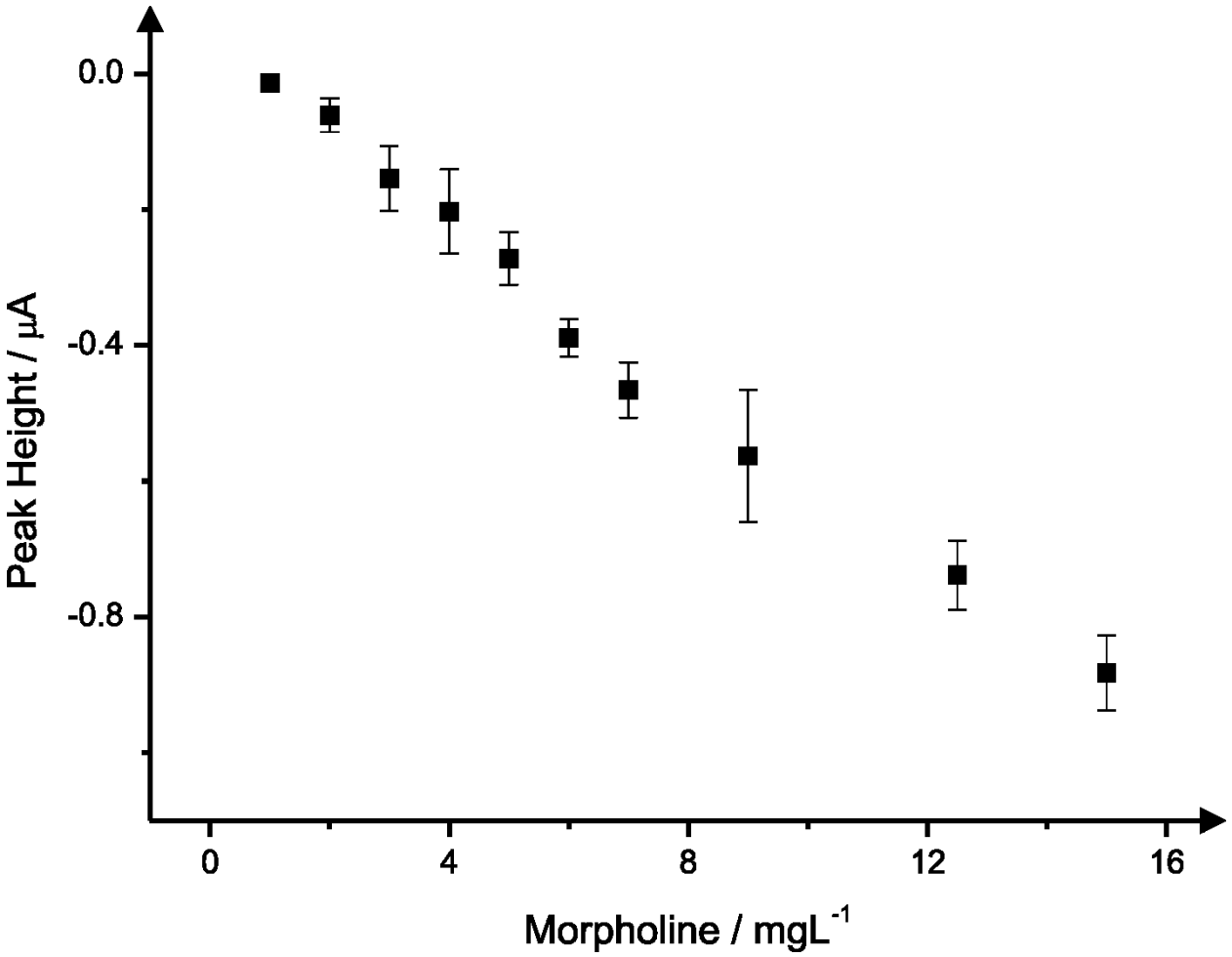

Figure 7.14 A typical calibration plot corresponding to additions of morpholine (1 – 15 mg L^{-1}) into a pH 10 carbonate buffer solution containing 0.1 mg mL^{-1} N-(4-Amino-2-Methyl-Phenyl)-Benzenesulfonamide. Data is from the analysis of the new peak observed at - 0.15 V (*vs*. Ag/AgCl) (data presented in figure 7.13). Error Bars arise from three measurements.

Figure 7.15 depicts the cyclic voltammetric responses from using SPGEs following additions of cyclohexylamine (1 – 10 mg L^{-1}) into a pH 10 Carbonate buffer solution containing 0.1 mg mL^{-1} N,N'-(1,4-phenylene)dibenzenesulfonamide; note that each measurement is conducted with a new SPGE. The electrochemical oxidation of the mediator to the corresponding sulfonimide and its electrochemical reduction are observed at + 0.07V (*vs*. Ag/AgCl) and at -0.01 V (*vs*. Ag/AgCl) respectively. The electrochemically oxidised mediator chemically reacts with cyclohexylamine. The reduction of this product then appears as a new peak observed at – 0.20 V (*vs*. Ag/AgCl) which increases relative to the concentration of cyclohexylamine. The resulting calibration plot corresponding to increasing concentrations of cyclohexylamine versus the voltammetric peak height (μA) are presented in

Figure 7.16. A linear response for the sensing of cyclohexylamine is readily achieved ($I_P/\mu A = -19.29$ x 10^{-2} $\mu A/mgL + 24.85$ x 10^{-2} μA; $R^2 = 0.9899$ $N = 3$). Furthermore, the limit of detection (3σ) for cyclohexylamine was determined to correspond to 0.9 mg L^{-1}. The proposed mechanism for this novel indirect electroanalytical protocol is summarized in Scheme 7.1.

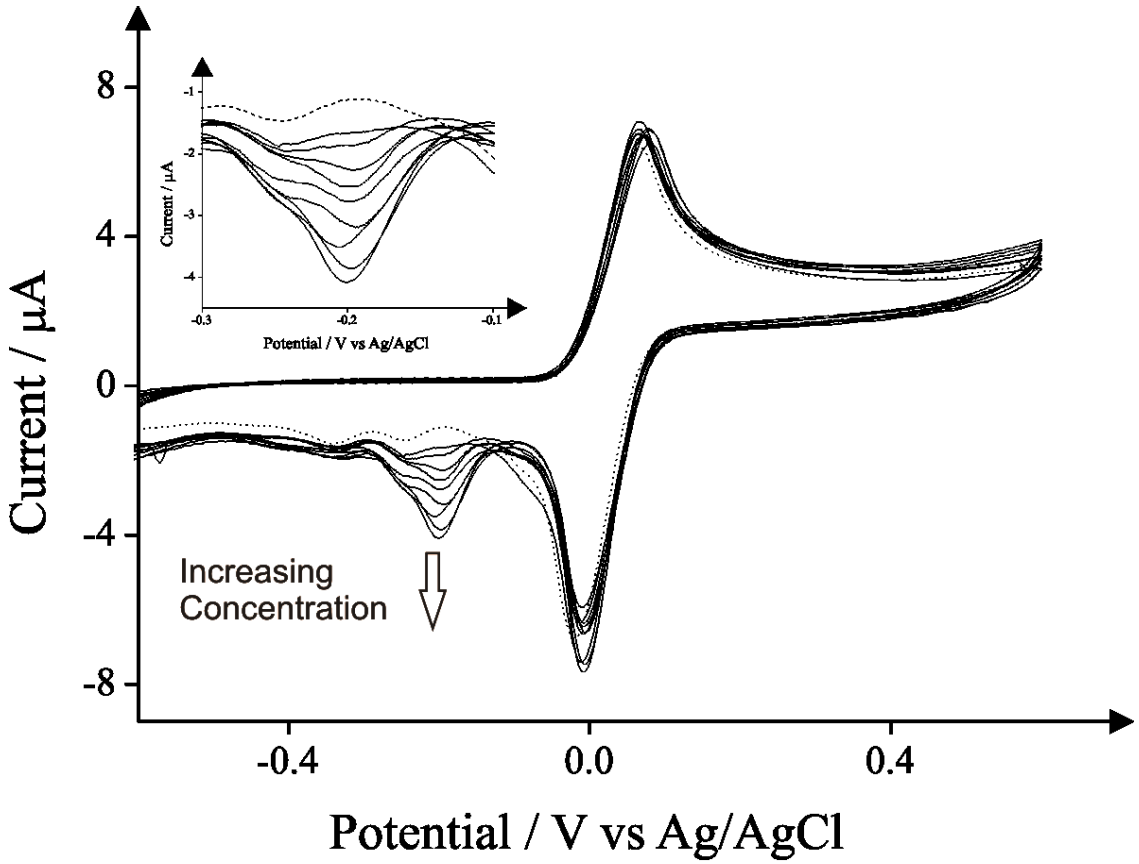

Figure 7.15 Typical cyclic voltammetric responses obtained using SPGEs following additions of cyclohexylamine (1 – 10 mg L^{-1}) into a pH 10 carbonate buffer solution containing 0.1 mg mL^{-1} N,N'-(1,4-phenylene)dibenzenesulfonamide. A new SPGE is used for each addition. Inset: zoom of the peak at potential - 0.2 V (*vs*. Ag/AgCl). Scan rate: 50 mVs^{-1}.

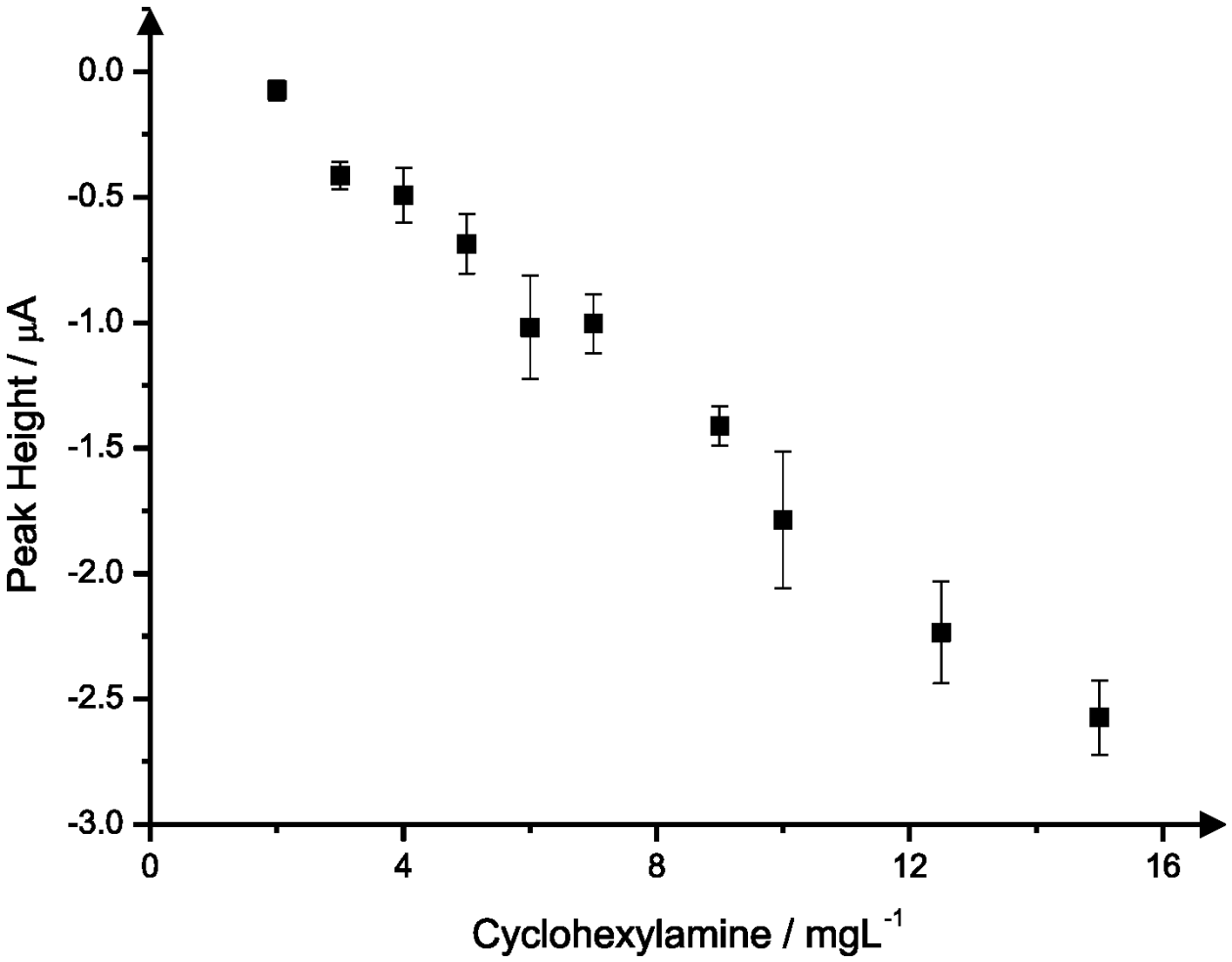

Figure 7.16 A typical calibration plot corresponding to additions of cyclohexylamine (1 - 15 mg L^{-1}) into a pH 10 carbonate buffer solution containing 0.1 mg mL^{-1} N,N'-(1,4-phenylene)dibenzenesulfonamide. The data presented in this figure is a result of the analysis of the new peak observed at - 0.2 V (*vs*. Ag/AgCl); data presented in figure 7.15 Error Bars arise from three measurements. New SPGEs electrodes were utilized each time.

7.4 CONCLUSIONS

The indirect sensing of morpholine and cyclohexylamine, two neutralizing amines widely used in water treatment in pH 10 carbonate buffer solutions using screen-printed graphite electrodes has been reported in this thesis for the first time. These economical screen-printed sensors provide an appealing alternative to the laboratory based methods for the detection of these neutralizing amines with potential to be applied easily into-the-field. Screen-printed graphite electrodes were demonstrated to allow lowest limits of detection 0.9 mg L^{-1} for cyclohexylamine and 1.0 mg L^{-1} for morpholine in ideal conditions using the mediators N,N'-(1,4-phenylene)dibenzenesulfonamide and N-(4-Amino-2-Methyl-Phenyl)-Benzenesulfonamide respectively. The two mediators are required for the detection of the two analytes as one mediator cannot measure both. Additionally the limits of detection for these amines are 10 times lower than the level of the FDA for food industry. Such sensors provide a potential solution to the common problem of the transition of laboratory-based analytical procedures to real world applications in the 'field' combining the low-cost benefits of carbon based materials with ease of mass production and facile use of screen-printed sensors. Note that the ability of the screen-printed sensors to be disposed after each measurement provide the advantage of avoiding the fouling of the working electrodes by organic compounds which are absorbed on the surface of the carbon-based working electrodes.

This electroanalytical protocol has the potential to be applied into sensing the target corrosion inhibitors in steam condensate. This real sample/matrix consists of pure water and in order for our approach to work, the steam would be expected to be condensated with the sample then spiked with our identified mediators and altering the pH to the optimum (pH 10) value. Note that the steam condensate will be either acidic or in the range 8-10 depending if the neutralizing amines are present or not. Consequently, it is hard to replicate a "real sample", which in this case, would be simply spiking deionised water (which has been done to prove our protocol). Future work is being coordinated with industries in order to explore the proposed analytical protocol for the implementation of sensing of neutralizing amines in steam condensate and has the potential to be used in an industrial or power generation cycle but note that cyclohexylamine concentrations would be much lower than 10 ppm for adequate pH control; such future work is suggested at the end of this thesis.

CHAPTER 8

CONCLUSIONS AND FUTURE WORK

8.1 OVERALL CONCLUSIONS

This thesis has reported some significant contributions to the field of electrochemistry and particularly electroanalysis developing sensors for measuring water quality. These sensors are mainly based on screen-printing technique with a view to be sensitive, cheap and portable in order to provide a potential solution to the transition of laboratory-based analytical procedures to real world applications "in-the-field" combining the low-cost benefits of carbon based materials with ease of mass production and facile use of screen-printed sensors.

Reported in chapter 5 are novel electroanalytical protocols for the detection of selenium (IV) and antimony(III) in drinking water at levels below the limits recommended by the European Union and World Health Organisation by using screen-printed graphite electrodes. Additionally the potential problematic occurrence of interferences has been explored. In the same chapter, the comparison of a novel analytical protocol for the indirect electrochemical detection of phenol and three chlorophenols within drinking water was compared with their direct electrochemical detection.

The development of a novel sensor for a point of site analysis at low levels of dissolved phosphorus in river water was presented in the sixth chapter. This provides a potential solution to the on-line monitoring of phosphorus in environmental samples and it forms a significant part of the highly desired evaluation of eutrophication in natural waters.

Finally, the introduction of the use of screen-printed electrodes for the detection of water treatment chemicals widely used in industrial water was successfully performed and presented in the seventh chapter. The novel electrochemical detection of amines such as cyclohexylamine and morpholine used as corrosion inhibitors to the steam condensate treatment was presented for the first time. The levels that these amines were detected are well below the recommended by the Food and Drug Administration (FDA) for food industries.

8.2 SUGGESTIONS FOR FUTURE WORK

In this thesis, novel electrochemical sensors have been developed and applied in the analysis of analytes which are important in the field of water analysis; a plethora of contaminants in drinking water and pollutants in environmental samples are shown to detected "in-the-field' with economical and portable screen-printed sensors. Additionally very little work focuses upon the application of the screen-printed sensors in the industrial water analysis where the on-line monitoring of the chemicals used as scale and corrosion inhibitors, oxygen scavengers, sludge dispersants and antifoaming agents is highly desired; hopefully this thesis has bridged this gap.

Future work is being coordinated with industries in order to explore the proposed analytical protocols for the implementation of sensing of neutralizing amines (mentioned in chapter seven) in steam condensate and has the potential to be used in an industrial or power generation plants. The proposed analytical protocol in chapter six for the detection of phosphorus compounds in natural water can be potentially applied in the monitoring of phosphate-based compounds traditionally used as scale inhibitors in boiler water treatment.

Screen-printed electrodes show great potential. However, electrode reproducibility and normalisation need to be tackled in order to turn them as viable sensors to further applications in the field of water quality.

Polymeric substrates used for the fabrication of the widely used screen-printed electrodes have limitations as they melt at temperatures 60^0C - 90^0C. Consideration of using polymers with higher melting points such as Polytetrafluoroethylene (PTFE) would contribute to the application of screen-printed sensors into high temperature water samples; this could enable the placement of such sensors into the condensate lines of a factory.

Finally, the incorporation of the necessary electrolytes to the three electrode configuration used in this thesis would overcome some limitations when these sensors are applied in weak supporting electrolyte samples or even to modify the pH of the samples. The incorporation could be achieved in the screen-printing process by adding another screen printing layer. In this case the desired electrolytes could be placed next to the working electrode surface (such as in the case of the silver/silver chloride reference electrode).

REFERENCES

1. S. E. Manahan, *Environmental Science and Technology*, 1997, CRC press LLC pg 7.
2. S. L. Phillips, D. A. Mack and W. D. MacLeod, *Analytical Chemistry*, 1974, 46, 345A-356A.
3. S. Ahuja, in *Monitoring Water Quality*, Elsevier B.V., 2013, p. 10.
4. H. B. Glasgow, J. M. Burkholder, R. E. Reed, A. J. Lewitus and J. E. Kleinman, *Journal of Experimental Marine Biology and Ecology*, 2004, 300, 409-448.
5. N. Pires, T. Dong, U. Hanke and N. Hoivik, *Sensors*, 2014, 14, 15458-15479.
6. S. Zhuiykov, *Sensors and Actuators B: Chemical*, 2012, 161, 1-20.
7. F. Lagarde and N. Jaffrezic-Renault, *Anal Bioanal Chem*, 2011, 400, 947-964.
8. J. Wang, *Accounts of Chemical Research*, 2002, 35, 811-816.
9. A. Hayat and J. L. Marty, *Sensors*, 2014, 14, 10432-10453.
10. P. Dell'Orco, J. Brum, R. Matsuoka, M. Badlani and K. Muske, *Analytical Chemistry*, 1999, 71, 5165-5170.
11. M. Schlesinger, *Applications of Electrochemistry in Medicine*, 2013, New York, Springer Science + Buisiness Media.
12. J. Krejčí, J. Prášek, L. Fujcik, S. Khatib, E. Hejátková, L. Jakubka and L. Giannoudi, *Microelectronics International: An International Journal*, 2004, 21, 20-24.
13. J.-M. Zen, A. Senthil Kumar, S.-C. Lee and Y. Shih, *Electroanalysis*, 2007, 19, 2369-2374.
14. P. Ekabutr, O. Chailapakul and P. Supaphol, *Journal of Applied Polymer Science*, 2013, 130, 3885-3893.
15. N. Serrano, A. Alberich, J. M. Díaz-Cruz, C. Ariño and M. Esteban, *TrAC Trends in Analytical Chemistry*, 2013, 46, 15-29.
16. J. P. Metters, R. O. Kadara and C. E. Banks, *Analyst*, 2011, 136, 1067-1076.
17. G. E. Fryxell and G. Cao, *Environmental Applications of Nanomaterials: Synthesis Sorbents and Sensors*, 2012, 2nd Edition Imperial College Press.
18. A. J. Bard and L. R. Faulkner, *Electrochemical Methods*, 2001, 2nd edition, Wiley, New York.
19. J. Wang, *Analytical Electrochemistry*, 2000, 2nd Edition, Wiley-VCH, New York.
20. A. C. Fisher, *Electrode Dynamics*, 2009, Oxford University Press, New York.
21. R. G. Compton and C. E. Banks, *Understanding Voltammetry*, 2007, 1st Ed., World Scientific Ltd.
22. F. Scholz, *Electroanalytical Methods*, 2010, Springer-Verlag Berlin Heidelberg.
23. A. E.Kaifer and M. Gomez-Kaifer, *Supramolecular Electrochemistry*, Toronto, Wiley-VHC, 1999.
24. C. G. Zoski, *Handbook of Electrochemistry*, 2007, 2001st Edition, Elsevier.
25. A. C. Testa and W. H. Reinmuth, *Analytical Chemistry*, 1961, 33, 1320-1324.
26. D. A. C. Brownson and C. E. Banks, *The Handbook of Graphene Electrochemistry*, 2014, Springer.
27. T. Hadjiioannou and C. Eustathiou, *Instrumental techniques of analysis*, University of Athens.
28. M. v. Stackelberg, M. Pilgram and V. Toome, *Z. Elektrochem.*, 1953, 57, 342.
29. F. Scholz, *Square-Wave Voltammetry*, 2007, Springer.
30. J. Mocak, A. M. Bond, S. Mitchell and G. Scollary, *Pure and Applied Chemistry*, 1997, 69, 297-328.
31. M. Thompson, S. L. R. Ellison and R.Wood, *Pure and Applied Chemistry*, 2002, 74, 835-855.
32. J. Heyrovský, *Chemické Listy*, 1922, 16, 256-264.
33. W. Kemula and Z. Kublik, *Analytica Chimica Acta*, 1958, 18, 104-111.
34. T. Navrátil, I. Švancara, K. Mrázová, K. Nováková, I. Šestáková, M. Heyrovský and D. Pelclová, *Sensing in Electroanalysis*, 2011, 6, 23-53.
35. K. Zarei, M. Atabati and H. Ilkhani, *Talanta*, 2006, 69, 816-821.

36. Y. He, Y. Zheng, M. Ramnaraine and D. C. Locke, *Analytica Chimica Acta*, 2004, 511, 55-61.
37. G. D. Zayats, V. T. Meryan, M.D.Revenco and D.G.Chiugureanu, *Analytical Letters*, 2002, 35, 577.
38. J.R.Donat and K.W.Bruland, *Anal. Chem.*, 1988, 60, 240-244.
39. C. Rojas, V. Arancibia, M. Gomez and E. Nagles, *International Journal of Electrochemical Science*, 2012, 7, 979-990.
40. A. M. M. Ali, M. A. Ghandour, S. A. El-Shatoury and S. M. Ahmed, *Electroanalysis*, 2000, 12, 155-158.
41. C. M. G. van den Berg and Z. Q. Huang, *Journal of Electroanalytical Chemistry and Interfacial Electrochemistry*, 1984, 177, 269-280.
42. J. Wang, J. Lu and R. Setiadji, *Talanta*, 1993, 40, 351-354.
43. C. M. G. Van Den Berg, *Journal of Electroanalytical Chemistry and Interfacial Electrochemistry*, 1986, 215, 111-121.
44. J. Wang and J. S. Mahmoud, *Journal of Electroanalytical Chemistry and Interfacial Electrochemistry*, 1986, 208, 383-394.
45. K. Yokoi and C. M. G. van den Berg, *Analytica Chimica Acta*, 1991, 245, 167-176.
46. C. M. G. Van den Berg and Z. Q. Huang, *Analytical Chemistry*, 1984, 56, 2383-2386.
47. G. T. F. Wong and L.-S. Zhang, *Talanta*, 1992, 39, 355-360.
48. B. Uslu and S. A. Ozkan, *Comb Chem High Throughput Screen*, 2007, 10, 495-513.
49. M. R. Smyth and J. G. Vos, *Analytical Voltametry*, 1992, Elsevier Science Pub.
50. P. Salaün, K. B. Gibbon-Walsh, G. M. S. Alves, H. M. V. M. Soares and C. M. G. van den Berg, *Analytica Chimica Acta*, 2012, 746, 53-62.
51. D. Merli, F. Ravasio, S. Protti, M. Pesavento and A. Profumo, *Talanta*, 2014, 130, 90-95.
52. V. Aumond, M. Waeles, P. Salaün, K. Gibbon-Walsh, C. M. G. van den Berg, P.-M. Sarradin and R. D. Riso, *Analytica Chimica Acta*, 2012, 753, 42-47.
53. K. Gibbon-Walsh, P. Salaün and C. M. G. van den Berg, *Analytica Chimica Acta*, 2012, 710, 50-57.
54. J. Wei, D. Yang, H. Chen, Y. Gao and H. Li, *Sensors and Actuators B: Chemical*, 2014, 190, 968-974.
55. F. Zavarise, D. Merli and A. Profumo, *Analytica Chimica Acta*, 2010, 668, 177-181.
56. A. Mohadesi and M. A. Taher, *Talanta*, 2007, 72, 95-100.
57. K. Fajerwerg, V. Ynam, B. Chaudret, V. Garçon, D. Thouron and M. Comtat, *Electrochemistry Communications*, 2010, 12, 1439-1441.
58. H. El Harmoudi, M. Achak, S. Lahrich, A. Farahi, L. El Gaini, M. Bakasse and M. A. El Mhammedi, *Arabian Journal of Chemistry*, DOI: http://dx.doi.org/10.1016/j.arabjc.2012.11.007.
59. M. A. El Mhammedi, M. Achak and M. Bakasse, *Arabian Journal of Chemistry*, 2013, 6, 299-305.
60. H. O. Pierson, in *Handbook of Carbon, Graphite, Diamonds and Fullerenes*, ed. H. O. Pierson, William Andrew Publishing, Oxford, 1993.
61. A. Kraft, *International Journal of Electrochemical Science*, 2007, 355-385.
62. L. S. Pan, *Diamond: Electronic Properties and Applications*, 1995 by Kluwer Academic Publishers.
63. R. Kalish, *Carbon*, 1999, 37, 781-785.
64. W. Haenni, P. Rychen, M. Fryda and C. Comninellis, in *Semiconductors and Semimetals*, eds. E. N. Christoph and R. Jürgen, Elsevier, 2004, vol. Volume 77, pp. 149-196.
65. M. Panizza and G. Cerisola, *Electrochimica Acta*, 2005, 51, 191-199.
66. M. A. Q. Alfaro, S. Ferro, C. A. Martínez-Huitle and Y. M. Vong, *Journal of the Brazilian Chemical Society*, 2006, 17, 227-236.
67. S. P. Satsangee, R. Jain, R. Shrivastava and S. Saxena, *Journal of The Electrochemical Society*, 2014, 161, H780-H786.

68. Ľ. Švorc, M. Rievaj and D. Bustin, *Sensors and Actuators B: Chemical*, 2013, 181, 294-300.
69. L. Bandžuchová, Ľ. Švorc, J. Sochr, J. Svítková and J. Chýlková, *Electrochimica Acta*, 2013, 111, 242-249.
70. A. Goodwin, A. L. Lawrence, C. E. Banks, F. Wantz, D. Omanović, Š. Komorsky-Lovrić and R. G. Compton, *Analytica Chimica Acta*, 2005, 533, 141-145.
71. D. Dragoe, N. Spătaru, R. Kawasaki, A. Manivannan, T. Spătaru, D. A. Tryk and A. Fujishima, *Electrochimica Acta*, 2006, 51, 2437-2441.
72. Y. Yardım, A. Levent, E. Keskin and Z. Şentürk, *Talanta*, 2011, 85, 441-448.
73. J. Wang, K. Li, C. Yang, Y. Wang and J. Jia, *Electrochemistry Communications*, 2012, 18, 51-54.
74. L. Codognoto, S. A. S. Machado and L. A. Avaca, *Diamond and Related Materials*, 2002, 11, 1670-1675.
75. C. Babyak and R. B. Smart, *Electroanalysis*, 2004, 16, 175-182.
76. L. Codognoto, S. T. Tanimoto, V. A. Pedrosa, H. B. Suffredini, S. A. S. Machado and L. A. Avaca, *Electroanalysis*, 2006, 18, 253-258.
77. C. D. Mendonça and S. A. S. Machado, *Meeting Abstracts*, 2014, MA2014-02, 2223.
78. Y. Song and G. M. Swain, *Analytica Chimica Acta*, 2007, 593, 7-12.
79. J. de Sanoit, E. Vanhove, P. Mailley and P. Bergonzo, *Electrochimica Acta*, 2009, 54, 5688-5693.
80. R. F. França, H. P. M. de Oliveira, V. A. Pedrosa and L. Codognoto, *Diamond and Related Materials*, 2012, 27–28, 54-59.
81. A. Wieckowski, *Interfacial Electrochemistry: Theory: Experiment and Applications*, Marcel Dekker, Inc., New York, 1999.
82. G. M. Jenkins and K. Kawamura, *Nature*, 1971, 231, 175-176.
83. V. K. Gupta, M. L. Yola, N. Atar, A. O. Solak, L. Uzun and Z. Üstündağ, *Electrochimica Acta*, 2013, 105, 149-156.
84. W. Geremedhin, M. Amare and S. Admassie, *Electrochimica Acta*, 2013, 87, 749-755.
85. J. Zolgharnein, T. Shariatmanesh and A. Babaei, *Sensors and Actuators B: Chemical*, 2014, 197, 326-333.
86. H. Yin, Q. Zhang, Y. Zhou, Q. Ma, T. liu, L. Zhu and S. Ai, *Electrochimica Acta*, 2011, 56, 2748-2753.
87. A.-E. Radi, H. M. Nassef and A. El-Basiony, *Dyes and Pigments*, 2013, 99, 924-929.
88. L. L. C. Garcia, L. C. S. Figueiredo-Filho, G. G. Oliveira, O. Fatibello-Filho and C. E. Banks, *Sensors and Actuators B: Chemical*, 2013, 181, 306-311.
89. J. Zolgharnein, T. Shariatmanesh and A. Babaei, *Sensors and Actuators B: Chemical*, 2013, 186, 536-544.
90. I. E. Mülazımoğlu, A. D. Mülazımoğlu and E. Yılmaz, *Desalination*, 2011, 268, 227-232.
91. L. Zhang, Y.-P. Wen, Y.-Y. Yao, Z.-F. Wang, X.-M. Duan and J.-K. Xu, *Chinese Chemical Letters*, 2014, 25, 517-522.
92. M. Á. Lorenzo, A. Sánchez Arribas, M. Moreno, E. Bermejo, M. Chicharro and A. Zapardiel, *Microchemical Journal*, 2013, 110, 510-516.
93. X. Dai, F. Qiu, X. Zhou, Y. Long, W. Li and Y. Tu, *Analytica Chimica Acta*, 2014, 848, 25-31.
94. P. Muthukumar and S. Abraham John, *Journal of Colloid and Interface Science*, 2014, 421, 78-84.
95. G. Lu, X. Yao, X. Wu and T. Zhan, *Microchemical Journal*, 2001, 69, 81-87.
96. M. L. Yola, N. Atar, M. S. Qureshi, Z. Üstündağ and A. O. Solak, *Sensors and Actuators B: Chemical*, 2012, 171–172, 1207-1215.
97. A. Stromquist, *Simple Screenprinting: Basic Techniques & Creative Projects*, Lark Books, 2004.
98. A. MacDougal, *Screen Printing Today: The Basics*, 2008, ST Media Group International Inc (2nd Ed.).
99. P. A. Serra, *Biosensors - Emerging Materials and Applications*, 2011, Intech.

100. F. G. Banica, *Chemical Sensors and Biosensors: Fundamentals and Applications*, 2012, John Wiley & Sons, Ltd.
101. F. D. Barlow and A. Elshabini, *Ceramic Interconnect Technology Handbook*, 2007, CRC PressTaylor & Francis Group.
102. J. P. Metters, M. Gomez-Mingot, J. Iniesta, R. O. Kadara and C. E. Banks, *Sensors and Actuators B: Chemical*, 2013, 177, 1043-1052.
103. F. Tan, J. P. Metters and C. E. Banks, *Sensors and Actuators B: Chemical*, 2013, 181, 454-462.
104. R. O. Kadara, N. Jenkinson and C. E. Banks, *Electrochemistry Communications*, 2009, 11, 1377-1380.
105. R. O. Kadara, N. Jenkinson and C. E. Banks, *Sensors and Actuators B: Chemical*, 2009, 142, 342-346.
106. M. Gómez-Mingot, S. Griveau, F. Bedioui, C. E. Banks, V. Montiel and J. Iniesta, *Electrochimica Acta*, 2014, 140, 42-48.
107. E. Khaled, H. N. A. Hassan, A. Girgis and R. Metelka, *Talanta*, 2008, 77, 737-743.
108. T. A. Ali, G. G. Mohamed, E. M. S. Azzam and A. A. Abd-elaal, *Sensors and Actuators B: Chemical*, 2014, 191, 192-203.
109. K. Keawkim, S. Chuanuwatanakul, O. Chailapakul and S. Motomizu, *Food Control*, 2013, 31, 14-21.
110. T. Tangkuaram, C. Ponchio, T. Kangkasomboon, P. Katikawong and W. Veerasai, *Biosensors and Bioelectronics*, 2007, 22, 2071-2078.
111. K. Yang, C. Freeman, R. Torah, S. Beeby and J. Tudor, *Sensors and Actuators A: Physical*, 2014, 213, 108-115.
112. M. Joo, B. Lee, S. Jeong and M. Lee, *Applied Surface Science*, 2011, 258, 521-524.
113. G. Nagy, R. E. Gyurcsányi, A. Cristalli, M. R. Neuman and E. Lindner, *Biosensors and Bioelectronics*, 2000, 15, 265-272.
114. A. Cranny, N. R. Harris, M. Nie, J. A. Wharton, R. J. K. Wood and K. R. Stokes, *Sensors and Actuators A: Physical*, 2011, 169, 288-294.
115. J. B. Véchembre and G. R. Fox, *Journal of Materials Research*, 2001, 16, 922-931.
116. D. E. Williams, K. Ellis, A. Colville, S. J. Dennison, G. Laguillo and J. Larsen, *Journal of Electroanalytical Chemistry*, 1997, 432, 159-169.
117. E. C. Rama, M. B. González-García and A. Costa-García, *Sensors and Actuators B: Chemical*, 2014, 201, 567-571.
118. M. M. S. Silva, A. C. M. S. Dias, M. T. Cordeiro, E. Marques Jr, M. O. F. Goulart and R. F. Dutra, *Talanta*, 2014, 128, 505-510.
119. N. Chandra Sekar, S. A. Mousavi Shaegh, S. H. Ng, L. Ge and S. N. Tan, *Sensors and Actuators B: Chemical*, 2014, 204, 414-420.
120. L. Rattfalt, F. Bjorefors, D. Nilsson, X. Wang, P. Norberg and P. Ask, *BioMedical Engineering OnLine*, 2013, 12, 64.
121. Y.-L. Yang, M.-C. Chuang, S.-L. Lou and J. Wang, *Analyst*, 2010, 135, 1230-1234.
122. G. Korotcenkov, *Handbook of Gas Sensor Materials*, 2013, Volume 1: Conventional Approaches, Springer Science+Business Media, LLC.
123. J. C. Whitaker, *Electronic Systems Maintenance Handbook*, 2001, 2nd edition, CRC Press LLC.
124. L. Aryasomayajula, *Pt-MWCNT and MWCNT Based Amperometri Biosensors for Glucose Sensing*, 2008, ProQuest LLC.
125. Y. Teng, C. Chen, C. Zhou, H. Zhao and M. Lan, *Sci. China Chem.*, 2010, 53, 2581-2586.
126. M. Khairy, R. O. Kadara and C. E. Banks, *Analytical Methods*, 2010, 2, 851-854.
127. N. A. Choudhry, D. K. Kampouris, R. O. Kadara, N. Jenkinson and C. E. Banks, *Analytical Methods*, 2009, 1, 183-187.
128. B. Šljukić, N. A. Malakhova, K. Z. Brainina, C. E. Banks and R. G. Compton, *Electroanalysis*, 2006, 18, 928-930.
129. T. J. Davies, M. E. Hyde and R. G. Compton, *Angewandte Chemie*, 2005, 117, 5251-5256.

130. F. G. Thomas and G. Henze, *Introduction to Voltammetric Analysis: Theory and Practice*, 2001, CSIRO Publishing.
131. I. Svancara, K. Kalcher, A. Walcarios and K. Vytras, *Electroanalysis with Carbon Paste Electrodes*, 2012, CRC Press Taylor & Francis Group, LLC.
132. J.-L. Chang, G.-T. Wei and J.-M. Zen, *Electrochemistry Communications*, 2011, 13, 174-177.
133. H.-H. Yang, M.-H. Chiu, K.-M. Chang and Y. Shih, *Journal of Electroanalytical Chemistry*, 2012, 682, 172-174.
134. P. W. Davies and F. Brink, *Review of Scientific Instruments*, 1942, 13, 524-533.
135. A. Fujishima, Y. Einaga, T. N. Rao and D. A. Tryk, *Diamond Electrochemistry*, 2005, Elsevier Science Ltd.
136. M. I. Montenegro, M. A. Queiros and J. L. Daschbach, *Microelectrodes: Theory and Applications*, 1990, Kluwer Academic Publishers.
137. E. Bernalte, C. Marín Sánchez and E. Pinilla Gil, *Sensors and Actuators B: Chemical*, 2012, 161, 669-674.
138. R. Güell, G. Aragay, C. Fontàs, E. Anticó and A. Merkoçi, *Analytica Chimica Acta*, 2008, 627, 219-224.
139. A. L. Alvarado-Gámez, M. A. Alonso-Lomillo, O. Domínguez-Renedo and M. J. Arcos-Martínez, *Journal of Electroanalytical Chemistry*, 2013, 693, 51-55.
140. E. Bernalte, C. M. Sánchez and E. P. Gil, *Analytica Chimica Acta*, 2011, 689, 60-64.
141. B. Silwana, C. van der Horst, E. Iwuoha and V. Somerset, *Electrochimica Acta*, 2014, 128, 119-127.
142. A. Sánchez, S. Morante-Zarcero, D. Pérez-Quintanilla, I. Sierra and I. del Hierro, *Electrochimica Acta*, 2010, 55, 6983-6990.
143. N. Lezi, C. Kokkinos, A. Economou and M. I. Prodromidis, *Sensors and Actuators B: Chemical*, 2013, 182, 718-724.
144. K. C. Honeychurch, J. P. Hart, D. C. Cowell and D. W. M. Arrigan, *Sensors and Actuators B: Chemical*, 2001, 77, 642-652.
145. S. Sadeghi and A. Garmroodi, *Materials Science and Engineering: C*, 2013, 33, 4972-4977.
146. H.-L. Fang, H.-X. Zheng, M.-Y. Ou, Q. Meng, D.-H. Fan and W. Wang, *Sensors and Actuators B: Chemical*, 2011, 153, 369-372.
147. S. Betelu, C. Vautrin-Ul and A. Chaussé, *Electrochemistry Communications*, 2009, 11, 383-386.
148. S. Betelu, C. Vautrin-Ul, J. Ly and A. Chaussé, *Talanta*, 2009, 80, 372-376.
149. O. Krystofova, L. Trnkova, V. Adam, J. Zehnalek, J. Hubalek, P. Babula and R. Kizek, *Sensors*, 2010, 10, 5308-5328.
150. M. Maczuga, A. Economou, A. Bobrowski and M. I. Prodromidis, *Electrochimica Acta*, 2013, 114, 758-765.
151. P. M. Hallam, D. K. Kampouris, R. O. Kadara, N. Jenkinson and C. E. Banks, *Analytical Methods*, 2010, 2, 1152-1155.
152. D. K. Kampouris, R. O. Kadara, N. Jenkinson and C. E. Banks, *Analytical Methods*, 2009, 1, 25-28.
153. S. Betelu, K. Polychronopoulou, C. Rebholz and I. Ignatiadis, *Talanta*, 2011, 87, 126-135.
154. L. Xiong, C. Batchelor-McAuley and R. G. Compton, *Sensors and Actuators B: Chemical*, 2011, 159, 251-255.
155. J.-M. Zen, Y.-S. Song, H.-H. Chung, C.-T. Hsu and A. Senthil Kumar, *Analytical Chemistry*, 2002, 74, 6126-6130.
156. R.-J. Zheng, Y.-M. Fang, S.-F. Qin, J. Song, A.-H. Wu and J.-J. Sun, *Sensors and Actuators B: Chemical*, 2011, 157, 488-493.
157. I. S. P. Savizi, H.-R. Kariminia, M. Ghadiri and R. Roosta-Azad, *Biosensors and Bioelectronics*, 2012, 35, 297-301.

158. J. P. Metters, R. O. Kadara and C. E. Banks, *Sensors and Actuators B: Chemical*, 2012, 169, 136-143.
159. C.-Y. Lin, V. S. Vasantha and K.-C. Ho, *Sensors and Actuators B: Chemical*, 2009, 140, 51-57.
160. M. Muchindu, T. Waryo, O. Arotiba, E. Kazimierska, A. Morrin, A. J. Killard, M. R. Smyth, N. Jahed, B. Kgarebe, P. G. L. Baker and E. I. Iwuoha, *Electrochimica Acta*, 2010, 55, 4274-4280.
161. B. R. Sljukic, R. O. Kadara and C. E. Banks, *Analytical Methods*, 2011, 3, 105-109.
162. S. I. R. Malha, J. Mandli, A. Ourari and A. Amine, *Electroanalysis*, 2013, 25, 2289-2297.
163. L. Gilbert, A. T. A. Jenkins, S. Browning and J. P. Hart, *Sensors and Actuators B: Chemical*, 2011, 160, 1322-1327.
164. S. Sanllorente-Méndez, O. Domínguez-Renedo and M. J. Arcos-Martínez, *Electroanalysis*, 2009, 21, 635-639.
165. S. Sanllorente-Méndez, O. Domínguez-Renedo and M. J. Arcos-Martínez, *Sensors*, 2010, 10, 2119-2128.
166. M. Khairy, D. K. Kampouris, R. O. Kadara and C. E. Banks, *Electroanalysis*, 2010, 22, 2496-2501.
167. E. Punrat, S. Chuanuwatanakul, T. Kaneta, S. Motomizu and O. Chailapakul, *Talanta*, 2013, 116, 1018-1025.
168. F. Arduini, F. Ricci, C. S. Tuta, D. Moscone, A. Amine and G. Palleschi, *Analytica Chimica Acta*, 2006, 580, 155-162.
169. M. Buleandra, A. A. Rabinca, C. Mihailciuc, A. Balan, C. Nichita, I. Stamatin and A. A. Ciucu, *Sensors and Actuators B: Chemical*, 2014, 203, 824-832.
170. M. Nurul Karim and H. J. Lee, *Talanta*, 2013, 116, 991-996.
171. W.-Y. Su, S.-M. Wang and S.-H. Cheng, *Journal of Electroanalytical Chemistry*, 2011, 651, 166-172.
172. J. Dou, A. Ding, L. Cheng, R. Sekar, H. Wang and S. Li, *Journal of Environmental Sciences*, 2012, 24, 956-962.
173. M. Albareda-Sirvent, A. Merkoçi and S. Alegret, *Analytica Chimica Acta*, 2001, 442, 35-44.
174. S. Timur, L. D. Seta, N. Pazarlioğlu, R. Pilloton and A. Telefoncu, *Process Biochemistry*, 2004, 39, 1325-1329.
175. K. A. Fähnrich, M. Pravda and G. G. Guilbault, *Biosensors and Bioelectronics*, 2003, 18, 73-82.
176. F. Arduini, S. Guidone, A. Amine, G. Palleschi and D. Moscone, *Sensors and Actuators B: Chemical*, 2013, 179, 201-208.
177. C. C. Mayorga-Martinez, F. Pino, S. Kurbanoglu, L. Rivas, S. A. Ozkan and A. Merkoci, *Journal of Materials Chemistry B*, 2014, 2, 2233-2239.
178. E. Moczko, G. Istamboulie, C. Calas-Blanchard, R. Rouillon and T. Noguer, *Journal of Polymer Science Part A: Polymer Chemistry*, 2012, 50, 2286-2292.
179. P. M. Hallam, D. K. Kampouris, R. O. Kadara and C. E. Banks, *Analyst*, 2010, 135, 1947-1952.
180. N. A. Choudry, D. K. Kampouris, R. O. Kadara and C. E. Banks, *Electrochemistry Communications*, 2010, 12, 6-9.
181. A. V. Kolliopoulos, J. P. Metters and C. E. Banks, *Analytical Methods*, 2013, 5, 3490-3496.
182. A. V. Kolliopoulos, J. P. Metters and C. E. Banks, *Analytical Methods*, 2013, 5, 851-856.
183. J. P. Smith, J. P. Metters, D. K. Kampouris, C. Lledo-Fernandez, O. B. Sutcliffe and C. E. Banks, *Analyst*, 2013, 138, 6185-6191.
184. K. G. Heumann, M. Wachsmann, *Z. Anal. Chem.*, 1989, 335, 755.
185. M. J. Fryer, *The Lancet*, 2000, 356, 943.
186. J. Szpunar, *Analyst*, 2005, 130, 442.
187. Panel on Dietary Antioxidants Nutrition Board Institute of Medicine, 2000.
188. R. Piech, W. W. Kubiak, *Electrochimica Acta*, 2007, 53, 584.
189. G. Gilron, *Integrated Environmental Assessment and Management*, 2012, 8, 194.
190. F. A. Bertolino, A. A. J. Torriero, E. Salinas R. Olsina, L. D. Martinez, J. and Raba, *Analytica Chimica Acta*, 2006, 572, 32.

191. European Commission, 1998, "Council Directive 98/83/EC of 93 November 1998 on the quality of water intended for human consumption (1998/1983/EC)."http://ec.europa.eu/environment/water/water-drink/index_en.html (Accessed: August 2012).
192. EPA, 1992, "National Primary Drinking Water Regulations." (http://water.epa.gov/drink/contaminants/basicinformation/selenium.cfm) (Accessed: August 2012).
193. Y. He, J. Moreda-Pineiro, C. M. Luisa, M. de la Guardia, *Journal of Analytical Atomic Spectrometry*, 1998, 13, 289.
194. H. Tao, J. W. H. Lam, J. W. McLaren, *Journal of Analytical Atomic Spectrometry*, 1993, 8, 1067.
195. P. M. Hallam, D. K. Kampouris, R. O. Kadara, C. E. Banks, *Analyst*, 2010, 135, 1947.
196. F.-H. Ko, S.-L. Chen, M.-H. Yang, *Journal of Analytical Atomic Spectrometry*, 1997, 12, 589.
197. C. Locatelli, *Electroanalysis*, 2004, 16, 1478.
198. M. Zelić, *Electroanalysis*, 2008, 20, 782.
199. J. Long, Y. Nagaosa, *Anal. Sci.*, 2007, 23, 1343.
200. J. P. Metters, R. O. Kadara, C. E. Banks, *Analyst*, 2011, 136, 1067.
201. J. Vandenhecke, M. Waeles, R. D. Riso, P.Corre, *Anal. Bioanal. Chem.*, 2007, 388, 929.
202. T. Navratil, M. Kopanica, *Crit. Rev. Anal. Chem.*, 2002, 32, 153.
203. N. Stozhko, E. Morosanova, L. Kolyadina, S. Fomina, *J. Anal. Chem.*, 2006, 61, 158.
204. J. Wang, B. Tian, *Analytica Chimica Acta*, 1993, 274, 1.
205. V. Beni, G. Collins, D. W. M Arrigan, *Analytica Chimica Acta*, 2011, 699, 127.
206. S. B. Adeloju, D. Jagner, L. Renman, *Analytica Chimica Acta*, 1997, 338, 199.
207. R. Inam, G. Somer, *Food Chem.*, 2000, 69, 345.
208. R. Inam, G. Somer, *Food Chem.*, 1999, 66, 381.
209. C. F. Pereira, F. B. Gonzaga, A. M. Guarita-Santos, J. R. SouzaDe, *Talanta*, 2006, 69, 877.
210. M. Ashournia, A. Aliakbar, *J. Hazard. Mater.*, 2009, 168, 542.
211. S. Zvonimir, S.-G. Jaroslava, M. Nikola, K. Snezana, *Food Chem.*, 2005, 92, 771.
212. L. Guanghan, L. Jianhua, H. Yiping, W. Fang, *Food Chem.*, 1996, 56, 177.
213. D. W. Bryce, A. Izquierdo, M. D. Luque de Castro, *Analytica Chimica Acta*, 1995, 308, 96.
214. Q. Zhang, X. Li, H. Shi, Hongzhou, Z. Yuan, *Electrochimica Acta*, 2010, 55, 4717.
215. R. W. Andrews, D. C. Johnson, *Anal. Chem.*, 1975, 47, 294.
216. R. S. Posey, R. W. Andrews, *Analytica Chimica Acta*, 1981, 124, 107.
217. S. H. Tan, S. P. Kounaves, *Electroanalysis*, 1998, 10, 364.
218. T. W. Hamilton, J. Ellis, T. M. Florence, *Analytica Chimica Acta*, 1979, 110, 87.
219. M. C. Santos, S. A. S. Machado, *J. Electroanal. Chem.*, 2004, 567, 203.
220. M. Alanyaliogu, U. Demir, C. Shannon, *J. Electroanal. Chem.*, 2004, 561, 21.
221. Z. Fijalek, A. Lozak, K. Sarna, *Electroanalysis*, 1998, 10, 846.
222. M. O. Solaliendres, A. Manzoli, G. R. Salazar-Banda, K. I. B. Eguiluz, S. T. Tanimoto, S. A. S. Machado, *J. Solid State Electrochem.*, 2008, 12, 679.
223. U. S. Environmental Protection Agency, *Water: Basic Information about Regulated Drinking Water Contaminants*, http://www.epa.gov, (Accessed Feb 2013).
224. U.S. Geological Survey, *U.S. Geological Survey*, 2012, 198.
225. C. A. Johnson, H. Moench, P. Wersin, P. Kugler and C. Wenger, *J. Environ. Qual.*, 2005, 34, 248.
226. W. Shotyk and M. Krachler, *Environmental Science & Technology*, 2007, 41, 1560.
227. M. Filella, P. A. Williams and N. Belzile, *Environmental Chemistry*, 2009, 6, 95.
228. K. A. Winship, *Adverse Drug React Acute Poisoning Rev*, 1987, 6, 67.
229. V. Potkonjak and M. Pavlovich, *Int Arch Occup Environ Health*, 1983, 51, 199.
230. H. Brieger, C. W. Semisch, 3rd, J. Stasney and D. A. Piatnek, *Ind Med Surg*, 1954, 23, 521.

231. P. Gross, M. L. Westrick, J. H. Brown, R. P. Srsic, H. H. Schrenk and T. F. Hatch, *AMA Arch Ind Health*, 1955, 11, 479.
232. K. E. Toghill, M. Lu and R. G. Compton*, *Int. J. Electrochem. Sci.*, 2011, 6, 3057.
233. Ashutosh, S. Sundar and N. Goyal, *Journal of Medical Microbiology*, 2007, 56, 143.
234. S. Sundar and J. Chakravarty, *International Journal of Environmental Research and Public Health*, 2010, 7, 4267.
235. Z. Farid, S. Bassily, D. C. Kent, A. Hassan, M. F. Abdel-Wahab and J. Wissa, *Br Med J*, 1968, 3, 713.
236. M. O. Andreae, J. F. Asmode, P. Foster and L. Van 't dack, *Analytical Chemistry*, 1981, 53, 1766.
237. World Health Organization, 2003, Antimony in drinking-water. Background document for preparation of WHO Guidelines for drinking-water quality, WHO/SDE/WSH/03.04/74, Geneva.
238. Council of the European Union, 1998, Council Directive 98/83 EC.
239. H. Matusiewicz and M. Krawczyk, *Journal of Analytical Atomic Spectrometry*, 2008, 23, 43.
240. M. N. Amin, S. Kaneco, K. Nomura, T. Suzuki and K. Ohta, *Microchim. Acta*, 2003, 141, 87.
241. É. C. Lima, J. L. Brasil and A. H. D. P. dos Santos, *Microchim. Acta*, 2004, 146, 21.
242. A. Iraji, D. Afzali, A. Mostafavi and M. Fayazi, *Microchim. Acta*, 2012, 176, 185.
243. P. Smichowski, Y. Madrid, M. B. de la Calle Guntinas and C. Camara, *Journal of Analytical Atomic Spectrometry*, 1995, 10, 815.
244. N. V. Semenova, L. O. Leal, R. Forteza and V. Cerda, *Anal Chim Acta*, 2005, 530, 8.
245. J. P. Metters, R. O. Kadara and C. E. Banks, *Analyst*, 2011, 136, 1067.
246. O. Domínguez-Renedo, M. Jesús Gómez González and M. Julia Arcos-Martínez, *Sensors*, 2009, 9, 219.
247. O. D. Renedo and M. Julia Arcos Martínez, *Electrochemistry Communications*, 2007, 9, 820.
248. K. C. Honeychurch, J. P. Hart, *TrAC Trends Anal. Chem.*, 2003, 22, 456.
249. O. Domínguez Renedo and M. J. Arcos Martínez, *Analytica Chimica Acta*, 2007, 589, 255.
250. K. C. Honeychuch, *Insciences*, 2012, 2, 1.
251. M. Lu, K. E. Toghill, M. A. Phillips and R. G. Compton, *Int. J. Environ. Anal. Chem.*, 2013, 93, 213.
252. DropSens (Spain), http://www.dropsens.com/; Accessed March 2013.
253. K. Z. Brainina and A. B. Chernyshova, *Talanta*, 1974, 21, 287.
254. M. M. Davila, M. P. F. M. S. Flores, M. P. Elizalde, J. Mattusch and R. Wennrich, *ECS Trans.*, 2007, 3, 1.
255. G. Gillain, G. Duyckaerts and A. Disteche, *Analytica Chimica Acta*, 1979, 106, 23.
256. G. Piccardi and R. Udisti, *Microchim. Acta*, 1979, 72, 447.
257. H. Guo, Y. Li, X. Chen, L. Nie, N. He, *Sensors*, 2005, 5, 284.
258. G. Fernekes and A. A. Koch, *J. Am. Chem. Soc.*, 1905, 27, 1224.
259. D. Li, J. Park and J.-R. Oh, *Analytical Chemistry*, 2001, 73, 3089-3095.
260. P. de Morais, T. Stoichev, M. C. P. Basto and M. T. S. D. Vasconcelos, *Talanta*, 2012, 89, 1-11.
261. U. S. E. P. A. (EPA), 1980.
262. M. Jin and Y. Yang, *Analytica Chimica Acta*, 2006, 566, 193-199.
263. The American Public Health Association, *16th edition*, 1985 part 510.
264. W. Frenzel, J. Oleksy-Frenzel and J. Mörlen, *Analytica Chimica Acta*, 1992, 261, 253-259.
265. H.-q. Ni, J. Dong, J.-j. Shi and W. Wang, *Journal of Separation Science*, 2010, 33, 1356-1359.
266. Y. Cun-guang, *Journal of Environmental Sciences*, 1998, 10, 76-86.
267. Y. Ito, Y. Tonogai, H. Suzuki, S. Ogawa, T. Yokoyama, T. Hashizume, H. Santo, K. I. Tanaka, K. Nishigaki and M. Iwaida, *Journal - Association of Official Analytical Chemists*, 1981, 64, 1448-1452.
268. R. J. Lacoste, S. H. Venable and J. C. Stone, *Analytical Chemistry*, 1959, 31, 1246-1249.
269. M. Ettinger, C. Ruchhoft and R. Lishka, *Analytical Chemistry*, 1951, 23, 1783-1788.

270. R. Azizur and A. A. Siddiqui, *International Journal of Pharmaceutical Sciences and Drug Research*, 2010, 2, 165-175.
271. G. V. Kornienko, N. V. Chaenko, N. G. Maksimov, V. L. Kornienko and V. P. Varnin, *Russ J Electrochem*, 2011, 47, 225-229.
272. J. Iniesta, P. A. Michaud, M. Panizza, G. Cerisola, A. Aldaz and C. Comninellis, *Electrochimica Acta*, 2001, 46, 3573-3578.
273. J. Wei, X. Zhu and J. Ni, *Electrochimica Acta*, 2011, 56, 5310-5315.
274. T. A. Enache and A. M. Oliveira-Brett, *Journal of Electroanalytical Chemistry*, 2011, 655, 9-16.
275. M. A. Rodrigo, P. A. Michaud, I. Duo, M. Panizza, G. Cerisola and C. Comninellis, *Journal of The Electrochemical Society*, 2001, 148, D60-D64.
276. K.-S. Lee, F. T. Short and D. M. Burdick, *Aquatic Botany*, 2004, 78, 197-216.
277. EPA, Environmental, Protection and Agency, *Working in Partnership with States to Address Phosphorus and Nitrogen Pollution through Use of a Framework for State Nutrient Reductions*, 2011, Washington, D.C.
278. O. Korostynska, A. Mason and A. Al-Shamma'a, *International Journal on smart Sensing and Intelligent Systems*, 2012, 5, 149-176.
279. E. A. Smith, P. B. Blanchard and S. Bargu, *Harmful Algae*, 2014, 35, 38-45.
280. S. Turki, A. Dhib, M. Fertouna-Bellakhal, V. Frossard, N. Balti, R. Kharrat and L. Aleya, *Ecological Engineering*, 2014, 67, 39-47.
281. G. M. Branch, R. H. Bustamante and T. B. Robinson, *Harmful Algae*, 2013, 24, 54-64.
282. S. Seoane, A. Puente, X. Guinda and J. A. Juanes, *Marine Pollution Bulletin*, 2012, 64, 2860-2866.
283. L. E. Fleming, C. Rivero, J. Burns, C. Williams, J. A. Bean, K. A. Shea and J. Stinn, *Harmful Algae*, 2002, 1, 157-168.
284. C. A. Weirich and T. R. Miller, *Current Problems in Pediatric and Adolescent Health Care*, 2014, 44, 2-24.
285. Y. Liu and J. Chen, in *Reference Module in Earth Systems and Environmental Sciences*, Elsevier, 2014, DOI: http://dx.doi.org/10.1016/B978-0-12-409548-9.09043-6.
286. N. F. Caraco, *Trends in Ecology & Evolution*, 1993, 8, 51-54.
287. Y. Bai, J. Tong, J. Wang, C. Bian and S. Xia, in *IET Nanobiotechnology*, Institution of Engineering and Technology, 2014, vol. 8, pp. 31-36.
288. EU, *Directive 2000/60/EC*, 2000, Establishing a framework for Community action in the field of water policy. Council Directive, Oct23, 2000.
289. J. Hem, *Study and interpretation of the chemical characteristics of natural water*, 1992, U.S. Geological Survey Water Supply Paper, 2254.
290. E.P.A., *Determination of Phosphorus by Semi-Automated Colorimetry*, 1993, Environmental Monitoring Systems Laboratory Office of Research and Development U.S. Environmental Protection Agency.
291. V. Ruiz-Calero and M. T. Galceran, *Talanta*, 2005, 66, 376-410.
292. L. Kröckel, H. Lehmann, T. Wieduwilt and M. A. Schmidt, *Talanta*, 2014, 125, 107-113.
293. Y.-S. Li, Y. Muo and H.-M. Xie, *Analytica Chimica Acta*, 2002, 455, 315-325.
294. N. Nakatani, D. Kozaki, W. Masuda, N. Nakagoshi, K. Hasebe, M. Mori and K. Tanaka, *Analytica Chimica Acta*, 2008, 619, 110-114.
295. M. S. A. C. Neves, M. R. S. Souto, I. V. Tóth, S. M. A. Victal, M. C. Drumond and A. O. S. S. Rangel, *Talanta*, 2008, 77, 527-532.
296. J. Murphy and J. P. Riley, *Analytica Chimica Acta*, 1962, 27, 31-36.
297. C. Warwick, A. Guerreiro and A. Soares, *Biosensors and Bioelectronics*, 2013, 41, 1-11.
298. L. Guanghan, W. Xiaogang, L. Yanhua and Y. Shenlai, *Talanta*, 1999, 49, 511-515.
299. Y. Udnan, I. D. McKelvie, M. R. Grace, J. Jakmunee and K. Grudpan, *Talanta*, 2005, 66, 461-466.
300. E. Akyilmaz and E. Yorganci, *Electrochimica Acta*, 2007, 52, 7972-7977.

301. E. M. d'Urso and P. R. Coulet, *Analytica Chimica Acta*, 1990, 239, 1-5.
302. Y. Xue, X. Zheng and G. Li, *Talanta*, 2007, 72, 450-456.
303. J. Jońca, V. León Fernández, D. Thouron, A. Paulmier, M. Graco and V. Garçon, *Talanta*, 2011, 87, 161-167.
304. A. N. Ejhieh and N. Masoudipour, *Analytica Chimica Acta*, 2010, 658, 68-74.
305. R. De Marco and C. Phan, *Talanta*, 2003, 60, 1215-1221.
306. Z. Chen, P. Grierson and M. A. Adams, *Analytica Chimica Acta*, 1998, 363, 191-197.
307. H. Hara and S. Kusu, *Analytica Chimica Acta*, 1992, 261, 411-417.
308. L. Gilbert, A. T. A. Jenkins, S. Browning and J. P. Hart, *Analytical Biochemistry*, 2009, 393, 242-247.
309. J. C. Quintana, L. Idrissi, G. Palleschi, P. Albertano, A. Amine, M. El Rhazi and D. Moscone, *Talanta*, 2004, 63, 567-574.
310. E. Y. Backheet, K. M. Emara, H. F. Askal and G. A. Saleh, *Analyst*, 1991, 116, 861-865.
311. M. C. Uprety and B. Revis, *Journal of Pharmaceutical Sciences*, 1964, 53, 1248-1251.
312. T. Suzuki, T. Hosokawa, M. Iwasaki, H. Komatsubara, Y. Makino, K. Matsubara, H. Morinaga, H. Suzuki, S. Takeda, M. Takemura and H. Takenaka, *Kurita Handbook of Water Treatment*, 1999, 2nd Edition, Kurita Water Industries Ltd., Tokyo.
313. C. De Waard and D. E. Milliams, *Corrosion*, 1975, 31, 177-181.
314. H. Yung, U. Kim, G. Seo, H. Lee and C. Lee, *Environ Eng Res*, 2009, 14, 195-199.
315. H. A. Carlson, *Industrial & Engineering Chemistry*, 1949, 41, 644-645.
316. R. R. Villa Jr, J. R. V. Paraon and K. A. Lichti, *Geothermal Resources Council Transactions*, 2002, 26, 679-686.
317. J. Luong, R. A. Shellie, H. Cortes, R. Gras and T. Hayward, *Journal of Chromatography A*, 2012, 1229, 223-229.
318. I. S. Cole, P. Corrigan, S. Sim and N. Birbilis, *International Journal of Greenhouse Gas Control*, 2011, 5, 749-756.
319. Y. S. Choi, S. Nesic and D. Young, *Environmental science & technology*, 2010, 44, 9233-9238.
320. V.-A. Glezakou, L. X. Dang and B. P. McGrail, *The Journal of Physical Chemistry C*, 2009, 113, 3691-3696.
321. S. Linnenberg, V. Darde, J. Oexmann, A. Kather, W. J. M. van Well and K. Thomsen, *International Journal of Greenhouse Gas Control*, 2012, 10, 1-14.
322. F. Valentini, V. Biagiotti, C. Lete, G. Palleschi and J. Wang, *Sensors and Actuators B: Chemical*, 2007, 128, 326-333.
323. K. Murugappan, J. Lee and D. S. Silvester, *Electrochemistry Communications*, 2011, 13, 1435-1438.
324. U. S. F. a. D. Administration, *Electronic Code of Federal Regulations*, 2014.
325. M. Joseph, V. Kagdiyal, D. K. Tuli, M. M. Rai, S. K. Jain, S. P. Srivastava and A. K. Bhatnagar, *Chromatographia*, 1993, 35, 173-176.
326. R. Lindahl, A. Wasterby and J.-O. Levin, *Analyst*, 2001, 126, 152-154.
327. R. Gilbert, R. Rioux and S. E. Saheb, *Analytical Chemistry*, 1984, 56, 106-109.
328. A. G. Kumbhar, S. V. Narasimhan and P. K. Mathur, *Talanta*, 1998, 47, 421-437.
329. R. Adams and K. A. Schowalter, *Journal of the American Chemical Society*, 1952, 74, 2597-2602.
330. National, Research and Council, *Acute Exposure Guideline Levels for Selected Airborne Chemicals*, 2007, Volume 5, Washington, D.C.
331. A. Asokan and M. J. Cho, *Biochimica et Biophysica Acta (BBA) - Biomembranes*, 2003, 1611, 151-160.